University of Ljubljana
Faculty of Mathematics and Physics

Dissertation Committee:
Janez Dolinšek, chairperson
Denis Arčon
Janez Bonča
Alexandros Lappas

STUDY OF ONE- AND TWO-DIMENSIONAL MAGNETIC SYSTEMS WITH SPIN-SINGLET GROUND STATE

by

Andrej Zorko

DISSERTATION

Ljubljana, October 2004

ACKNOWLEDGEMENTS

I would first like to acknowledge the financial support of the Slovenian Ministry of Education, Science and Sport through the Young Researcher educational program.

Second, I would like to thank both of my supervisors, Janez Dolinšek for giving me an opportunity to become a member of the Magnetic Resonance Group and for his continuous guidance, as well as Denis Arčon for all the stimulating discussions and valuable hints, given during the process of making this Thesis, and for being a true mentor in every respect. My thanks go also to Robert Blinc, the head of the Solid State Physics department at "Jožef Stefan" Institute, Ljubljana, for accepting me in the department.

I would also like to express my sincere gratitude to Alexandros Lappas from the Institute of Electronic Structure and Laser, FORTH, Heraklion, for providing and characterizing virtually all the samples used in this investigation as well as for our long-lasting collaboration in the field of magnetism in lower dimensions. I am also grateful to Hiroshi Kageyama from Gradual School of Science, Kyoto, for providing a $SrCu_2(BO_3)_2$ single crystal.

I thank Zvonko Jagličić from Institute of Mathematics, Physics and Mechanics, Ljubljana, for performing magnetic susceptibility measurements, and Marko Hrovat from the Electronic Ceramics Department at "Jožef Stefan" Institute, for his assistance in the synthesis of doped $SrCu_2(BO_3)_2$ compounds.

Last but not least, I thank Janez Bonča and Samir El Shawish from the Department of Theoretical Physics at "Jožef Stefan" Institute for our collaboration on calculation of ESR spectra in low-dimensional magnetic systems, currently underway.

ABSTRACT

A comprehensive study of magnetic properties of two different families of low-dimensional compounds exhibiting spin gap is presented in this Thesis. The emphasis is put on two recently discovered systems, the one-dimensional Haldane system $PbNi_2V_2O_8$ and the two-dimensional orthogonal dimer system $SrCu_2(BO_3)_2$. The ground state, low-energy excited states, as well as the effect of doping and magnetic anisotropy on the magnetism of these two systems is investigated via magnetic resonance measurements. The proposed picture of the dominant magnetic anisotropy in the Haldane system $PbNi_2V_2O_8$ is improved on the basis of X-band electron spin resonance (ESR) and symmetry arguments. Additionally, the ^{51}V nuclear magnetic resonance (NMR) designates the VO_4 tetrahedra as exchange bridges for relatively strong interchain exchange in the $PbNi_2V_2O_8$ system. Similarly, the X-band ESR linewidth anisotropy of the $SrCu_2(BO_3)_2$ single crystal allows accurate determination of the major magnetic anisotropy contributions in this system. In addition to the well-accepted interdimer Dzyaloshinsky-Moriya coupling, the intradimer components are quantitatively evaluated and shown to be substantial. The pattern of the Dzyaloshinsky-Moriya vectors is constructed using the symmetry operations of the corresponding space group. Second, the doping effect on the spin-singlet ground states of both parent materials is studied. The impurity substitutional doping of the $PbNi_2V_2O_8$ compound on Ni^{2+} magnetic sites is consistent with the valence-bond-solid model, which predicts liberated $S = 1/2$ end-chain spins. These spins are shown to be strongly ferromagnetically coupled. Besides, by comparing the magnetic resonance results of the Mg-doped and Co-doped compounds, also the spin nature of the dopants is found to have a pronounced effect on the development of the low-temperature spin correlations. On the other hand, doping of the $SrCu_2(BO_3)_2$ system seems to be much more difficult task. In this respect, the results on the Li-intercalation are rather contradictory, but the general conclusion could be that the spin gap is much more robust in this compound.

Keywords: spin liquid, Haldane-gap state, dimer-gap state, spin-vacancy induced antiferromagnetism, electron spin resonance, nuclear magnetic resonance, Dzyaloshinsky-Moriya interaction, single-ion anisotropy

PACS: 75.50.Mm, 75.30.Gw, 76.30.-v, 76.60.-k

POVZETEK

Ta disertacija vključuje podrobno študijo magnetnih lastnosti dveh različnih družin nižje-dimenzionalnih spojin s spinsko energijsko režo. Pod drobnogled sta vzeta dva nedavno odkrita sistema, enodimenzionalni Haldaneov sistem $PbNi_2V_2O_8$ in dvodimenzionalni sistem ortogonalnih dimerov $SrCu_2(BO_3)_2$. Značilnosti osnovnega stanje in nizkoležečih vzbujenih stanj ter efekt dopiranja in magnetne anizotropije na magnetizem omenjenih sistemov smo preučevali s pomočjo magnetno-resonančnih spektroskopskih metod. Veljavna slika oblike dominantnega člena magnetne anizotropije v Haldaneovem sistemu $PbNi_2V_2O_8$ je nadgrajena s pomočjo rezultatov meritev elektronske spinske resonance (ESR) v področju X in uporabo simetrijskih argumentov. Meritve jedrske magnetne resonance (NMR) na jedrih ^{51}V omogočajo označitev VO_4 tetraedrov kot mediatorjev relativno močne izmenjalne sklopitve med verigami v sistemu $PbNi_2V_2O_8$. Podobno v sistemu $SrCu_2(BO_3)_2$ meritve širine absorpcijskih spektrov ESR dovoljujejo natančno določitev dominantnih členov magnetne anizotropije v tem sistemu. Poleg že uveljavljene interdimerne interakcije Dzyaloshinsky-Moriya je ocenjena tudi velikost intradimerne interakcije, katere velikost je znatna. Dodatno je na podlagi simetrijskih operacij prostorske grupe kristala $SrCu_2(BO_3)_2$ izdelan še vzorec vektorjev Dzyaloshinsky-Moriya. Nadaljnji predmet raziskave je vpliv dopiranja na osnovno singletno stanje obeh sistemov. Substitucijsko dopiranje z nečistočami na mestih ionov Ni^{2+} v spojini $PbNi_2V_2O_8$ je v skladu s tako imenovanim modelov "valence-bond solid", ki napoveduje nastanek prostih spinov $S = 1/2$ ob nečistočah. Rezultati meritev kažejo, da so inducirani spini močno feromagnetno sklopljeni. Dodatna primerjava magnetno-resonančnih rezultatov med spojinami dopiranimi z magnezijem in s kobaltom pokaže, da ima na razvoj nizkotemperaturnih spinskih korelacij bistven vpliv tudi spinska narava dopantov. V nasprotju s sistemom $PbNi_2V_2O_8$ je dopiranje spojine $SrCu_2(BO_3)_2$ precej bolj zahtevno. Rezultati interkalacije litija v to spojino se zdijo nekoliko kontradiktorni, vendar pa bi v splošnem lahko zaključili, da je spinska energijska reža v tem spinskem sistemu mnogo bolj obstojna.

Ključne besede: spinska tekočina, Haldaneovo stanje z energijsko režo, dimerno stanje z energijsko režo, antiferomagnetizem kot posledica spinskih nečistoč, elektronska spinska resonanca, jedrska magnetna resonanca, interakcija Dzyaloshinsky-Moriya, anizotropija na posameznem mestu

CONTENTS

1 INTRODUCTION TO SPIN-GAP SYSTEMS

1.1 Magnetism in Lower Dimensions

Low-dimensional quantum magnetic systems have been receiving considerable attention in the last two decades. Enhanced experimental and theoretical efforts were triggered by the discovery of superconductivity in two-dimensional cuprates [1], since the parent cuprate insulators are now considered the best examples of planar spin $S = 1/2$ antiferromagnets with isotropic and predominantly nearest-neighbor exchange interaction. The pseudogap, which manifests itself as a partial suppression of the excitation spectrum corresponding to a transfer of spectral weight of magnetic excitations from low to higher energy in underdoped high-temperature superconductors in the normal phase below a characteristic temperature, as well as antiferromagnetic fluctuations have been observed [2]. Their interconnections with the tendency of copper pairing in the superconducting phase have been at the heart of the debates in the last decade. Different experimental techniques were successful in observing these phenomena among which are also NMR spectroscopy [2, 3] and interlayer tunneling resistivity experiments [4]. These experiments indicate the predominant role of the spin over the orbital degrees of freedom in the formation of the pseudogap. For this reason, also the magnetism of other low-dimensional antiferromagnets exhibiting an energy gap in their excitation spectrum, attributed to the spin system, is of special interest. One can then waggishly remark that the fascinating field of copper oxides, vanadates, and nickelates opened up merely as a side product of the two-dimensional superconducting cuprates. However, the investigation of a reach assortment of the fundamental magnetic phenomena appearing in these systems has also an appeal of its own.

On the other hand, the early development of a coherent theory of magnetism in one dimension is dating back to the first half of the previous century and is strongly correlated to the progress in the field of quantum mechanics. This is due to the fact that linear spin chains often allow analytical and numerical solutions whereas this is usually not the case in higher dimensions. Another strong aspect enabling a blossom of the field of low dimensional magnetism that one encounters nowadays, is the prominent development of the solid-state chemistry, which is now able of tailoring various “exotic” systems with peculiar as well as potentially technologically useful magnetic properties. There are numerous experimental and theoretical reports on the topics of the magnetism in lower dimensions recently published in the literature. Comprehensive reviews of the present state of affairs are for instance provided by Lemmens *et al*. [5] and Katsumata [6].

The low-energy excitations are frequently due to spin degrees of freedom. In such systems the magnetic properties can often be described by the Heisenberg exchange

Hamiltonian. The route to low-dimensional magnetism is paved by one of the two building principles potentially responsible for the reduction of the spin dimension from the three-dimensional physical space. The first one is due to enlarged distances of missing bridging ions (most often the oxygen ions) corresponding to a particular direction or even two directions within the crystal structure. Second, the Kanamori-Goodenough superexchange rules yield vanishing antiferromagnetic exchange in the case when the two interacting magnetic moments define the right angle with the bridging oxygen ion [7, 8]. Compounds that incorporate these structural aspects exhibit a number of unusual magnetic properties that are related to strong quantum fluctuations. They can be characterized by strong electronic correlations controlled by the exchange parameters, exchange topology and a possible presence of spin impurities.

To begin with the magnetism in lower dimension let us first highlight the magnetic properties of the simplest and relatively well-understood Heisenberg system. This is a uniform $S = 1/2$ spin chain with only nearest-neighbor antiferromagnetic exchange coupling. The solution of this problem dates to a distant history of quantum mechanics. Already in 1931 Bethe came to the conclusions that the ground state is a many-body spin singlet state, that it has no energy gap to the excited states and that the spin correlations decay slowly as a power low of distance [9]. Anderson described the ground state as a superposition of all possible singlet pairings of the chain, which is known as the resonating valence-bond state [10]. Assuming negligible spin anisotropy and interchain interactions the ground state remains nonmagnetically ordered even at zero temperature. Due to the delocalized nature of singlet pairs, the excitations to the triplet state become gapless. The lowest-lying spinon excitations were rigorously calculated to have the dispersion relation of the form $E(k) = (\pi/2)|J||\sin k|$, with k as a normalized wave vector along the chains [11]. Since the latter expression resembles the classical spin-wave dispersion $E(k) = |J||\sin k|$, it was assumed for a long time that the Heisenberg model with larger spin value smoothly converges to the classical case.

However, contrary to this expectation, Haldane's conjecture in 1983 that the ground states of the Heisenberg spin chains strongly depend on the value of the spin came out rather as a surprise [12, 13]. Namely, if the chain consists of half-integer spins it should exhibit quasi-long-range order as in the case of $S = 1/2$ spins. Any slight perturbation such as a marginal interchain coupling or magnetic anisotropy will decrease quantum fluctuations, which act opposite to magnetic ordering, and thus a long-range ordered ground state will be restored. On the contrary, integer-spin systems show true short-range order in their ground state with the spin correlation functions decaying exponentially. Moreover, ground state is robust to external perturbations to a relatively high extent. This is due to an energy gap (Haldane gap) between the ground state and the lowest-lying excited state present in the excitation spectrum of an integer-spin system, which is not the case with half-integer spin systems [13]. As the gap originates from spin degrees of freedom, it is conventionally called a spin gap.

1.2 Origin of the Energy Gap in Magnetic Excitation Spectrum

Although the detailed structures of the ground states of the systems exhibiting spin gap differ, they share an important concept, namely, the singlet formation of pairs of spins. For an antiferromagnetically coupled pair of localized $S = 1/2$ spins, the quantum mechanical ground state is the well-known antisymmetric combination of the Néel states, $\left(|\uparrow\downarrow\rangle - |\downarrow\uparrow\rangle\right)/\sqrt{2}$, which does not have a classical counterpart. However, in macroscopic spin systems the pair formation becomes more difficult since each spin has in general several nearest neighbors. Consequently, most macroscopic spin systems with translational symmetry exhibit Néel order at low temperatures, attributed also to a presence of spin anisotropies as discussed below. However, some of them still prefer a ground state based on the singlet pair formation.

The central concept of describing these low-dimensional quantum spin systems is that of a spin liquid. The ground state is nonmagnetic and highly disordered. It is characterized by the absence of the long-range magnetic order, which is due to strong quantum fluctuations. In this respect the $S = 1/2$ Heisenberg spin chain is regularly addressed as the critical spin liquid due to the algebraic decay of spin correlations. The spin gap in one and two dimensions can be attributed to the integer nature of spins, a special exchange topology, frustration of the underlying spin lattice or dimerization, which is the consequence of a broken translational symmetry.

1.2.1 Overview of Spin-Gap Systems in One Dimension

Spin-Peierls Transition and Alternating Exchange

In one dimension many different systems are known to exhibit the spin gap in their excitation spectrum. The origin of the spin-gap behavior in spin-Peierls systems is a lattice dimerization, which may set-in in the case of soft lattices in the direction of the chains and if the chains are well magnetically separated. The phase transition from the uniform to the dimerized spin chains at a finite temperature is characterized by alternating deformation of the spin chains, which is also the origin of the alternating exchange coupling as presented in Fig. 1.1. Although the dimerization increases the elastic energy of the underlying lattice, the transition may still be possible if the singlet pair formation compensates for the energy increase. The ground state structure of the spin-Peierls system is thus a stacking of spin-singlet pairs.

The first experimentally observed spin-Peierls systems were organic compounds [14, 15], however, the discovery of such transition also in inorganic $CuGeO_3$ compound [16] and NaV_2O_5 spin system [17] expanded the horizons of this field. This is mainly a consequence of the

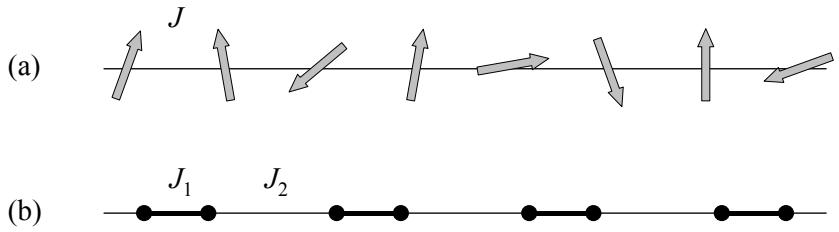

Fig. 1.1: (a) Spin $S = 1/2$ chain with the uniform antiferromagnetic exchange coupling. (b) The "singlet" ground state of the dimerized lattice below the spin-Peierls transition, which is the origin of the alternation of the exchange interaction.

availability of large single crystals of considerable quality in case of inorganic spin-Peierls compounds due to their high thermal stability with respect to the organic systems. Second, doping of inorganic compounds, to be addressed in the next subsection, is also more feasible.

A similar structure to that of a spin-Peierls ground state is observed if a "static" alternation of the exchange is intrinsically provided by the crystal structure itself. The case of temperature-independent alternating exchange on linear chains was, for instance, observed in $Cu(NO_3)_2 \cdot 2.5\ H_2O$ system [18] and also recently recognized in the $(VO)_2P_2O_7$ compound [19], which was for a long time mistreated as a spin ladder system.

Competing Antiferromagnetic Interactions

The next possible mechanism leading to spin-gap behavior in one dimension is sufficient frustration due to next-nearest-neighbor antiferromagnetic exchange interaction. It was shown by Majumdar and Ghosh that when the next-nearest exchange accounts for exactly half of the nearest-neighbor exchange, the Heisenberg model is exactly solvable and has a two-fold degenerated singlet ground state [20]. This solution was recently used also as a guide for constructing various more or less artificial spin Hamiltonians with the spin-liquid ground state and gapped magnetic excitations [21].

Haldane chains

All the above-presented mechanisms have geometrical reasons for two particular spins to form the singlet bond. However, in the case of $S = 1$ spin chains, the origin of the spin-gap character of the ground state lies in the integer spin value. As initially conjectured by Haldane [13], the integer spin systems exhibit a singlet ground state. Currently the best and also well-established approximation of the ground state of a realistic $S = 1$ spin chain is the one given by Affleck *et*

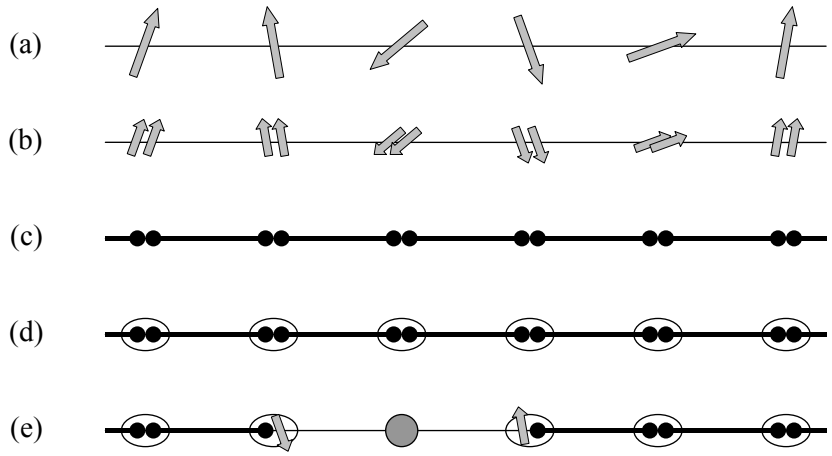

Fig. 1.2: Within the valence-bond-solid model (a) each spin $S = 1$ on the uniform chain is decomposed into (b) two $S = 1/2$ spin degrees of freedom. (c) The adjacent spins are paired into singlets and (d) the two $S = 1/2$ spins at each side are symmetrized to restore the original spin $S = 1$. (e) The introduction of a spin vacancy breaks two valence bonds and liberates two $S = 1/2$ degrees of freedom on the neighboring sites.

al., who proposed the valence-bond-solid model [22]. In this model, the singlet nature of the ground state, the gap to the first excited state and the short-range exponentially decaying spin correlations are correctly predicted [23] by considering two valence bonds emerging from each site and terminating in the two neighboring sites as illustrated in Fig. 1.2. Each valence bond contracts two of the $S = 1/2$ variables to form a singlet. It is constructed in the following way: first, the $S = 1$ spin at each site is decomposed into two $S = 1/2$ spin degrees of freedom. Next, the singlet bonds between adjacent liberated half-integer spins are made. At the end, the two $S = 1/2$ spins at each site are symmetrized. Intuitively, the existence of the spin-singlet ground state can be understood as if the strength of the valence bonds is much larger than the "force" needed to align the two spin degrees of freedom within each ion. The $S = 1/2$ dimer and the $S = 1$ Haldane Hamiltonians were, in fact, shown to belong to the same class, allowing a crossover between them by a continuous change of parameters [24]. Due to quantum many-body effects, the Haldane gap is suppressed with respect to the isotropic exchange ($\Delta = 0.41J$) as accurately determined from exact diagonalization of the Haldane Hamiltonian [25].

The Haldane gap was first observed in the $CsNiCl_3$ system [26]. Because of the existence of the Néel order at low temperatures (see Fig. 1.4) a clear conclusion was impossible at that time. Another model material is $[Ni(C_2H_8N_2)_2(NO_2)]ClO_4$, abbreviated as NENP, which shows a spin gap and no Néel ordering [27]. Since then various other Haldane systems have been reported (as presented in Fig. 1.4) with the last one being $PbNi_2V_2O_8$ spiral-chain system [28]. The magnetic resonance measurement on the latter parent system and different doped materials is one of the topics of this Thesis and will be thoroughly presented in chapter 3.

The validity of the valence-bond-solid model in real systems was directly confirmed for the first time by observing liberated $S = 1/2$ degrees of freedom when the Haldane bonds were intentionally broken by introducing spin vacancies to partially replace the $S = 1$ spins [29]. However, it has to be emphasized that the valence-bond-solid ground state is only an approximation of the realistic ground state for $S = 1$ spin chain with only the nearest-neighbor exchange coupling. Namely, it is an exact solution of the following Hamiltonian

$$H = J\sum_i \left(\mathbf{S}_i \cdot \mathbf{S}_{i+1} + (\mathbf{S}_i \cdot \mathbf{S}_{i+1})^2/3\right). \tag{1.1}$$

The first excited state is a single triplet excitation with the Haldane gap corresponding to the wave vector at the boundary of the Brillouin zone ($q = \pi$). The next excited state is a two-magnon continuum beginning at the energy of two Haldane gaps at wave vector $q = 0$ [30, 31].

1.2.2 Spin Ladders – Crossover from One to Two Dimensions

The spin ladder systems serve as a bridge between one- and two-dimensional spin systems. A spin ladder system is an $S = 1/2$ antiferromagnetic square lattice with finite width and infinite length. The simplest representative of such compounds is a two-leg spin ladder with an approximately equal or larger exchange coupling of spins along rungs than along legs of the ladder [32]. The ground state is a composition of singlets formed on the rungs with the spin gap to the first excited state again suppressed due to the intraleg interaction. A model representative of the two-leg ladder system is $SrCu_2O_3$ compound. On the other hand, the recently synthesized two-leg ladder CaV_2O_5 is even more straightforward since the intrachain interaction is small compared with the intrarung interaction making the system quasi-zero-dimensional [33].

There is an interesting feature associated with ladder systems when more than two legs are coupled. Namely, the ladders with an even number of legs have a spin gap and the true spin-liquid nature of the ground state, while odd-leg ladders are gapless and exhibit a power-law falloff of the spin correlation functions [34], which is a quantum manifestation of the fact that an even number of half-integer spins can be arranged into a spin singlet. The model systems for the n-leg ladders are $Sr_{n-1}Cu_{n+1}O_{2n}$ compounds [34]. With increasing number of legs we arrive at two dimensions, but the magnitude of the spin gap goes to zero. This is an indication why only few two-dimensional systems exhibiting the spin gap are known.

1.2.3 Spin Gap in Two Dimensions

The first possible route to the gapped excitation spectrum in two dimensions is modified exchange topology. This mechanism is realized in the 1/5-depleted square lattice of the CaV_4O_9

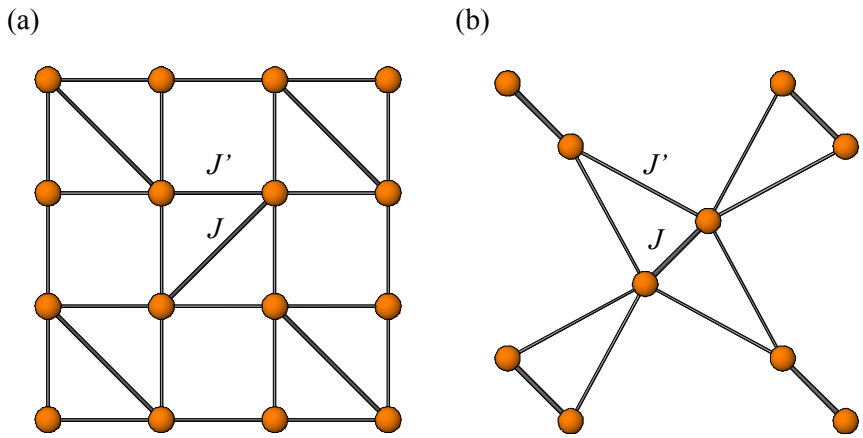

Fig. 1.3: (a) The Shastry-Sutherland lattice with nearest-neighbor antiferromagnetic exchange *J'* and selected antiferromagnetic bond interactions *J*. (b) The arrangement of Cu^{2+} ($S = 1/2$) sites within the crystallographic *ab* planes of the $SrCu_2(BO_3)_2$ compound. The nearest-neighbor exchange *J* and the next-nearest-neighbor exchange *J'* are accounted for within the orthogonal dimer model. The two lattices are topologically equivalent.

system [35], where the ground state is a two-dimensional arrangement of plaquette singlet units of four V^{4+} ions possessing spin $S = 1/2$ [36]. Second, sufficient geometrical frustration may also lead to spin gap. Frustration is expressed in the Kagomé lattice, where the antiferromagnetically coupled triangles share corners instead of sites in contrast to the familiar triangular lattice [37], and in the Shastry-Sutherland lattice [38]. Many other more or less artificial models have been theoretically discussed in the literature. For instance, the net spin model is a generalization of the Majumdar-Gosh model for any spin in one and two dimensions [39]. However, unfortunately, as a general rule these theoretical models do not correspond to any known physical system.

Although the Shastry-Sutherland model on a square lattice with selected diagonal (next-nearest-neighbor) bonds presented in Fig. 1.3a seems rather artificial, there is, in fact, a physical realization of this model. Namely, the $SrCu_2(BO_3)_2$ system was recognized to be topologically equivalent to the two-dimensional Shastry-Sutherland lattice [40, 41]. The equivalent Hamiltonian for the $SrCu_2(BO_3)_2$ system in conventionally called the orthogonal dimer model [42] due to the orthogonal arrangement of Cu^{2+} $S = 1/2$ dimers in the $SrCu_2(BO_3)_2$ compound shown in Fig. 1.3b. The ground state of the model Hamiltonian taking into account the antiferromagnetic exchange coupling *J* with the nearest-neighbor Cu^{2+} magnetic moment and the antiferromagnetic exchange *J'* to four next-nearest neighbors,

$$H = J\sum_{(i,j)} \mathbf{S}_i \cdot \mathbf{S}_j + J'\sum_{\{l,m\}} \mathbf{S}_l \cdot \mathbf{S}_m \,, \tag{1.2}$$

is a simple product of singlet states on each dimer, while the lowest lying magnetically excited state is a single triplet excitation localized on one of the dimers [42].

A more thorough introduction into the magnetic properties of the $SrCu_2(BO_3)_2$ compound will be given in chapter 4. There the second topic of this Thesis, namely the magnetic resonance measurement on this two-dimensional spin-gap system will be comprehensively presented.

1.3 Effects of Anisotropy, 3D Exchange and Impurity Doping on the Gapped Singlet Ground States

As presented in the preceding section, there are not many systems exhibiting spin-liquid ground states. This is due to the fact that physical systems often exhibit perturbations to the ideal Heisenberg Hamiltonian that are not negligible. The parameters that may significantly affect the ground state properties and the low-lying magnetic excitations of a particular low-dimensional spin system are interchain/interlayer exchange coupling, magnetic anisotropy, and the dilution of the spin network by inhomogeneities introduced to the system in a form of impurities. In principle, due to the energy gap characteristic for spin-gap systems, the gaped ground states are usually robust to these perturbations up to a certain degree. However, when the external perturbation is raised above a definite threshold value it effectively lowers the energy of excitations at a certain point in the reciprocal space to such extent that a transition to the long-range ordered state is induced.

For example, the importance of the interchain exchange $J_\perp$ with Z nearest chains and the magnetic anisotropy D_{cf} in the form of the single-ion anisotropy with tetrahedral symmetry (for explanation see the subsequent chapter) on the Haldane ground state is reflected on the Sakai-Takahashi phase diagram [43]. In Fig. 1.4 several $S = 1$ spin-chain systems are placed on this diagram including the $PbNi_2V_2O_8$ and $SrNi_2V_2O_8$ systems [44]. As evident, both perturbations oppose the Haldane ground state. However, the gaped state is quite robust.

Another way to induce magnetic ordering in Haldane systems is the introduction of spin vacancies. For magnetic ordering to set-in it was theoretically predicted that the fraction of the introduced impurities into an integer-spin systems with disordered ground state has to exceed some critical threshold value x_c [45]. This mechanism is known by the name "order-by-disorder effect" [46], since the introduced disorder in a form of spin vacancies, in effect, induces long-range order in the spin system. It was actually the initial idea for testing the validity of the valence-bond-solid model in Haldane systems to introduce spin vacancies, which effectively brake the valence bonds and introduce $S = 1/2$ degrees of freedom at the host spin sites neighboring the impurity sites providing that the exchange coupling between the host and the impurity spins is sufficiently weak (see Fig. 1.2). The effective fractional spins $S = 1/2$ were

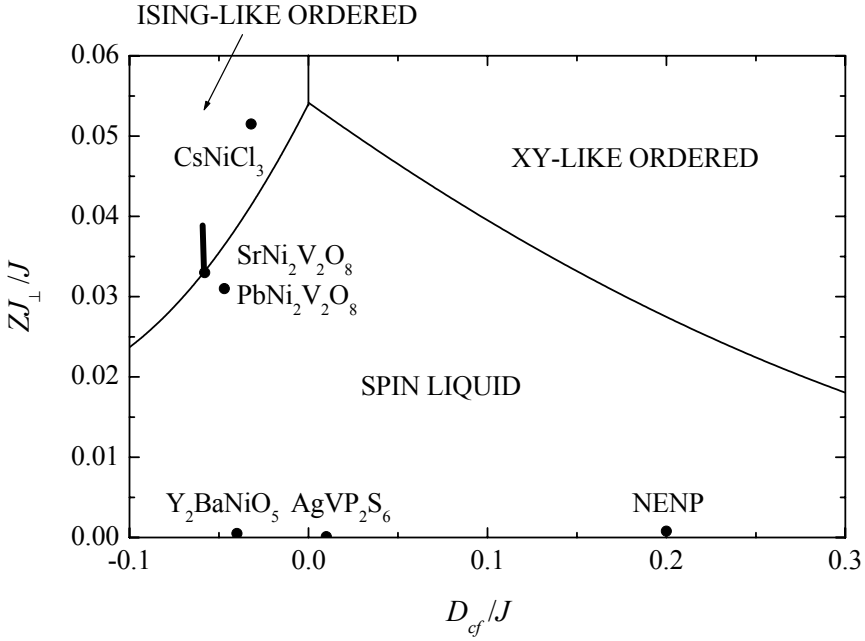

Fig. 1.4: The Sakai-Takahashi $J_\perp$-D_{cf} phase diagram of weakly coupled one-dimensional spin $S = 1$ chains (Ref. 43) with the position of some well-characterized Haldane systems (Ref. 44). Vertical bar indicates the uncertainty of the parameters for the $SrNi_2V_2O_8$.

theoretically explained by exact diagonalization of finite open chains [47]. These calculations revealed that the four lowest-lying energy states in a finite chain are the singlet and the triplet states whose separation approaches zero exponentially with increasing chain length while there is, on the other hand, the Haldane gap to the next energy level. Such liberated spins were, in fact, observed for the first time in the NENP Haldane system by means of ESR [29, 48].

The "order-by disorder effect" is known to show up in spin $S = 1/2$ systems possessing spin gap such as the spin-Peierls system $CuGeO_3$ [16] or the two-leg spin ladder compound $SrCu_2O_3$ [49]. The breaking of the spin-Peierls ground state for the long-range Néel-ordered state in the $CuGeO_3$ compound occurs for very low doping levels and irrespective of the nature of the substitution on either the Cu^{2+} or the Ge^{4+} site [5]. For instance, in the case of Zn doping on copper site there exists no critical concentration for the observation of the long-range order at low temperatures. Similar observations have been reported for the case of Zn-doped two-leg ladder system $SrCu_2O_3$ [49, 50]. Since the phenomenon of enhanced antiferromagnetic correlations is found to occur in several models and cluster geometries, a common simple explanation based on the valence-bond character of the spin correlations was given [51]. The antiferromagnetic order and the rapid collapse of the spin gap is a consequence of the appearance of $S = 1/2$ spin states near vacancy sites. This effect can be easily understood in the case of strong dimerization (spin-Peierls systems) or large ratio between the intrarung and the intraleg exchange (ladder systems). In this case weakly interacting "loose" $S = 1/2$ spins are created next to impurity sites. However, when the dimerization is small or the intrarung

exchange is not dominant, the $S = 1/2$ states are spread over several lattice spacings enhancing the spin-spin correlations at short distances [50, 52]. The magnetized segments of chains interact with neighboring chains resulting in the long-range ordering [53]. The induced liberated spins form an energy band, which appears below the lowest-lying magnetic excitation and effectively closes the spin-gap at relatively low doping concentrations.

Although the suppression of the spin gap and the enhancement of the antiferromagnetic correlations have been observed in different $S = 1/2$ spin-liquid systems, the vacancy-induced order in a Haldane system was not observed in the past despite a reach ensemble of the Haldane systems. However, recently Uchiyama *et al*. observed magnetic ordering also in Haldane-gap systems in the case of $PbNi_{2-x}Mg_xV_2O_8$ compounds [28].

Theoretical as well as experimental studies of impurity doping in spin-gap systems found general interest also as a step towards understanding the phenomenon of the superconductivity. At first sight, the two types of systems might not seem interconnected. For instance, in high-T_c compounds mobile carriers destroy the long-range Néel order on a square lattice leading to the opening of the pseudogap for spin and charge excitations. On the other hand, the transition from nonmagnetic gapped state to a magnetically ordered gapless state is induced by localized spin vacancies in dimerized spin chains or even-leg spin ladders. However, the effect of the mobile carriers on the gapped excitations of spin liquids should be directly related to the problem of the high-temperature superconductivity [5]. Corresponding theoretical studies of weakly hole-doped ladders confirmed the tendency of holes towards binding [32]. This mechanism is an inherent consequence of the nature of the ground state of the undoped two-leg ladder. Coupled holes thus minimize the number of "damaged" spin singlets [54]. In fact, Uehara *et al*. were the first to report superconductivity in the hole-doped chain/ladder system $Sr_{0.4}Ca_{13.6}Cu_{24}O_{41.84}$ in the case of applied pressure [55]. Additionally, it has been recently predicted that in the case of Li^+-hole-doped ladders the spin-gap character should be robust due to the formation of a dopant-magnon bound state just below the spin gap, in clear contrast to the Zn^{2+} vacancy doping [56].

Even though the general effect of the impurity-induced ordering in spin-gap systems is well accepted by now, it still lacks a coherent theory. For this reason experimental insight into the problem should come useful, which was our initial motivation for performing magnetic resonance experiments on the Mg-doped and also Co-doped $PbNi_2V_2O_8$ compounds. Second, also the doping effect on the two-dimensional dimer model $SrCu_2(BO_3)_2$ should be of interest, especially in connection to the possible occurrence of the superconductivity, as the Cu planes resemble the situation encountered in the high-T_c cuprates. Since there is virtually no experimental data on doping the $SrCu_2(BO_3)_2$ systems, we employed a number of experimental techniques, the outcome of which is reported in this Thesis.

Second, this work also addresses the question of magnetic anisotropy present in both families of materials. As already discussed above, the anisotropy can have a pronounced effect

on the ground state and the excited states properties of spin systems. When trying to produce a "general" theory about a certain phenomenon originating from the spin system it is, therefore, essential to have a broad general knowledge about the magnetic anisotropy of the system. Magnetic resonance measurements are ideal for addressing these open questions.

The structure of the Thesis is organized as follows: in the next chapter a general theory about the magnetic resonance absorption in magnetic systems will be given, which is necessary to understand the experimental results of electron spin resonance and nuclear magnetic resonance measurements presented in the subsequent two chapters. Chapter 3 will focus on the magnetic properties of the one-dimensional Haldane system $PbNi_2V_2O_8$ and the compounds obtained from this parent material by Mg- and Co-doping on nickel sites as well as on the isostructural $SrNi_2V_2O_8$ system. The magnetic ordering of the doped materials will also receive a considerable attention. Chapter 4 will be devoted to the magnetic properties of the two-dimensional spin-gap system $SrCu_2(BO_3)_2$. An upgraded picture about the magnetic anisotropy in this system will be given and the importance of the spin-phonon coupling mechanism will be highlighted. At the end of this chapter out attempts of doping this two-dimensional compound will be presented. Concluding remarks will briefly be given in chapter 5.

Bibliography

[1] J. G. Bednorz, K. A. Müller. Possible high-Tc superconductivity in the Ba-La-Cu-O system, *Z. Phys. B* **64**, 189 (1986).

[2] T. Auler, M. Horvatić, J. A. Gillet, C. Berhtier, Y. Berthier, P. Ségransan, J. Y. Henry. ^{63}Cu and ^{89}Y NMR study of the optimally doped $YBa_2Cu_3O_{6.94}$ single crystal, *Phys. Rev. B* **56**, 11274 (1997).

[3] B. Batlogg, V. J. Emery. Crossovers in cuprates, *Nature* **382**, 20 (1996).

[4] T. Shibauchi, L. Krusin-Elbaum, M. Li, M. P. Maley, P. H. Kes. Closing the pseudogap by Zeeman splitting in $Bi_2Sr_2CaCu_2O_{8+y}$ at high magnetic fields, *Phys. Rev. Lett.* **86**, 5763 (2001).

[5] P. Lemmens, G. Güntherodt, C. Gros. Magnetic light scattering in low-dimensional quantum spin systems, *Phys. Rep*. **375**, 1 (2003).

[6] K. Katsumata. High-frequency electron spin resonance in magnetic systems, *J. Phys.: Condens. Matter* **12**, R589 (2000).

[7] J. Kanamori. Superexchange interaction and symmetry properties of electron orbitals, *J. Phys. Chem. Solids* **10**, 87 (1959).

[8] J. B. Goodenough. Theory of the role of covalence in the perovskite-type manganites [La, *M*(II)]MnO_3, *Phys. Rev*. **100**, 564 (1955).

[9] H. A. Bethe. Zur Theorie der Metalle. I. Eigenwerte und Eigenfunktionen der linearen Atomkette, *Z. Phys*. **71**, 205 (1931).

[10] P. W. Anderson. Resonating valence bonds - new kind of insulator, *Mater. Res. Bull*. **8**, 153 (1973).

[11] J. des Cloizeaus, J. J. Pearson. Spin-wave spectrum of the antiferromagnetic linear chain, *Phys. Rev*. **128**, 2131 (1962).

[12] F. D. M. Haldane. Continuum dynamics of the 1-D Heisenberg anti-ferromagnet - identification with the O(3) non-linear sigma-model, *Phys. Lett*. **93A**, 464 (1983).

[13] F. D. M. Haldane. Nonlinear field theory of large-spin Heisenberg antiferromagnets: semiclassically quantized solitons of the one-dimensional easy-axis Néel state, *Phys. Rev. Lett*. **50**, 1153 (1983).

[14] J. W. Bray, H. R. Hart, L. V. Interrante, I. S. Jocobs, J. S. Kasper, G. D. Watkins, S. H. Wee, J. C. Bonner. Observation of a spin-Peierls transition in a Heisenberg antiferromagnetic linear-chain system, *Phys Rev. Lett*. **35**, 744 (1975).

[15] S. Huizinga, J. Kommendour, G. A. Sawatzky, B. T. Thole, K. Kopinga, W. J. M. de Jong, J. Roos. Spin-Peierls transition in N-methyl-N-ethyl-morpholinium-ditetracyanoquinodimethanide [MEM-$(TCNQ)_2$], *Phys. Rev. B* **19**, 4723 (1979).

[16] M. Hase, I. Terasaki, K. Uchinokura. Observation of the spin-Peierls transition in linear Cu^{2+} (spin-1/2) chains in an inorganic compound $CuGeO_3$, *Phys. Rev. Lett.* **70**, 3651 (1993).

[17] M. Isobe, Y. Ueda. Magnetic susceptibility of quasi-one-dimensional compound α'-NaV_2O_5 - possible spin-Peierls compound with high critical temperature of 34 K, *J. Phys. Soc. Jpn.* **65**, 1178 (1996).

[18] J. C. Bonner, S. A. Fridberg, H. Kobayashi, D. L. Meier, H. W. J. Blöte. Alternating linear-chain antiferromagnetism in copper nitrate $Cu(NO_3)_2 \cdot 2.5\ H_2O$, *Phys. Rev. B* **27**, 248 (1983).

[19] A. W. Garrett, S. E. Nagler, D. A. Tennant, B. C. Sales, T. Barnes. Magnetic excitations in the S = 1/2 alternating chain compound $(VO)_2P_2O_7$, *Phys. Rev. Lett.* **79**, 745 (1997).

[20] C. K. Majumdar, D. P. Ghosh. On next-nearest neighbor interaction in linear chains. I, *J. Math. Phys.* **10**,1388 (1969).

[21] B. Kumar. Quantum spin models with exact dimer ground sates, *Phys. Rev. B* **66**, 024406 (2002).

[22] I. Affleck, T. Kennedy, E. H. Lieb, H. Tasaki. Rigorous results of valence-bond ground states in antiferromagnets, *Phys. Rev. Lett*. **59**, 799 (1987).

[23] I. Affleck, T. Kennedy, E. H. Lieb, H. Tasaki. Valence bond ground-states in isotropic quantum antiferromagnets, *Commun*. *Math. Phys.* **115**, 477 (1988).

[24] A. K. Kolezhuk, H.-J. Mikesha. Models with exact ground states connecting smoothly the S = 1/2 dimer and S = 1 Haldane phases of one-dimensional spin chains, *Phys. Rev. B* **56**, R11380 (1997).

[25] O. Golinelli, Th. Jolicoeur, R. Lacaze. Finite-lattice extrapolations for a Haldane-gap antiferromagnet, *Phys. Rev. B* **50**, 3037 (1994).

[26] W. J. L. Buyers, R. M. Mora, L. W. Armstrong, M. J. Hogan, P. Gerlach, K. Hirakawa. Experimental evidence for the Haldane gap in a spin-1 nearly isotropic antiferromagnetic chain, *Phys. Rev. Lett.* **56**, 371 (1986).

[27] J. P. Renard, M. Verdaguer, L. P. Regnault, W. A. C. Erkelens, J. Rossatmignod, W. G. Stirling. Presumption for a quantum energy-gap in the quasi one-dimensional S = 1 Heisenberg-antiferromagnet $Ni(C_2H_8N_2)_2NO_2(ClO_4)$, *Europhys. Lett.* **3**, 945 (1987).

[28] Y. Uchiyama, Y. Sasago, I. Tsukada, K. Uchinokura, A. Zheludov, T. Hayashi, N. Miura, P. Böni. Spin-vacancy-induced long-range order in a new Haldane-gap antiferromagnet, *Phys. Rev. Lett*. **83**, 632 (1999).

[29] M. Hagiwara, K. Katsumata, I. Affleck, B. I. Harpelin, J. P. Renard. Observation of S = 1/2 degrees of freedom in an S = 1 linear-chain Heisenberg antiferromagnet, *Phys. Rev. Lett.* **65**, 3181 (1990).

[30] I. Affleck. Theory of electron spin resonance in Haldane-gap antiferromagnets, *Phys. Rev. B* **46**, 9002 (1992).

[31] M. Takahashi. Monte Carlo calculation of elementary excitation of spin chains, *Phys. Rev. Lett*. **62**, 2313 (1989).

[32] E. Dagotto, J. Riera, D. J. Scalapino. Superconductivity in ladders and coupled planes, *Phys. Rev. B* **45**, 5744 (1992).

[33] Y. Ueda, M. Isobe. Magnetic properties of AV_2O_5 (A = Li, Na, Cs, Ca, Mg), *J. Magn. Magn. Mater.* **177-181**, 741 (1998).

[34] E. Dagotto, T. M. Rice. Surprises on the way from one- to two-dimensional quantum magnets: The ladder materials, *Science* **271**, 618 (1996).

[35] S. Taniguchi, T. Nishikawa, Y. Yasui, Y. Kobayashi, M. Sato, T. Nishioka, M. Kotani, K. Sano. Spin gap behavior of S = 1/2 quasi-two-dimensional system CaV_4O_9, *J. Phys. Soc. Jpn.* **64**, 2758 (1995).

[36] K. Kodama, H. Harashina, H. Sasaki, Y. Kobayashi, M. Kasai, S. Tanigutchi, Y. Yasui, M. Sato, K. Kakurai, T. Mori, M. Nishi. Study of spin-gap formation in quasi-two-dimensional S = 1/2 system CaV_4O_9: Neutron scattering and NMR, *J. Phys. Soc. Jpn.* **66**, 793 (1997).

[37] L. Limot, P. Mendels, G. Collin, C, Mondelli, B. Ouladdiaf, H. Mutka, N. Branchard, M. Mekata. Susceptibility and dilution effects of the Kagomé bilayer geometrically frustrated network: A Ga NMR study of $SrCr_{9p}Ga_{12-9p}O_{19}$, *Phys. Rev. B* **66**, 144447 (2002); and references therein.

[38] B. S. Shastry, B. Sutherland. Exact ground state of a quantum mechanical antiferromagnet, *Physica* **108B**, 1069 (1981).

[39] H. Q. Lin, J. L. Shen, H. Y. Shik. Exactly soluble quantum spin models on a double layer: The net spin model, *Phys. Rev. B* **66**, 184402 (2002).

[40] H. Kageyama, K. Onizuka, Y. Ueda, N. V. Mushnikov, T. Goto, K. Yoshimura, K. Kosuge. Magnetic anisotropy of $SrCu_2(BO_3)_2$ with a two-dimensional orthogonal dimer lattice, *J. Phys. Soc. Jpn*. **67**, 4304 (1998).

[41] H. Kageyama, K. Yoshimura, R. Stern, N. V. Mushnikov, K. Onizuka, M. Kato, K. Kosuge, C. P. Slichter, T. Goto, Y. Ueda. Exact dimer ground state and quantized magnetization plateaus in the two-dimensional spin system $SrCu_2(BO_3)_2$, *Phys. Rev. Lett*. **82**, 3168 (1999).

[42] S. Miyahara, K. Ueda. Exact dimer ground state of the two dimensional Heisenberg spin system $SrCu_2(BO_3)_2$, *Phys. Rev. Lett.* **82**, 3701 (1999).

[43] T. Sakai, M. Takahashi. Effect of the Haldane gap on quasi-one-dimensional systems, *Phys. Rev. B* **42**, 4537 (1990).

[44] A. Zheludov, T. Masuda, I. Tsukada, Y. Uchiyama, K. Uchinokura, P. Böni. Magnetic excitations in coupled Haldane spin chains near the quantum critical point, *Phys. Rev. B* **62**, 8921 (2000).

[45] E. F. Shender, S. A. Kivelson. Dilution-induced order in quasi-one-dimensional quantum antiferromagnets, *Phys. Rev. Lett*. **66,** 2384 (1991).

[46] J. Villain, R. Bidaux, J. P. Carton, R. Conte. Order as an effect of disorder, *J. Phys. - Paris* **41**, 1263 (1980).

[47] T. Kennedy. Exact diagonalizations of open spin-1 chains, *J. Phys.: Condens. Matter* **2**, 5737 (1990).

[48] S. H. Glarum, S. Geschwind, K. M. Lee, M. L. Kaplan, J. Michel. Observation of fractional spin $S = 1/2$ on open ends of $S = 1$ linear antiferromagnetic chains: nonmagnetic doping, *Phys. Rev. Lett.* **67**, 1614 (1991).

[49] M. Azuma, Y. Fujishiro, M. Takano. Switching of the gapped singlet spin-liquid state to an antiferromagnetically ordered state in $Sr(Cu_{1-x}Zn_x)_2O_3$, *Phys. Rev. B* **55**, R8658 (1997).

[50] Y. Motome, N. Katoh, N. Fukuwara, M. Imada. Impurity effect on spin ladder systems, *J. Phys. Soc. Jpn.* **65**, 1949 (1996).

[51] M. Laukamp, G. B. Martins, C. Gazza, A. L. Malvezzi, E. Dagotto. Enhancement of antiferromagnetic fluctuations induced by nonmagnetic impurities: Origin and predictions for NMR experiments, *Phys. Rev. B* **57**, 10755 (1998).

[52] G. B. Martins, E. Dagotto, J. A. Riera. Rapid suppression of the spin gap in Zn-doped $CuGeO_3$ and $SrCu_2O_3$, *Phys. Rev. B* **54**, 16032 (1996).

[53] H. Fukuyama, T. Tanimoto, M. Saito. Antiferromagnetic long range order in disordered spin-Peierls systems, *J. Phys. Soc. Jpn.* **65**, 1182 (1996).

[54] E. Dagotto. Spin-gap and superconductivity in ladder compounds, *J. Electron Spectrosc.* **117-118**, 223 (2001).

[55] M. Uehara, T. Nagata, J. Akimitsu, H. Tkahashi, N. Mori, K. Kinoshita. Superconductivity in the ladder material $Sr_{0.4}Ca_{13.6}Cu_{24}O_{41.84}$, *J. Phys. Soc. Jpn.* **65**, 2764 (1996).

[56] A. Läuchli, D. Poiblanck, T. M. Rice, S. R. White. Li-induced spin and charge excitations in spin ladders. *Phys. Rev. Lett.* **88**, 257201 (2002).

2 MAGNETIC RESONANCE IN MAGNETIC SOLIDS

2.1 Electron Spin Resonance

The general term electron magnetic resonance stands for magnetic resonance absorption experiments performed on an ensemble of magnetic moments corresponding to localized or itinerant electrons. In principle, such absorption can be seen in the case of paramagnetic compounds containing transition elements with incomplete inner shells, in ordinary metals, in magnetically ordered systems and in case of imperfections in insulators, which may trap electrons or holes [1]. In this respect the expression electron spin resonance (ESR) can be assigned to experiments with paramagnetic species in the case when the magnetic moments originate primarily from the spin momentum as in iron-group metals, as well as for the resonant absorption in ferromagnetically or antiferromagnetically ordered state.

The ESR technique often provides additional information to the information obtained by bulk magnetic susceptibility measurements. ESR can reveal the development of electronic correlations in magnetic solids when changing the temperature, the magnetic field, or some other external parameter. This is due to the fact that electrons serve as local probes in ESR measurements so that the spectra directly reflect fluctuations of the local magnetic fields present at a particular site in the crystal or at a particular wave-vector.

2.1.1 Effective Spin Hamiltonian

Electrons, which are localized at magnetic sites in incompletely filled electronic shells, are in a state different from a free-ion state. This is because of the interaction of each magnetic ion with its surroundings. The crystal-field (CF) effect accounts for the interaction of the paramagnetic ion with its diamagnetic neighbors. The second type of interaction that a particular magnetic moment encounters in a crystal is an interaction with other magnetic moments. The simplest crystal-field interaction is the electrostatic effect due to surrounding charges. This mechanism is, in fact, dominant for the rare-earth metals, which are characterized by incompletely filled 4*f* shell. The crystal field is much larger in the case of iron-group metals. The main reason is that 3*d* electrons range over the outer region of an ion. In general, the orbitals of magnetic ions corresponding to free electrons in *d* shells directly overlap with orbitals of neighboring diamagnetic ions in a magnetic solid. The resulting covalency effect overshadows the direct electrostatic interaction and drastically enhances the strength of the crystal field [2].

In the case of performing magnetic resonance analysis in a magnetic solid, the so-called effective spin Hamiltonian is of great interest. To obtain such form of the Hamiltonian one has

to take into account also the spin-orbit coupling (LS coupling) in addition to the fundamental ionic potential and the crystal field. However, the relative "size" of the former interaction with respect to the crystal-field interaction varies appreciably between different groups of magnetic materials. Between the two types of the perturbative interaction LS coupling is the superior one in rare-earth metals. Magnetic moments are in such materials consequently directly proportional to the total angular momentum **J**. The effect of the crystal field, which can be treated as a perturbation, is then simply to eliminate the degeneracy of the energy levels corresponding to the incompletely filled electronic shell. In this respect it affects magnetic properties of a particular material. On the other hand, in the iron-group metals the crystal-field effect is much larger compared to both the thermal energy *kT* and the spin-orbit coupling. As a consequence, it has to be considered as a perturbation upon the ionic potential before taking into account the LS coupling. In effect, it splits the degenerated energy levels of a given orbital momentum **L** of the ion and can cause the familiar "quenching" of the expected values of this operator, $\langle \mathbf{L} \rangle = 0$ [1]. The spin-orbit coupling, which can be written as $H_{LS} = \lambda \mathbf{L} \cdot \mathbf{S}$ for the states of definite orbital momentum **L** and spin momentum **S** [3], and the Zeeman energy term, corresponding to the energy of the magnetic moment in the applied magnetic field $H_Z = \mu_B (g_0 \mathbf{S} + \mathbf{L}) \cdot \mathbf{B}_0$, can be considered as a further perturbation. Here μ_B is the Bohr magneton and g_0 = 2.0023 the free-electron *g*-factor. The result is the effective Hamiltonian, which has for a nondegenerate orbital ground state $|0\rangle$ split-off by the crystal field, the following form [4]

$$H_S = \sum_{\mu,\nu} g_0 \mu_B B_\mu \left(\delta_{\mu,\nu} - \lambda \Lambda_{\mu,\nu} \right) S_\nu - \lambda^2 S_\mu \Lambda_{\mu,\nu} S_\nu - \mu_B^2 B_\mu \Lambda_{\mu,\nu} B_\nu \,, \tag{2.1}$$

where μ and ν represent Cartesian components and the components of the tensor $\underline{\mathbf{\Lambda}}$ are defined as

$$\Lambda_{\mu,\nu} = \sum_n \frac{\langle 0 | L_\mu | n \rangle \langle n | L_\nu | 0 \rangle}{E_n - E_0} . \tag{2.2}$$

Here the sum runs over all the excited states corresponding to a given shell. Since a spin wave function is independent of an orbital wave function, **S** is left as an operator in Eq. (2.1). In the view of electron spin resonance only the first two terms of this equation are potentially important. The first one introduces the anisotropic *g*-factor tensor with components $g_{\mu,\nu} = g_0 \left(\delta_{\mu,\nu} - \lambda \Lambda_{\mu,\nu} \right)$, which define the compact form of the Zeeman interaction

$$H_Z = \mu_B \mathbf{S} \cdot \underline{\mathbf{g}} \cdot \mathbf{B}_0 . \tag{2.3}$$

The second term is the origin of the single-ion anisotropy. It represents the anisotropy energy for the spin direction and can be written in the local frame, in which it takes a diagonal form, as

$$H_{cf} = D_{cf} S_z^2 + E_{cf} \left(S_x^2 - S_y^2 \right). \tag{2.4}$$

The anisotropy parameters D and E are related to the principal values of the Λ-tensor as

$$D_{cf} = -\left(\Lambda_{zz} - \frac{1}{2}\left(\Lambda_{xx} + \Lambda_{yy}\right)\right)\lambda^2,$$
$$E_{cf} = -\frac{1}{2}\left(\Lambda_{xx} - \Lambda_{yy}\right)\lambda^2. \tag{2.5}$$

It is worth mentioning that the singe-ion anisotropy Hamiltonian has no effect on the ESR in systems with $S = 1/2$, as both spin states have the same energy.

In ionic crystals with localized electrons there is another important type of interaction of the localized magnetic moment with its surroundings, i.e., the coupling to other magnetic moments. The exchange interaction

$$H_{ex} = \sum_{(i,j)} J_{ij} \mathbf{S}_i \cdot \mathbf{S}_j \tag{2.6}$$

is usually much larger than the magnetic-dipole interaction. The sum in Eq. (2.6) runs over all pairs of spins. Essentially, there are two different mechanisms leading to this type of spin coupling [5]. The first one is the so-called direct exchange, which is due to the quantum exchange term of the Coulomb interaction and favors parallel alignment of interacting spins. The second one, the kinetic exchange, can be obtained from the Hubbard model in the second order perturbation in kinetic transfer term, when electrons are nominally localized. Such type of exchange interaction supports antiferromagnetic ordering. It is generally dominant in iron-group oxides and fluorides.

When, however, the exchange interaction between two paramagnetic ions in magnetic compounds arises via anions situated somewhere near them, i.e., the superexchange interaction, it depends also on the relative position of the participating ions and not only on the distance between them.

In the same manner as the orbital moments induced by the LS coupling depend on the orientation of the spin **S** with respect to the crystal axes, the same mechanism adds to an additional anisotropic part to the isotropic exchange interaction. In the first order perturbation one can derive the antisymmetric anisotropic exchange interaction, called Dzyaloshinsky-Moriya (DM) interaction, which has the form

$$H_{DM} = \sum_{(i,j)} \mathbf{D}_{ij} \cdot \mathbf{S}_i \times \mathbf{S}_j \,. \tag{2.7}$$

Such antisymmetric form of the spin interaction was first suggested by Dzyaloshinsky to account for the phenomenon of the occurrence of weak ferromagnetism [6]. A microscopic derivation of this interaction was later given by Moriya [7] together with the symmetry restraints that the Dzyaloshinsky-Moriya vectors $\mathbf{D}_{ij}$ must obey. The symmetry arguments are based on the space group symmetry of a particular crystal. Further, the result of the second

order perturbation calculation is the symmetric anisotropic exchange. In its principal frame this interaction can be written as

$$H_{ae} = \sum_{(i,j)} d_{ij} S_i^z S_j^z + e_{ij} \left(S_i^x S_j^x - S_i^y S_j^y \right). \tag{2.8}$$

This interaction is also called the pseudo-dipolar interaction because of the formal similarity of its form with the dipolar interaction. The size of the two anisotropic terms can be estimated as $D \sim (\Delta g / g) \cdot J$ and $d \sim (\Delta g / g)^2 \cdot J$, where Δg accounts for the *g*-shift from the free electron value. These estimations are only approximate since the isotropic exchange in reality acts between the ground and the excited spin states at a given site as evident from the exact result of the perturbative calculation [4]. On the other hand, *J* stands for the exchange between the ground state of the two interacting ions. Furthermore, the estimation of the size of the DM vectors suffers a further faultiness. Namely, as already stressed, it critically depends on the local symmetry. For instance, if there is a center of inversion present in the midpoint of two coupled spins the DM interaction will be identically equal to zero.

The last interaction to be mentioned explicitly in this subsection is the magnetic dipolar coupling between isolated moments displaced by vector $\mathbf{r}_{ij}$,

$$H_{dd} = \frac{\mu_0 (g\mu_B)^2}{4\pi} \sum_{(i,j)} \left(\frac{\mathbf{S}_i \cdot \mathbf{S}_j}{r_{ij}^3} - \frac{3(\mathbf{S}_i \cdot \mathbf{r}_{ij})(\mathbf{S}_j \cdot \mathbf{r}_{ij})}{r_{ij}^5} \right). \tag{2.9}$$

It is often inferior to the magnetic exchange anisotropy, especially in low-dimensional systems with low degree of local symmetry, where also the *g*-shifts are significant. The second condition to be fulfilled for this statement to be valid is that the isotropic exchange has to be considerable.

The hyperfine interaction of the electrons with the nuclei is usually negligible in magnetically dense systems. For this reason it can be ignored in explanation of ESR absorption in magnetic solids. However, it proves to be essential in nuclear magnetic resonance (NMR), as it will be presented latter in this chapter.

2.1.2 General Theory of Magnetic Resonance Absorption

The way to a general quantum-mechanical description of the magnetic resonance was paved by Kubo and Tomita [8]. In essence this is a linear-response theory, where the response of the system of magnetic moments depends linearly on the external disturbance. The authors split the spin Hamiltonian into two parts, the term $H_0 = H_{ex} + H_Z$ and the magnetic anisotropy part $H' = H_{cf} + H_{DM} + H_{ae} + H_{dd}$, which was then treated as a perturbative correction. The Hamiltonians within the former term commute with each other, while they do not commute with the Hamiltonians included in the latter term.

In the high-temperature limit, when the energy of thermal fluctuations is much larger than the Zeeman energy splitting, an ESR absorption spectrum is determined by thermal-averaged fluctuations of the transverse magnetization operator $M^x = g\mu_B \sum_i S_i^x$, since it is given by the imaginary part of the dynamical susceptibility

$$\chi''(\omega) = \frac{\omega V}{2k_B T} \int_{-\infty}^{\infty} \left\langle M^x(t) M^x(0) \right\rangle e^{-i\omega t} \, \mathrm{d}t \,. \tag{2.10}$$

The static magnetic field direction is usually denoted as the *z* direction. The operator M^x is coupled to the linearly polarized magnetic field $B_{mw}^x = B_{mw}^0 \cos\omega_0 t$ oscillating with angular Larmor frequency of $\omega_0 = g\mu_B B_0 / \hbar$. This coupling induces transitions between energy levels split in the external magnetic field. In the X-band ($\omega_0 \approx 60\,\mathrm{GHz}$) the energy splitting accounts for approximately 0.45 K in the temperature scale. Transforming the magnetization operator into interaction representation by transformation $\widetilde{M}(t) = e^{-iH_0 t/\hbar} M(t) e^{iH_0 t/\hbar}$ and taking into account the operators relations $\left\langle \widetilde{M}^{\pm}(t) \widetilde{M}^{\pm}(0) \right\rangle = 0$ allows one to rewrite the Eq. (2.10) into the form

$$\chi''(\omega) = \frac{\omega V}{8k_B T} \int_{-\infty}^{\infty} \left(\left\langle \widetilde{M}^{+}(t) M^{-}(0) \right\rangle e^{-i(\omega-\omega_0)t} + \left\langle \widetilde{M}^{-}(t) M^{+}(0) \right\rangle e^{-i(\omega+\omega_0)t} \right) \mathrm{d}t \,, \tag{2.11}$$

which demonstrates that resonant absorption is peaked at $\pm\omega_0$. In fact, in the limiting case when there is no magnetic anisotropy ($H' = 0$), the spectrum would simply consist of two δ-functions. The time dependence of the correlation functions $\left\langle \widetilde{M}^{\pm}(t) M^{\mp}(0) \right\rangle$ due to anisotropy is thus responsible for finite linewidths, lineshifts and the shape of the absorption spectra in general. Usually the linewidth is small compared to the Larmor frequency. This further allows one to neglect the contribution to the spectrum peaked at the negative frequency.

According to the Kubo-Tomita derivation, the normalized electron-spin-resonance absorption spectrum can be expressed as the Fourier transform of the relaxation function $\varphi(t) = \left\langle \widetilde{M}^{+}(t) M^{-}(0) \right\rangle \Big/ \left\langle M^{+} M^{-} \right\rangle$,

$$I(\omega) = \int_{-\infty}^{\infty} \varphi(t) \exp[i(\omega - \omega_0)t] \mathrm{d}t \,. \tag{2.12}$$

In the case of Gaussian random processes the relaxation function is approximated by

$$\varphi(t) = \exp\left(-\int_0^t (t-\tau) \psi(\tau) \, \mathrm{d}\tau \right), \tag{2.13}$$

where the spin correlation function $\psi(\tau) = \left\langle \left[\widetilde{H}'(\tau), M^{+}(0)\right] \left[M^{-}(0), \widetilde{H}'(0)\right] \right\rangle \Big/ \hbar^2 \left\langle M^{+} M^{-} \right\rangle$ fluctuates on the time scale of the electron correlation time $\tau_c = 1/\omega_e \approx \hbar/J$ since the anisotropic Hamiltonian is modulated by the isotropic exchange interaction in the interaction picture. Here the square brackets $[A, B]$ denote the commutator of the operators *A* and *B*. This approximately yields a Gaussian function $\psi(\tau) = \psi(0) \mathrm{e}^{-\tau^2/2\tau_c^2}$.

2.1.3 Exchange Narrowing of the Absorption Spectra

Since the exchange coupling constant in principle spans a large interval of possible values, it is worth testing two limiting cases of the magnitude of the electron correlation time with respect to the parameter t describing the decay of the relaxation function. In the case when the spin correlation function decays slowly ($t \ll \tau_c$) the spin correlation function can be replaced by the second moment of the absorption spectrum

$$M_2 = \hbar^2 \psi(0) = \left\langle \left[H', M^+\right] \left[M^-, H'\right] \right\rangle \Big/ \left\langle M^+ M^- \right\rangle , \tag{2.14}$$

which yields a Gaussian-shaped relaxation function and consequently also Gaussian profile of the absorption spectrum. The peak-to-peak linewidth of the derivative ESR spectrum is in this case given by

$$\delta B_{pp}^{G} = \frac{2}{g\mu_B} \sqrt{M_2} \, . \tag{2.15}$$

In the second limiting case, usually encountered in real systems, the spins fluctuate very rapidly ($t \gg \tau_c$) due to large exchange coupling constant with respect to the observed linewidths. The integral defining the relaxation function in Eq. (2.13) can then be approximated by

$$\int_0^t (t-\tau)\psi(\tau)\,\mathrm{d}\tau = \psi(0)\left(t \int_0^{t\to\infty} \mathrm{e}^{-\tau^2/2\tau_c^2}\,\mathrm{d}\tau - \int_0^{t\to\infty} \tau\, \mathrm{e}^{-\tau^2/2\tau_c^2}\,\mathrm{d}\tau \right) \approx \sqrt{\frac{\pi}{2}}\psi(0)\tau_c t \, , \tag{2.16}$$

which sets the relaxation function as an exponentially decaying function. The Fourier transform consequently yields the Lorentzian lineshape of the absorption spectrum with the peak-to-peak linewidth

$$\delta B_{pp}^{L} = \sqrt{\frac{\pi}{6}} \frac{2}{\hbar g \mu_B} M_2 \tau_c \approx \sqrt{\frac{\pi}{6}} \frac{2}{g\mu_B} \frac{M_2}{J} \, . \tag{2.17}$$

It should be stressed that the Lorentzian shape is expected for frequencies when (ω - ω_0) $\ll \omega_e$, or equivalently for magnetic fields (B - B_0) $\ll \hbar\omega_e/g\mu_B$, while the decay is faster in the tails of the spectrum, since it is determined by the relaxation function time dependence around $t = 0$. This fact ensures finite values of the second moment, contrary to the second moment of the purely Lorentzian line that diverges. The second aspect to be highlighted is the occurrence of the exchange narrowing in the case of rapid electronic spin fluctuations. Namely, a comparison of Eq. (2.15) and Eq. (2.17) clearly demonstrates that the Lorentzian linewidth is suppressed with respect to the Gaussian one by approximately the factor of $\sqrt{M_2}/J$. Since the second moment is proportional to the square of the magnetic anisotropy present in the system and the isotropic exchange is normally much larger, the introduced factor is quite small.

A further correction of the value of the expected linewidth is possible if the electron correlation time is estimated more accurately [9]. Taking into account also the fourth moment of the absorption spectrum

$$M_4 = \left\langle \left[H - H_Z, \left[H', M^+\right]\right] \left[H - H_Z, \left[H', M^-\right]\right] \right\rangle \Big/ \left\langle M^+ M^- \right\rangle , \tag{2.18}$$

the linewidth of the Lorentzian lineshape is given by the expression

$$\delta B_{pp}^{L} = \frac{C}{g\mu_B} \left(\frac{M_2^3}{M_4} \right)^{1/2} . \tag{2.19}$$

The constant C appearing in the above equation is not strictly determined in a sense that both the second and the fourth momentum of the real Lorentzian profile diverge. For this reason it is necessary to artificially suppress the contributions from the tails. In this respect it is worth mentioning that the strong exchange coupling condition (B - B_0) $\ll \hbar\omega_e/g\mu_B$ is usually fulfilled in magnetic solids up to the degree that the deviation of the spectrum from the Lorentzian shape is not experimentally observable at all. There are different ways of solving the problem of infinite moments known in the literature [10]. The common approach is to examine the cut-off Lorentzian curve with the cut-off field at an arbitrary value. The calculated constant $C = \pi/3$ is in this case independent of the exact position of the cut-off point. However, intuitively more reasonable are the approximation of the absorption spectrum with a product function of the Lorentzian curve and the Gaussian function $\exp\left(-(B - B_0)g\mu_B/\sqrt{2}J\right)^2$ or a product function of the Lorentzian and the exponentially decaying function $\exp\left(-|B - B_0|g\mu_B/J\right)$. In the former case the calculation of the moments yields the constant $C = 2\sqrt{\pi/6}$ while the latter approximation gives $C = 2\pi/\sqrt{6}$.

The method of moments, initially derived by Van Vleck [11], requires the knowledge of infinite number of moments to completely describe the lineshape. However, computation of exact moments from a known model Hamiltonian can become a formidable labor when the order of the moment increases. For this reason it is usual to consider only the moments up to the fourth order in the ESR and up to the sixth order in the NMR analysis [12].

2.1.4 Effect of Spin Diffusion on the Absorption Spectra

In spin systems it often turns out at higher temperatures that the Gaussian approximation of the decay of the spin correlation function $\psi(\tau)$ is not justified. The diffusional contribution to the decay of this function rather dictates a slower time dependence of the form [13]

$$\psi(\tau) \propto \tau^{-d/2} , \tag{2.20}$$

where d represents the dimensionality of the spin system. In one- and two-dimensional systems such diffusional dependence leads to a diverging exponent of the relaxation function in the approximation given by Eq. (2.16). In reality, this additional mechanism affects the resonant spectra in a way that they get broader and change their shape from Lorentzian towards the Gaussian lineshape.

The effect of the spin diffusion mechanism is reflected in the relaxation function only through the secular part of the anisotropy Hamiltonian, i.e., the part commuting with the Hamiltonian H_0. On the other hand, the nonsecular terms contribute the Lorentzian component to the absorption due to their characteristic oscillating time dependence in the interaction representation originating from the Zeeman interaction. These oscillations average out the effect of diffusional decay of the spin correlation function.

In one-dimensional systems with the isotropic exchange as the dominant spin interaction the relaxation function can be analytically calculated, $\varphi(t) = \exp\left(-(\Gamma t)^{3/2}\right)$, in the case when the contribution of the secular part of anisotropy Hamiltonian to the second moment M_2^s is of the same order as the overall second moment M_2. The parameter in the exponential decay is determined as $\Gamma = \left(4M_2^s/3\hbar^2\right)^{2/3}\tau_c^{1/3}$ [13]. The Fourier transform then yields an absorption spectrum decaying somewhere in-between the Lorentzian and the Gaussian curve with an increased linewidth of the order Γ.

Another condition to be fulfilled to observe such kind of time dependence of the relaxation function in one dimension is for temperature to be considerable compared to the characteristic temperature of the spin system J/k_B. For this reason, it is the increasing of the temperature that enables the observation of the deviation of the lineshape from the Lorentzian shape and the broadening of the absorption spectra.

On the other hand, there is no universal picture about the lineshape in two-dimensional systems when the diffusional mechanism is efficient. However, the deviations of the experimentally observed ESR spectra from the Lorentzian shape have been observed and successfully ascribed to the presence of spin diffusion [14]. Although the effect can be present in two dimensions, it is usually much less significant than in one dimension [15]. The relatively fast decay of the spin correlation function $\psi_{3D}(\tau) \propto \tau^{-3/2}$ in thee dimensions suppresses the divergence of the exponent in Eq. (2.13) completely so that the lineshape remains Lorentzian.

However, the diffusional decay of the electronic spin correlation functions is often not detectable by ESR experiments even in low-dimensional magnetic systems. Although these systems may be characterized as having a reduced dimensionality due to the dominant exchange along a chain or within a plane, also the interchain or interlayer exchange coupling can still be large compared to the magnetic anisotropy terms regulating the linewidth of the absorption spectra. In such cases the decay of a nonequilibrium spin polarization is effectively happening in three dimensions.

2.1.5 Temperature Dependence of the Linewidth

An exact calculation of the second and the fourth moment of the ESR absorption spectra determining the linewidth through Eq. (2.19) is possible only in the limit of infinite temperature. In this case the static spin correlations of the products of spin operators acting on different lattice sites, can be neglected. In general one is dealing with the assignment of computing four-spin correlation functions since the magnetic anisotropy Hamiltonian is quadratic in spin operators. When the spin operators acting on *N* different crystal sites are treated as completely uncorrelated and the density matrix is approximated by unity, the following equations are found useful when calculating the moments

$$\begin{aligned} &\mathrm{Tr}\left(S_i^{\alpha} S_j^{\beta}\right) = \delta_{ij}\delta_{\alpha\beta}\frac{1}{3}S(S+1)(2S+1)^N, \\ &\mathrm{Tr}\left(S_i^{\alpha} S_i^{\beta} S_j^{\mu} S_j^{\nu}\right) = \frac{\delta_{\alpha\beta}\delta_{\mu\nu}}{(2S+1)^N}\mathrm{Tr}\left(\left(S_i^{\alpha}\right)^2\right)\mathrm{Tr}\left(\left(S_j^{\mu}\right)^2\right). \end{aligned} \tag{2.21}$$

For instance, if we include the dipole interaction, the antisymmetric Dzyaloshinsky-Moriya interaction and the symmetric anisotropic exchange (Eq. (2.9-2.11)) into the calculation of the second moment, the above relations yield [10]

$$\begin{aligned} M_2^{\infty} = \frac{S(S+1)}{N}\sum_{(i,j)}\Bigg[&\frac{1}{3}\left(\left(D_{ij}^{x}\right)^2 + \left(D_{ij}^{y}\right)^2 + 2\left(D_{ij}^{z}\right)^2 + 2\left(d_{ij}+e_{ij}\right)^2 + 4B_{ij}\left(d_{ij}+e_{ij}\right)\right) + \\ &+\frac{9}{2}\left(\frac{\mu_0}{4\pi}\right)^2(g\mu_B)^4\left(1+\cos^2\theta_{ij}\right)/r_{ij}^6\Bigg]. \end{aligned} \tag{2.22}$$

The only mixed terms appearing in this expression couple both symmetric interactions. The mixing occurs only with the truncated (secular) part of the dipolar interaction commuting with the Hamiltonian H_0. This produces parameters $B_{ij} = 3\mu_0(g\mu_B)^2\left(1-3\cos^2\theta_{ij}\right)/8\pi r_{ij}^3$, where θ_{ij} stands for the angle between the external magnetic field $\mathbf{B}_0$ and the $\mathbf{r}_{ij}$ vector. Contrary, the last term represents the contribution of the total magnetic dipole interaction [16]. Namely, in the instance of strong isotropic exchange it is not sufficient to include only the truncated part as Van Vleck did when introducing the method of moments for describing the absorption spectra [11]. The reason for this is that the satellite lines, originating from the nonsecular part of the dipolar coupling, merge with the central line.

The calculation of the general expression of the fourth moment is much more involved, which is why it will not be explicitly given at this point. Although tedious, the calculation for special cases when one of the magnetic anisotropy terms dominates is possible and will be presented at a later stage when analyzing the ESR results.

At finite temperatures the assumption of completely uncorrelated spin operators in not strictly valid any more. The static spin correlations that set-in at temperatures of the order of the

isotropic exchange require the relations given by Eq. (2.21) to be corrected. An indicator about the influence of this short-range order effect is simply the deviation of the static magnetic susceptibility from the Curie dependence typical for isolated magnetic moments. The impact of the static spin correlations is reflected in the thermal average of products of spin operators through normalized static correlation functions $C_{ij}(T)$ [17], which are defined by the equation

$$\mathrm{Tr}\left(S_i^{\alpha} S_j^{\beta}\right) = \frac{1}{3} S(S+1)(2S+1)^N C_{ij}(T)\delta_{\alpha\beta}. \tag{2.23}$$

These correlation functions depend, apart from the temperature, only on the distance between the two spins if we include into the density matrix only the isotropic exchange, which is supposed to be the largest part of the spin Hamiltonian. It is also worth mentioning that the trace of any odd number of spin operators remains equal to zero at temperatures large compared to the Zeeman splitting [18], $\mathrm{Tr}\left(S_i^{\alpha}\right) = \mathrm{Tr}\left(S_i^{\alpha} S_j^{\beta} S_k^{\gamma}\right) = 0$. On the other hand, the actual four-spin correlation functions can be decoupled according to the following decoupling scheme [17]

$$\begin{aligned}\mathrm{Tr}\left(S_i^{\alpha} S_j^{\beta} S_m^{\mu} S_n^{\nu}\right) = &\left(\frac{1}{3} S(S+1)\right)^2 (2S+1)^N \\ &\left(C_{im}(T)C_{jn}(T)\delta_{\alpha\mu}\delta_{\beta\nu} + C_{in}(T)C_{jm}(T)\delta_{\alpha\nu}\delta_{\beta\mu}\right).\end{aligned} \tag{2.24}$$

It turns out that the contributions to the second moment from the symmetric and the antisymmetric part of the anisotropy Hamiltonian remain decoupled even at finite temperatures, so that the second moment can be written as [18]

$$M_2(T) = M_2^s(T) + M_2^a(T), \tag{2.25}$$

where the temperature dependence arises from the temperature evolution of the spin correlation functions. In general these functions approach zero when increasing the temperature for $i \neq j$. At high temperatures the most important are the corrections due to the nearest neighbors while at lower temperatures also the correlations to more distant neighbors have to be taken into account. As the analytical solution of the short-range correlations effect is not possible, this approach is usually limited to temperatures $k_B T \geq J$ [17]. The calculation of the fourth moment taking into account also spin correlations is extremely complicated task, which is why this parameter is usually considered to be temperature independent.

2.1.6 Magnetic Resonance in the Vicinity of Critical Points

In principle, there are three different temperature intervals of interest when performing magnetic resonance absorption experiments on magnetic solids, which undergo a transition to a magnetically ordered state below some critical temperature T_c. Namely, the high-temperature interval ($T \gg T_c$) where only short-range correlations potentially play a role and the spin

diffusion mechanism may be relevant, the temperatures just above the critical temperature ($T \geq T_c$), where precursor effects of long-range ordering are present, and temperatures below T_c, for which appreciable internal magnetic field due to magnetic ordering are crucial for understanding the resonant spectra.

In the critical region there is an intrinsic difference between ferromagnetic and antiferromagnetic materials. That is, in ferromagnets the contribution of the spin correlations at wave-vector $\mathbf{q} = 0$ gets critically enhanced while these correlations are diminished in antiferromagnets in the light of staggered (alternating) correlations at wave-vector $\mathbf{q}_0$ at the antiferromagnetic zone center, which tend to dominate near antiferromagnetic transitions. If looked at in the light of a snapshot picture, increasing clusters of ordered spins begin appearing when approaching the transition point of a system. Also the mean-squared amplitudes of the staggered Fourier component of the magnetic-moment distribution increases, which can be properly accounted for by the wave-length-dependent static susceptibility $\chi(\mathbf{q}, t = 0)$. On the other hand, also the dynamical aspect of the critical fluctuations is important. Namely, when approaching the transition temperature the average lifetime of a cluster of ordered spins will be increased. This effect, called the critical slowing-down of spin fluctuations, is expressed by the decrease of the relaxation rate $\Gamma(\mathbf{q}, T)$ of the spin correlation functions and, in effect, adds to the increased fluctuation amplitudes. Both the static and the dynamic effect contribute to a significant line broadening of the ESR absorption spectra in the vicinity of the phase-transition temperature. Not to get too philosophical at this point, some expressions for the development of the magnetic resonance parameters in the critical region will be presented in the next chapters, when appropriate.

2.2 Nuclear Magnetic Resonance

The techniques of nuclear magnetic resonance (NMR) can be also successfully applied to the study of the electronic properties of solids. The virtue of this experimental method is that it can provide us with a probe that is only weakly coupled to the electronic system, allowing for precise determination of the local magnetic fields present in the material under investigation. Thus it often gives additional information to that obtained by electron spin resonance, where electrons directly serve as experimental probes. Because of the effectively weak coupling, which is usually much weaker than the leading Zeeman term, the NMR results are also easier to interpret. Nuclear magnetic resonance is sensitive to the time-averaged local magnetic fields through the position of the absorption lines as well as to certain spectral components of fluctuating fields. The fluctuations affect the linewidth and the relaxation times of nuclei.

2.2.1 Origins of Internal Fields and Frequency Shifts of NMR Spectra

In the light of the size of different interactions determining nuclear magnetic resonance (NMR) spectra of a certain kind of nuclei in a particular material, there is a considerable difference between nonmagnetic [1, 19] and magnetic materials, which can also exhibit ferromagnetic [20] or antiferromagnetic order [21]. Namely, the relatively small corrections to the energy of a nucleus in the external magnetic field can be for nonmagnetic solids associated with the dipolar field of other nuclei and atomic diamagnetism reflected in chemical shifts. On the other hand, the electronic dipolar fields are several orders of magnitude larger than the corresponding nuclear fields, and the atomic hyperfine fields of magnetic ions possibly 10^6 times larger.

As the rate of the nuclear spin-spin relaxation and also the NMR linewidth scale with the size of the local field, $1/T_2 \approx \gamma B_{loc}$, where γ is the gyromagnetic ratio, the NMR spectra at first sight seem to be unobservable in magnetic solids. However, electronic fluctuations due to the isotropic exchange between magnetic moments play a crucial role in this respect. Namely, if during the Larmor period $T_L \approx \left(\gamma B_{eff}\right)^{-1}$ (B_{eff} is an effective field, which is the sum of the external magnetic field and the static component of the local field arising whether from dipolar or hyperfine origin) the local field fluctuates rapidly, what a particular nucleus effectively sees is the time-averaged local field. The fluctuating transverse components of the local field oscillating at the Larmor frequency $\nu_L = \left(2\pi T_L\right)^{-1}$ contribute to the spin-spin and the spin-lattice relaxation (T_1-relaxation). In addition, the spin-spin relaxation is effected by those longitudinal components of the local field fluctuating at very low frequencies ($\nu \ll \nu_L$), since these produce a distribution in T_L.

A typical frequency dependence of the amplitude of the local field for both the dipolar and the hyperfine interaction at temperatures appreciably above the ordering temperature has a step-like dependence with a step of a temperature-rounded shape annihilating the local field, which occurs at the value of the exchange frequency [21]. The rapid reorientation of electronic spins caused by generally very strong isotropic exchange makes the amplitude of the local field spectral components $\left|B_{loc}(\omega = 0)\right| \approx \left|B_{loc}(\omega = \omega_L)\right|$ severely attenuated with respect to the value one would expect in the static picture. The necessary condition for NMR to be observable in magnetic materials is for exchange energy to be sufficiently large to satisfy the condition

$$\frac{1}{T_{1,2}^{\min}} > \frac{\left(\gamma B_{loc}(\omega = 0)\right)^2}{\omega_e}, \tag{2.26}$$

where $T_{1,2}^{\min}$ is the smallest value of the relaxation times still experimentally observable. The above equation again clearly shows the effect of the exchange narrowing mechanism. It is also worth mentioning that the amplitude of the local field varies with the degree of order in electronic system and is thus quite temperature dependent.

The internal fields at the nucleus produced by the electronic spin moments can be classified into three broad classes depending on the nature of the atoms under investigation in the magnetic solid. In the first class of nuclei of nonmagnetic atoms, the main anisotropic addition to the Zeeman Hamiltonian $H_Z = -\gamma\hbar\mathbf{I}_i \cdot \mathbf{B}_0$ for the nucleus at site *i* originates from the dipole interaction between the nuclear spin $\mathbf{I}_i$ and the average electronic spin moments of surrounding paramagnetic ions $\langle \mathbf{S}_j \rangle$. The static dipolar field $\langle \mathbf{B}_d \rangle$ can be obtained from the dipolar Hamiltonian

$$H_i^d = -\gamma\hbar\mathbf{I}_i \cdot \mathbf{B}_d = -\gamma\hbar\mathbf{I}_i \cdot \frac{\mu_0 g\mu_B}{4\pi} \sum_j r_{i,j}^{-3} \left(\mathbf{S}_j - 3\mathbf{r}_{i,j} \left(\mathbf{S}_j \cdot \mathbf{r}_{i,j} \right) / r_{i,j}^2 \right), \tag{2.27}$$

when the time-averaged value of the electronic spin is taken into account. In the Eq. (2.27) the summation extends over all magnetic sites *j*, which are at the distance $r_{i,j}$ from the nucleus. The static field is proportional to the time-average of electronic magnetic moments and thus to the uniform magnetization of the system. In the paramagnetic phase this interaction is nonzero only in the case of applied external magnetic field $\mathbf{B}_0$, which partially polarizes the electronic system. However, the dipolar magnetic field $\mathbf{B}_d$ and the external field need not be parallel since the electronic *g*-tensor is in general anisotropic. This is even more pronounced if magnetic ordering sets in.

In the second group are nuclei of magnetic ions. These nuclei of the paramagnetic atoms are subjected to the intense hyperfine fields, which arise from the interaction of the nucleus with electrons within the same paramagnetic ions. In addition to the dipolar Hamiltonian (Eq. (2.27)), anisotropy terms of the form

$$H_i^{hf} = \mathbf{I}_i \cdot \underline{\mathbf{A}}_i \cdot \mathbf{S}_i \tag{2.28}$$

determine the properties of NMR absorption of the nucleus at site *i*. The static hyperfine magnetic field $\mathbf{B}_{hf} = -\underline{\mathbf{A}}_i \cdot \langle \mathbf{S}_i \rangle / \gamma\hbar$ is usually so intense to produce significant lineshifts or even makes the resonant absorption experimentally unobservable [21]. In the one-electron theory the hyperfine interaction can be expressed in the following form [22]

$$H_i^{hf} = \frac{\mu_0 \gamma\hbar g\mu_B}{4\pi} \left(\frac{8\pi}{3} |\psi(0)|^2 \mathbf{I}_i \cdot \mathbf{S}_i - \frac{\mathbf{I}_i \cdot (\mathbf{S}_i - \mathbf{L}_i)}{r^3} + \frac{3(\mathbf{I}_i \cdot \mathbf{r})(\mathbf{S}_i \cdot \mathbf{r})}{r^5} \right). \tag{2.29}$$

The first term represents the Fermi contact interaction being nonzero only for *s* electrons, which have a nonzero probability of being found exactly at the point of the nucleus. In such case the last two terms are zero due to the spherical distribution of the electron density. These two terms are the orbital and the spin dipole energy terms. For several electrons outside the closed shell the operators in Eq. (2.29) are taken as the sum operators for the entire ion. However, this conventional one-electron theory has its shortcomings, as it cannot predict hyperfine fields for ions with net spin but no unpaired *s* electrons. In fact, if an ion is in the *S* orbital state and has a

net spin the spin and the orbital dipole contributions will be zero, however, the ion can still have appreciable local fields arising from the Fermi contact term. In Mn^{2+} this hyperfine field can be of the order of 70 T [22]. The many-electron contribution to the hyperfine coupling includes the polarization effect involving core electrons. Namely, the incompletely filled shell with $L \neq 0$ distorts the closed shell and, in turn, causes an interaction with the nuclear magnetic moment [22]. The calculation of the hyperfine tensor is thus far from being trivial, which is why it is usually taken phenomenologically as an anisotropic tensor and is not calculated from the first principles.

The last class joins nuclei of partially magnetic ions. For such materials there is an appreciable overlap between the wave functions of electrons of nominally nonmagnetic ions and those wave functions of electrons from paramagnetic ions. As a consequence a space redistribution of electrons at the nonmagnetic sites appears. This can be explained in the light of the amount of covalency present in bonds as follows. To the extent that an orbital of the paramagnetic ion is mixed with an orbital of the diamagnetic ion in the bonding function, it is reduced in the antibonding function. This means that, to the degree that bonding occurs, the unpaired electron in the antibonding orbital has the character of the initial orbital of the diamagnetic ion. Consequently, an imbalance at nonmagnetic ion characteristic of the symmetry of its initial orbital occurs in the sense that the unpaired electron in the antibonding orbital, with spin parallel to that of the paramagnetic ion, can produce its characteristic hyperfine field. In this way even at ions with paired *s* electrons there can be significant hyperfine coupling of the Fermi contact type [23]. The effective hyperfine interaction can be written for partially magnetic ions as a sum of transferred hyperfine contributions

$$\widetilde{H}_i^{hf} = \mathbf{I}_i \cdot \sum_j \underline{\widetilde{\mathbf{A}}}_{i,j} \cdot \mathbf{S}_j \ , \tag{2.30}$$

where the sum runs over all the neighboring paramagnetic sites *j* that effect the spatial distribution of electrons on the diamagnetic site *i*. From the size and the shape of the transferred hyperfine tensor $\underline{\widetilde{\mathbf{A}}}_{i,j}$ one can in principle deduce the orbital character and the extent of collaboration of the electrons from the diamagnetic species with the paramagnetic electrons in formation of the covalent bonding.

As demonstrated in this section, the line position reveals information on the time-averaged value of the local fields. The resonance frequency strictly follows the temperature evolution of the averaged spin moment when the coupling constants (dipolar and hyperfine) are assumed to be temperature independent.

Before turning to the theoretical discussion of the line-broadening due to fluctuating local fields, another major source of anisotropy in the case when $I \geq 1$ has to be introduced, i.e., the nuclear quadrupole interaction. This coupling arises from the interaction between nuclear

quadrupole moment Q with the electric field gradients (EFG) V_{ij} existing at the nucleus and is described by the Hamiltonian [19]

$$H_Q = \frac{e^2 qQ}{4I(2I-1)}\left(3I_Z^2 - I(I+1) + \frac{1}{2}\eta\left(I_+^2 + I_-^2\right)\right). \tag{2.31}$$

The above Hamiltonian is written in the principal frame of the EFG tensor with the principal values by convention taken as $eq = |V_{ZZ}| \geq |V_{YY}| \geq |V_{XX}|$, while the asymmetry parameter is defined as $\eta = (V_{XX} - V_{YY})/V_{ZZ}$. In the presence of high magnetic fields applied to the nuclear system the quadrupole Hamiltonian can be treated as a perturbation to the Zeeman coupling. In this case several resonance frequencies appear. The first order frequency shifts for the transition between nuclear states are then given by

$$\nu_m^{(1)} = \frac{E_{m-1} - E_m}{h} = -\nu_Q\left(m - \frac{1}{2}\right)\left(3\cos^2\theta - 1 + \eta\left(1 - \cos^2\theta\right)\cos 2\phi\right), \tag{2.32}$$

with $\nu_Q = 3e^2 qQ/4I(2I-1)h$ and θ, ϕ as the polar and the azimuthal angles of the magnetic field direction in the principal frame of the EFG tensor. For half-integer spins the central transition $-1/2 \leftrightarrow 1/2$ is a delta-function not shifted by the quadrupole interaction from the Larmor frequency ν_L while the satellite lines appear as symmetrically displaced delta-functions with respect to the central line. In the second-order perturbation also the central transition gets shifted, while the satellites remain symmetric. The quadrupole frequency shift of the central transition is a minor effect compared with the shifts of the satellites in strong magnetic fields as it is of the order of ν_Q^2/ν_L. The angular dependence of this transition is explicitly given by [24]

$$\begin{aligned}\nu_{1/2}^{(2)} = -\frac{16}{3}\frac{\nu_Q^2}{\nu_L}\Bigg[&\left(-\frac{27}{8} + \frac{9}{4}\eta\cos 2\phi - \frac{3}{2}(\eta\cos 2\phi)^2\right)\cos^4\theta + \\ &+\left(\frac{30}{8} - \frac{1}{2}\eta^2 - 2\eta\cos 2\phi + \frac{3}{4}(\eta\cos 2\phi)^2\right)\cos^2\theta + \\ &+\left(-\frac{3}{8} + \frac{1}{3}\eta^2 - \frac{1}{4}\eta\cos 2\phi - \frac{3}{8}(\eta\cos 2\phi)^2\right)\Bigg].\end{aligned} \tag{2.33}$$

When working with powder samples a proper distribution of the Euler angles has to be taken into account. Additionally, also the probability of a certain nuclear spin transition has to be considered. This probability is given by the square of the matrix element responsible for the transition between two states,

$$W_{m-1,m} \propto \left|\langle m-1|I^+|m\rangle\right|^2 = I(I+1) - (m-1)m. \tag{2.34}$$

For the abovementioned reason the heights of the satellite lines are suppressed with respect to the central line or can even be completely wiped out, especially if a distribution of the electric field gradient is present.

2.2.2 Relaxation and Linewidths

As noted earlier, the observability of the nuclear magnetic resonance in magnetic material depends on the magnitude of certain spectral components of the fluctuating local fields or equivalently the fluctuating electron spin correlation functions. The amplitude of the fluctuations varies with the degree of order in the electronic system and is, therefore, quite temperature dependent. The general expressions for line broadening and spin-lattice relaxation in the case of large exchange coupling were derived by Moriya [25] using the Kubo-Tomita general theory of magnetic resonance. In principle, the general theory presented in sections 2.1.2 and 2.1.3 for the electron spin resonance applies also to the case of the nuclear magnetic resonance if the electron magnetization operators are replaced with the nuclear magnetization operators. However, it is somewhat more edifying to speak in the language of local fields arising from the interaction of the nucleus with the surrounding electrons.

The fluctuations in the local field are defined as $\mathbf{b}(t) = \mathbf{B}_{loc}(t) - \langle \mathbf{B}_{loc} \rangle$. As already explained, the time-averaged field contributes to the shift of the resonance frequency while the fluctuations, on the other hand, are themselves responsible for finite homogeneous linewidth. Similar as it was already presented for the case of electron spin resonance (Eq. 2.12), a normalized absorption line in NMR experiments can be expressed in terms of the relaxation function of transverse nuclear magnetization $M(t)$, as

$$I_n(\omega) = \int_{-\infty}^{\infty} \varphi_n(t) \exp[i(\omega - \omega_0)t] \mathrm{d}t \,, \tag{2.35}$$

where the angular Larmor frequency is given by $\omega_0 = \gamma \left| \mathbf{B}_0 + \langle \mathbf{B}_{loc} \rangle \right|$. The relaxation function is related to the correlation function [26]

$$\psi_n(\tau) = \gamma^2 \left(\langle \{ b_z(\tau) b_z(0) \} \rangle + \frac{1}{2} \mathrm{e}^{i\omega_0 \tau} \langle \{ b_+(\tau) b_-(0) \} \rangle \right), \tag{2.36}$$

through the familiar expression given by Eq. (2.13). By agreement the index z again denotes the direction of the external magnetic field and $\{AB\}$ stands for the symmetrized product of two operators. Once again, as with ESR, if the electron correlation time is small compared to the spin-spin relaxation time the exponent of the relaxation function will be a linear function of time. Lorentzian lineshape is then expected. The expression for the spin-spin relaxation time, which is related to the full width at half height (FWHH) of the absorption spectrum in the frequency units as $\Delta\nu = 1/\pi T_2$ in the picture of the homogeneous broadening, can be derived to have the following appearance

$$\frac{1}{T_2} = \gamma^2 \int_0^{\infty} \left(\langle \{ b_z(\tau) b_z(0) \} \rangle + \frac{1}{2} \langle \{ b_x(\tau) b_x(0) + b_y(\tau) b_y(0) \} \rangle \cos \omega_0 \tau \right) \mathrm{d}\tau \,. \tag{2.37}$$

Introducing the spectral density of the fluctuating local field

$$\mathcal{J}_{\alpha,\beta}(\omega) = 1/\pi \int_{-\infty}^{\infty} \left\langle \left\{ b_\alpha(\tau) b_\beta(0) \right\} \right\rangle \cos \omega\tau \, \mathrm{d}\tau \,, \tag{2.38}$$

the Eq. (2.37) can be rewritten as

$$\frac{1}{T_2} = \frac{\pi\gamma^2}{2} \left(\mathcal{J}_{zz}(0) + \frac{1}{2} \mathcal{J}_{yy}(\omega_0) + \frac{1}{2} \mathcal{J}_{xx}(\omega_0) \right). \tag{2.39}$$

The first term represents contributions arising from the secular part of the perturbing Hamiltonian defining the local field while the transverse correlation functions represent the nonsecular part. The spin-spin relaxation thus probes dynamic as well as static components of the local magnetic fields. The spin-lattice relaxation, on the other hand, in governed solely by the transverse fluctuations

$$\frac{1}{T_1} = \gamma^2 \int_0^{\infty} \left\langle \left\{ b_x(\tau) b_x(0) + b_y(\tau) b_y(0) \right\} \right\rangle \cos \omega_0 \tau \, \mathrm{d}\tau = \frac{\pi\gamma^2}{2} \left(\mathcal{J}_{yy}(\omega_0) + \mathcal{J}_{xx}(\omega_0) \right). \tag{2.40}$$

Consequently, it is affected only by the fluctuations of the local magnetic fields at the Larmor frequency. Since electron correlations normally persist for much shorter times than the nuclear Larmor period, the nuclear relaxation times are simply determined by the spectral density of fluctuating field at zero frequency.

The magnetic field fluctuations are of course correlated to electronic spin fluctuations through Eqs. (2.27-2.30). To be precise, if we write a coupling term between a nuclear spin $\mathbf{I}_i$ at site i and the ionic spin $\mathbf{S}_j$ at site j in the general form (accounting for the hyperfine as well as the dipolar coupling)

$$H_{hf}^{i} = \mathbf{I}_i \cdot \underline{\mathbf{A}}_{i,j} \cdot \mathbf{S}_j \tag{2.41}$$

and identify electron spin fluctuations from the equation spin polarization as $\delta\mathbf{S} = \mathbf{S} - \langle \mathbf{S} \rangle$, the expressions for the nuclear relaxation times governed by the coupling to the system of paramagnetic electrons can be transformed into the following general form

$$\begin{aligned} \frac{1}{T_1} &= \frac{1}{2\hbar^2} \int_{-\infty}^{\infty} \sum_{j,k} \sum_{\mu,\nu} \left(A_{i,j}^{x,\mu} + i A_{i,j}^{y,\mu} \right) \left(A_{i,k}^{x,\nu} - i A_{i,k}^{y,\nu} \right) \left\langle \left\{ \delta S_j^{\mu}(\tau) \delta S_k^{\nu}(0) \right\} \right\rangle \cos \omega_0 \tau \, \mathrm{d}\tau, \\ \frac{1}{T_2} &= \frac{1}{2\hbar^2} \int_{-\infty}^{\infty} \sum_{j,k} \sum_{\mu,\nu} \left(\left(A_{i,j}^{z,\mu} A_{i,k}^{z,\mu} \right) + \frac{1}{2} \mathrm{e}^{i\omega_0 t} \left(A_{i,j}^{x,\mu} + i A_{i,j}^{y,\mu} \right) \left(A_{i,k}^{x,\nu} - i A_{i,k}^{y,\nu} \right) \left\langle \left\{ \delta S_j^{\mu}(\tau) \delta S_k^{\nu}(0) \right\} \right\rangle \right) \mathrm{d}\tau. \end{aligned} \tag{2.42}$$

The temperature dependence of the NMR relaxation times in magnetic solids can be in principle obtained by calculating the time dependence of the electron spin correlation functions. In this respect the NMR analysis demands less theoretical efforts than ESR. This is due to the fact that nuclear resonance strictly samples local properties in magnetic solids. That is, a nucleus at a

particular site resonates independently of other nuclei, which is due to the linearity of the nuclear perturbing Hamiltonian in the electronic spin operators. Its resonance spectrum is determined by electronic fluctuations and correlations sensed at a particular wave-vector [26]. It is the same argument that explains why only the knowledge of two-spin correlation functions is needed in NMR, while ESR in its essence requires the information about the four-spin correlation functions. In the above-presented way also the nuclei can serve as an experimental probe for detecting the temperature evolution of the spin correlations in the spin system of the paramagnetic electrons.

At the end of this chapter, few words on the effect of the nonmagnetic mechanism (i.e., the quadrupole coupling) on the nuclear relaxation are in place. The influence of this interaction on the shift of the resonance line has already been highlighted from the static point of view. However, one has to include dynamical aspect for this coupling to be able to induce relaxation. In liquids such feature is provided by rapid reorientations of molecules, which produces fluctuations of local electric field gradients. On the other hand, for the quadrupole coupling to be effective in inducing relaxation in solids phonons have to be taken into account. Such lattice vibrations modulate EFG tensors. It is well established that the spin-lattice relaxation times, for instance, should scale linearly with the temperature if direct phonon processes are dominant, which account for the single phonon creation of annihilation processes. On the other hand, if the phonons are inelasticaly scattered on the spin system as in the case of the Raman processes, the increase of the relaxation rate is much steeper (T^2 to T^7 depending on the temperature with respect to the Debye temperature) [19].

Bibliography

[1] C. P. Slichter, *Principles of Magnetic Resonance, 3rd Enlarged and Updated Edition* (Springer-Verlag, Berlin, 1990).

[2] G. E. Pake. *Paramagnetic Resonance* (W. A. Benjamin, New York, 1962), p. 48.

[3] W. Low. Paramagnetic Resonance in Solids, in *Solid State Physics, Supplement 2*, edited by F. Seitz, D. Turnbull (Academic Press, New York, 1960), p. 8.

[4] K. Yosida, *Theory of Magnetism* (Springer-Verlag, Berlin, 1996).

[5] P. W. Anderson. New approach to the theory of superexchange interaction, *Phys. Rev.* **115**, 2 (1959).

[6] I. Dzyaloshinky. A thermodynamic theory of "weak" ferromagnetism of antiferromagnetisc, *J. Phys. Chem. Solids* **4**, 241 (1958).

[7] T. Moriya. Anisotropic superexchange interaction and weak ferromagnetism, *Phys. Rev.* **120**, 91 (1960).

[8] R. Kubo, K. Tomita. A general theory of magnetic resonance absorption, *J. Phys. Soc. Jpn*. **9**, 888 (1954).

[9] Y. Tazuke, K. Nagata. EPR linewidths of a one-dimensional Heisenberg antiferromagnet $CsMnCl_3 2 \cdot H_2 0$, *J. Phys. Soc. Jpn*. **38**, 1003 (1975).

[10] T. G. Castner, M. S. Seehra. Antisymmetric exchange and exchange-narrowed electron-paramagnetic-resonance linewidths, *Phys. Rev. B* **4**, 38 (1971).

[11] J. H. Van Vleck. The dipolar broadening of magnetic resonance lines in crystals, *Phys. Rev*. **74**, 1168 (1948).

[12] J. E. Gulley, D. Hone, D. J. Scalapino, B. G. Silbernagel. Exchange narrowing: Magnetic resonance lineshapes and spin correlations in paramagnetic $KMnF_3$, $RbMnF_3$, and MnF_2, *Phys. Rev. B* **1**, 1020 (1970).

[13] P. M. Richard. Magnetic resonance in one- and two-dimensional systems, in *Local Properties of Low-Dimensional Antiferromagnets*, edited by K. A. Müller (Nord Holland Publishing Company, Amsterdam, 1976), p. 539.

[14] P. M. Richards, M. B. Salamon. Exchange narrowing of electron spin resonance in a two-dimensional system, *Phys. Rev. B* **9**, 32 (1974).

[15] J.-C. Bissey, N. Filloleau, N.-B. Chanh, R. Berger, S. Flandrois. Exchange interaction as studied by EPR in a two-dimensional molecular composite $[NH_3\text{-}(CH_2)_4\text{-}NH_3]MnCl_4$, *Solis State Comm.* **106**, 385 (1998); and references therein.

[16] B. R. Cooper, F. Keffer. Paramagnetic resonance width in iron and nickel, *Phys. Rev.* **125**, 896 (1962).

[17] Z. G. Soos, T. T. P. Cheung, K. T. McGregor. Exchange narrowing in correlated spin systems: local field contributions, *Chem. Phys. Lett*. **46**, 600 (1977).

[18] Z. G. Soos, K. T. McGregor, T. T. Cheung, A. J. Silverstein. Antisymmetric and anisotropic exchange in ferromagnetic copper(ii) layers, *Phys. Rev. B* **16**, 3036 (1977).

[19] A. Abragam. *Principles of Nuclear Magnetism* (Oxford University Press, Oxford, 1961).

[20] A. M. Portis, R. H. Lindquist. Nuclear Resonance in Ferromagnetic Materials, in *Magnetism, Vol. II, Part A*, edited by G. T. Rado, H. Suhl (Academic Press, New York, 1965), p. 357.

[21] V. Jaccarino. Nuclear Resonance in Atiferromagnets, in *Magnetism, Vol. II, Part A*, edited by G. T. Rado, H. Suhl (Academic Press, New York, 1965), p. 307.

[22] A. J. Freeman, R. E. Watson. Hyperfine Interaction in Magnetic Materials, in *Magnetism, Vol. II, Part A*, edited by G. T. Rado, H. Suhl (Academic Press, New York, 1965), p. 167.

[23] R. G. Shulman, V. Jaccarino. Nuclear magnetic resonance in paramagnetic MnF_2, *Phys. Rev*. **108**, 1219 (1957).

[24] P. P. Man. Quadrupole coupling in nuclear magnetic resonance, general, in *Encyclopedia of Analytical Chemistry*, edited by R. A. Meyers (John Wiley & Sons, Chichester, 2000), p. 12224.

[25] T. Moriya. Nuclear magnetic resonance in antiferromagnets, *Prog. Theor. Phys*. **16**, 23 (1956).

[26] P. Heller. NMR and Neutron Scattering Studies Near Phase Transitions in Uniaxial Antiferromagnets, in *Local Properties of Low-Dimensional Antiferromagnets*, edited by K. A. Müller (Nord Holland Publishing Company, Amsterdam, 1976), p. 445.

3 SPIN CORRELATIONS AND MAGNETIC ANISOTROPY IN 1D HALDANE SYSTEM $PbNi_{2-x}(Mg,Co)_xV_2O_8$

3.1 Crystal Structure and Magnetic Properties

The first synthesis of the $PbNi_2V_2O_8$ compound was reported in the late 1990s by Uchiyama *et al*. [1]. The system is isomorphous to $SrNi_2V_2O_8$ material, whose structure is known for almost two decades [2]. These compounds possess a tetragonal unit cell (space group $I4_1cd$) with lattice constants given for the Pb-based material as a = 12.16 Å and c = 8.32 Å. The corresponding unit cell is presented in Fig. 3.1. The only ions possessing magnetic moment are the Ni^{2+} ions with the spin quantum number S = 1. In a general case applicable to all of the iron-group metals surrounded by oxygen ligands, the orbital moment of Ni^{2+} ions is expected to be effectively quenched by a strong crystal field. Thus the magnetic structure of $PbNi_2V_2O_8$ material consist of S = 1 effective moments forming peculiar helical arrangement. The spiral-shaped chains of edge-shared NiO_6 octahedra extend parallel to the crystal c axis as shown in Fig 3.1b. The nearest neighbor exchange links two Ni^{2+} ions through two oxygen bridges (see Fig. 3.4). On the other hand, the interchain magnetic exchange coupling is suggested to be provided by the VO_4 tetrahedra. Pb^{2+} ions are located between Ni^{2+} chains and are not expected to play any major role in the magnetism of this compound. From the structural point of view the system is thus expected to be quasi-one-dimensional.

Indeed, the magnetic properties prove that $PbNi_2V_2O_8$ compound can be in first approximation considered as a one-dimensional spin system. All the Ni^{2+} sites and the nearest-neighbor (intrachain) bonds are crystallographically equivalent. The corresponding dominant isotropic exchange is antiferromagnetic. Its size $J = k_B \cdot 95\,\mathrm{K}$, which is considerable, was evaluated from the temperature dependence of the susceptibility curve at high temperature [1], i.e., above the temperature of 120 K where the susceptibility curve exhibits a maximum. Similar value was obtained also from the inelastic neutron scattering (INS) profiles [1, 3] which, however, yield slightly higher value of the nearest-neighbor exchange, $J = k_B \cdot 110\,\mathrm{K}$, if only the nearest-neighbor interaction is considered. The mismatch was argued to be due to intrinsically different information obtained from the two experimental techniques as cold neutrons investigate only low-energy excitations of the system. Employing thermal-neutron diffraction [4] has improved the disagreement and also showed that both the next-nearest neighbor intrachain exchange ($J' = k_B \cdot 5\,\mathrm{K}$) as well as the interchain coupling ($J_\perp = -k_B \cdot 2\,\mathrm{K}$) are considerable. It should be noted that the latter one is of a ferromagnetic character.

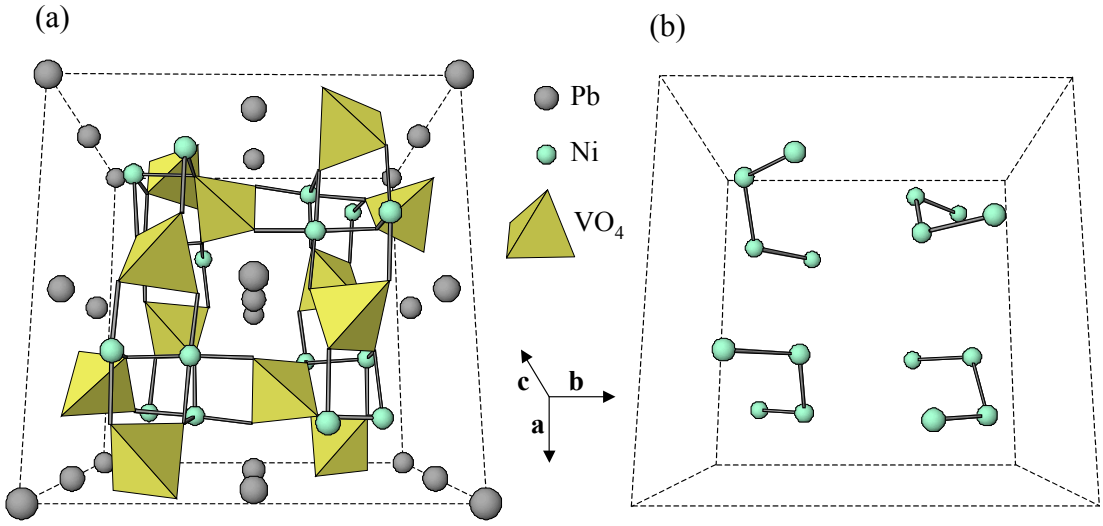

Fig. 3.1: (a) The unit cell of the $PbNi_2V_2O_8$ crystal structure with VO_4 tetrahedra in addition to smaller and larger spheres representing nickel and lead ions, respectively. (b) The spiral-shaped chains of Ni^{2+} $S = 1$ spins.

Regarding the reported isotropic exchange coupling constants $PbNi_2V_2O_8$ system can be considered as a quasi-one-dimensional quantum Heisenberg antiferromagnet. The temperature dependence of the low-temperature susceptibility reflects an activation behavior proving the existence of the Haldane ground state in the case of the $PbNi_2V_2O_8$ compound [1]. Due to the presence of the spin gap the magnetic response of a Haldane system is expected to vanish when the temperature is lowered below the characteristic spin-gap temperature. Second, the singlet nature of the Haldane ground state dictates a characteristic field dependence of the magnetization at low temperatures. A sudden increase of this parameter occurs above the critical value of the magnetic field where the lowest triplet-like magnetically excited state crosses the energy level of the ground state. The values of the intrinsic energy gaps characteristic for noninteracting Haldane chains as estimated from the neutron scattering experiments are $\Delta_{\parallel} = k_B \cdot 36\,\mathrm{K}$ for the spin wave excitation polarized along the spin chains and $\Delta_{\perp} = k_B \cdot 46\,\mathrm{K}$ for the transverse excitations [3]. The "three-dimensional" energy gaps are significantly suppressed (by roughly a factor of 2) with respect to the intrinsic values due to the interchain exchange. It is also worth noting that the lowest-lying Haldane excitations are highly mobile triplet-like excitations and occur near the center of the antiferromagnetic zone.

Uchiyama *et al*. [1] also reported the synthesis of impurity-doped $PbNi_{2-x}Mg_xV_2O_8$ compounds and showed that these materials exhibit a peak in the susceptibility curve below approximately 3.5 K characteristic for the phase transition to the Néel long-range-ordered phase. This ordering was further confirmed by thermodynamical measurements of the specific heat. The dilution dependence of the Néel temperature exhibits a steep increase for low vacancy

concentration, has a maximum of ~3.5 K around $x = 0.16$ and gradually decreases above this concentration [5]. The interesting feature of the $PbNi_{2-x}Mg_xV_2O_8$ compounds is that the lower critical concentration of spin vacancies is either zero or very close to this value. Since the pure $PbNi_2V_2O_8$ compound is positioned in the close vicinity of the phase boundary with the easy-axis ordered state on Sakai-Takahashi phase diagram as shown in Fig. 1.4, this shouldn't come as a surprise. Actually, the isostructural compound $SrNi_2V_2O_8$ was reported to be positioned just across this quantum phase boundary according to the results of the inelastic neutron scattering experiments [3]. However, this statement was deduced from the fit of the absorption peak in a rather unconvincing manner. The presence of diffuse and phonon scattering in the absorption peaks at low energy disabled the authors to exclude the existence of an energy gap smaller than $k_B \cdot 12\,\mathrm{K}$. Moreover, powder diffraction experiments also failed to detect any magnetic Bragg reflection proving that the ordered moment is small, if present at all [3]. In fact, the magnetic field dependence of the magnetization in this compound is very similar to the one in the Pb-based system [6]. The observed sudden increase of the slope in the magnetization curve is usually considered as one of the fundamental evidences for the presence of the spin gap.

The most important origin of the magnetic anisotropy in $PbNi_2V_2O_8$ system is reported to be the slight distortion of NiO_6 octahedra [1]. Following the initial proposal, up to date all the studies of the parent and the doped materials considered the main magnetic anisotropy term of the uniaxial single-ion form $D_{cf}S_i^{z\,2}$. The z axis is taken to coincide with the crystal c axis. The inelastic neutron diffraction experiments yield a negative value of $D_{cf} = -k_B \cdot 5.2\,\mathrm{K}$, which corresponds to a magnetic easy axis parallel to the crystal c axis [3, 4].

A more precise picture about the appearance of the magnetic anisotropy still has to be worked out since the assumption about the form of the major anisotropy contribution was based on the symmetry of the crystal structure and thus ignored the local symmetry at a particular Ni^{2+} site, which in fact determines the actual form of the single-ion magnetic anisotropy. For this reason the distortion of the NiO_6 octahedra, which can be provided only by accurate structural measurements, has to be examined more thoroughly and implemented into the anisotropy Hamiltonian. Second, additional anisotropy mechanisms have to be considered. In this respect Dzyaloshinsky-Moriya interaction could be vital as we are dealing with a low-dimensional system with a low degree of symmetry at a local level and substantial exchange coupling, all the basic ingredients for an appreciable antisymmetric anisotropic exchange interaction.

Despite the fact that the crossover from the Haldane state to the three-dimensionally ordered state is now experimentally quite well established and confirmed, some details still remain unclear. Namely, the competition between the three-dimensional correlations and the one-dimensional Haldane excitations is particularly vague. Also the microscopic nature of the ordering mechanism in still not well understood.

The next unresolved problem in the lead-nickel vanadate system under investigation is the influence of the vicinity of the phase-transition point between the disordered spin-liquid ground state and the long-range ordered state on the spin correlations. This corresponds to the Pb-based system and even more to the Sr-based one, reportedly being on the verge of the three-dimensional ordering instability. Furthermore, the present state of experimental findings seems to be somewhat contradicting for the latter compound.

All the above-mentioned open questions can be most elegantly answered by a combination of structural information and spectroscopic measurements capable of investigating the local magnetic properties. The best tool for the investigation of the magnetic anisotropy present on the local level thus seems to be electron spin resonance, which directly probes the magnetic anisotropy. Furthermore, this method offers insight into the development of the electron spin correlations as a function of both the temperature as well as the level of doping.

As the occurrence of long-range ordering is directly related to the development of three-dimensional spin correlations while the excitations in the pure Haldane state are of one-dimensional nature, magnetic resonance techniques seem to be an appropriate tools for investigating the cross-over behavior in the doped samples being directly sensitive to these correlations. In this regard nuclear spin resonance can provide complementary point of view with respect to the electron spin resonance if nuclei only weakly interacting with the electronic system are used as local probes. In this way static as well as dynamic properties of the electronic correlations can be investigated from the external perspective.

For the above-mentioned reasons we decided to perform ESR measurements [7, 8] and ^{51}V NMR measurements [8, 9] on the family of $PbNi_{2-x}Mg_xV_2O_8$ compounds as well as on the $PbNi_{2-x}Co_xV_2O_8$ samples and the Sr-based undoped system. All the measurements were performed on powder samples since single crystals are, unfortunately, not available at present. The next section will highlight the results and present an appropriate interpretation of the magnetic resonance measurement employed on the parent $PbNi_2V_2O_8$ material. Measurements on the doped systems will be presented in the section 2.3, followed by the section on the magnetic resonance findings in the $SrNi_2V_2O_8$ material. At the end of this chapter some concluding remarks gathering and highlighting the major results will be given.

3.2 Magnetic Resonance Measurements on the Parent Material

As already mentioned, NMR and ESR techniques can provide complementary information about the electronic correlations in the system. ESR in its essence offers information on the direct response of the electronic magnetic moments to the microwave magnetic field. On the other hand, NMR can provide a local probe only weakly coupled to the electronic magnetic

system. For this reason we have chosen to carry out the ^{51}V NMR measurements since vanadium sites should be involved in the formation of the relatively strong interchain exchange bonds between Ni^{2+} sites and should thus be appreciably coupled to the electronic system.

3.2.1 Magnetic Anisotropy and the Dynamics of Spin Correlations as Determined by ESR

The X-band ESR measurements on the $PbNi_2V_2O_8$ compound were performed in the temperature range between room temperature and 5 K. The representative spectra for the temperatures above 40 K are presented in Fig. 3.2a. For lower temperatures accurate measurements were not possible due to the fact that the observed signal loses its intensity when lowering the temperatures as well as it exhibits a rather strong broadening. The derivative ESR spectra in the above mentioned temperature range were satisfactory fitted by the "broad"-Lorentzian distribution taking into account the two Lorentzian-shape contributions, one centered at the positive magnetic field B_c and the other one at the negative magnetic field -B_c as described in subsection 2.1.2,

$$I(B) = -\frac{16A}{\pi}\delta B\left(\frac{(B-B_c)}{\left(4(B-B_c)^2+\delta B^2\right)^2}+\frac{(B+B_c)}{\left(4(B+B_c)^2+\delta B^2\right)^2}\right). \tag{3.1}$$

In the above expression parameter A represents the intensity of the signal, while δB is related to the observed linewidth. In the case when the contribution of the second term is only minor this latter parameter corresponds to the full width at half height (FWHH) of the absorption spectrum or to $\sqrt{3}$-times the peak-to-peak linewidth (δB_{pp}) of the corresponding derivative ESR spectrum. At lower temperatures some spurious signals come into existence at low magnetic fields, which could be due to intrinsic ESR signal of the resonator that we use or could also indicate on the presence of some impurity phases in the sample. However, the intensity of these features is marginal, which makes them unobservable by x-ray diffraction measurements. For this reason they will be neglected in the forthcoming discussion.

The temperature evolution of the ESR intensity corresponding to $A(T)$ in the Eq. (3.1) is shown in Fig. 3.2b. It roughly follows the temperature dependence of the static susceptibility of this sample indicating that the observed signal can be safely attributed to the magnetic Ni^{2+} moments on the Haldane chains. We have also verified the absolute value of the ESR intensity using the standard reference $CuSO_4 \cdot 5H_2O$ and proved that the value of the measured intensity corresponds to the value of static susceptibility within the experimental error [7]. The explanation for the observed discrepancy in the temperature behavior of the static susceptibility and the ESR intensity can be found in the Kramers-Kronig relation

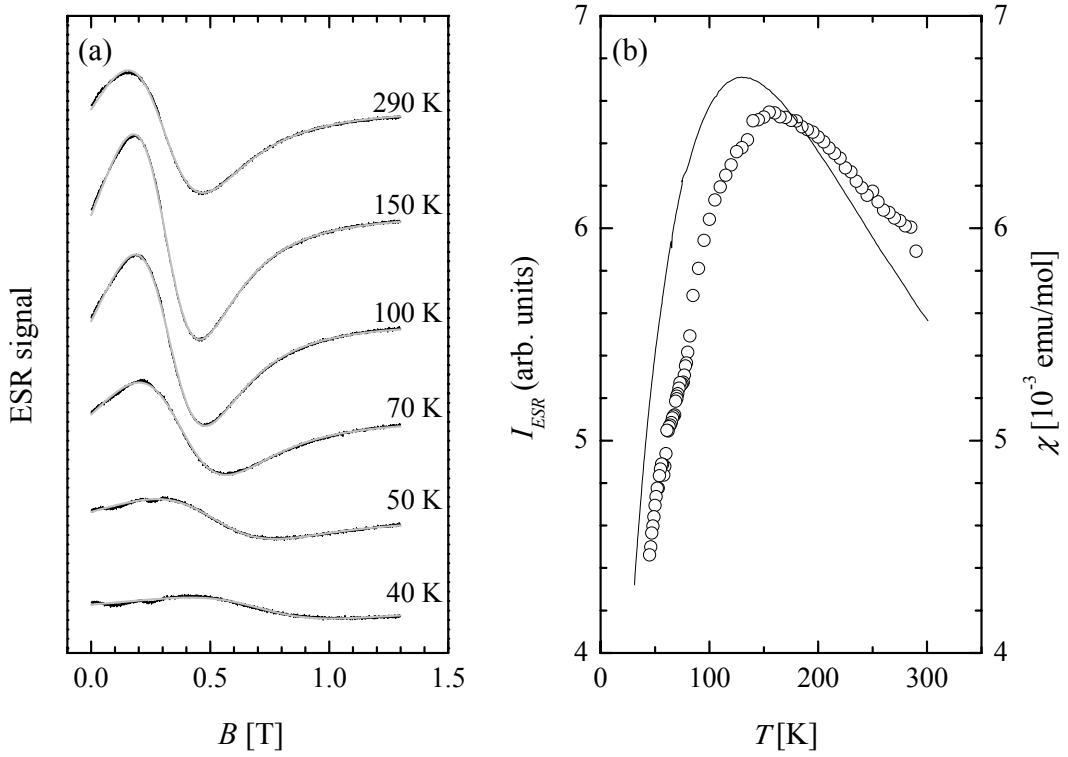

Fig. 3.2: (a) X-band ESR spectra of the $PbNi_2V_2O_8$ powder sample with gray lines representing the corresponding fits to the "broad"-Lorentzian lineshape given by Eq. (3.1). (b) A comparison of the temperature evolution of the ESR intensity (○) with the static magnetic susceptibility (**—**).

$$\chi_0 = \chi'(0) = \frac{1}{\pi} \mathrm{P} \int_{-\infty}^{\infty} \frac{\chi''(\omega)}{\omega} \mathrm{d}\omega , \tag{3.2}$$

where the function P stands for taking the principal part of the integral. In the case when the signal is narrow with respect to the center position ω_0 the proportionality of the static susceptibility and the intensity of the ESR spectrum, which is the integral under the absorption curve, is obvious. A slight experimental difference is that ESR preferably detects $\chi''(B)$ to $\chi''(\omega)$. On the other hand, when the observed signals are as broad as in our case the proportionality of the intensity and the static susceptibility is only approximate, which is believed to be the origin of the mismatch presented in Fig 3.2b.

The linewidth and the *g*-factor of the ESR absorption lines show two significantly different characters when changing the temperature with a crossover occurring around 150 K (see Fig. 3.3). This fact indicates that the electron correlations determining the ESR absorption profiles are changing appreciably around this temperature. In what follows in this subsection the two different regimes will be separately presented.

High-Temperature Behavior

At temperatures above the temperature where the ESR linewidth shows a minimum, both the linewidth as well as the *g*-factor increase moderately with temperature as shown in Fig. 3.3. In general, at temperatures above the characteristic spin temperature determined by the exchange coupling one expects that both of these parameters would become temperature independent. Namely, the localized spins can be treated as uncorrelated at sufficiently high-temperatures due to intense thermal spin fluctuations. However, there are several possible mechanism, which can induce temperature dependence of these two parameters even at temperatures far above the exchange temperature.

The first possible source of the high-temperature linewidth increase is the diffusional decay of the spin correlation function. As described in subsection 2.1.4, the algebraic decay of this function can cause significant line broadening in low-dimensional systems. The spin polarization decay is severely reduced in purely one-dimensional systems due to limited paths of exchange interaction, which, in effect, are responsible for averaging out the line-broadening mechanisms. However, when the spin diffusion effect is important also the lineshape changes from the Lorentzian towards the Gaussian shape. Since the experimental spectra nicely correspond to Lorentzian function, the spin diffusion is expected not to play an important role in the determination of the $PbNi_2V_2O_8$ ESR spectra. This experimental finding could also be predicted beforehand. Namely, the relatively strong interchain exchange coupling makes the investigated system only quasi-one-dimensional. The rate of the out-of-chain diffusion is of the order of $J_\perp/\hbar$ [10] and thus much faster than the X-band ESR frequency. Hence the spin system behaves like three dimensional on the ESR timescale. The decay of the spin correlations is consequently not confined to only one dimension, which makes the spin diffusion process unaffected.

The second mechanism, which can lead to temperature-dependent linewidths at high temperatures, is also intrinsic to the spin system. Namely, at temperatures $T \sim J/k_B$ static spin correlations reflecting the presence of the short-range correlations vary appreciably with the temperature thus making the ESR linewidth and the *g*-factor temperature dependent (see subsection 2.1.5). One would usually expect to observe major changes at temperatures around the exchange temperature, however, in low-dimensional spin systems the short-range correlations effect can be observed up to considerably higher temperatures, i.e., even to $T \sim 10J/k_B$ [11]. Moreover, the short-range order present in the system affects also the *g*-factor of the ESR absorption lines due to the presence of the internal magnetic fields induced by the clusters of ordered spins.

The third possible source of the high-temperature linewidth increase can be sought in the coupling of the spin system and the underlying lattice. In general, as the density of the phonons

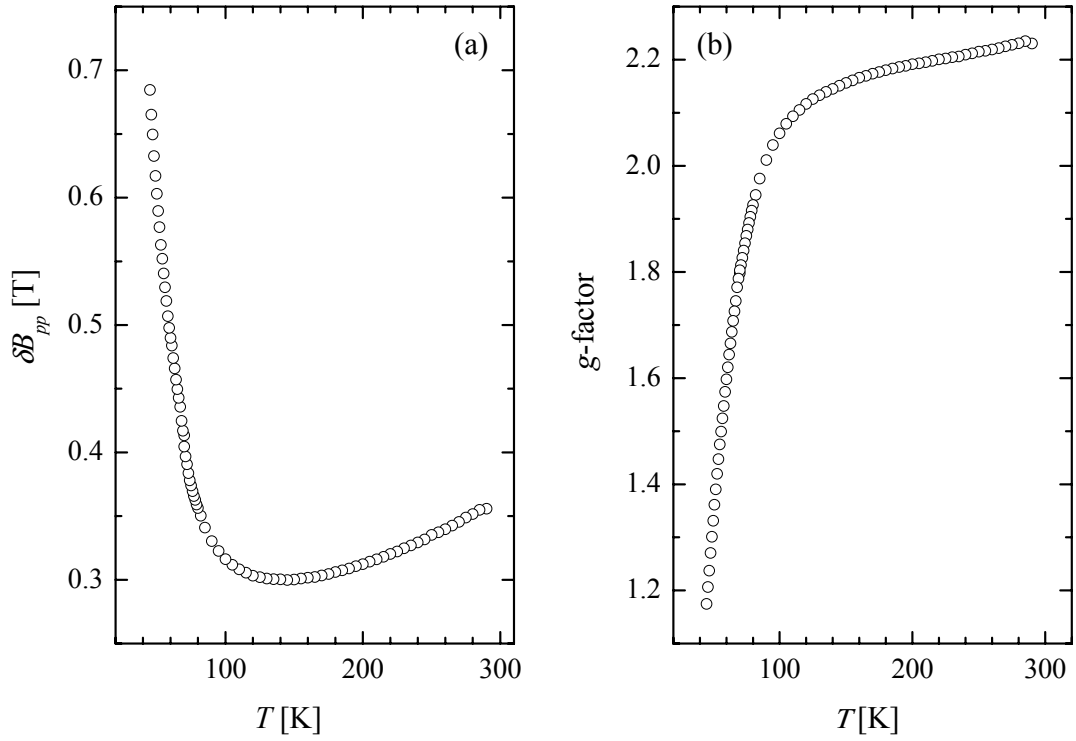

Fig. 3.3: (a) The temperature dependence of the peak-to-peak linewidth and (b) the *g*-factor of the X-band ESR spectra of the $PbNi_2V_2O_8$ powder sample.

rises with the temperature, the lifetime broadening effects become more and more important. The vibrations of the lattice time-modulate the magnetic anisotropy felt by paramagnetic moments, thus possibly leading to the ESR linewidth broadening. The effect of the phonon on the Dzyaloshinsky-Moriya interaction proposed by Seehra *et al*. [12] can be also quantitatively evaluated. In the next chapter this mechanism will be shown to be responsible for the high-temperature linewidth increase in the $SrCu_2(BO_3)_2$ system. On the other hand, it may also be important in $PbNi_2V_2O_8$ systems if the configuration of the Ni^{2+} spin chains is looked at from a "closer" perspective, as it will be argued in the following. The coupling of the spin system to the lattice would invoke line-broadening effect, however, it is expected not to have a major influence on the center position of the ESR lines. Fig. 3.3 then implies that the high-temperature increase of the linewidth as well as the increase of the *g*-factor is mostly due to the presence of static short-range spin correlations in the system.

Let us now focus on the observed magnitude as well as the temperature and the angular dependence of the ESR linewidth. The spectra are rather broad, which is the reflection of appreciable spin anisotropy present in the spin system. The Lorentzian shape of the absorption spectra indicates that motional-narrowing process is effective. If we suppose the major anisotropy to originate from the single-ion anisotropy and to have the form $D_{cf}S_z^2$ [1] with

$D_{cf} = -k_B \cdot 5.2\,\mathrm{K}$ as determined by inelastic neutron scattering experiments [3, 4], the second moment (Eq. (2.14)) and the fourth moment (Eq. (2.18)) entering the expression for the expected linewidth have the following forms

$$\begin{aligned} M_2 &= \frac{D_{cf}^2}{2}\left(1+\cos^2\theta\right), \\ M_4 &= 4J^2 D_{cf}^2\left(1+\cos^2\theta\right), \end{aligned} \tag{3.3}$$

where θ denotes the angle between the external magnetic field and the direction of the easy axis, which has been proposed to lie parallel to the crystal *c* axis. Averaging the above equations over the parameter θ with an assumption of an isotropic powder distribution and plugging the obtained expression in the Eq. (2.19), one can obtain the value of the expected infinite-temperature linewidth

$$\delta B_{pp} = \frac{\pi}{3\sqrt{3}} \frac{1}{g\mu_B} \frac{D_{cf}^2}{J} = 0.12\,\mathrm{T}\,. \tag{3.4}$$

When deriving this equation the constant term $C = 2\pi/6$ appearing in Eq. (2.19) was taken into account as explained in the paragraph following this equation. The evaluated linewidth is of the correct order of magnitude, however, it is about three-times to small if we refer to the room-temperature value. As the lineshape is the Lorentzian curve, the spin diffusion capable of breaking the validity of the Eq. (2.19) as well as the *g*-factor anisotropy cannot be responsible for the above discrepancy. Thus there seems to be some additional spin anisotropy terms so far not considered in the literature. Two possible sources will be considered in what follows.

First, in the original paper on the magnetic properties of the $PbNi_2V_2O_8$ system the single-ion anisotropy term was suggested to have the easy-axis form with the easy axis pointing along the crystal *c* direction [1]. This proposal was made on the basis of the tetragonal crystal symmetry of the investigated system. Such an assumption may well be valid on a macroscopic scale as evident from the orientational effect, where Ni^{2+} chains tend to align along the direction of a strong magnetic field when put into a liquid media [1]. However, one cannot turn a blind eye to this proposal when performing microscopic experiments like ESR or INS, which are sensitive to the local magnetic structure. The form of the single-ion magnetic anisotropy term is determined by the local arrangement of the ligand O^{2-} ions surrounding a particular Ni^{2+} ion and the onsite magnetic anisotropy does not necessary point along the crystal *c* axis.

In the case of the cubic crystal-field symmetry the lowest lying orbital state of an octahedrally coordinated Ni^{2+} ion ($3d^8$ configuration) is a singlet, while two triply degenerate energy states lie significantly above this state due to the strong crystal-field [13]. The ESR technique then probes the magnetic dipole transitions within the singlet ground state when the corresponding three $S = 1$ spin states are split in the external magnetic field. The orbital

momentum of the ground state is "quenched" and partially restored by the spin-orbit coupling, which mixes a finite amount of the six excited orbital states into the ground state. This, for instance, explains the deviations of the measured *g*-factor from the free-electron value in the investigated compound. In an undistorted octahedral environment the Ni^{2+} ions encounters an isotropic *g*-shift and no single-crystal anisotropy as all of the principal values of the Λ-tensor introduced in subsection 2.1.1 are equal [14]. However, if the symmetry is less than cubic the two triplet states will be split leading to finite single-ion anisotropy. It is the local arrangement of the six O^{2-} ions around each Ni^{2+} ion that determines the size and the principal axes of the Λ-tensor and thus the single-ion anisotropy. If the distortion of the O^{2-} octahedron is for instance tetrahedral the D_{cf} term will be the only one present in the effective crystal-field spin Hamiltonian given by Eq. (2.4).

There are different approaches regarding how to consider the effect of the distorted ligand environment. The most straightforward method and at the same time the only accessible for someone that is not a "molecular-bonding" chemist is the crystal field approach [15], which treats the crystal-field interactions of a particular ion with the surrounding ligands from the perspective of the point-charge electrostatic potential being the dominant interaction. As such it is directly applicable only to rare-earth ions, where the covalency effect is not significant. For Ni^{2+} ions surrounded by O^{2-} at a distance of 2 Å [2] significant overlap of the atomic orbitals is expected.

For the above-mentioned reason the determination of the single-ion anisotropy tensor in the case of the $PbNi_2V_2O_8$ compound is far from being trivial. A further complication is provided by the fact that the distortion of the O^{2-} octahedra has practically no symmetry judging from the crystal structure of the $SrNi_2V_2O_8$ compound [2] and recent highly accurate determination of the crystal structure of the $PbNi_{1.88}Mg_{0.12}V_2O_8$ system [16] as presented in Fig. 3.4. The crystal structure of the $PbNi_2V_2O_8$ compound is expected to be very similar, which is reflected also in the similar ESR signals of the Mg-doped and the pristine sample, as will be presented in the following section. Since the overlap of atomic orbitals is expected to play the major role in determining the principal tensor of the single-ion anisotropy, the direction of the principal axes would not be accurate enough without using molecular-orbital computation programs. However, since the distortion of the NiO_6 octahedron is quite general the D_{cf} and E_{cf} term of the same order are expected. This has not been considered so far in any of the theory and experiments on $PbNi_2V_2O_8$.

Second, the Dzyaloshinsky-Moriya antisymmetric exchange interaction between the neighboring Ni^{2+} ions (Eq. (2.7)) should be appreciable in the investigated system due to the fact that there is no center of inversion at the midpoint between them. Symmetry arguments led Keffer [17] to the conclusion that in the case of the superexchange interaction the Dzyaloshinsky-Moriya vector points in the direction $\mathbf{n}_b^i \times \mathbf{n}_b^j$, where $\mathbf{n}_b^i$ is the normalized

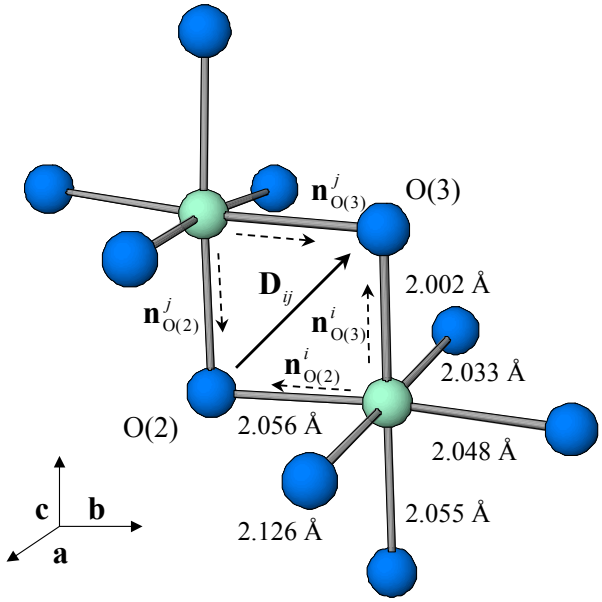

Fig. 3.4: The two neighboring distorted NiO_6 octahedra with the nickel-oxygen distances corresponding to the case of $PbNi_{1.88}Mg_{0.12}V_2O_8$ at 300 K [16]. The broken arrows represent the direction of the vectors from the nickel ions to the bridging oxygen ions while the solid arrow corresponds to the Dzyaloshinsky-Moriya vector between the two Ni^{2+} ions.

vector connecting the *i*-th interacting magnetic moment with the ion acting as the bridge for the superexchange. If there are two pathways as in Fig. 3.4, the corresponding DM vector will be of the form

$$\mathbf{D}_{ij} = D\left(\mathbf{n}^{i}_{O(2)} \times \mathbf{n}^{j}_{O(2)} + \mathbf{n}^{i}_{O(3)} \times \mathbf{n}^{j}_{O(3)}\right), \tag{3.5}$$

with $D \approx \Delta g/g \cdot J$ as explained in chapter 2. If the accurate crystal structure is taken into account the DM interaction can be evaluated to be of the size $D_{ij} \approx 0.15\Delta g/g \cdot J \approx k_B \cdot 1.5\,\mathrm{K}$ with the DM vector pointing approximately perpendicular to the Ni-Ni direction as indicated in Fig. 3.4.

The estimated DM vector is rather large and should thus effect the spin configuration at low temperatures. However, it cannot alone account for the observed linewidth. The experimental linewidth is thus probably due to a combined effect of both the single-ion anisotropy terms as well as the Dzyaloshinsky-Moriya interaction. The discrepancy between Eq. (3.4) and experiment thus comes of no surprise. However, it seems at this stage impossible to give any firm statement about the anisotropy of the $PbNi_2V_2O_8$ system without performing an experiment on a single crystal.

Mid-Temperature Behavior

As evident from Fig. 3.3 there is an apparent change of the temperature dependence of the ESR parameters in the $PbNi_2V_2O_8$ spin system coming into existence below approximately 150 K. The signal seems to progressively change its character from the high-temperature to the low-temperature nature. Something similar, though a bit different, was also reported by Date *et al*. [18] for the $[Ni(C_2H_8N_2)_2(NO_2)]ClO_4$ system (NENP) in the first ESR experiment performed on Haldane systems. The authors of this report observed an exchanged-narrowed signal at the *g*-factor close to the free electron value at high-temperatures and another signal significantly shifted towards higher fields emerging at temperatures below approximately the temperature corresponding to the Haldane gap. Although the two signals overlapped, they were able to separate the two contributions in the mid-temperature regime. Since this initial ESR study numerous experimental reports on different Haldane systems [19, 20] as well as theoretical calculations [21, 22] concerning the ESR in Haldane systems have been published. However, all of them focus on the low-temperature behavior, where only the lowest-lying magnetic excitations are expected to be contributing significantly to the ESR signal. At low temperatures the transitions within the lowest lying triplet state at $q = \pi$ dominate the ESR spectra. On the other hand, the transitions from the singlet ground state to this excited state are not allowed due to the fact that the momentum transfer in the ESR measurements is limited to $\Delta q \approx 0$.

With the use of the established facts let us now try to understand what would the low-temperature ESR absorption spectrum of $PbNi_2V_2O_8$ spin system look like. If there were no anisotropy terms in the spin system the ESR spectrum would be simply a δ-function located at the *g*-value corresponding to the free-electron value. The anisotropy splits the zero-field energy values of the three modes. The corresponding magnetic field diagrams are schematically presented in Fig. 3.5 for magnetic fields applied parallel to the principal axes of the single-ion anisotropy tensor. The corresponding curves for the external field parallel to the *z* principal axis are given by [19]

$$E^{x,y}(q) = \left[(g\mu_B B)^2 + v^2 (q-\pi)^2 + \frac{\left(E_x^2 + E_y^2\right)}{2} \pm \right.$$
$$\left. \pm \left(\frac{\left(E_x^2 - E_y^2\right)^2}{4} + (g\mu_B B)^2 \left(\left(E_x^2 + E_y^2\right) + 4v^2 (q-\pi)^2 \right) \right)^{1/2} \right]^{1/2}, \tag{3.6}$$
$$E^z(q) = \left[E_z^2 + v^2 (q-\pi)^2 \right],$$

where the isotropic *g*-factor and excitation "velocity" *v* have been assumed. The relations for the other two directions of the magnetic field are obtained by the circular permutation of the indexes *x*, *y* and *z*. Due to the powder nature of the compound under investigation the only non-

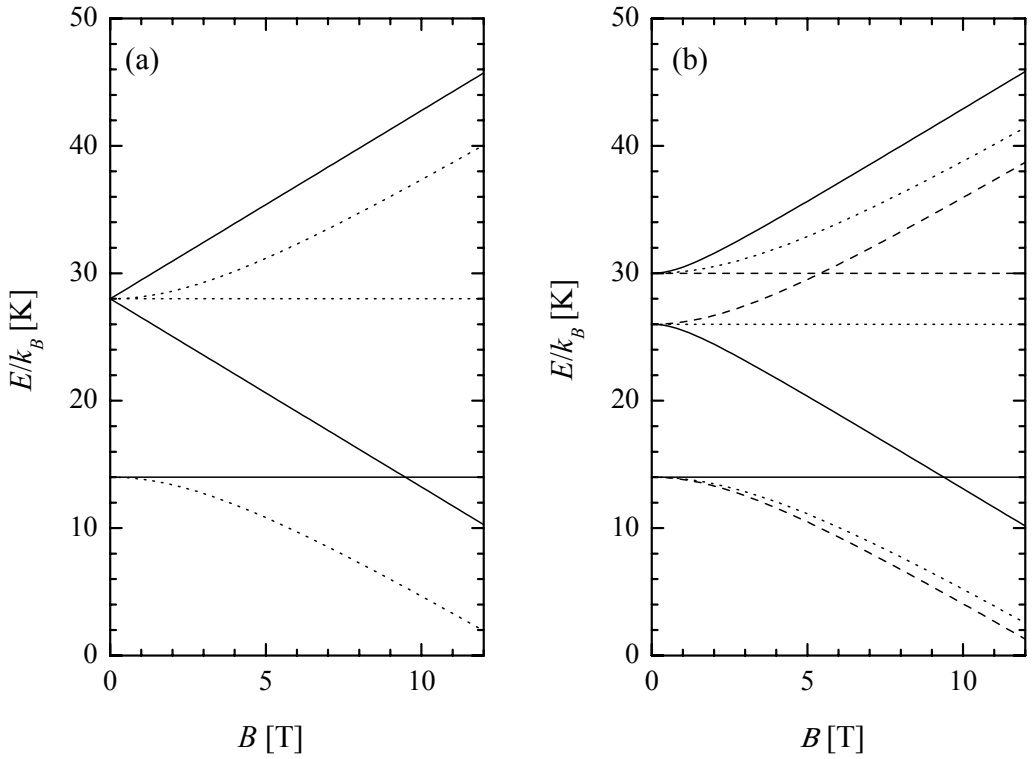

Fig. 3.5: The energy splitting of the lowest triplet excitation at the center of the antiferromagnetic zone in the external magnetic field (a) with and (b) without axial symmetry as given by Eq. (3.6). The plots correspond to the external magnetic field oriented along the easy axis denoted by z (—), along the x (--) and along the y (····) principal axes.

model-dependent parameter is the lowest energy gap, which Zheludov *et al*. measured in the INS measurements, $E_{\parallel} = k_B \cdot 14\,\mathrm{K}$. Next they assumed what seem to be an unjustifiable assumption of the tetragonal symmetry of the single-ion anisotropy tensor as argued above, and obtained the energy gap for the two magnons corresponding to fluctuations of the staggered magnetization in the two directions perpendicular to the easy axis, $E_{\perp} = k_B \cdot 28\,\mathrm{K}$. These gaps are somewhat lower than the intrinsic Haldane gaps due to interchain exchange.

The energy diagram of these three excitations in the case of the external field parallel and perpendicular to the easy axis is shown in Fig. 3.5a for $g = 2.2$. The two δ-function signals for the direction of the external field parallel to the easy axis corresponding to the resonance frequency $\nu = 9.3\,\mathrm{GHz}$ that we use in X-band are centered at $B_{\parallel}^{1} = 9.17$ T and $B_{\parallel}^{2} = 9.78$ T. Second, if the magnetic field were applied in the direction perpendicular to the easy axis the $\Delta m = 1$ transition would be observed at the field $B_{\perp} = 1.73$ T. As the perpendicular directions represent a two-dimensional space one would expect to observe the major part of the ESR signal in a powder sample at $B_{\perp}$. It turns out that there is another important effect of the anisotropy on

the ESR absorption spectra. Namely, the Zeeman splitting becomes wave-vector dependent, which introduces finite linewidths [21]. In Fig. 3.5b additional splitting of the two perpendicular modes due to E_{cf} is shown. The situation is more complicated in this case, however, a general conclusion would be that the position of the lowest transition moves towards higher fields.

Although we do not know an exact form of the single-ion anisotropy and the corresponding energy gaps, we can generally state that the low-temperature ESR signal in the Haldane system is shifted towards higher magnetic fields with respect to the high-temperature paramagnetic phase due to the zero-field energy splitting of the lowest-lying triplet excitation. In this sense the experimentally observed rather strong reduction of the measured *g*-factor in the $PbNi_2V_2O_8$ system can be understood in terms of a gradual shift of the center of the ESR signal from the single-ion paramagnetic excitations to the collective Haldane excitations. This change of the character is due to the Boltzman repopulation of the energy levels when lowering the temperature, which effectively suppresses the observability of the transitions within the magnon continuum. Regarding the increase of the observed X-band ESR linewidth, on the other hand, the answer in less clear. Such behavior could be due to the change of the spin dynamics when entering the Haldane regime. However, a more definite answer can be given only if the temperature dependence of the spin correlation functions is calculated for this system.

3.2.2 ^{51}V nuclei – Spies for Electronic System

The ^{51}V (I = 7/2) NMR measurements were performed in an external magnetic field of $B_0 = 6.34\,\mathrm{T}$. The temperature dependence of the spectra as well as the evolution of their first moment in the parent $PbNi_2V_2O_8$ sample is shown in Fig. 3.6. As evident their shape and linewidth do not change much with temperature. The lineshape is characteristic of the quadrupole-perturbed Zeeman Hamiltonian additionally almost isotropicly broadened, as will be argued below. Already a quick inspection of the NMR absorption lines reveals the presence of shoulders characteristic for the quadrupole interaction. On the other hand, the center of the line, which is determined by the first moment of the absorption line, shifts with the temperature appreciably. A sharp resonance at 71.72 MHz, particularly strong at higher temperatures, is due to a presence of Cu nuclei at or around our probe and will be neglected in what follows.

Role of Transferred Hyperfine Interaction in $PbNi_2V_2O_8$ System

Let us first focus on the center position of the absorption lines. The shift of the NMR line from the expected Larmor frequency for diamagnetic ^{51}V nuclei, $\nu_L^{dia} = 70.974\,\mathrm{MHz}$, is considerable, especially at higher temperatures. The reference frequency corresponds to $VOCl_3$, which is

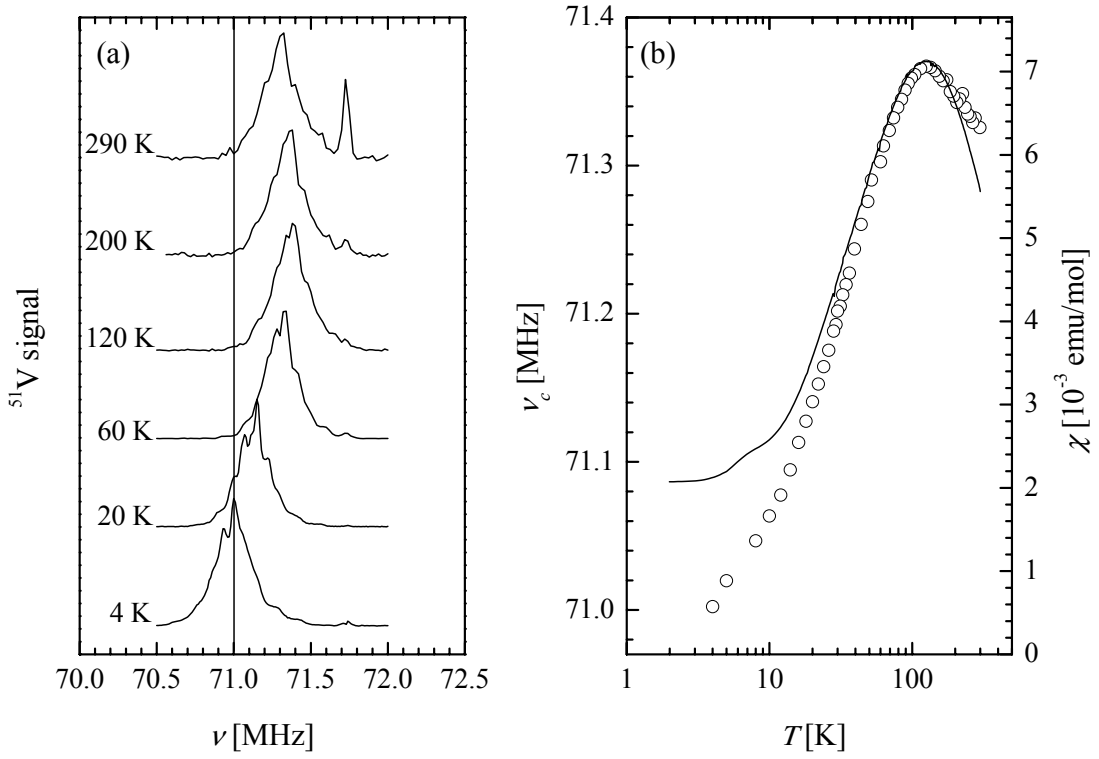

Fig. 3.6: (a) ^{51}V NMR spectra of $PbNi_2V_2O_8$ measured in the external magnetic field of 6.34 T at selected temperatures. The vertical line represents the center position of the spectrum at 4.2 K. The sharp resonance at 71.7 MHz is due to copper nuclei extrinsic to the compound under investigation. (b) Comparison of the temperature dependence of the center of the NMR spectra, as determined by the first moment (○), with the static magnetic susceptibility (—). Note that the frequency scale begins at 70.974 MHz, which is the position of the expected ^{51}V Larmor frequency.

taken as the reference for ^{51}V (I = 7/2) NMR measurements with zero chemical shift. The value of the shift of the center NMR position in $PbNi_2V_2O_8$ at room temperature is thus around 300 kHz, or equivalently $\Delta\nu/\nu_L = 0.4\,\%$. Such a large shift at the V^{5+} site, which is diamagnetic, can only be explained by a substantial coupling of ^{51}V nuclei with the surrounding electrons belonging to the paramagnetic Ni^{2+} sites.

This statement can be put on even firmer grounds if the temperature dependence of the lineshift is compared to the dependence of the magnetic susceptibility. The susceptibility curve was measured in a high magnetic filed of 5 T to imitate the NMR experimental conditions as accurately as possible. However, this curve does not deviate from the measurements in a low magnetic field since the magnetization-versus-magnetic-field dependence is linear at room temperatures and at the lowest accessible temperature of 2 K. As apparent from Fig. 3.6 the two quantities, i.e., the magnetic susceptibility and the center position of the NMR lines have the same tendency of changing with temperature. There are differences some of which can,

however, be qualitatively explained. Namely, the low temperature deviation of the susceptibility from the decreasing dependence with decreasing temperature is attributed to a small quantity of "impurities" present in the system [23]. Such a Curie upturn can be also due to the presence of $S = 1/2$ spins emerging at the ends of the chains, which terminate on the surface of the grains.

As explained in chapter 2, the main interactions of the vanadium nucleus (belonging to the nonmagnetic ion) with its surroundings in a magnetic system are expected to be the quadrupole coupling, the dipole interaction between the nuclear magnetic moment and the neighboring paramagnetic moments, and the transferred effective hyperfine interaction due to the mixing of electronic wave functions between the vanadium orbitals and the orbitals of the oxygen ligands, which are supplementary mixed by the nickel orbitals. The first interaction can in principle lead to the frequency shift of the central line ($-1/2 \rightarrow 1/2$). However, this shift is due to the second order perturbation and is in out experiment a minor effect since we prove later on that the quadrupole frequency is rather small. Moreover, the quadrupole interaction is not expected to change much with the temperature. The dipolar interaction with surrounding magnetic moments also does not produce any lineshifts in a powder sample, since it can be represented by a traceless tensor. The only origin of the observed drift of the line from the frequency expected in case of diamagnetic V^{5+} ions can thus be the isotropic part of the effective transferred hyperfine coupling, which is according to Eq. (2.30) written in the form

$$\widetilde{H}_i^{hf} = \mathbf{I}_i \cdot \sum_j \underline{\widetilde{\mathbf{A}}}_{i,j} \cdot \mathbf{S}_j \,. \tag{3.7}$$

Here the summation extends over the nearby paramagnetic neighbors that disturb the distribution of the electrons from the otherwise completely occupied V^{+5} shells. The hyperfine tensor can be conveniently decomposed into the isotropic and the traceless anisotropic part, $\underline{\widetilde{\mathbf{A}}}_{i,j} = A_{ij}^{iso}\,\underline{\mathbf{I}} + \underline{\widetilde{\mathbf{A}}}_{i,j}^{an}$. This decomposition proves to be useful in the analysis of the center position in powder samples since only the isotropic part has a nonzero contribution. Anisotropic part of the hyperfine coupling tensor, on the other hand, leads to a characteristic anisotropic broadening of the NMR spectra. The determination of the magnitude of the isotropic part can be our initial assignment. Trying to accomplish this goal, we follow the procedure introduced by Sulman and Jaccarino [24] for the case of paramagnetic MnF_2.

For setting the reference of the zero paramagnetic frequency shift we choose the value of the first moment of the absorption line at 4 K, where the spin susceptibility is expected to be negligible due to its activation dependence at low temperatures. This value of almost exactly $\nu_L^0 = 71\,\mathrm{MHz}$ can serve as a better reference for determining the temperature dependence of the frequency shifts due to interactions with the surrounding paramagnetic centers than the Larmor frequency corresponding to the purely diamagnetic case, $\nu_L^{dia} = 70.974\,\mathrm{MHz}$, since we may also have a chemical shift of that order present in the material. From the measured frequency shift at

room temperature, $\Delta\nu = 300\,\mathrm{kHz}$, we can then calculate the corresponding isotropic hyperfine coupling using the Eq. (3.7)

$$\widetilde{A}_{i,j}^{iso} = \frac{h\Delta\nu 2N_A g\mu_B}{6\chi_{mol}B_0} \approx k_B \cdot 0.17\,\mathrm{mK}\,. \tag{3.8}$$

When deriving the expression in Eq. (3.8) it was assumed that the average value of the spin moment at the paramagnetic site is given by relation $2N_A g\mu_B \langle S_j \rangle = \chi_{mol} \cdot B_0$. Further, all of the six nearest neighboring Ni^{2+} ion that are connected to the V^{5+} site were equally considered though the distance to the vanadium nucleus varies from 3.33 Å to 3.48 Å and the geometry of the exchange paths also changes.

The V^{5+} sites evidently act as partially magnetic ions. The covalency effect induces a space redistribution of the 3*s* and 3*p* electrons that manifests itself in a partially unpaired character of the vanadium *s* and *p* electrons. These electrons are then responsible for the transferred hyperfine coupling. Since the *s* electrons are the only type of electrons that can lead to isotropic frequency shifts due to the Fermi contact interaction (see Eq. (2.29) and the corresponding explanation) the percentage of the *s* electrons taking a part in the covalent bonding can be estimated. This fraction is connected to the amount of the *s* electrons at V^{5+} site becoming unpaired. If there was one unpaired electron in the vanadium 3*s* shell it would produce the isotropic hyperfine coupling sensed by the vanadium nucleus, which is according to Eq. (2.29) of the order

$$A_{3s}^{iso} = \frac{\mu_0}{4\pi} g\mu_B \gamma\hbar \frac{8\pi}{3} |\psi(0)|_{3s}^2 = k_b \cdot 0.4\,\mathrm{K}\,. \tag{3.9}$$

When deriving this estimation the density of the *s*-type electronic wave function at the nucleus for the V^{5+} ion, $|\psi(0)|_{3s}^2 = 601\,\text{Å}^{-3}$, was calculated from the tables of ionic wave functions [25]. Comparison of the magnitudes of the transferred hyperfine coupling (Eq. (3.8)) and the hyperfine coupling corresponding to an unpaired 3*s* electron at vanadium site reveals the percentage of vanadium 3*s* electron being unpaired, the fraction being $w \approx 2.5 \cdot 10^{-3}$.

In the same manner also the fraction of the unpaired 3*p* electrons at vanadium site could be estimated, assuming that one would have a single crystal at one's disposal. However, as already mentioned, in powder samples the resulting anisotropic frequency shift due to the anisotropic part of the transferred hyperfine interaction is averaged out.

Possible NMR Line-Broadening Mechanisms

The ^{51}V NMR spectrum of the $PbNi_2V_2O_8$ obtained by a long averaging is shown in Fig. 3.7a. Let us first try to explain the linewidth of the central transition ($-1/2 \rightarrow 1/2$). According to Eq.

(2.33) the second order contribution of the quadrupole coupling to the central transition is of the order of $5\nu_Q^2/\nu_L$. The quadrupole frequency can be very roughly estimated from the positions of the shoulders in the absorption spectrum (Eq. (2.32)) to be around $\nu_Q \approx 80\,\mathrm{kHz}$. The corresponding value of the linewidth of the central transition provided by the quadrupole coupling, $\delta\nu_Q \approx 1\,\mathrm{kHz}$, is almost two orders of magnitude smaller than the experimental linewidth of the central transition $\delta\nu_0 = 60\,\mathrm{kHz}$, measured as the full width at half height.

The next interaction worth considering is the estimated isotropic hyperfine coupling (Eq. (3.8)), which corresponds to the frequency of $\nu_{iso} \approx 21\,\mathrm{MHz}$. However, due to the fluctuating nature of the electronic correlations strong reduction of this frequency is expected. The anticipated line broadening due to the fluctuations of the isotropic hyperfine interaction can be estimated from the expression for the spin-spin relaxation time given by Eq. (2.42) or by using the method of moments introduced in Chapter 2 in connection with the electron spin resonance. The full frequency width at half height is then given by [24]

$$\delta\nu_{iso} \approx \frac{2}{h}\sqrt{\frac{\pi}{2}}\frac{M_2}{\hbar\omega_e} \approx \frac{\sqrt{2\pi}Z}{h}\left(A_{i,j}^{iso}\right)^2 \frac{S(S+1)}{3\sqrt{2J^2Z'S(S+1)/3}} \approx 15\,\mathrm{Hz}\,, \tag{3.10}$$

where $Z = 6$ represents the number of nearest-neighbor paramagnetic ions and the exchange frequency is approximated by $\omega_e = \sqrt{2J^2Z'S(S+1)/3\hbar^2}$ [26] with $Z' = 2$ as the number of the nearest paramagnetic neighbors for each magnetic moment. For obtaining this expression it was assumed that the electronic spins are completely uncorrelated (Eq. (2.21)), that the electronic fluctuations are virtually isotropic in the paramagnetic phase, and that $\delta\mathbf{S} \approx \mathbf{S}$. Due to the very rapid electronic fluctuations the contribution of the isotropic hyperfine exchange is drastically reduced by a factor of 10^6 from the expected value $6\nu_{iso} \approx 21\,\mathrm{MHz}$. The contribution to the line broadening due to this interaction is thus even by two orders of magnitude smaller than the quadrupole interaction.

The next step is to evaluate the dipolar coupling between the nuclear magnetic moments and the electronic paramagnetic moments. For this purpose it is convenient to rewrite the dipolar coupling given by Eq. (2.27) in the tensor notation characteristic for the hyperfine tensor,

$$H_{hf}^{i} = \mathbf{I}_i \cdot \sum_j \underline{\mathbf{A}}_{i,j}^{d} \cdot \mathbf{S}_j\,. \tag{3.11}$$

Here the coupling tensor has the following form assuming an isotropic *g*-factor [27]

$$\underline{\mathbf{A}}_{i,j}^{d} = \frac{\mu_0\gamma\hbar g\mu_B}{4\pi}\sum_j \frac{3\mathbf{n}_{i,j}\otimes\mathbf{n}_{i,j} - \underline{\mathbf{1}}}{r_{i,j}^3}\,, \tag{3.12}$$

where $\mathbf{n}_{i,j}$ represents the normalized vector $\mathbf{r}_{i,j}$ connecting the nucleus at site *i* with the neighboring paramagnetic spin at site *j*.

In the paramagnetic state every time-averaged magnetic moment of Ni^{2+} paramagnetic ion would lie parallel to the external magnetic field assuming that the anisotropy of the susceptibility tensor is negligible. Actually, there is a slight difference of the magnetic susceptibility values measured for the external field applied along the three crystal axes [1], however, this can be neglected for our purposes. The dipole tensor can be evaluated from the crystal structure. For the vanadium nucleus at the position $r=(0.9181a, 0.2641a, 0.2984c)$ within the prime cell the coupling tenors $\mathbf{A}_{ij}^{d}$ was numerically calculated to have the following form in the crystal frame

$$\underline{\mathbf{A}}_{ij}^{d} = \gamma\hbar\tilde{\mu}\begin{bmatrix} -0.28 & \sim 0 & \sim 0 \\ \sim 0 & 0.46 & \sim 0 \\ \sim 0 & \sim 0 & -0.18 \end{bmatrix}[\mathrm{mT}], \tag{3.13}$$

where $\tilde{\mu}=\langle\mu\rangle/\mu_B$ corresponds to the normalized paramagnetic moment. In this calculation virtually all the neighbors (10^5 nearest Ni^{2+} sites) have been taken into account. As all the vanadium sites within the prime cell are crystallographically equivalent, all the ^{51}V nuclei have the same eigenvalues of the hyperfine tensors, although the principal axes change when moving from site to site within the prime cell. However, as we are dealing with powder samples, all the directions of the external magnetic field in the crystal frame are equally probable so that there is effectively only one ^{51}V site. It is worth noting that the value of the local field produced at a certain nucleus is substantially suppressed with respect to the order-of-magnitude value $\mu_0 g\mu_B\langle S_i\rangle/4\pi r^3 \approx \tilde{\mu}\cdot 25\,\mathrm{mT}$ due to the symmetry of the crystal system. The frequency shifts $|\Delta\nu|=\gamma/2\pi\cdot B_{loc}$ corresponding to the three eigenvalues of $\underline{\mathbf{A}}_{ij}^{d}$ are sizable only if the maximum spin moment $\tilde{\mu}=g\sqrt{S(S+1)}=2.8$ is taken into account. In this case it amounts to $|\Delta\nu|\approx 15\,\mathrm{kHz}$. However, one should not forget that due to exchange narrowing mechanism a significant reduction of the estimated static value is expected, and second, the magnitude of the average magnetic moment of the Ni^{2+} ion is in the paramagnetic phase only a fraction of the maximum moment $\tilde{\mu}=3\cdot 10^{-2}$ as can be calculated from the molar susceptibility. Thus also the direct electron-nucleus dipole coupling is of insignificant importance.

A possible way out is to introduce also anisotropic part of the transferred hyperfine coupling tensor. The expression for the linewidth due to fluctuating paramagnetic moments is then similar to that given by Eq. (3.10)

$$\delta\nu \approx \frac{\sqrt{2\pi}}{h}\frac{S(S+1)}{3\sqrt{2J^2Z'S(S+1)/3}}\sum_j\frac{1}{2}\left(\tilde{A}_{i,j}^{xx\,2}+\tilde{A}_{i,j}^{yy\,2}\right)+\tilde{A}_{ij}^{zz\,2}, \tag{3.14}$$

which applies to a further simplification that the magnetic field is directed parallel to the *z*-principal axis of the hyperfine tensor [28]. To account for the experimentally observed width of the central transition, which is around $\delta\nu_0 = 60\,\mathrm{kHz}$, the anisotropic part of the transferred

hyperfine tensor would have to be according to Eq. (3.10) about 60-times larger than the isotropic part. To estimate if this value is physically plausible let us again evaluate the hyperfine interaction of an unpaired vanadium 3*d* electron as it was done above for the 3*s* electron. Expression equivalent to Eq. (3.9) is [24]

$$A_{3p}^{an} = \frac{\mu_0}{4\pi} g\mu_B \gamma\hbar \frac{2}{5}\left\langle \frac{1}{r^3} \right\rangle_{3p} = k_b \cdot 15\,\mathrm{mK}, \tag{3.15}$$

where the expectation value of the inverse cube of the distance between the 3*p* electron and the core, $\left\langle 1/r^3 \right\rangle_{3p} = 38.8\,\text{Å}^{-3}$, can again be calculated from the atomic wave functions for the V^{5+} ion [25]. The value A_{3p}^{an} is very close to the required one $\widetilde{A}_{i,j}^{an} \approx 60\widetilde{A}_{i,j}^{iso} = 10\,\mathrm{mK}$, which certainly throws a shadow of a doubt on this mechanism.

However, the polarization effect of the paramagnetic moments in the external magnetic field has been neglected so far. Namely, the average value of the spin moment at room temperature in the field of 6.34 T is $\langle S \rangle = 1.5 \cdot 10^{-2}$ as can be deduced from the value of the static susceptibility. Due to the powder nature of the sample the transferred hyperfine coupling anisotropy is reflected in the broadening of the central-line transition according to the estimation

$$h\delta\nu_0 \approx \widetilde{A}_{i,j}^{an} \langle S \rangle. \tag{3.16}$$

Interestingly, this expression yields the anisotropic hyperfine interaction $\widetilde{A}_{i,j}^{an} = 0.19\,\mathrm{mK}$ virtually identical to the estimated isotropic part and requires an acceptable fraction of an unpaired 3*p* electron at V^{5+} site of the order of couple of percents.

Another possible candidate to account for the broad central ^{51}V NMR lines is the chemical shift anisotropy, which has been so far neglected, as it is usually not observable in magnetic systems due to the dominancy of the coupling of the nuclei with the paramagnetic electrons. However, as the above detailed analysis has shown, this latter coupling is severely attenuated by the rapid electron fluctuations. For this reason the anisotropic part of the chemical shift tensor can become a "chief player". In this case the local magnetic field for the vanadium nucleus at site *i* would be of the following form

$$\mathbf{B}_i = \mathbf{B}_0 \left(1 - \underline{\boldsymbol{\sigma}}_i\right) - \frac{1}{\gamma\hbar} \sum_j \underline{\widetilde{\mathbf{A}}}_{i,j} \cdot \langle \mathbf{S}_j \rangle. \tag{3.17}$$

The origin of the chemical shift in diamagnetic substances is two-fold. First the electronic currents induced by the external magnetic field produce diamagnetic contribution to the local field at a given nuclear site, and second, the distorted electronic shells produce a paramagnetic contribution. Both of the two mechanisms produce lineshift proportional to the external field.

For the nucleus of the V^{5+} ion it is quite common for the isotropic chemical shift to be negative and of the order of several hundred ppm [29, 30], with this value being closely related

to the coordination number of O^{2-} ligands around the vanadium ion [29]. Moreover, for the VO_4 tetrahedra also a significant anisotropy of the chemical-shift tensor is quite characteristic. This parameter, which denotes the difference between the principal values and the isotropic part of the chemical-shift tensor, can be close to the value of the isotropic part [29]. From the linewidth of the central transition, $\delta\nu_0 = 60\,\mathrm{kHz}$, it can be evaluated that the anisotropic terms of this tensor should be of the order of 450 ppm if this is the main broadening mechanism, which is again a reasonable value for the nucleus of the V^{5+} ion sitting in the center of an oxygen tetrahedron [29]. As the profile appears quite symmetric, the value of the asymmetry parameter should then be around $\eta = (\sigma_2 - \sigma_1)/(\sigma_3 - \sigma_1) \approx 0.5$, where σ_i stands for the principal values $\sigma_1 \le \sigma_2 \le \sigma_3$ of the chemical-shift tensor.

If the chemical-shift tensor is introduced, we have to examine also its effect on the center position of the NMR absorption line. As the isotropic part of this tensor should be in VO_4 octahedra of the same order as the anisotropic components, the isotropic lineshift can be estimated to be $\Delta\nu^{is} = \delta\nu_0/2 = 30\,\mathrm{kHz}$, which can thus well be the origin of the difference of the center position measured at the lowest temperature and the expected center position of ^{51}V spectra in $PbNi_2V_2O_8$.

Thus it looks like that both the anisotropy of the transferred hyperfine coupling as well as the chemical shift anisotropy could explain the rather broad central NMR transition. A closer look of the detailed NMR spectrum of $PbNi_2V_2O_8$ recorded at room temperature (Fig. 3.7a) reveals that the absorption line appears a bit anisotropic. This anisotropic feature can be most probably related to the anisotropy of these two interactions. Unfortunately, both broadening mechanisms scale linearly with the value of the external magnetic field, which makes them inseparable in a powder sample even when this parameter is changed. However, to show that the line-broadening and the shift are indeed of the magnetic origin, a comparison of the central-transition line in the magnetic field of 6.34 T with a profile measured in almost three-times lower field of 2.35 T is shown in Fig. 3.7b. The scaling of the line position is rather good as the peaks are shifted with respect one to another only by 3%. Also the linewidth increases by increasing the field from 29 kHz to 60 kHz. However, the ration of the linewidth increase 2.1 is somewhat below the ration of the two corresponding field values, 2.7. In Fig. 3.7b where the spectra are plotted against the normalized frequency shift, the spectrum recorded at the lower value of the magnetic field appears for this reason broader. This is most probably the signature of the quadrupole broadening contribution, which becomes more important at lower fields as it scales with the inversed Larmor frequency.

Since the lineshape is relatively complex, the linewidth of the overall experimental absorption spectrum is a less informative and a less accurately defined parameter. For this reason the analysis of the second moment of the line seems the most reasonable approach. However, as evident from Fig. 3.6 the lineshape in general does not change significantly with

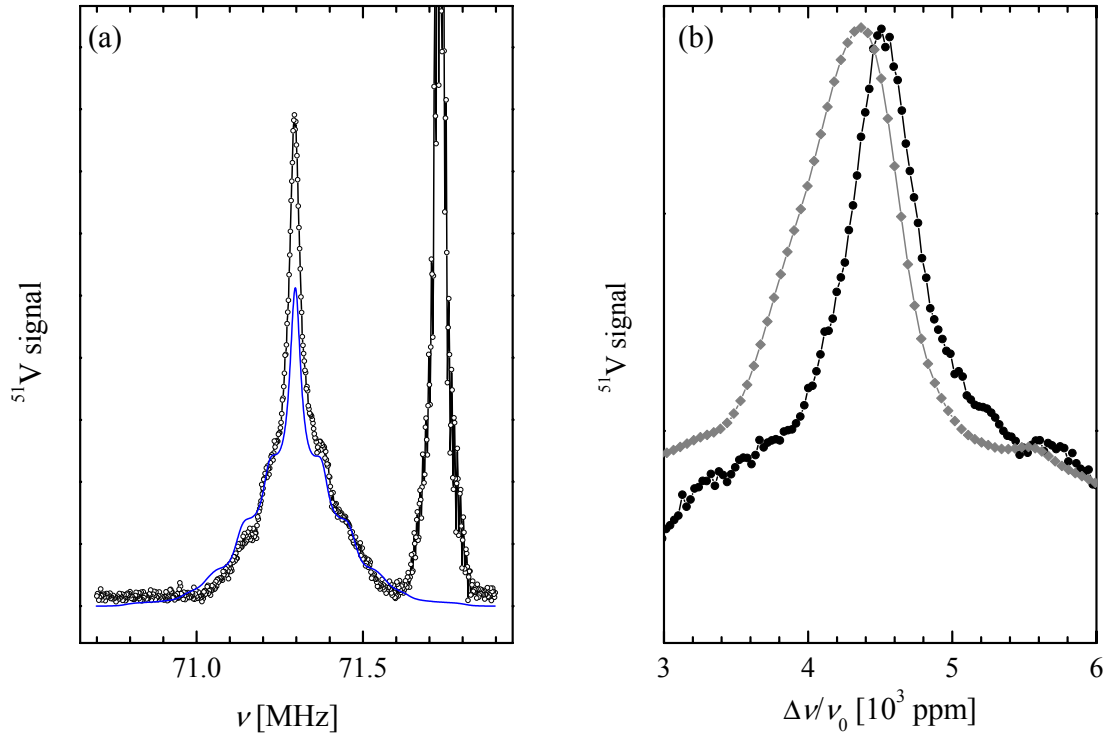

Fig. 3.7: (a) Quadrupole split ^{51}V NMR spectrum of the $PbNi_2V_2O_8$ system at room temperature compared with the modeled spectrum given by the solid line. The measured peak at 71.7 MHz is due to copper impurities. (b) A comparison of the central line of the ^{51}V NMR spectra at room temperature recorder in 2.35 T (◆) and 6.34 T (●) and plotted against the normalized frequency shift.

the temperature. This observation is a rather expected feature if one bears in mind that the shape of the absorption spectra determined by the quadrupole interaction and the chemical shift anisotropy is expected to remain more or less unchanged over the whole temperature range if there is no structural phase transition. It further suggests that the paramagnetic-electron spin dynamics remains unchanged on a rather long timescale of the nuclear magnetic resonance, which is in line with the mobile character of the Haldane spin excitations even in the low-temperature range. A more detailed presentation of the second moment is given in the next section, where the comparison with the linewidth behavior in the doped samples is made.

Absorption Profiles

From all the above-mentioned arguments it would by delusional to think that one would be able to accurately fit the experimental powder lineshape considering all the possible mechanism that may be involved. For this reason, we present only a simplified justification for the appearance

of the overall lineshape. We treat the quadrupole mechanism as the major interaction shaping the absorption profile and then introduce additional isotropic broadening, which makes the profile smoother. For a specific set of parameters $(\cos\theta, \varphi)$ the spectrum would according to Eq. (2.32) and Eq. (2.33) consist of seven δ-functions representing the central line and the six symmetrically placed satellites. In line with Eq. (2.34) the "amplitudes" of these lines would be in the relation $7:12:15:16:15:12:7$. We have undertaken the task of calculating the powder average of the quadrupole absorption spectrum in a numerical manner. A uniform distribution of the parameters $\cos\theta$ and φ has been assumed. The obtained spectrum was then additionally broadened using the convolution of the pure quadrupole spectrum with a Lorentzian distribution of the width corresponding to the central transition. The asymmetry parameter η = 0.88 was calculated from the position of only the four closest O^{2-} ligands forming the VO_4 tetrahedron with a particular vanadium ion, and the value of the quadrupole frequency was determined as $\nu_Q \approx 85\,\text{kHz}$. The resulting theoretical spectrum for the case when 10^5 points from the corresponding parameter space were taken into account is shown in Fig. 3.7a.

As expected, the numerically calculated absorption profile is only in a qualitative agreement with the experimental lineshape. The problem of the difference with satellites and the central line occurs because the satellites are a result of the first order perturbation while the central line is calculated in the second order. To calculate the absorption profile with a greater fidelity an exact knowledge of the anisotropic transferred hyperfine coupling is needed. In this case one should in principle jointly treat the quadrupole interaction and the hyperfine coupling in a perturbative manner. This would be a proper way to handle the problem since both of the interactions are of a comparable size when an average spin value in the paramagnetic state is considered.

3.3 Magnetic Resonance Measurements on Doped Materials

The magnetic resonance measurements on doped samples were aimed to provide a further insight into the impurity-doping ordering effect observed in the $PbNi_{2-x}(Mg,Co)_xV_2O_8$ compounds. The responsible microscopic mechanism is believed to be the breaking of valence bonds representative for the Haldane ground state as explained in the introductory chapter. However, the introduced impurities drag along a variety of unexpected phenomena, among which is also the "order-by-disorder effect" observed for the first time in the Haldane system in $PbNi_2V_2O_8$ [1]. For the liberated spins to exhibit a long-range order at low temperatures appreciable coupling between them is required, the nature of which is rather unclear. Since magnetic resonance techniques are able to probe a particular magnetic system on a local level, they seem to be an appropriate choice for addressing the remaining open questions.

The materials used in the magnetic resonance experiments can be labeled as solid solutions. The position of the cation (Mg^{2+}, Co^{2+}) replacements for the Ni^{2+} ion is randomly distributed, however, the phase purity of all the samples was again verified by x-ray diffraction measurements. The structural measurements revealed that the cations effectively replace the Ni^{2+} ions while leaving the crystal structure virtually unaffected [16, 23, 31].

3.3.1 ESR Detection of Liberated End-Chain Spins in Doped Materials

The majority of ESR measurements were performed in the X-band ($\nu_L = 9.35\,\mathrm{GHz}$), however, few absorption spectra were recorded also in a high magnetic field at the Larmor frequency of $\nu_L = 96\,\mathrm{GHz}$ in order to be able to discuss the possible broadening mechanisms present in the $PbNi_{2-x}(Mg,Co)_xV_2O_8$ system.

In the Mg-doped samples the broadening effect due to the introduced impurities is not so colossal as in Co-doped compounds. The spectra recorded at room temperature are presented in Fig. 3.12 appearing later in this section, where also the discussion on the possible broadening mechanisms in both families of materials in given. But first, let us focus on the temperature dependence of the ESR parameters obtained in the Mg-doped samples. The fitting of the powder absorption spectra remains satisfactory with the "broad"-Lorentzian function introduced by Eq. (3.1). The temperature dependence of the peak-to-peak width and the changes observed in the center position of the ESR spectra are presented in Fig. 3.8. A rather interesting feature of the doped materials is that the behavior of their parameters is much more complex than in the pristine sample. For instance, below room temperature the evolution of the linewidths in doped samples follows the decreasing behavior of the linewidth in the pure sample, however, the first minima are shifted towards lower temperatures and the increase below that temperature is much less intense. Second, a maximum of this parameter is observed around 30 K, where the signal in the pure compound, on the contrary, is not observable any more. The decreasing tendency of the linewidth is again reversed around 10 K. The center of the line follows very similar routine as can be seen from the *g*-factor. The temperature dependence of the latter parameter is thus roughly reversed with respect to the linewidth.

Diverse nature of ESR Centers in Doped Samples

The dependence of the *g*-factor implies that there are in fact two different contributions to the ESR signal in all doped samples. The presence of an additional kind of a paramagnetic center is further supported by the ESR intensity, which exhibits an increase below 20 K (see Fig. 3.9). This is once again atypical for the pristine sample where the presence of the spin gap drives the

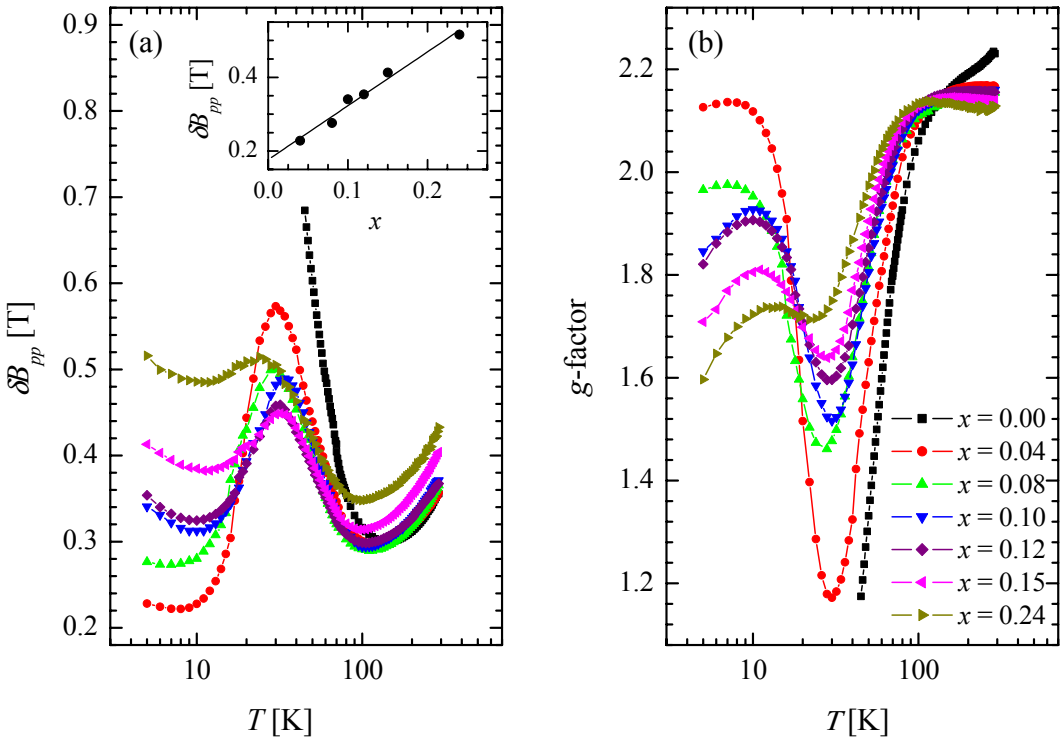

Fig. 3.8: The temperature dependence of the X-band ESR (a) peak-to-peak linewidth and (b) *g*-factor for the $PbNi_{2-x}Mg_xV_2O_8$ family. The inset to part (a) shows the linear dependence (solid line) of the linewidth on the doping level at 5 K.

intensity of the detected signal towards zero. Moreover, it seems that the deviation of all the parameters from the temperature dependences characteristic for the parent compound nicely evolves with the level of doping. This fact indicates that impurities indeed induce additional ESR signal, becoming increasingly important at temperatures around and below the spin-gap value.

The temperature evolution of the absorption spectra described above can be easily understood if the liberated end-chain spins are considered. Namely, the spectra can be imagined to be composed of two component, the high-temperature broad signal characteristic for the Haldane material, and the low-temperature contribution with a slightly narrower linewidth in the crossover regime around 50 K. If the two spin centers are coupled so that their exchange coupling is much stronger than their *g*-factor difference, one expects the two contributions to the absorption spectrum not to be resolved as a direct consequence of rapid spin fluctuations arising from this exchange coupling [32]. The expected *g*-factor for the "exchange-averaged" line would then read

$$\langle g \rangle = \frac{g_1\chi_1 + g_2\chi_2}{\chi_1 + \chi_2}, \tag{3.18}$$

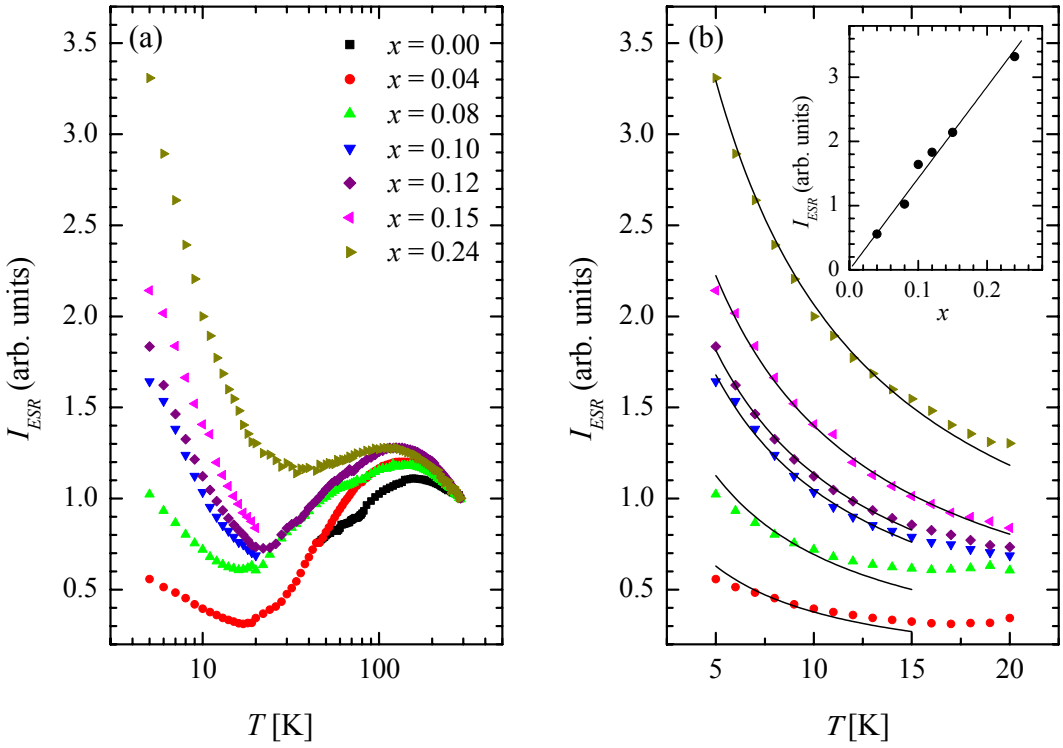

Fig. 3.9: The temperature dependence of the ESR intensity of the $PbNi_{2-x}Mg_xV_2O_8$ compounds (a) in the temperature range between room temperature and 5 K and (b) in the low-temperature regime. The solid lines correspond to fits with the Curie-Weiss model given by Eq. (3.30). The inset to figure (b) shows the scaling of the intensity at 5 K.

where $\chi_{1,2}$ stands for the corresponding susceptibilities of the two ESR centers at a given temperature. At higher temperatures, where the susceptibility of the broad Haldane signal is dominant, the *g*-factor in doped compounds follows the one measured in the parent material. However, at temperatures around 50K the high-temperature signal begins disappearing and the low-temperature paramagnetic centers take over the initiative. For this reason the signal experiences a shift towards higher *g*-values characteristic for free electrons liberated at chain ends by the nonmagnetic Mg^{2+} impurities. The same argumentation also applies to the temperature dependence of the linewidth.

As the values of the local minima and maxima of the *g*-factor and the linewidth as well as the linear low-temperature increase of the ESR intensity (inset to Fig. 3.9b) evidently scale with the doping level, one can safely state that the origin of the low-temperature signal are the broken Haldane bonds due to the presence of nonmagnetic impurities, which tear apart the uniform chains. Virtually simultaneously with our observations [7] also Smirnov *et al*. published similar remarks about the presence of the liberated $S = 1/2$ degrees of freedom. Their conclusions were drawn both on the paramagnetic as well as the antiferromagnetic resonance measurements [33].

Coupling of Liberated End-Chain Spins

The low-temperature spectra observed in vacancy-doped $PbNiV_2O_8$ compounds somewhat differ from the typical $S=1/2$ end-chain ESR signals observed in the prototypical Haldane systems NENP. Namely, in our case they are appreciably broader (more than on order of magnitude) from all the signals induced in the latter system by nonmagnetic impurities (Zn^{2+} [34, 35] and Cd^{2+}, Hg^{2+} [34]) and comparable, although still broader, than the cases when dopants in NENP had spin [36]. Trying to explain the unexpectedly broad low-temperature ESR lines a comparison of the spectra corresponding to the $PbNi_{1.85}Mg_{0.15}V_2O_8$ sample recorded at 5 K in X-band and in high magnetic field ($\nu_L = 96\,\mathrm{GHz}$) is made in Fig. 3.10. The peak-to-peak linewidths are almost unchanged with the corresponding values increasing from $\delta B_{pp}^{X} = 0.429(5)\,\mathrm{T}$ to $\delta B_{pp}^{HF} = 0.445(5)\,\mathrm{T}$ when increasing the resonance frequency by approximately a factor of 10. If the linewidth was due to individual noninteracting $S=1/2$ end-chain spins the width should have scaled linearly with the frequency as a result of the *g*-factor anisotropy as was observed in vacancy-doped NENP [34]. In this case deviation of the lineshape towards an anisotropic shape would be expected. However, if the liberated spins are coupled the effective anisotropy Hamiltonian of the coupled-spin system should be of the form $D^*\tilde{S}_z^2$, where $\tilde{S}_\alpha$ represents the spin operator of the two-spin system. This interaction makes the linewidth non-frequency dependent in the first order. Such fictitious coupling term between two interacting $S=1/2$ spins can be shown to result from the magnetic dipole interaction and the anisotropic exchange, which may be for a ferromagnetically coupled spins both treated similarly. The effective single-ion anisotropy term is then given in the case of the uniaxial symmetry by [37]

$$D^* = -3\frac{\mu_0}{4\pi}\frac{(g\mu_B)^2}{r^3} - \frac{3d}{2}, \tag{3.19}$$

where the first term is due to the dipolar interaction between spins at a distance $r = 5.04\,\text{Å}$ and the second term is the symmetric anisotropic exchange, which is of the order $d = (\Delta g/g)^2 \tilde{J}'$ with $\tilde{J}'$ as the effective exchange constant as explained in chapter 2. The magnetic field emerging from the dipolar coupling can be evaluated from the above equation, $B^d = 45\,\mathrm{mT}$. The contribution to the linewidth of the second term, on the other hand, is of the order of $3d/2g\mu_B \approx 90\,\mathrm{mT}$ if the next-nearest neighbor interaction J' between Ni^{2+} spins introduced in the opening section of this chapter is taken as an approximation for the effective exchange coupling $\tilde{J}'$ between $S=1/2$ spins. Though the later statement seems to be an overestimation since the next-nearest exchange in the undoped chain should be dominantly determined by the overlapping of the Ni^{2+} and O^{2-}orbitals, the joint contribution of the two mechanisms still does not account for the experimentally observed linewidths, which turn out to be as large as 515 mT

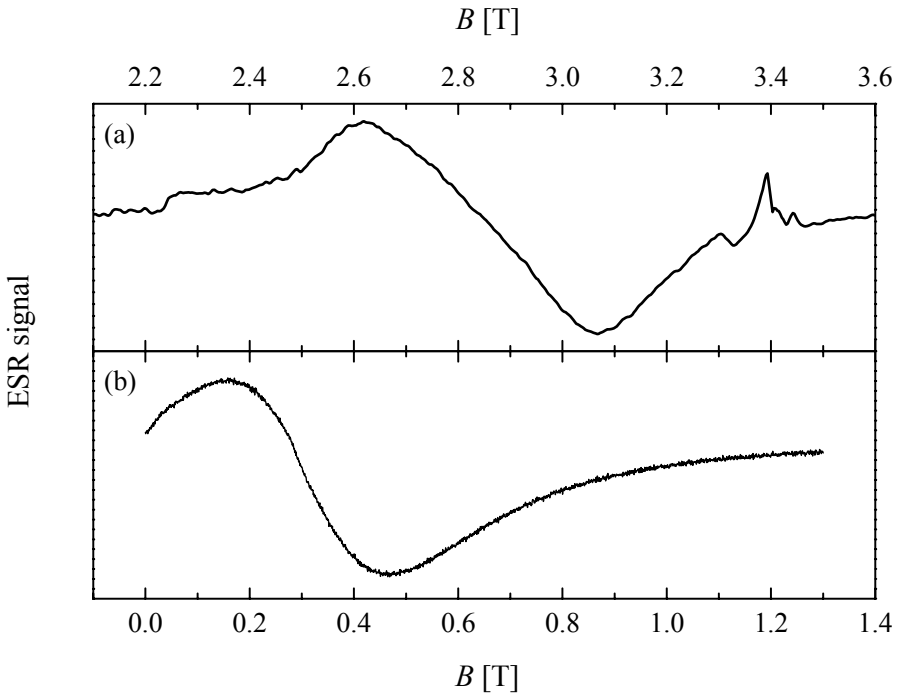

Fig. 3.10: A comparison of (a) the high-field (ν_L = 96 GHz) ESR spectrum with (b) the X-band spectrum (ν_L = 96 GHz) recorded at 5 K in the $PbNi_{1.85}Mg_{0.15}V_2O_8$ compound. Note that the magnetic field range is the same in both cases.

at 5 K in the case of the largest doping level (see Fig. 3.8). Moreover, the above estimations correspond to the static limit when the exchange narrowing due the spin fluctuations is disregarded.

Clearly, the presented simple picture does not offer a satisfactory explanation for the observed low-temperature ESR signal behavior, as the corresponding anisotropy contributions are not large enough. Second, the *J'* coupling is reported to be antiferromagnetic, which implies singlet ground state of the two liberated end-chain spins. Evidently, our experimental findings of the intensity of the low-temperature signal growing with the decreasing temperature are in a contradiction with this picture. There is, however, an additional binding mechanism coupling the two spins neighboring the spin vacancy site providing that also interchain coupling is present. Shender and Kivelson proposed the following mechanism for the doped Haldane system [38], which is schematically presented in Fig. 3.11. By virtue of the interchain exchange coupling the end-chain spin at one of the sites neighboring the impurity induces a "pocket" of staggered magnetization on the neighboring chain. This "pocket" couples again to the end-chain spin on the other side of the impurity-broken chain. This effective second order coupling is dependent on the number of the neighboring chains *Z*, the staggered "susceptibility" χ_π and the interchain exchange $J_\perp$ through the expression $J'_{eff} = Z\chi_\pi J_\perp^2$. It was initially proposed that such an effective coupling should be of a antiferromagnetic nature, however, Zheludov *et al*. [4]

argued that it should really be ferromagnetic as it is also obvious from our schematic picture. It should also be stresses that the end-chain $S = 1/2$ spins are delocalized staggered "pockets", which roughly extend ξ lattice sites away from the impurities, ξ being the correlation length. For clarity this delocalized nature of the impurity-liberated spins is not shown in Fig. 3.11. From the parameters obtained by inelastic neutron scattering experiments the effective ferromagnetic chain-end spin coupling was roughly estimated to be $J'_{eff} \approx 2\,\mathrm{K}$, which is of the same order as the next-nearest neighbor antiferromagnetic uniform-chain coupling.

Due to the semi-quantitative nature of this prediction and the errors of the inelastic neutron scattering parameters originating from the powder nature of the investigated samples [4] the effective exchange could have a rather different value. Our experimental low-temperature spectra of Mg-doped samples predict higher values of end-chain-spin exchange, which can be then the origin of appreciably larger magnetic anisotropy as given by Eq. (3.19). The exchange narrowing mechanism averages the contribution of such anisotropy term to the ESR linewidth at temperatures much higher than the critical ordering temperature due to rapid spin fluctuations. However, in the vicinity of the phase transition to the magnetically ordered state, occurring in our case around 3.5 K or below this temperature depending on the doping concentration, a critical slowing-down of spin fluctuations is expected. The theory of the critical ESR linewidth broadening was developed for the case of the single-ion anisotropy [39] and the dipolar anisotropy [40]. As explained in the subsection 2.1.6 the broadening of the resonance lines in the vicinity of the antiferromagnetic phase transition is a joined effect of the critical enhancement of the staggered spin correlations $\left\langle S^z_{\mathbf{q}_o} S^z_{-\mathbf{q}_o} \right\rangle$ corresponding to the wave vector in the center of the antiferromagnetic zone $\mathbf{q}_0$ (static effect) and the reduction of the relaxation rate $\Gamma(\mathbf{q}_0)$ of the fluctuations of staggered magnetization due to the increase of the average life time of the clusters of antiferromagnetically ordered spins (dynamic effect). In the close vicinity of the phase-transition temperature the antiferromagnetic mode dominates and dictates the linewidth [41]

$$\delta B \propto \frac{\left\langle S^z_{\mathbf{q}_o} S^z_{-\mathbf{q}_o} \right\rangle}{\Gamma(\mathbf{q}_0)} \xi^2 , \tag{3.20}$$

with ξ as the correlation length.

The low-temperature increase of the linewidth below 10 K in all the doped samples at first sight seems to correspond to critical slowing down of spin fluctuations just above the ordering temperature. Similarly, the low-temperature deviations of the *g*-factor from the free-electron value towards lower values correspond to a building-up of sizable internal magnetic fields [42]. However, such critical effects are usually expected to be observable only in the close vicinity of the phase transition $(T - T_N)/T_N \leq 0.1$. On the other hand, the low temperature increase of the linewidth and the shift of the *g*-factor towards lover values resemble the behavior

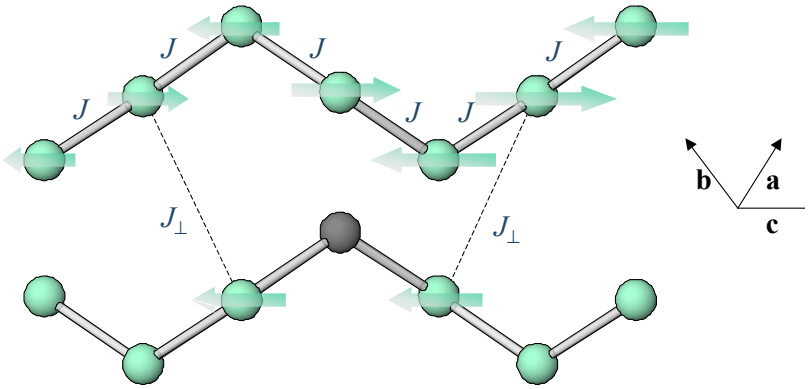

Fig. 3.11: Effective ferromagnetic coupling of the two S = 1/2 end-chain spins liberated next to the impurity site through the "pocket" of staggered magnetization induced on one of the neighboring chains. For clarity the delocalized nature of the end-chain spins is not shown.

happening in all the samples below 100 K. In that temperature region the observed dependence was successfully attributed to the presence of the single-ion anisotropy, which is as we have shown also the property of the paramagnetic centers active at low temperatures.

The consequence of the "pockets" of staggered magnetization on the chains neighboring the spin vacancy site is two fold [7]. First, they provide the basics for the coupling between the two liberated spins, and second, the ordered Ni^{2+} spins inside staggered magnetization also give rise to an effective dipolar interaction with the end-chain spins. This coupling has been estimated to have the value of approximately 130 mT [7] taking into account the exponentially decaying nature of the average spin moments with the distance from the impurity site within the staggered "pockets", which is an appreciable value, though still far to small to account for the experimental observations. The fact that the low-temperature linewidth increases with the level of doping implies that its nature cannot be entirely explained by the anisotropic interactions between the two liberated spins neighboring a particular impurity site (Eq. (3.19)). The comparison of the line broadening obtained from the ESR measurements at 5 K reveals that the linewidth increase is virtually linear as shown in the inset to Fig. 3.8a. Such a linear dependence has been attributed before to the coupling between the delocalized clusters of the end-chain spins [43]. Since each impurity induces end-chain spin clusters, which decay with the characteristic correlation length, the neighboring clusters between two consecutive impurities on a particular chain interact with each other. Apart from the effective single-ion anisotropy interaction given by Eq. (3.19) for each effective $S = 1$ impurity-induced spin originating from the two ferromagnetically coupled $S = 1/2$ end-chain spins, there is thus additional magnetic coupling between the effective $S = 1$ spins progressively getting larger with the doping level. The extrapolated zero-doping-level value of the linewidth at 5 K $\delta B_{pp}^{x=0} = 177\,\mathrm{mT}$ can thus be

assigned to be due to the intrinsic magnetic anisotropy of uncoupled effective $S = 1$ impurity-induced spin.

The temperature dependence of the intensity of the low-temperature ESR signal as presented in Fig. 3.9 can be interpreted in the light of cooperative three-dimensional phenomena resulting in the Curie-Weiss-like behavior,

$$I_{ESR} = \frac{C}{T - T_N}. \tag{3.21}$$

From Fig. 3.9b one can safely conclude that the agreement of the above model with the experiments is decent, especially for higher level of doping. The fitting parameters are collected in Table 3.1. The Néel temperature for all the samples was predetermined by the value of the phase-transition temperature obtained from the specific heat measurements [5].

Table 3.1: The fitting parameters of the Curie-Weiss law given by Eq. (3.21) corresponding to the low-temperature ESR signal in $PbNi_{2-x}Mg_xV_2O_8$. The constant C and the ratio C/x have arbitrary units.

x	0.04	0.08	0.10	0.12	0.15	0.24
T_N	2.5 K	3.0 K	3.3 K	3.4 K	3.5 K	3.4 K
C	4.7	9.0	13.5	15.2	18.9	27.4
C/x	118	113	135	127	126	114

The observed scaling of the constant C with the level of doping x as evident from the ratio C/x speaks in favor of liberated spins (strongly ferromagnetically coupled as we have discusses) being responsible for the occurrence of the low-temperature signal. However, apart from the thee-dimensional cooperative mechanism being responsible for the rapid decrease of the intensity of this signal with temperature another mechanism has been considered in literature to explain such behavior [44]. Namely, the coupling of the impurity-induced spins to the thermal excitations on the Haldane chains causes similar decay of the ESR signal. We have also considered this mechanism to explain out ESR experiment and have concluded that the agreement between the theory and the experiment is of about the same quality [7]. Thus it seems most probable that the low-temperature ESR intensity is determined by both the three-dimensional antiferromagnetic correlations and the one-dimensional thermal excitations on the chain.

Smirnov *et al*. argued in their ESR report [33] that the liberated spins should remain paramagnetic, i.e., are not coupled appreciably, at low temperatures, which is exactly opposite to our picture of strongly ferromagnetically coupled end-chain $S = 1/2$ spins. Their assumption

was based on their observation of the paramagnetic signal in doped samples just above the transition temperature, which showed no zero-field splitting. However, their absorption lines were considerably broad and also the powder nature should average out such features. In fact, a conformation consistent with our hypothesis came latter on by precise specific heat measurements performed by Masuda *et al*. [45]. They fitted the observed temperature dependence of the heat capacity to the Schottky-dependence and concluded that one spin vacancy effectively induces one $S = 1$ spin.

It should be also emphasized that in the mid-temperatures crossover regime a single almost Lorentzian resonance line is observed. This indicates that the end-chain spins are strongly coupled to the triplet Haldane excitations. Thus the one-dimensional excitations seem to coexist with the three-dimensional correlations emerging from the end-chain spins. The two other possibilities that either the Haldane excitations would destroy the staggered magnetization corresponding to the delocalized nature of the end-chain spins or that mobile excitations do not penetrate into these staggered structure of spins can be ruled out as also recently reported by Smirnov *et al.* [46].

Impurity Broadening of Ni^{2+} ESR Absorption Lines

Now, let us look back at the ESR spectra of $PbNi_{2-x}(Mg,Co)_xV_2O_8$ compounds recorded at room temperature and focus on their dependence on the level of doping. As evident from Fig. 3.12 both types of impurities, Mg^{2+} ($S = 0$) and Co ($S = 3/2$), cause line broadening with respect to the parent compound. The broadening initiated by vacancies is clearly present as the linewidth in the case of the highest doping level ($x = 0.24$) is by the factor of 1.22 higher than the linewidth in the undoped material. On the other hand, the effect of dopants having spin is much more drastic. Already at the doping level of $x = 0.08$ the spectrum is on the limit of observability in X-band and the linewidth is enlarged by a factor of approximately 2.5. Thus the extra broadening mechanism responsible for the observed effect has to incorporate the spin nature of the dopants.

As presented in Fig. 3.12a all room-temperature spectra could be satisfactory fitted by the "broad"-Lorentzian profile given by Eq. (3.1). However, a spurious narrow signal is present in several different samples at the position corresponding to the free-electron *g*-value. This later contribution to the ESR spectra does not show any consistency of changing with the level of doping or the spin nature of the dopants. On the contrary, it proves to be sample-dependent as the intensity of the narrow line varies from sample to sample within the same nominal stochiometry. For this reason it can be safely attributed to the presence of impurities in the

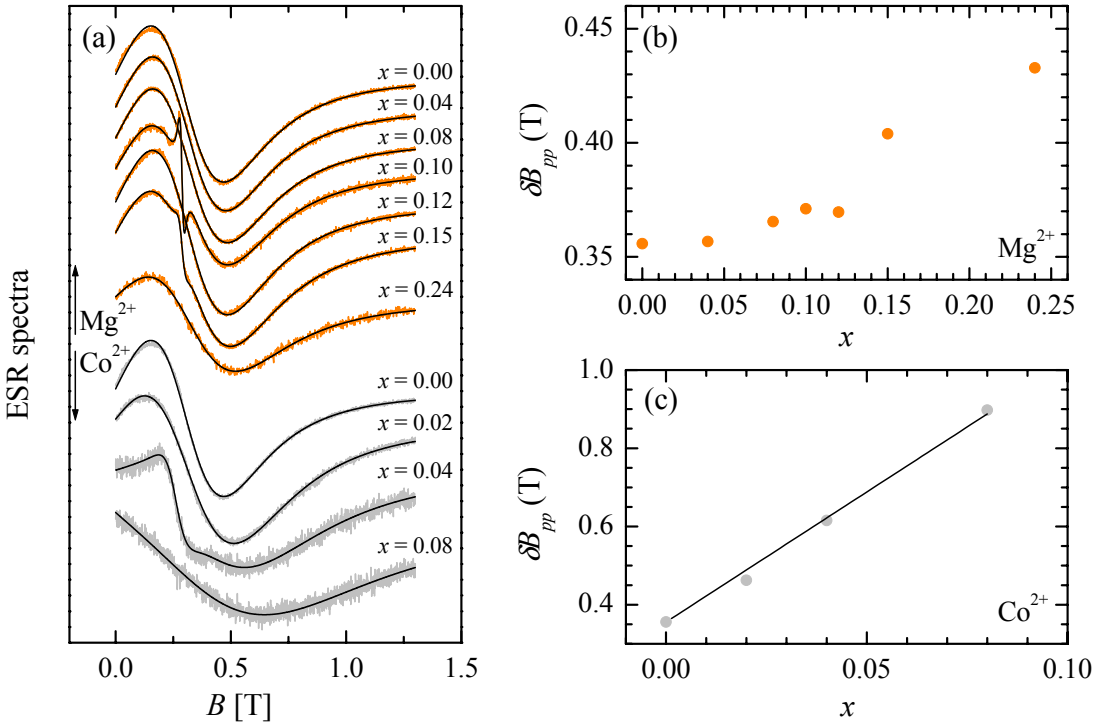

Fig. 3.12: (a) The evolution of X-band ESR spectra in $PbNi_{2-x}(Mg,Co)_xV_2O_8$ upon the level of doping recorded at room temperature, with black lines corresponding to "broad"-Lorentzian curves (Eq. (3.1)) with an additional narrow component where needed. The level of the impurity broadening is shown for (b) Mg^{2+} and (c) Co^{2+} impurities with the latter type causing linear increase of the observed linewidth.

sample. As the intensity of the narrow component does not exceed a percent of the total ESR intensity in any of the cases, such impurities are also invisible in x-ray diffraction patterns.

Let us begin with the case of the vacancy doping where the broadening effect is not that prominent. The introduced vacancies do not have any sizable effect on the crystal structure of the materials as evident from the detailed structural measurements [16, 23]. Since the single-ion anisotropy at Ni^{2+} sites as the dominant broadening mechanism depends on the local structure (predominantly of the NiO_6 octahedra), it can be assumed that it does not change much when dopants are introduced. If one supposed that the exchange coupling of the "boundary" $S = 1$ spins is greatly altered it would not be hard to imagine a possible mechanism leading to the doping-dependent linewidth. Namely, the recorded spectra are exchange narrowed, with the exchange constant entering the denominator of the expression for the expected linewidth (see Eq. (2.17)). If the vacancies decrease the average value of the exchange interaction sensed by Ni^{2+} spins this mechanism would lead to the broadening of the lines. In the extreme case when the exchange of the boundary Ni^{2+} spins with the neighboring impurity sites was completely diminished the average exchange would scale with $1-x/2$ leading in the case of $x = 0.24$ to an

enhancement of the linewidth by a factor of 1.13. As reported above, the measured broadening effect is rather more pronounced and second, there is no real background to send the exchange to zero. On the contrary, the overlap of the orbitals of the two ions is still present. However, the lack of one spin on one of the two interacting sites can have a pronounced effect, so that only a complete calculation based on atomic-orbital overlap can resolve the issue on to what extent the average exchange interaction is changed.

The changes of the average exchange probably cannot account for the experimentally observed broadening. Another mechanism, presumably being important in the case of one-dimensional magnetic systems, is the effect of the introduced impurities on the spin diffusion [47]. The diffusional decay of the spin correlation function can play a crucial role in determining the absorption spectrum in the low-dimensional systems where the exchange pathways are severely limited. The impurity introduced into a spin chain alters the diffusion rate along the chain, where the rate across the impurity site depends on the size of the impurity spin and the coupling of the end-chain spins to the impurity spin [48]. If the impurity is nonmagnetic the diffusion rate is greatly suppressed, which should cause appreciable broadening. However, in the case of the $PbNi_2V_2O_8$ system the interchain exchange is appreciable, which somewhat alleviates the intensity of the broadening effect and can legitimately account for out measurements.

When changing the impurity from Mg^{2+} to another spinless cation Zn^{2+} the characteristics of the low-temperature antiferromagnetic ordering do not change [49]. This fact indicates that the impurities are not directly involved in the formation of the long-range order in vacancy-doped $PbNi_2V_2O_8$. However, when the spinless dopant is exchanged with an impurity possessing a spin, the situation is radically changed. Namely, in the case of Cu^{2+} doping ($S = 1/2$) no phase transition could be detected down to 2 K for low doping concentrations [49], while Co^{2+} ($S = 3/2$) ions appreciably increase the phase-transition temperature, which rises to 7.2 K in the case of $PbNi_{1.92}Co_{0.08}V_2O_8$ [31].

Our ESR measurements also show a severe difference between the Mg- and the Co-doped case. The observed profiles can be described by single “broad”-Lorentzian line, which speaks in favor of strong exchange coupling of the two spin species. When a cobalt ion Co^{2+} ($3d^7$ configuration) is placed in an octahedral environment of cubic symmetry the lowest lying orbital state stays triply degenerated even after the spin-orbit coupling is introduced. A small distortion of the cubic symmetry of the ligands, as in our case, splits this ground-state degeneracy. However, a considerable orbital character is expected to remain in the orbital ground state. For instance, if a Co^{2+} ion is octahedrally surrounded by ligands producing crystal field of cubic symmetry the *g*-factor is isotropic but significantly shifted with respect to the free-electron value, i.e., $g = 4.3$ [13]. The *g*-factor tensor becomes anisotropic when the local symmetry is lowered, however, the mean *g*-factor remains around the above value. In our case

there is no evidence of a spectral component present at such a high value of the *g*-factor. We can thus conclude that the observed signal in the $PbNi_{2-x}Co_xV_2O_8$ compounds is due to Ni^{2+} ions.

The extreme broadening of the ESR spectra due to the presence of a small concentration of Co^{2+} impurities has been reported before in several different systems [32, 50]. The presence of strong spin-orbit coupling in Co^{2+} ions results in this ion being a fast relaxing one. The phonons, which modulate the local crystal fields, cause rapid spin-lattice relaxation of the non-Boltzman Co^{2+} spin density. The spin lattice relaxation time can be of the order of 10^{-12} s at room temperature [32]. The extreme broadening can be then attributed to the Co-Ni exchange J^* combined with the Co^{2+} spin-lattice relaxation. The effect of the cobalt impurity on the linewidth is determined by the relative rate at which the magnetic energy flows from the host system to the impurity system with respect to the rate for the energy flow between the impurity system and the lattice. The expected linewidth is then expressed by the equation [32]

$$\delta B = \delta B_0 + \frac{\eta}{1-\eta}\delta B_{imp}\,, \tag{3.22}$$

where δB_0 and δB_{imp} correspond to the linewidth of the pure system and the contribution of the dopant, respectively, while η represent the ratio between the rate of the impurity's spin-lattice relaxation and the host-impurity energy transfer rate determined by the exchange coupling of the two spin species. When the spin lattice relaxation is slow compared to the characteristic time of the exchange the "bottleneck effect" is present. Therefore, a spin-lattice relaxation rate of the same order as the host-impurity exchange rate is required before relaxation effects significantly broaden the resonance.

The comparison of the temperature evolution of the ESR linewidths in the parent and the Co-doped material with the lowest impurity concentration (x = 0.02) is presented in Fig. 3.13. This level of doping turns out to be the only one that offers traceable ESR signals in the X-band. As clearly illustrated in the inset of this figure, the difference between the linewidth of the doped and the parent samples grows with temperature up to around 150 K. Above the latter temperature it approximately settles at around $\delta B_{imp} \approx 120\,\mathrm{mT}$. The small downturn at higher temperatures will be discussed later. The spin-lattice relaxation rate of the Co^{2+} impurities is temperature dependent, due to the changes of the phonon density with the temperature. It increases with increasing temperature and is in our case approximately of the same order as the host-impurity spin correlation time around 55 K (see Fig. 3.13), which seems to correspond to a mid-temperature point between the "bottleneck" regime and the strong-impurity-relaxation regime. Spin-lattice relaxation is expected to be due to Raman two-phonon processes and can be written as [51]

$$\frac{1}{T_1} = a\left(\frac{T}{\theta_D}\right)^7 \int_0^{\theta_D/T} \frac{x^6\, \mathrm{e}^x \mathrm{d}x}{\left(e^x - 1\right)^2}\,. \tag{3.23}$$

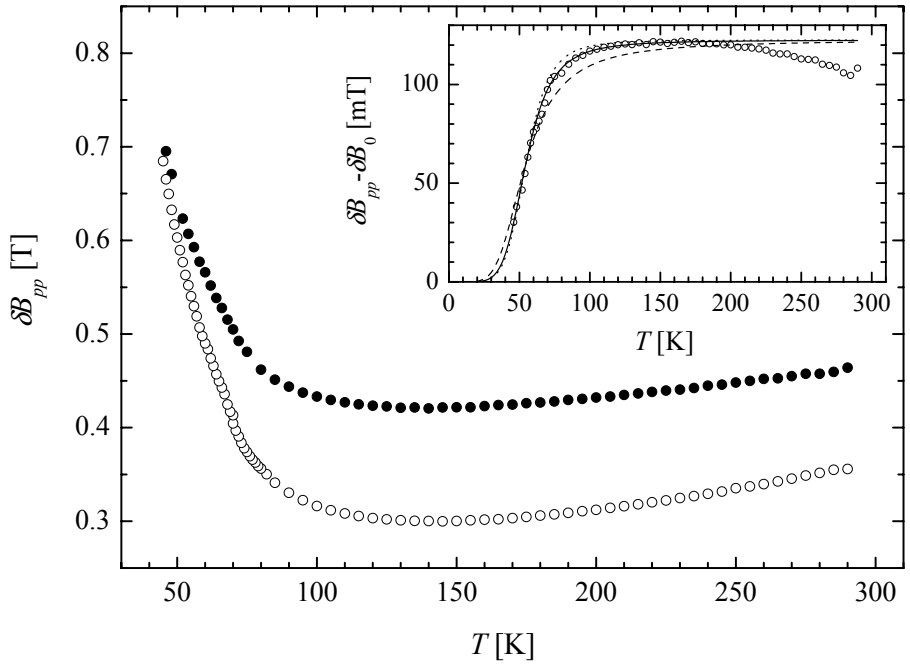

Fig. 3.13: A comparison of the temperature-dependent ESR linewidth in the parent $PbNi_2V_2O_8$ (○) and $PbNi_{1.98}Co_{0.02}V_2O_8$ (●) compounds. The inset shows a bottleneck-type of the difference between the linewidth of the two materials explained by rapid spin-lattice relaxation of Co^{2+} ions. The lines represent the predicted curves for the Debye temperature values of $\theta_D = 300$ K (**--**), $\theta_D = 500$ K (**—**) and $\theta_D = 700$ K (····).

Here θ_D stands for the Debye temperature in the Debye model of the phonon spectrum [52], the parameter x is defined as $x = \hbar\omega / k_B T$ and the constant a depends on the strength of the spin-phonon coupling. Both of the constants are not known, however, the latter one does not occur in the expression for the expected linewidth (Eq. (3.22)) if we set $\eta(55\,\mathrm{K}) = 1$ as the experimental impurity broadening reaches half of the saturated value at the temperature of 55 K (see inset to Fig. 3.13). In this case the temperature-dependent ratio of the impurity spin-lattice relaxation rate to the host-impurity exchange relaxation rate can be expresses as

$$\eta(T) = \frac{T_1(55\,\mathrm{K})}{T_1(T)}. \tag{3.24}$$

The fit of the model described through the Eqs. (3.22)-(3.24) with the experimental impurity-dependent linewidth for the $PbNi_{1.98}Co_{0.02}V_2O_8$ compound is shown in the inset to Fig. 3.13. The best agreement is reached when the Debye temperature is set to $\theta_D = 500$ K (solid line). This is, in fact, the only free parameter of the model if the saturated value of the impurity-induced linewidth is taken as $\delta B_{imp} = 120$ mT, which seems to correspond to the experimental behavior most accurately. The obtained Debye temperature has a reasonable value. However, to see the real effect of this parameter on the temperature dependence of the impurity-induced broadening,

the corresponding curve is compared with the curves obtained for somewhat different values of the parameter θ_D; $\theta_D = 300\,\mathrm{K}$ (dashed line) and $\theta_D = 700\,\mathrm{K}$ (doted line) in the inset of Fig. 3.13b. As evident the slope of these curves depends on the Debye temperature considerably, which allows us to make a final estimation of this parameter in the $PbNi_2V_2O_8$ system, $\theta_D = 500(50)\,\mathrm{K}$. Unfortunately, no other measurement yielding the Debye temperature of the investigated system has been reported yet, which leaves us with no reference. However, as already mentioned the obtained Debye temperature has a reasonable value, which further supports the otherwise very pleasing agreement between the experiment and the theory.

The temperature dependence of the impurity-induced contribution to the ESR linewidth seems ho have a maximum around 150 K, which contradicts the model prediction of the monotonic dependence. A possible scenario would be that the presence of the impurities possessing spin alters the decay of the spin correlation function of the Ni^{2+} system due to the coupling of the host spins with the impurity spins. As latter spins are strongly coupled to the lattice they effectively act as sinks for the transfer of the magnetic energy from the spin to the lattice system. The resulting rapid decay of nonequilibrium spin density at the impurity sites can significantly change the development of the short-range spin correlations.

The saturated impurity-induced contribution to the host-spin ESR linewidth obtained from the above fitting procedure, $\delta B_{imp} = 120\,\mathrm{mT}$, can be also theoretically described. In the limit when the isotropic exchange between the impurity and the host spins is considered as the leading impurity-host interaction, this contribution to the linewidth has the following form in the limit of infinite temperature [50]

$$\delta B_{imp} \approx \frac{1}{\sqrt{3}} \frac{32}{g\mu_B} \frac{\left(J^*\right)^2 S^*\left(S^*+1\right)}{3\hbar\omega_e} \frac{x}{2}, \tag{3.25}$$

where S^* represent the size of the impurity spin. In the above expression the characteristic exchange frequency governing the decay of the host-spin relaxation function should be determined by the value of the host-host exchange, $\omega_e = \sqrt{2J^2 Z' S(S+1)/3\hbar^2}$. The resulting host-impurity exchange coupling is then evaluated from the experimental parameters to be $J^* = k_B \cdot 11\,\mathrm{K}$, a value an order of magnitude below the Ni-intrachain exchange. The cobalt spin-lattice relaxation time, which is approximately equal to the impurity-host spin correlation time around 55 K, is thus of the order of $5 \cdot 10^{-12}$ s at this temperature.

It is also worth emphasizing that Eq. (3.25) yields a linear dependence of the ESR linewidth increase upon the doping concentration. This fact is clearly manifested in the case of $PbNi_{2-x}Co_xV_2O_8$ compounds as apparent from Fig. 3.12c. Second, we argued above that the observed ESR signal corresponds to the Ni^{2+} spins as only a single Lorentzian line is observed. This argument can now be endorsed by the rapid spin-lattice relaxation of the single-ion Co^{2+} impurities, which enormously broadens the signal of the Co^{2+} spin system.

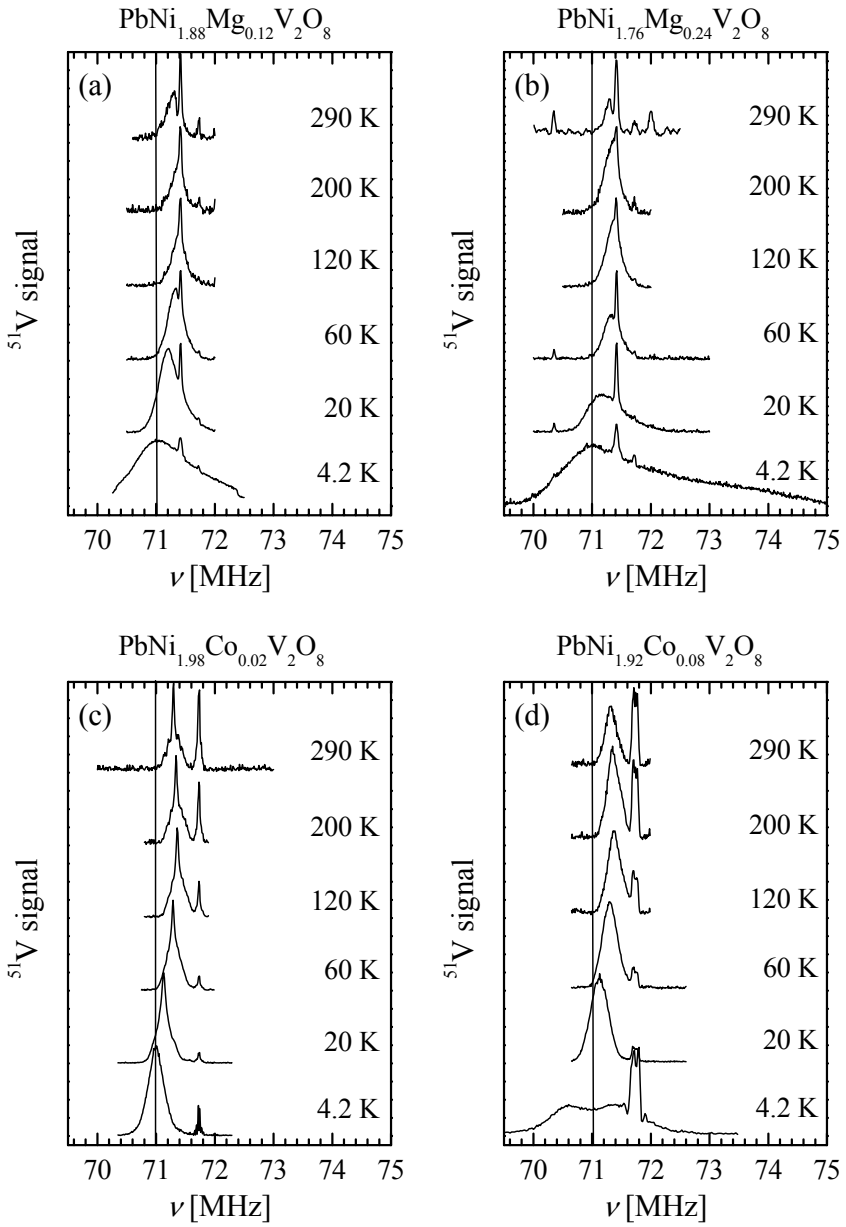

Fig. 3.14: ^{51}V NMR spectra at selected temperatures in (a) $PbNi_{1.88}Mg_{0.12}V_2O_8$, (b) $PbNi_{1.76}Mg_{0.24}V_2O_8$, (c) $PbNi_{1.98}Co_{0.02}V_2O_8$, and (d) $PbNi_{1.92}Co_{0.08}V_2O_8$ with the vertical line corresponding to the line position of the parent material at 4.2 K.

3.3.2 Competition of 1D and 3D Spin Correlations as Revealed by NMR

The difference of the outcome of the ^{51}V NMR measurements performed on the pristine $PbNi_2V_2O_8$ sample and the (Mg,Co)-doped samples is quite intriguing. As in ESR experiments also in NMR the nature of the doping ion seems to play an important role in the development of the low-temperature absorption spectra.

At high temperatures with respect to the value of the isotropic exchange J all the measured spectra are qualitatively similar to the undoped case as can be verified by comparing Fig. 3.14 and Fig. 3.6a. There is, however, an additional narrow component present in both Mg-doped samples. The nature of this queer feature was initially argued to be possibly intrinsic to the system [9]. However, it is probably due to a small amount of a different phase or due to impurities as also observed by ESR in these samples. Due to the fact that the intensity of the narrow component is small compared to the broad component, it will be neglected in what follows.

Obviously, the exchange-narrowing mechanism, which is effective in the case of the undoped sample, has a major role also in the doped samples. When decreasing the temperature, in contrast, a pronounced distinction of NMR spectra in different samples is found. The ^{51}V spectra become broader compared to the undoped case. In addition to the temperature dependence the degree of broadening is dopant dependent as well as it depends on the level of doping. Furthermore, the broadening of the Co-doped samples seems to result in symmetrical lineshapes at low temperatures in a striking contrast to the Mg-doped samples, which exhibit lineshapes of pronounced anisotropy at very low temperatures. This fact indicates that the character of the spin-correlation functions is essentially different when Mg^{2+} is replaced by Co^{2+} as will be further elucidated below. This fact may well be responsible for the enhancement of the Néel temperature in cobalt-doped samples.

Coupling of ^{51}V Nuclei to Electronic System

First, let us focus on the first moment (M_1) of the measured NMR absorption lines. Fig. 3.15a demonstrates that dissimilarity in the temperature evolution of this parameter in Mg-doped samples exists with respect to the undoped compound below approximately 120 K. The monotonic decrease of M_1 in the pristine sample can be, as already emphasized, related to the spin-gap character of the Haldane state. However, both Mg-doped samples exhibit a minimum of the first moment, occurring at 7 K and at 14 K in the $PbNi_{1.88}Mg_{0.12}V_2O_8$ and $PbNi_{1.76}Mg_{0.24}V_2O_8$ samples, respectively. The trend above the minima can be assigned to the presence of 1D excitation, which survive down to very low temperatures also in doped samples. The observed reverse in the behavior of the center position below the minima suggests that 3D spin correlations become substantial, which can be understood as a precursor effect due to the vicinity of the phase-transition temperature. Such behavior is in accordance with the ESR results presented in the previous subsection, where it was shown that both kinds of magnetic excitations seem to coexist in the “mid-temperature” range. The observed evolution of M_1 in Mg-doped compounds, however, somewhat defers from the temperature dependence of the

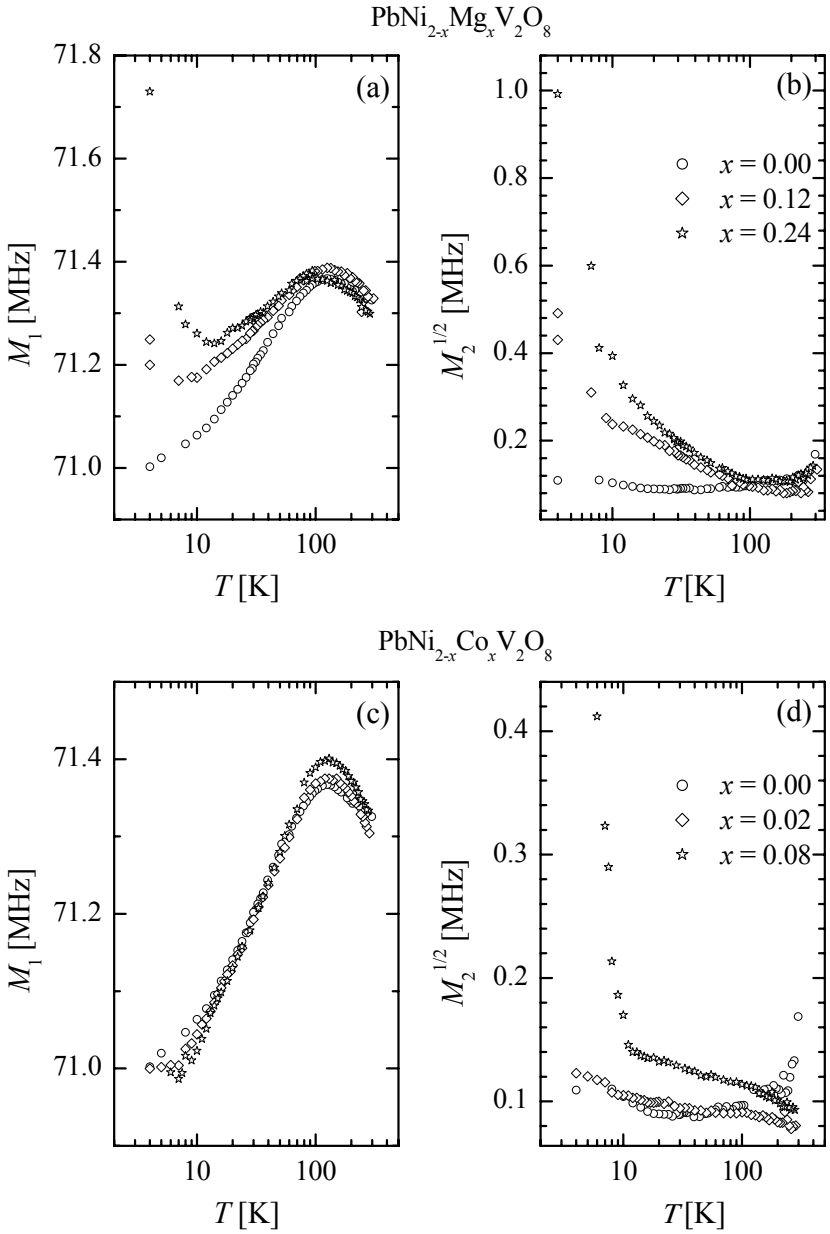

Fig. 3.15: The temperature dependence of (a) the first and (b) the square root of the second moment of the ^{51}V NMR spectra in $PbNi_{2-x}Mg_xV_2O_8$ compounds as well as (c) the first and (d) the second moment in the case of $PbNi_{2-x}Co_xV_2O_8$ compounds.

magnetic susceptibility in these samples at low temperatures [1]. Susceptibility of the $PbNi_{1.76}Mg_{0.24}V_2O_8$ sample, for instance, shows a monotonic increase with decreasing temperature with the value corresponding to 4.2 K being around 6-times greater that the room-temperature value.

One has to bear in mind that measuring magnetic moment corresponds to a static response, while the NMR spectra reflect also the dynamical aspect of the electronic spin

correlations. Thus dissimilarities are expected to set in especially near the phase transitions, where the slower decay of the electron spin-correlation functions significantly affects the appearance of the NMR spectra [53]. Second, it has to be stressed that the magnetic susceptibility measurements were performed in a low magnetic field of 0.1 T while the resonant field in the NMR experiments is much higher ($B_0 = 6.34\,\mathrm{T}$). It turns out, as will be discussed below, that external magnetic field of the order of several tesla significantly alters the nature of spin ordering in doped samples. For the above-mentioned reasons it is not surprising that NMR center position deviates from the dependence expected purely on basis of the magnetic susceptibility.

On the contrary to the Mg-doped samples, in Co-doped samples the agreement between M_1 (Fig. 3.15c) and the spin susceptibility [31] is much better. However, as both the Mg-doped and the Co-doped compounds undergo a magnetic phase transition to reportedly the antiferromagnetic ground state [1, 23, 31], the apparently dissimilar behavior is rather surprising. Moreover, the low-temperature ^{51}V NMR spectra belonging to the two different dopants are radically different indicating that the spin correlations evolve in much different manner in the two families of materials. In Fig. 3.15b and 3.15d the analysis of associated second moment is presented for the Mg-doped and Co-doped systems, respectively. The relative changes of the linewidth are much more drastic in the case of vacancy doping, though, it has to be emphasized that the concentrations of magnesium as a dopant are higher than the concentration of cobalt.

Magnetic-Ordering Effects Reflected in NMR Spectra of Mg-Doped Compounds

The temperature evolution of the second moment shows a drastic dependence on the level of Mg impurities, an effect again evidently expressed below approximately 120 K. While in the pure sample this parameter is virtually temperature independent, in both Mg-doped samples the increase of the linewidth below this temperature is substantial. Additionally, the absorption spectra experience also a qualitative change from the high-temperature symmetric to a low-temperatures asymmetric powder-like lineshape. In the vicinity of the phase-transition point the strength of the exchange narrowing mechanism must be significantly suppressed with respect to the parent material, which would correspond to slowing-down of electronic spin fluctuations. More precisely, the typical correlation time of spin fluctuations must become comparable with the time-scale of the NMR spin-spin relaxation. Large increase of the linewidth thus again suggests on the development of 3D spin correlations in doped samples as explained below. In principle, there are, however, different possible mechanisms, which could lead to the observed anisotropy of absorption spectra.

The expected temperature variation of the lineshape can be predicted from the known structure of the material and a presumed spin arrangement. In this context it is instructive to first model the NMR lineshapes and calculate the corresponding linewidth for various possible kinds of interactions of vanadium nuclei with the electronic system in a static limit, which should apply for the spin-ordered state. Second, the spin impurities either of a spinless nature or not introduce inhomogeneities into the system. However, as our samples are "solid solutions" the impurities are randomly distributed, which seems as the major obstacle for theoretical calculations of the NMR spectra. Since the impurities are in average relatively far away (in the case of the highest Mg doping level there is in average seven Ni^{2+} sites between consecutive impurity sites), let us first treat the spin chains as uniform. This approximation can be made in NMR in a contrast to the low-temperature ESR measurements since the NMR detects an average signal of all the vanadium nuclei while the ESR measures only the end-chain spin clusters at low temperatures.

The dipolar coupling of a particular ^{51}V nucleus with surrounding paramagnetic moments is the first suitable candidate for describing the low-temperature lineshape evolution. For the paramagnetic phase it was already shown (Eq. (3.13) and the discussion below it) that the contribution of the dipolar coupling between a particular vanadium nucleus and surrounding paramagnetic moments is negligible, $\delta\nu \approx 15\,\mathrm{kHz}$, compared to the observed line-broadening even if one supposes an unrealistic completely ferromagnetic arrangement of paramagnetic centers. However, in the case of the antiferromagnetic transition the wave-vector-dependent susceptibility corresponding to the center of the antiferromagnetic zone is expected to diverge and second, the fluctuations within the emerging clusters are supposed to slow-down. Both of the spin-ordering effects can of course have a radical effect on the NMR absorption profiles [53]. For this reason the antiferromagnetic ordering of spin moments should be of particular interest as the doped systems encounter a transition to antiferromagnetically ordered state at low temperatures. This situation will be in fact considered below in the relation to the case of Co-doping, where it will be shown that frequency shifts of maximum 0.5 MHz are expected for the ordered phase. However, in the case of magnesium as the dopant it is not of an actual interest in as high magnetic fields as we use in our NMR experiments.

It has been experimentally verified by different techniques that the application of relatively small magnetic fields changes the magnetic ground state and that the antiferromagnetically ordered state is not the ground state anymore. By measuring the heat-capacity temperature dependence in the magnetic field and the magnetization curves Masuda *et al*. [45] accomplished that for the cases of low doping concentrations ($x \leq 0.04$), the critical field, which destroys the antiferromagnetic spin arrangement in favor of the paramagnetic one, does not exceed 3-4 T. Additionally, Lappas *et al*. [23] draw a similar conclusion for the case of high doping level ($x = 24$) based on the behavior of the static as well as the dynamic

susceptibility. The changes in the susceptibility show that below the phase-transition temperature the antiferromagnetic character of spin correlations is significantly reduced in the presence of a relatively low external magnetic field while ferromagnetic correlations are enhanced. This phenomenon was attributed to the metamagnetism of the investigated material, which is characteristic for magnetic materials with a strong easy axis anisotropy [54]. In such systems the phase transition to the paramagnetic state can be characterized by simple reversal of the local spin directions. The strong anisotropy prevents the spins from rotating away from the easy axis, as is the usual case for the spin-flop systems with only small amount of magnetic anisotropy. In the case of the $PbNi_{1.76}Mg_{0.24}V_2O_8$ compound the critical magnetic field driving the system from the antiferromagnetic state to the paramagnetic state is only slightly above 1 T at zero temperature and decreases towards zero when approaching the transition temperature from below.

Next, we consider the transferred hyperfine interaction. If we assume that the isotropic hyperfine coupling constants of each vanadium nucleus with the six nearest Ni^{2+} paramagnetic moments have the same value, this interaction would effectively cancel out in the antiferromagnetically ordered state, since the vanadium ion is coupled to four spins on one chain and two spins on the neighboring chain. Moreover, the variation of the Ni-V distances and Ni-O-V angles is not appreciable [16] indicating that all the six isotropic hyperfine coupling constants should be more or less identical. However, as discussed in the previous paragraph, the ferromagnetic spin correlations should be characteristic for the $PbNi_{1.76}Mg_{0.24}V_2O_8$ system in the experimental magnetic field of 6.34 T when lowering the temperature. Such correlations dominantly enhanced in the direction of the easy axis, produce large frequency shifts of maximal $\delta\nu^{iso} = 21\,\mathrm{MHz}$ (see subsection 3.2.2) when the easy axis lies parallel to the external magnetic field. In the general case of the magnetic easy axis making an angle θ with the direction of the magnetic field the expected NMR line would lie at the frequency $\nu = \nu_0 + \delta\nu^{iso}\cos\theta$. In the case of the uniformly distributed powder sample the corresponding lineshape is box-shaped since the probability of the external magnetic field making the angle θ with respect to the direction of the dipolar field is proportional to $\cos\theta$. The profile will remain symmetric even if the distribution of the polar angles θ is not uniform. If we now take into account also the impurities, this additional variable breaks the homogeneity of the Ni^{2+} spin chains. However, due to the powder nature of the sample, the corresponding NMR absorption line should stay symmetric.

On the other hand, also the anisotropic part of the transferred hyperfine coupling should be appreciable. Although the "contact" of the *p* electrons with the vanadium nucleus is some 15-times weaker than the *s*-electron one as calculated in subsection 3.2.2, the former orbitals extend much further away from the nucleus. Consequently, one would expect them to considerably mix with the oxygen-bridge orbitals causing also a sizable *p*-orbital covalency effect. As the

anisotropic interaction originating from *p* electrons exhibits a typical $\left(3\cos^2\theta_i - 1\right)$-type of anisotropy with θ_i denoting the angle between the axis of the *p* orbital and the *i*-th principal axis of the hyperfine tensor [55], the experimental uniaxial-type anisotropic absorption spectrum is expected. The center of the theoretical spectrum originating from the *p*-electron covalency effect is, however, not shifted, which is why we attribute the temperature shift of the first moment of the experimental spectra at lower temperatures to the isotropic part of the hyperfine coupling tensor. The scaling of this shift together with the scaling of the linewidth with the level of doping thus seem to correspond to increasing ferromagnetic correlations in the direction of the easy axis at low temperatures.

Unfortunately, the above consideration can not go beyond mere speculations since we are dealing with a rather complicated system in the sense of the magnetism, which is additionally inhomogeneous and even more tragically no single crystal are obtainable. It may well be that the electron correlations characteristic for the metamagnetic phase are much more complicated and possibly influenced by some other electron-electron anisotropic interactions like the Dzyaloshinsky-Moriya interaction in addition to the crystal-field anisotropy.

Phase Transition in Co-Doped Compounds

Contrary to the magnesium case the NMR spectra of the Co-doped compounds show much more moderate behavior when approaching the phase transition. The spectra are significantly less broadened (see Fig. 3.15) and remain symmetric even in the close vicinity of the phase-transition temperature. In addition, due to the fact that $PbNi_{1.92}Co_{0.08}V_2O_8$ shows a transition to the magnetically ordered state already at $T_N = 7.17\,\mathrm{K}$, we were able to inspect also the transition point. An interesting feature of the ^{51}V NMR absorption lines below the transition temperature is that they split into a doublet, which is symmetrically positioned around the frequency of 71 MHz as shown in Fig. 3.16a. The peak-to-peak linewidth acts as an order parameter as evident from Fig. 3.16b. However, the relatively broad absorption peaks prevent us to accurately determine this splitting in the close vicinity of the phase transition point making the analysis of the corresponding critical exponent practically impossible. Thus it looks like the vanadium nuclei are sensing the two sublattice magnetizations consistent with the antiferromagnetic nature of the ground state.

In the light of the experimental facts given above for the Mg-doped samples the antiferromagnetic order at 6.34 T would look unrealistic. However, the magnetizations versus magnetic field measurement on the $PbNi_{1.92}Co_{0.08}V_2O_8$ sample significantly differ from the Mg-doped cases. It seems that in Co-doped materials the magnetic order is more sustainable than in Mg-doped compounds. Namely, there is no hump in the magnetization curve of

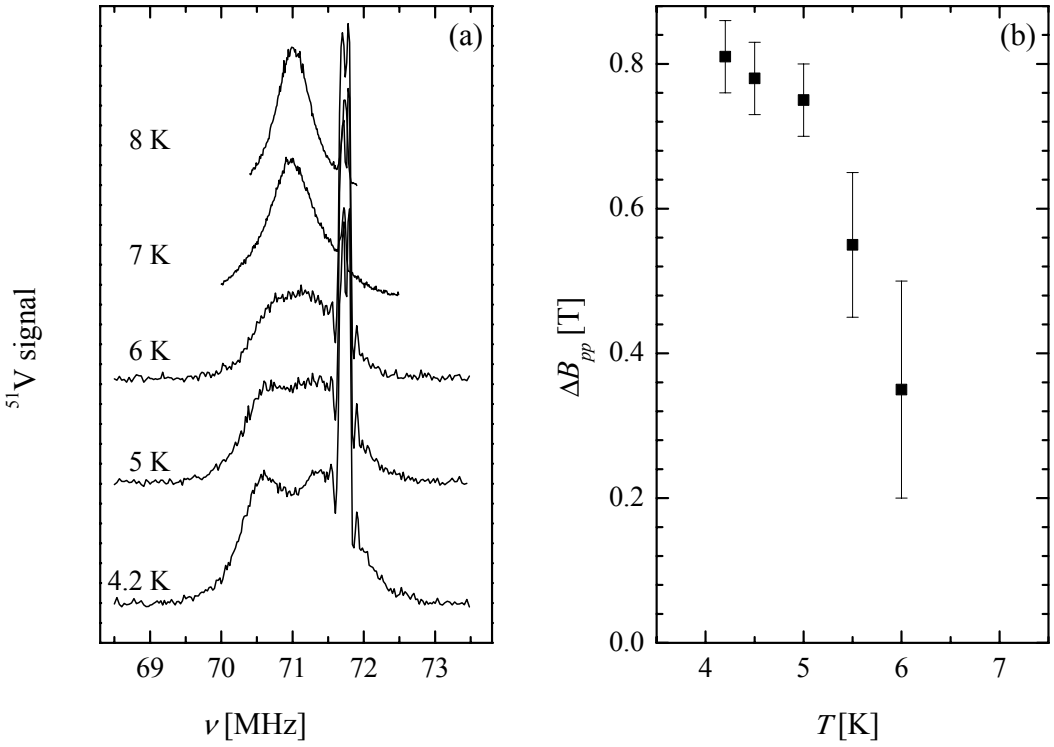

Fig. 3.16: (a) Low-temperature ^{51}V NMR absorption spectra of $PbNi_{1.92}Co_{0.08}V_2O_8$ near the phase-transition temperature of 7.17 K. (b) The evolution of the peak-to-peak NMR linewidth representing an order parameter.

$PbNi_{1.92}Co_{0.08}V_2O_8$ characteristic of the braking of the antiferromagnetic order up to the value of the magnetic field that we use, contrary to the magnesium family [45]. For this reason the antiferromagnetic order of spins should be considered when calculating the lineshape near or below the phase transition.

The expected NMR frequency shift for the vanadium nuclei at site *i* in the magnetically ordered state is in principle determined by the transferred hyperfine coupling and the dipolar coupling of the ^{51}V nuclei with the six surrounding Ni^{2+} ordered magnetic moments,

$$\Delta\nu_i = \frac{1}{h}\sum_j \tilde{A}_{i,j}^{iso}\cos\theta\langle S_j\rangle + \frac{1}{h}\sum_j \left(\underline{\tilde{\mathbf{A}}}_{i,j}^{an}\cdot\langle\mathbf{S}_j\rangle\right)_z + \Delta\nu^d\cos\theta' . \tag{3.26}$$

The first term corresponds to the isotropic hyperfine shift where θ is the angle between the external magnetic field (*z* direction) and the direction of spin orientation. The anisotropic transferred hyperfine tensor in the second term is written in the laboratory frame with *z* as the direction of the external magnetic field and the last term indicates the frequency shift due to dipolar field pointing at angle θ' with respect to the external magnetic field. If the spin chain were again considered as uniform the isotropic hyperfine interaction would vanish as discussed above. In clear contrast to the case of the Mg-doped samples, this is consistent with the first

moment of the resonant spectra in Co-doped samples exhibiting the activation dependence similar to the parent material. Unfortunately, we cannot make the same statement about the anisotropic part, since the pathways of the six V-Ni bonds are rather complicated. To draw a firm conclusion one would have to know the exact form of the anisotropic hyperfine tensor. However, as the experimental spectra do not show any significant anisotropy above the phase-transition temperature, also this contribution must cancel out. The next possible interaction is the dipolar magnetic coupling. While the true antiferromagnetic ground state is a complicated (not classically imaginative) spin arrangement, our basic approximation will be the classical Néel state with the coupled spins pointing in the opposite direction and aligned parallel to the crystal *c* axis. Such a state with the spins on neighboring chains with the same *c* axis fractional cell coordinate coupled antiferromagnetically, gives the best explanation for the purely magnetic neutron diffraction pattern observed in the ordered phase in both the Mg- and Co-doped materials [23, 31] and is consistent with the interchain exchange being ferromagnetic. This is because the interchain interaction was assumed to couple the two nearest neighbors in adjacent chains, which are in fact displaced by *c*/4 along the *c*-direction [3]. The anisotropy field due to the dipolar interaction can again be calculated from the known crystal structure.

With the above-proposed spin arrangement the dipolar field sensed by the vanadium nuclei has appreciably larger values than for the paramagnetic spin arrangement. For the nucleus at position $r = (0.5819a, 0.2641a, 0.2984c)$ it is given by

$$\mathbf{B}_i^d = -\frac{1}{\gamma\hbar}\sum_j \mathbf{A}_{ij}^{AFM} \cdot \langle \mathbf{S}_j \rangle = \tilde{\mu}(-41, -5.6, 6.1)[\mathrm{mT}]. \tag{3.27}$$

The maximum frequency shift, corresponding to the external magnetic field applied parallel to the internal dipolar field is thus of the order of $|\Delta\nu^d| \approx 470\,\mathrm{kHz}$, where the estimated average value of $\langle\mu\rangle \approx \mu_B$ corresponding to the antiferromagnetically ordered state was used [31]. Such an experimentally deduced reduction of the average Ni^{2+} magnetic moment with respect to the spin only value $2.8\mu_B$ has been argued by Lappas *et al*. [23] to possibly arise from at least two different origins, the first one being low-dimensional "zero point" fluctuations and the second one the nickel-oxygen covalency effect. This observation is in accord with the remarks presented in subsection 3.2.1, where the magnetic anisotropy including the crystal field and the Dzyaloshinsky-Moriya interaction was argued to lead to canting of spins from the direction of the spin chains. The above expression for the local field at a particular ^{51}V nucleus due to dipolar interaction with antiferromagnetically ordered paramagnetic Ni^{2+} ions has been calculated by taking into account "all" the neighbors of the chosen ^{51}V nucleus within the several prime cells away. However, this time the appearance of the dipolar field does not critically depend on the number of considered neighbors as it does in the paramagnetic phase (see the explanation below Eq. (3.13)). It has to be noted that the dipolar field vector (Eq. 3.27)

is directly applicable only for the ^{51}V site, for which it was calculated. But since all the sites are crystallographically equivalent, changing position to different vanadium sites, in effect, only exchanges the components of this vector and possible their sign. If has been also numerically verified that this is indeed the case and, moreover, the *c* component is within the sign equal for all vanadium nuclei within the prime cell as can also be expected in the first place. That is to say, a general V^{5+} position within the prime cell can be generated with the use of four-fold screw-axis symmetry operator lying along the crystal *c*-direction.

If the isotropic distribution of the angle values is assumed corresponding to the powder nature of the sample, the predicted lineshape will be of box shape. Due to homogeneous linewidth broadening it would be, however a bit rounded with the distance between the two shoulders roughly given by $\Delta\nu_i = 2\left|\Delta\nu^d\right| = 0.95\,\mathrm{MHz}$. This value satisfactory corresponds to the peak-to-peak linewidth observed in the ordered state of the $PbNi_{1.92}Co_{0.08}V_2O_8$ system (Fig. 3.16b), which is though a bit smaller due to strong homogeneous line broadening.

However, the apparent discrepancy of the observed spectrum and the one predicted from the above-presented model is the presence of an unexpected central dip in the experimental line. The inhomogeneity of the system due to spin vacancies cannot account for this feature due to the fact that the powder spectrum corresponding to a distribution of the dipolar fields rather looks like a bell-like profile. Such a double-peaked spectrum could, however, correspond to canting of Ni^{2+} spins away from the crystal *c* direction. It is most likely, that the average spins have also a nonzero component within the *ab* crystal plane, due to local crystal field symmetry and the Dzyaloshinsky-Moriya interaction favoring perpendicular arrangement of interacting spins. In addition, this would explain the reduction of the average nickel momentum in the ordered state from $2.8\mu_B$ to approximately μ_B as observed by neutron scattering [23, 31].

As in the case of Mg-doping there are too many noncontrollable variables in the system to draw a definite conclusion about which of the possible interactions is the most influential at low temperatures. However, there is unambiguously a drastic difference between the development of the spin correlations in the vacancy-doped and spin-doped $PbNi_2V_2O_8$ system. This point can be further examined by comparison of the spin-lattice relaxation in these compounds.

Spin-Lattice Relaxation

To get further insight into the development of the low-temperature spin correlations we measured also the ^{51}V spin-lattice relaxation time using the saturation-recovery method in the parent as well as in doped compounds. As expected the room-temperature value of this parameter $T_1^{RT} = 1.7\,\mathrm{ms}$ proved to be sample independent, while it showed a rather diverse behavior in different samples when decreasing the temperature. In the parent material the spin-

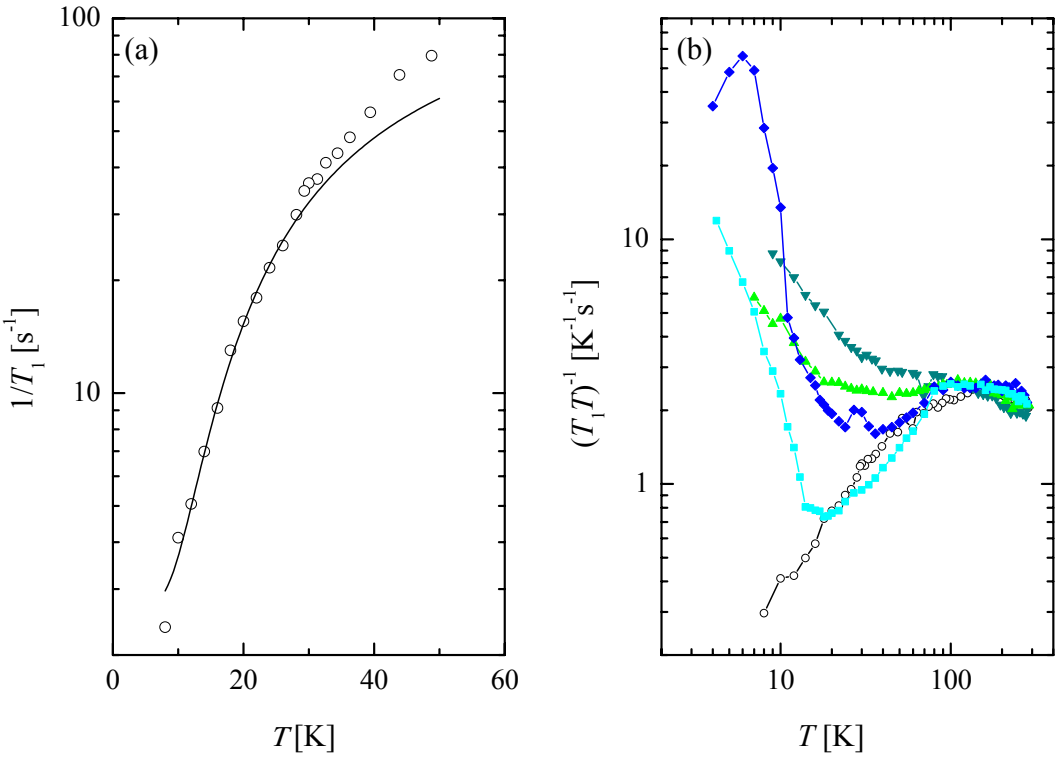

Fig. 3.17: The activation dependence of the $PbNi_2V_2O_8$ low-temperature spin-lattice relaxation rate with the solid line corresponding to the model given by Eq. (3.30). (b) The temperature dependence of the spin-lattice relaxation rate divided by temperature in the compounds $PbNi_{1.88}Mg_{0.12}V_2O_8$ (▲), $PbNi_{1.76}Mg_{0.24}V_2O_8$ (▼), $PbNi_{1.98}Co_{0.02}V_2O_8$ (◆) and $PbNi_{1.92}Mg_{0.08}V_2O_8$ (■) compared with the parent compound (○).

lattice relaxation shows strong temperature dependence. The relaxation time monotonously increases and changes its size by roughly three orders of magnitude at 4.2 K with respect to the room-temperature value. When plotting $(T_1T)^{-1}$ as a function of the temperature this parameter shows very similar evolution as the magnetic susceptibility of the sample (see Fig. 3.17) proving that paramagnetic electrons are involved in the dominant spin-lattice relaxation mechanism of the vanadium nuclei.

As discussed in the previous section, the transferred hyperfine coupling of the ^{51}V nuclei at site i with the Ni^{2+} magnetic moments at sites j is the dominant mechanism producing time-dependent local magnetic fields. The expression for the spin-lattice relaxation time in the limit of infinite temperature can then be derived by the use of Eq. (2.42) and the assumption of the Gaussian time distribution of spin-correlation functions [26]

$$\left\langle \left\{ \delta S_j^{\mu}(t) \delta S_k^{\nu} \right\} \right\rangle = \delta_{j,k} \delta_{\mu,\nu} \frac{S(S+1)}{3} e^{-(\omega_e t)^2/2}, \tag{3.28}$$

to have the following form

$$\frac{1}{T_1} = \sqrt{\frac{\pi}{2}} \frac{1}{h} \frac{S(S+1)}{3\hbar\omega_e} \sum_j \frac{1}{2} \left(\widetilde{A}_{i,j}^{xx\,2} + \widetilde{A}_{i,j}^{yy\,2} \right). \tag{3.29}$$

Here $Z = 6$ denotes the number of the nearest Ni^{2+} neighbors of each vanadium nucleus, *z* is the direction of the external magnetic field and the exchange frequency is given by $\omega_e = \sqrt{2J^2 Z' S(S+1)/3\hbar^2}$ [26]. The spin-lattice relaxation time corresponding to the above estimated isotropic part of the transferred hyperfine tensor $\widetilde{A}_{\mathrm{i,j}}^{iso} = k_B \cdot 0.17\,\mathrm{mK}$ is then of the order of $T_1^{iso} = 250\,\mathrm{ms}$, which is two orders of magnitude above the measured value at room temperature. On the other hand, as mentioned above the relaxation rate in the pristine sample shows characteristic features of vanadium nuclei relaxing primary due to the coupling with the paramagnetic electrons. For this reason, it is natural to assume that the anisotropic part of the transferred hyperfine tensor dominates over the isotropic part. Thus the former components should be approximately an order of magnitude larger than the latter one to account for the experimentally observed relaxation rates. This experimental observation is also in accord with the development of the ^{51}V NMR powder-like lineshape in Mg-doped samples at low temperatures, where the asymmetric absorption lines was proposed to be dictated by this same electron-nucleus interaction.

Next, let us turn to the temperature evolution of the spin-lattice relaxation time. The changes of this parameter with temperature can be traced back to the changes of the electron correlation functions $\left\langle \left\{ \delta S_j^{\mu}(t) \delta S_k^{\nu} \right\} \right\rangle$. Changing from the physical to the reciprocal space the time-integral of these correlation functions can be shown to be proportional to the dissipative part of the dynamic wave-vector-dependent susceptibility $\chi''(\mathbf{q}, \omega_0)$, which in turn, determines the temperature evolution of the spin-lattice relaxation time as well as the line shape [56].

In the pure Haldane system the spin-lattice relaxation rate is then expected to show activation behavior due to the singlet nature of the ground state with the dominant contributions originating from the center of the Brillouin zone, $q \approx 0$, and from the wave vectors at the zone boundary $q \approx \pi$ corresponding to the antiferromagnetic spin correlations [57, 58]. The phenomenological fit of the spin-lattice relaxation rate for temperatures below the spin gap value to the equation of the form

$$\frac{1}{T_1} = \frac{1}{T_1^0} + \frac{1}{T_1^{\infty}} \mathrm{e}^{-\Delta_{av}/k_B T} \tag{3.30}$$

yields an "average" spin gap value $\Delta_{av} = k_B \cdot 51(1)\,\mathrm{K}$ and the relaxation rate at zero temperature $\left(T_1^0\right)^{-1} = 2.7(1)\,\mathrm{s}^{-1}$ (Fig. 3.17a). The latter parameter corresponds to the relaxation caused by some other relaxation mechanism, which becomes important only at extremely low temperatures. On the other hand, the model parameter $\left(T_1^{\infty}\right)^{-1}$ is not relevant, since at high temperatures interactions between excited magnon modes brake down the validity of this simple picture and therefore the Eq. (3.30) cannot be applied.

Haldane *et al.* showed that at very low temperatures ($\mu_B(B-B_c) \gg k_B T$, where $B_c = 14-19$ T [1] is the critical field where the lowest-lying magnetic excitation crosses the energy level of the ground state) the ferromagnetic contribution dominates, while in the opposite limit ($\mu_B(B-B_c) \ll k_B T$) the antiferromagnetic one gives the leading contribution [57]. As the energy gap in the center of the Brillouin zone ($q \approx 0$) is by a factor of two larger than the spin-gap corresponds to the magnetic excitations at the center of the antiferromagnetic zone ($q \approx \pi$), the experimentally deduced energy gap seems to have a reasonable value. Namely, the difference of the critical field in $PbNi_2V_2O_8$ and the static magnetic field used in our experiments corresponds to the temperature of 7 K, which means that we are in between the two limiting regimes. A further complication is that the presence of the magnetic anisotropy terms splits the lowest magnon dispersion into three branches. Interbranch as well as intrabranch magnon transitions are then possible, which further complicates the theoretical calculation of the spin-lattice relaxation [57]. Furthermore, it has been theoretically as well as experimentally deduced that the Haldane gap increases as a function of the temperature, which makes the analysis even more complex [59]. A comparison of the measured dynamical spin gaps obtained from the nuclear spin-lattice relaxation with the static gaps corresponding to the static spin susceptibility in different Haldane system showed that the former gaps always have somewhat but not appreciably larger values than the latter ones [60], which is in line with our experimental findings.

In the presence of spin impurities the treatment of the system is of course even more involved. The contribution to the relaxation rate from the $S = 1/2$ degrees of freedom liberated by spin vacancies was also argued to have an activation-like character [57]. However, our measurement presented in Fig. 3.17b reveal a drastically different behavior for both Mg-doped and Co-doped samples. Since the calculation of the temperature dependence of the spin-lattice relaxation is far from being trivial in inhomogeneous systems only a qualitative description is given below.

The spin-lattice relaxation starts to deviate from the case of the pristine sample already below approximately 120 K in Mg-doped samples and at significantly lower temperatures in the Co-doped samples, which seems to correspond nicely with to temperature development of the linewidths of the corresponding ^{51}V NMR spectra (Fig. 3.15). The behavior of the Co-doped samples is more or less expected. In the systems, which undergo magnetic phase transition to the antiferromagnetically ordered state, critical antiferromagnetic fluctuations are expected to determine the relaxation rate in the close vicinity of the phase-transition point [53]. As already explained at several occasions, the precursor effects of antiferromagnetically ordered clusters of spins above the transition temperature have a twofold effect on the system of ^{51}V nuclei. First, the spatial aspect is expressed in the divergent character of the wave-vector-dependent susceptibility corresponding to the wave vector of AFM ordered spins, and second, the time

correlations become long-lived due to the slowing-down of spin fluctuation. Consequently, the spin-lattice relaxation rate should exhibit critical behavior of the form $(T_1)^{-1} \propto ((T - T_N)/T_N)^{-p}$ in the vicinity of the phase transition with the critical exponent *p* reflecting the dimensionality as well as static and dynamic aspects of AFM spin fluctuations [61]. However, such critical behavior is usually observed only in a close vicinity of the phase-transition temperature, $((T - T_N)/T_N) \leq 0.1$.

Our measurements of the spin-lattice relaxation in Co-doped samples show all the characteristics of critical behavior. There is a peak in the relaxation time accruing at 7 K in the case of $PbNi_{1.92}Co_{0.08}V_2O_8$, which nicely corresponds to the transition temperature of 7.17 K and the observed splitting of the absorption line. The peak in the relaxation rate proves that magnetic ordering still takes place despite the relatively large value of the static magnetic field. This gives a firm conformation of our assumption that metamagnetism is not present in this system in magnetic field up to 6.34 T, which is the origin for understanding the difference of the low-temperature spectra between Mg-doped and Co-doped compounds. The transition temperature of the other Co-doped sample is, unfortunately, below our lowest attainable temperature. The critical exponent *p* could not be determined, due to the fact that the critical regime with a constant *p*-value is too narrow with respect to our experimental accuracy.

On the other hand, the Mg-doped samples show drastically different characteristics in terms of the spin-lattice relaxation. Namely, as mentioned above, the relaxation starts deviating from the parent sample already below 120 K and shows no evidence of the presence of gapped excitations. The increase of the parameter $(T_1T)^{-1}$ is also much more moderate than in the case of spin-doped materials. The evolution of the spin correlations in the two families is thus again proven to be rather different.

3.4 Gap-Like Behavior of Magnetic Properties in $SrNi_2V_2O_8$

As mentioned in the opening section of this paragraph, the present state of the experimental findings regarding the low-temperature magnetic properties of the $SrNi_2V_2O_8$ system is rather contradictory. The nature of the ground state of this spin system is thus still ambiguous. There was a suggestion made by Zheludov *et al*. [3] that $SrNi_2V_2O_8$ compound should be unlike the isomorphous system $PbNi_2V_2O_8$ positioned on the magnetically ordered side of the Sakai-Takahashi phase diagram. This conclusion was drawn according to the bulk magnetic measurements and inelastic neutron scattering results. Below $T_N = 7\,\mathrm{K}$ the system should undergo a transition to a weak-ferromagnetic-like magnetically ordered ground state. However, the authors also reported that they were unable to detect any magnetic Bragg reflections in the presumably ordered phase, which lead them to a conclusion that the ordered moment is very

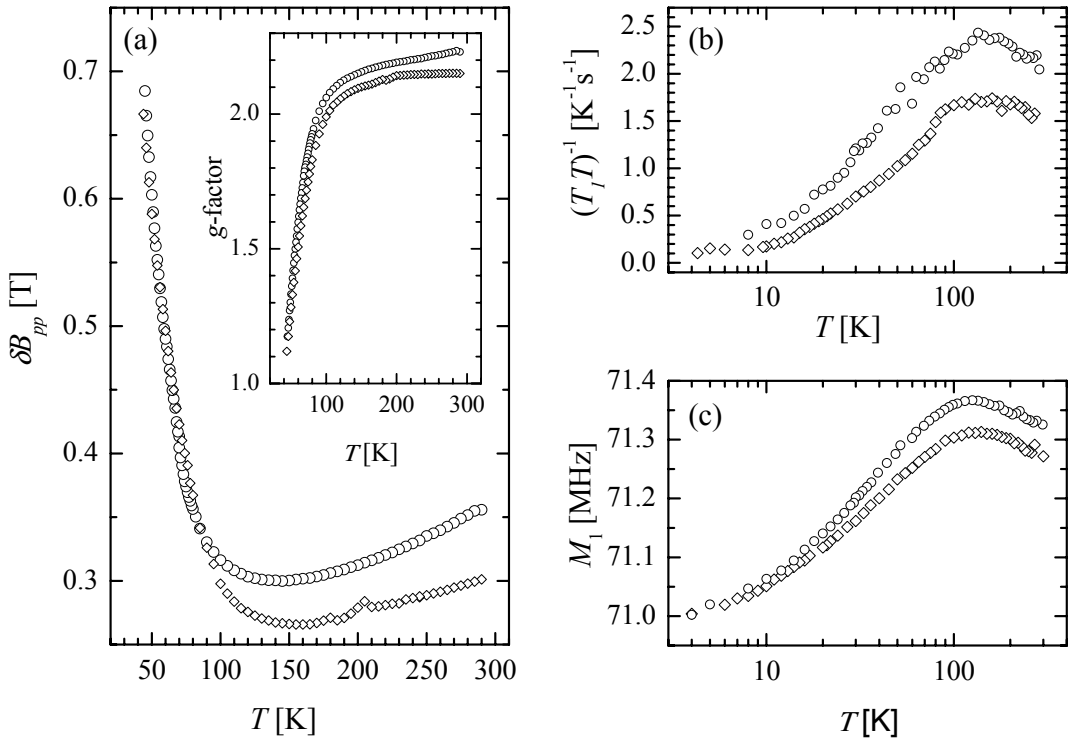

Fig. 3.18: Temperature dependence of (a) the X-band ESR linewidth and *g*-factor (inset) as well as (b) ^{51}V NMR spin-lattice relaxation and (c) NMR line position of $PbNi_2V_2O_8$ (○) and $SrNi_2V_2O_8$ (◇) compounds.

small. They also left an open possibility of a finite energy gap because of strong diffuse and phonon scattering dominating the INS spectra at low energy transfers.

Since the magnetic ordering is accompanied by a significant change in the behavior of the time and the space dependence of the spin correlation functions, magnetic resonance measurements probing the local spin fluctuations should prove valuable for addressing the unresolved questions, which is why we performed X-band ESR as well as ^{51}V NMR measurement on the $SrNi_2V_2O_8$ compound. The comparison with the $PbNi_2V_2O_8$ Haldane-gap system is summarized in Fig. 3.18.

Let us first make a closer inspection on the ESR results. The spectrum measured at room temperature is again exchange-narrowed as in the Pb-based compound. However, it appears to be observably narrower, i.e., by approximately 15%. When lowering the temperature the spectra of the $SrNi_2V_2O_8$ compound become more and mode similar to the case of $PbNi_2V_2O_8$. This observation is valid not only for the linewidth behavior but also for the *g*-factor shift. The Ni^{2+} signal becomes practically unobservable below 40 K in the field-window that we use. For temperatures much bellow this temperature only an irregular ESR signal intrinsic to the resonator that we use is observed together with some narrow features with the Curie-like dependence around the free-electron *g*-value, which seem to correspond to impurities. However,

there is no drastic change observable around the temperature of 7 K. We were also not able to detect any antiferromagnetic resonance in X-band as well as in high-frequency ESR measurements. From ESR measurements one would then conclude that the nature of spin correlations of both vanadates is very similar at low temperatures. However, as the signal intrinsic to the investigated systems is absent, it is not wise to draw a definite conclusion about the ground state of the $SrNi_2V_2O_8$ system at this point based only on the nonexistence of the ESR signal. In this respect additional NMR measurement prove to be irreplaceable. Before changing the theme, the difference of the high-temperature ESR parameters should be revisited. Namely, in addition to the difference of the room-temperature linewidth of the two materials, also the slopes of the increase of this parameter as well as the *g*-factor seem to be different for the two materials. A remarkable feature is that the linear fit of the high-temperature linewidth data gives very similar "zero-temperature" constant values, i.e., $\delta B_{lin}^{Pb}(0) = 0.227(2)\,\mathrm{mT}$ and $\delta B_{lin}^{Sr}(0) = 0.222(2)\,\mathrm{mT}$, which again suggests on a common origin of the ESR signal. The different values of the slopes would then probably correspond to somewhat different behavior of the short-range correlations effect. Similar conclusion could also be drawn from the comparison of the magnetic susceptibility, which shows a reduction in the $SrNi_2V_2O_8$ system with respect to the $PbNi_2V_2O_8$ system, although the general temperature behavior is very similar. Thus the room-temperature susceptibility value is reduced from $\chi_{mol}^{Pb} = 5.6 \cdot 10^{-3}$ emu/mol corresponding to Pb-based compound to $\chi_{mol}^{Sr} = 4.0 \cdot 10^{-3}$ emu/mol in $SrNi_2V_2O_8$ system.

Next, let us take a closer look at the ^{51}V NMR results. In Figs. 3.18b and 3.18c only the temperature evolution of the spin-lattice relaxation and the center of the absorption lines are presented. The spectra and their width are not shown since they are very similar for both types of vanadates in the whole temperature range. Also the overall temperature dependence of the two NMR parameters presented in Fig. 3.18 is quite alike. The discrepancy in the high-temperature region can be attributed to the difference of the magnetic susceptibilities in the two compounds as mentioned in the preceding paragraph since both the spin-lattice relaxation and the center of the resonance probe spin correlations due to the dominant magnetic interaction sensed by vanadium nuclei originating from the paramagnetic-electrons spin system.

More interesting should be the comparison of the NMR results in the low-temperature region. Namely, both the center position as well at the spin-lattice relaxation rates become very similar in both of the systems. This unambiguously proves that the static as well as the dynamic behavior of the local magnetic fields, or equivalently spin correlations, are practically the same in Sr-based and Pb-bases systems. The magnetic ordering, reportedly occurring in the $SrNi_2V_2O_8$ system below 7 K [3] can thus safely be ruled out, at least in out compound, which is quite pure according to the performed structural analysis. If the spins ordered in three dimensions the spin-lattice relaxation would certainly show the typical deviations at least in the vicinity of the transition point as shown for the doped $PbNi_2V_2O_8$ materials (see Fig. 3.17).

3.5 Discussion on Magnetic Resonance Results

In this chapter a comprehensive study of magnetic resonance employed on the quasi-one-dimensional $PbNi_{2-x}(Mg,Co)_xV_2O_8$ system has been given. The presented survey includes ESR as well as NMR measurements, both techniques yielding information on the development of the electron spin correlations as a function of the temperature and doping. Regarding NMR, ^{51}V nuclei have been chosen since they provide only weakly interacting local probes for the electronic system. Since both techniques are sensitive to the static and the dynamic part of the electronic correlations on a local scale, they are able to offer additional information on magnetic anisotropy governing the electronic correlations to that information already established from the bulk magnetic measurements.

With the use of the ESR measurements performed on the parent $PbNi_2V_2O_8$ compound we were able to show that the previously proposed model of the dominant part of the magnetic anisotropy interaction sensed by each Ni^{2+} magnetic moment, which is of the uniaxial symmetry, is if fact inadequate. Namely, the easy-axis-type of the single-ions anisotropy interaction neglects the local (non)symmetry thus throwing a shadow of a doubt on the accuracy of the determined magnetic parameters characteristic for this Haldane spin system. In addition, it has been argued that also other sources of magnetic anisotropy should be important due to the distortion of NiO_6 octahedra. In this respect the Dzyaloshinsky-Moriya interaction between nearest-neighbor Ni^{2+} spins has been evaluated and shown to be possibly of the same order of magnitude as the presumably dominant single-ion anisotropy.

The disappearance of the ESR signal from the experimental X-band window at temperatures around the spin gap temperature of approximately 43 K has been argued to be due to the change of the character of the spin excitations when entering the Haldane phase. On the other hand, no drastic changes are observed in ^{51}V NMR spectra recorded on the pristine compound in the whole temperature region between room temperature and 4.2 K. One could at first sight correlate these findings with an assumption that the vanadium nuclei are not coupled to the spin system of the paramagnetic moments. However, there are several experimental facts proving that the ^{51}V nuclear system does communicate with the system of Ni^{2+} spins. This communication designates the vanadium ions in the $PbNi_2V_2O_8$ as being partially magnetic. Their magnetic character originates from the electron spin system and is due to the covalency effect. Thus we have been able to associate the temperature dependence of the first moment of the NMR spectra with the imbalance of the electron distribution on vanadium sites, which gives rise to an effective transferred hyperfine interaction at these sites. The *s*-character of this anisotropic interaction was evaluated to arise from the portion of approximately $2.5 \cdot 10^{-3}$ of the unpaired 3*s* vanadium electrons. On the other hand, a single crystal would be needed to be able

to perform a similar estimation about the redistribution of the vanadium 3*p* electrons since these electrons do not induce lineshifts in the powder samples.

On the other hand, the isotropic part of the transferred hyperfine interaction as the dominant nuclear anisotropy cannot account for the width of the observed spectra as it is severely attenuated by the rapid electron fluctuations. To examine the width of the central NMR transition line we employed the anisotropic part of this interaction as well as the chemical-shift tensor anisotropy, which together with the quadrupole coupling determine the absorption profiles.

The importance of the transferred hyperfine interaction at vanadium sites can be related to the relatively strong interchain exchange coupling. The VO_4 tetrahedra thus clearly act as connecting bridges for the Ni-Ni exchange between adjacent chains. The resulting quasi-one-dimensional character of the $PbNi_2V_2O_8$ system determines the position of the system on the Sakai-Takahashi phase diagram close to the borderline between the Haldane disordered ground state and magnetically ordered ground state.

In contrast, the isomorphous $SrNi_2V_2O_8$ compound was previously reported to be positioned on the ordered side of this phase diagram as shown in Fig. 1.4. This system was reported to undergo a long-range magnetic ordering below 7 K according to the inelastic neutron scattering results [3]. Our ESR and even more the ^{51}V NMR measurements unambiguously indicate that the real situation is in fact different. Namely, there is no qualitative difference between the evolution of the electronic correlations in the Pb-based and Sr-based system. The overall temperature dependence of the NMR lineshape and the position of the line as well as the spin-lattice relaxation time reveal the presence of the spin gap also in the $SrNi_2V_2O_8$ compound down to the temperature of the liquid helium.

The crossover between the magnetically disordered and ordered ground state and the precursor effects of this transition have been, on the other hand, successfully studied in the vacancy-doped $PbNi_{2-x}Mg_xV_2O_8$ and the spin-doped $PbNi_{2-x}Co_xV_2O_8$ compounds. The ESR experiments performed on the former family revealed that there are two diverse origins of the paramagnetic signal. The first dominating at high temperatures corresponds to the Haldane system as in the pristine compound. However, at temperatures below the characteristic temperature of the spin gap the end-chain contribution overshadows the first one. Due to rather broad resonance profiles at very low temperatures we drew a conclusion that the liberated $S = 1/2$ degrees of freedom are in fact ferromagnetically coupled, which was later confirmed also with thermodynamic measurement [45].

In the mid-temperature range the two kinds of spin excitations in vacancy-broken chains seem to coexist as evident from the ESR and the NMR experiments. Namely, there is a uniform transition of the linewidths and the position of the line from the Haldane-dictated character to the dependence due to three-dimensional spin correlations. This observation goes hand in hand

with other experimental findings. In cases of low Mg-doping concentrations, i.e. below $x = 0.04$, several experimental techniques revealed that clusters of antiferromagnetic order of the end-chain spins coexists with Haldane-ordered clusters of the remaining Ni^{2+} spins. These conclusions have been drawn from the specific heat measurements, magnetic entropy and magnetization measurements [45], as well as from magnetic resonance measurements [33, 46] simultaneously observing paramagnetic and antiferromagnetic resonance. At larger doping concentrations (like we use in our experiments) no magnetic phase separation has been observed. However, our experiments show that the character of the spin excitations and its evolution is qualitatively the same also in samples with higher doping level.

Due to severe broadening of the ESR absorption lines in the case of Co-doping, the comparison of the effect of vacancy versus spin doping on the development of the electronic correlations on Haldane chains has been studied only by NMR. These measurements unexpectedly revealed that the nature of the spin correlations at temperatures close to the ordering temperature significantly differs in the two families of materials, at least in the relatively high static magnetic field of 6.34 T that was used in our experiments. That is to say, in Mg-doped samples the antiferromagnetic ordering is destroyed by the presence of the magnetic field in favor of the ferromagnetic correlations as evidenced from the first and the second moment of absorption spectra, which is in line with the metamagnetic transition. On the other hand, the antiferromagnetic-type of correlations is much more sustainable in the Co-doped samples as already reflected in higher values of the transition temperatures in the first place. Thus the coupling between the nonuniform pockets of staggered magnetization induced in the neighborhood of the impurity sites, which tend to order at low temperatures, seems to be much stronger in the case of Co dopant. This can be traced back to effectively stronger interaction between clusters of antiferromagnetically ordered spins originating from the spin character of the Co dopant, which is the root to stronger antiferromagnetic correlations in Co-doped samples with respect to the Mg-doped samples. On the other hand, our high-temperature measurements show that the average Ni-Ni interchain interaction is very similar in all the samples. Namely, the NMR lineshift reflecting the interchain polarization effect does not change with the doping.

The survival of the antiferromagnetic spin correlations in the $PbNi_{1.92}Co_{0.08}V_2O_8$ system was experimentally expressed in various NMR parameters. The most convincing are the sharp peak of the spin-lattice relaxation curve at 7 K and the double-peaked character of the NMR absorption profile below this temperature indicating the presence of two sublattice magnetizations.

Another strikingly different aspect between the Mg- and Co-doping is the dependence of the ESR linewidth on the nature of the dopant and the level of doping. While in the case of the vacancy doping the moderate increase of the linewidth at high temperatures can probably be assigned to partially limited diffusion of non-Boltzman spin polarization due to spin vacancies,

the Co impurities act as effective sinks for the magnetic energy from the host spin system. This is a consequence of Co^{2+} ions being strongly coupled to lattice vibrations. The interpretation of the ESR data of $PbNi_{1.98}Co_{0.02}V_2O_8$ compound allowed us to evaluate the Ni-Co exchange interaction to be of the order of $k_B \cdot 10\,\mathrm{K}$ as well as provided an insight into the phonon system. The model predicted a reasonable value of the Debye temperature ($\theta_D \approx 500\,\mathrm{K}$) and a rather convincing bottleneck behavior of the temperature dependence of the impurity broadening mechanism.

Bibliography

[1] Y. Uchiyama, Y. Sasago, I. Tsukada, K. Uchinokura, A. Zheludov, T. Hayashi, N. Miura, P. Böni. Spin-vacancy-induced long-range order in a new Haldane-gap antiferromagnet, *Phys. Rev. Lett*. **83**, 632 (1999).

[2] R. Wichman, H. Müller-Buschbaum. SrNi2V2O8: ein nuer Strukturtyp der Erdalkali-Oxometallate, *Rev. Chim. Miner*. **23**, 1 (1986).

[3] A. Zheludov, T. Masuda, I. Tsukada, Y. Uchiyama, K. Uchinokura, P. Böni. Magnetic excitations in coupled Haldane spin chains near the quantum critical point, *Phys. Rev. B* **62**, 8921 (2000).

[4] A. Zheludov, T. Masuda, K. Uchinokura, S. E. Nagler. Zone-boundary excitations in coupled Haldane spin chain systems $PbNi_2V_2O_8$ and $SrNi_2V_2O_8$, *Phys. Rev. B* **64**, 134415 (2001).

[5] K. Uchinokura, Y. Uchiyama, T. Masuda, Y. Sasago, I. Tsukada, A. Zheludov, T. Hayashi, N. Miura, P. Böni. Phase diagram of spin-vacancy-induced antiferromagnetism in a new Haldane compound $PbNi_2V_3O_8$, *Physica B* **284-288**, 1641 (2000).

[6] A. Lappas. Private communications.

[7] A. Zorko, D. Arčon, A. Lappas, J, Giapintzakis, C. Saylor, L. C. Brunel. Effect of vacancy doping on the Haldane spin-liquid state in $PbNi_{2-x}Mg_xV_2O_8$, *Phys. Rev. B* **65**, 144449 (2002).

[8] D. Arčon, A. Zorko, A. Lappas. X-band ESR and ^{51}V NMR study of the Haldane system $PbNi_{2-x}Mg_xV_2O_8$, to be published in *Appl. Magn. Reson*. **27**.

[9] D. Arčon, A. Zorko, A. Lappas. ^{51}V NMR study of the doped chain compounds $PbNi_{2-x}Mg_xV_2O_8$, *Europhys. Lett.* **65**, 109 (2004).

[10] V. Kataev, K.-Y. Choi, M. Grüninger, U. Ammerahl, B. Büchner, A. Freimuth, A. Revcolevschi. Strong anisotropy of the superexchange in the copper-oxygen chains of $La_{14-x}Ca_xCu_{24}O_{41}$, *Phys. Rev. Lett.* **86**, 2882 (2001).

[11] Z. G. Soos, T. T. P. Cheung, K. T. McGregor. Exchange narrowing in correlated spin systems: local field contributions, *Chem. Phys. Lett*. **46**, 600 (1977).

[12] M. S. Seehra, T. C. Castner. The paramagnetic line width in $Cu(HCOO)_2 \cdot 4H_2O$, *Phys. Kondens. Materie* **7**, 185 (1968).

[13] J. R. Pilbrow. *Transition Ion Electron Paramagnetic Resonance* (Oxford University Press, Oxford, 1990).

[14] G. E. Pake. *Paramagnetic Resonance* (W. A. Benjamin, New York, 1962), p. 64.

[15] W. Low. Paramagnetic resonance in solids, in *Solid State Physics, supplementary Vol. 2*, edited by F. Seitz and D. Turnbull (Academic Press, New York, 1960), p. 8.

[16] I. Mastoraki, A. Lappas, J. Giapintzakis, D. Többens, J. Hernández-Velasco. Relation of crystal structure to magnetic properties in the quasi-one-dimensional compound $PbNi_{1.88}Mg_{0.12}V_2O_8$, *J. Solid State Chem.* **177**, 2404 (2004).

[17] F. Keffer. Moriya interaction and the problem of the spin arrangements in βMnS, *Phys. Rev.* **126**, 896 (1962).

[18] M. Date, K. Kindo. Elementary excitations in the Haldane state, *Phys. Rev. Lett.* **65**, 1659 (1990).

[19] L. C. Brunel, T. M. Brill, I. Zaliznyak, J. P. Boucher, J. P. Renard. Magnon spin resonance in the Haldane spin chain $Ni(C_2H_8N_2)NO_2ClO_4$, *Phys. Rev. Lett*. **69**, 1699 (1992).

[20] S. Kimura, H. Ohta, M. Motokawa, T. Yokoo, J. Akimitsu. ESR study on Haldane system Y_2BaNiO_5 in submilimeter wave region, *J. Magn. Magn. Mater.* **177-181**, 624 (1998).

[21] I. Affleck. Theory of electron spin resonance in Haldane-gap antiferromagnets, *Phys. Rev. B* **46**, 9002 (1992).

[22] M. Oshikawa. ESR in Haldane gap systems revisited, *Prog. Theor. Phys. Suppl*. **145**, 253 (2002).

[23] A. Lappas, V. Alexandrakis, J. Giapintzakis, V. Pomjakushin, K. Pressides, A. Shenck. Impurity-induced ordering in the Haldane-gap compound $PbNi_{2-x}Mg_xV_2O_8$ (x = 0.24), *Phys. Rev. B* **66**, 014428 (2002).

[24] R. G. Shulman, V. Jaccarino. Nuclear magnetic resonance in paramagnetic MnF_2, *Phys. Rev*. **108**, 1219 (1957).

[25] E. Clementi, C. Roetti. Roothaan-Hartree-Fock atomic wavefunctions: Basis functions and their coefficients for ground and certain excited states of neutral and ionized atoms, $Z \leq 54$, *At. Data Nucl. Data Tables* **14**, 177 (1974).

[26] T. Moriya. Nuclear magnetic relaxation in antifferomagnetics, *Prog. Theor. Phys.* **16**, 23 (1956).

[27] A. Schweiger, G. Jeschke. *Principles of pulsed electron Paramagnetic Resonance* (Oxford University Press, Oxford, 2001), p. 30.

[28] J. E. Gulley, D. Hone, D. J. Scalapino, B. G. Silbernagel. Exchange narrowing: Magnetic resonance lineshapes and spin correlations in paramagnetic $KMnF_3$, $RbMnF_3$, and MnF_2, *Phys. Rev. B* **1**, 1020 (1970).

[29] S. Hayashi, K. Hayamizu. ^{51}V NMR chemical shift and anisotropy in solid metavanadates, *Bull. Chem. Soc. Jpn.* **63**, 961 (1990).

[30] B. A. Gee, A. Wong. Vanadium-51 MAS and static NMR studies of the binary V_2O_5-WO_3 system, *J. Phys. Chem. B* **107**, 8382 (2003).

[31] I. Mastoraki, A. Lappas, R. Schneider, J. Giapintzakis. Spin-gap and antiferromagnetic correlations in low-dimensional $PbNi_{2-x}A_xV_2O_8$ (A = Mg, Co), *Appl. Phys. A* **74** (Suppl.), S640 (2002).

[32] J. E. Gulley, V. Jaccarino. Impure exchange-coupled paramagnets: Electron paramagnetic-resonance studies, *Phys. Rev. B* **6**, 58 (1972).

[33] A. I. Smirnov, V. N. Glazkov, H.-A. Krug van Nidda, A. Loidl, L. N. Demianets, A. Ya. Shapiro. Paramagnetic and antiferromagnetic resonance in the diamagnetically diluted Haldane magnet $PbNi_2V_2O_8$, *Phys. Rev. B* **65**, 174422 (2002).

[34] S. H. Glarum, S. Geschwind, K. M. Lee, M. L. Kaplan, J. Michel. Observation of fractional Spin S = 1/2 on open ends of S = 1 linear antiferromagnetic chains: nonmagnetic doping, *Phys. Rev. Lett.* **67**, 1614 (1991).

[35] Y. Ajiro, T. Uchikawa, T. Asano, M. Mekata, N. Mori. ESR of "the magnetic dangling bond" in the Haldane state, *J. Phys. Soc. Jpn*. **66**, 971 (1997).

[36] M. Hagiwara, K. Katsumata, I. Affleck, B. I. Harpelin, J. P. Renard. Observation of S = 1/2 degrees of freedom in an S = 1 linear-chain Heisenberg antiferromagnet, *Phys. Rev. Lett.* **65**, 3181 (1990).

[37] H. Manaka, I. Yamada. Crossover from S = 1/2 to S = 1 Haldane state in the ferromagnetic and antiferromagnetic alternating Heisenberg chain system $(CH_3)_2CHNH_3CuCl_3$ observed with EPR at 24 GHz, *Phys. Rev. B* **62**, 14279 (2000).

[38] E. F. Shender, S. A. Kivelson. Dilution-induced order in quasi-one-dimensional quantum antiferromagnets, *Phys. Rev. Lett*. **66,** 2384 (1991).

[39] H. Mori. Paramagnetic resonance line width in antiferromagnets, *Prog. Theor. Phys.* **30**, 578 (1963).

[40] D. L. Huber. Critical-point anomalies in the electron-paramagnetic resonance linewidth and in the zero-field relaxation time of antiferromagnets, *Phys. Rev. B* **6**, 3180 (1972).

[41] P. M. Richard. Magnetic Resonance in One- and Two-Dimensional Systems, in *Local Properties of Low-Dimensional Antiferromagnets*, edited by K. A. Müller (Nord Holland Publishing Company, Amsterdam, 1976), p. 539.

[42] K. Nagata, Y. Tazuke. Short range order effects on the EPR frequencies in Heisenberg linear chain antiferromagnets, *J. Phys. Soc. Jpn*. **32**, 337 (1972).

[43] V. N. Glazkov, A. I. Smirnov, R. M. Eremina, G. Dhalenne, A. Revcolevschi. Magnetic resonance of spin clusters and triplet excitations an a spin-Peierls magnet with impurities, *JETP* **93**, 143 (2001).

[44] P. P. Mitra, B. I. Harpelin. Temperature dependence of the electron-spin-resonance spectrum of the chain-end S = 1/2 modes in an S = 1 antiferromagnetic chain, *Phys. Rev. B* **45**, 5299 (1992).

[45] T. Masuda, K. Uchinokura, T. Hayashi, N. Miura. Impurity-induced antiferromagnetic phase in a doped Haldane system $Pb(Ni_{1-x}Mg_x)_2V_2O_8$, *Phys. Rev. B* **66**, 174416 (2002).

[46] A. I. Smirnov, V. N. Glazkov, T. Masuda, K. Uchinokura, L. N. Demianets, A. Ya. Shapiro. Microscopic magnetic phase separation at the impurity stimulated antiferromagnetic ordering of two spin-gap magnets, *Physica B* **329-333**, 699 (2003).

[47] D. Hone, K. G. Petzinger. Spin correlations in impure linear Heisenberg chains, *Phys. Rev. B*. **6**, 245 (1972).

[48] P. M. Richard. Electron-spin resonance in the impurity doped Heisenberg linear chain $(CH_3)_4NMnCl_3$:Cu, *Phys. Rev. B* **10**, 805 (1974).

[49] K. Uchinokura, T. Masuda, Y. Uchiyama, R. Kuroda. Impurity-induced antiferromagnetic phase in a new Haldane-gap compound $PbNi_2V_2O_8$, *J. Magn. Magn. Mater.* **226-230**, 431 (2001).

[50] K. Nagata, T. Nishino, T. Hirosawa, T. Komatsubara. EPR in the impure Heisenberg linear chain $CsMn_{1-x}Co_xCl_3 \cdot 2H_2O$, *J. Phys. Soc. Jpn*. **44**, 813 (1978).

[51] A. Zorko, D. Arčon, K. Biljaković, C. Carcel, J. M. Fabre, J. Dolinšek. Spin-Peierls fluctuations in $(TMTTF)_2Br$ studied by pulsed electron spin resonance spin-lattice relaxation, *Phys. Rev. B* **64**, 172404 (2001).

[52] N. W. Ashcroft, N. D. Mermin. *Solid State Physics* (Sounders College Publishing, Fort Worth, 1976), p 457.

[53] T. Moriya. Nuclear magnetic resonance near the Curie temperature, *Prog. Theor. Phys*. **28**, 371 (1962).

[54] E. Stryjewski, N. Giordano. Metamagnetism, *Adv. Phys*. **26**, 487 (1977).

[55] M. Tinkham. Paramagnetic resonance in dilute iron group fluorides. II. Wave functions of the magnetic electrons, *Proc. Roy. Soc. (London) A* **236**, 549 (1956).

[56] P. Heller. NRM and neutron scattering studies near phase transitions in uniaxial antiferromagnets, in *Local Properties of Low-Dimensional Antiferromagnets*, edited by K. A. Müller (Nord Holland Publishing Company, Amsterdam, 1976), p. 445.

[57] J. Sagi, I. Affleck. Theory of nuclear relaxation in Haldane-gap antiferromagnets, *Phys. Rev. B* **53**, 9188 (1996).

[58] Th. Jolicoeur, O. Golinelli. σ model study of Haldane-gap antiferromagnets, *Phys. Rev. B* **50**, 9265 (1994).

[59] D. Sénéchal. Mass gap of the nonlinear-σ model through the finite temperature effective action, *Phys. Rev. B* **47**, 8353 (1993).

[60] Y. Itoh, H. Yasuoka. Interrelation between dynamical and static spin gaps in quantum spin systems, *J. Phys. Soc. Jpn.* **66**, 334 (1997).

[61] C. Bourbonnais. Nuclear relaxation and electronic correlations in quasi-one-dimensional organic conductors. I. Scaling theory, *J. Phys. I* **3**, 143 (1993).

4 MAGNETISM OF 2D ORTHOGONAL DIMER SYSTEM $SrCu_2(BO_3)_2$

4.1 Structural Properties and Related Magnetic Character

Although the initial synthesis of the $SrCu_2(BO_3)_2$ compound was reported in 1991 [1], it did not arouse any major interest of the scientific society until the break of the millennium when this particular system was rediscovered by Kageyama *et al.* [2]. The intense response of the theoreticians as well as experimentalists that followed the latter contribution, and is still in progress, can be attributed to the relatively uncomplicated basic model Hamiltonian, which can account for the fundamental magnetic properties. The second factor, crucial for the scientific triumph of this system, is the successful manufacture of high-purity single crystals of $SrCu_2(BO_3)_2$ by traveling solvent floating zone method [3], which enormously simplifies the study of the anisotropy of its magnetic character.

The unit cell of the $SrCu_2(BO_3)_2$ compound has tetragonal symmetry ($I\bar{4}2m$) [1] with cell constants $a = 8.982$ Å and $c = 6.664$ Å at room temperature [4]. As shown in Fig. 4.1, the crystal structure consists of consecutive $CuBO_3$ layers displaced by Sr^{2+} ions. All the Cu^{2+} sites possessing spin $S = 1/2$ are crystallographically equivalent. Pairs of nearest copper neighbors within rectangular CuO_4 groups are interconnected by planar BO_3 groups. In this way a novel two-dimensional network of copper dimers is formed with the neighboring pairs oriented perpendicular to each other. Due to the layered structure also the magnetic character of this system is two-dimensional. Namely, the dominant magnetic exchange interaction pathways are the antiferromagnetic intradimer exchange *J* and the antiferromagnetic exchange interaction of each copper magnetic moment with the four next-nearest neighbors *J'*, which are taken into account by the so-called two-dimensional orthogonal dimer model [5]. The system is topologically equivalent to the Shastry-Sutherland model [6], artificially constructed almost twenty years before this first experimental realization of the model was recognized (see Fig. 1.3). The model Hamiltonian

$$H = J\sum_{(i,j)} \mathbf{S}_i \cdot \mathbf{S}_j + J'\sum_{\{l,m\}} \mathbf{S}_l \cdot \mathbf{S}_m, \tag{4.1}$$

with the first sum representing the exchange between pairs of nearest neighbors and the second one pairs of next-nearest neighbors, has an exactly soluble eigenstate. This state, which is also the ground state of the model up to the critical ratio of the exchange constants $(J'/J)_c = 0.68$ [7], is a simple product state of singlets on each dimer, called the dimer singlet state. Above this critical ratio an intermediate state of either helical order [8] or more probably plaquette singlet nature [7, 9] is believed to exist for the Shastry-Sutherland model. However, for the next-nearest

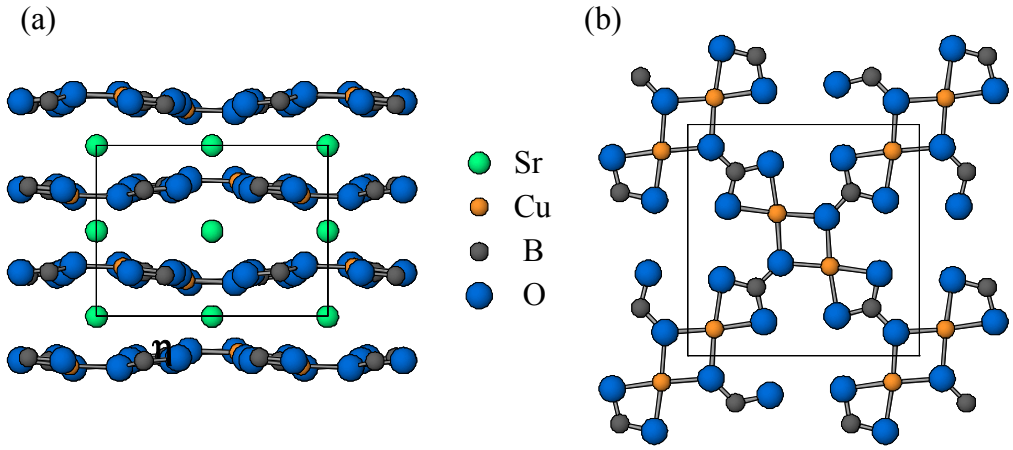

Fig. 4.1: (a) Crystal structure of the $SrCu_2(BO_3)_2$ compound as viewed along the crystal *c* axis and (b) the structure of a $CuBO_3$ layer. The rectangles represent the unit cell.

exchange greater than the intradimer one the Shastry-Sutherland spin system resembles the two-dimensional square-lattice Heisenberg model, which exhibits an antiferromagnetically ordered ground state providing a finite coupling between planes. It is believed that the crossover from the nonmagnetic ground state to the magnetically ordered state occurs around $\left(J'/J\right)_c \approx 0.7$ [10]. A direct evidence of the dimer singlet ground state was given by ^{63}Cu NMR experiments [11]. The four-fold splitting of the central absorption line and the coherent spin-echo oscillations were attributed to nuclear spins strongly coupled within pairs and, on the other hand, orders of magnitude weaker coupling between different dimers. As the nuclear coupling is mediated by the electronic system, these observation serves as an unequivocal indicator of the dominancy of spin correlations within the dimer in the ground state of the system.

For the $SrCu_2(BO_3)_2$ system various sets of exchange parameters have been proposed in the literature [5, 12, 13], among which the values $J = k_B \cdot 85\,\mathrm{K}$ and $J' = 0.63J$ reproduce the temperature dependence of the magnetic susceptibility most accurately [13]. Thus the ground is of spin-liquid type, although the system is positioned in the close vicinity of the quantum-phase-transition borderline. The dimer singlet state remains the ground state even if the finite interlayer coupling $J_{\|} = 0.09J$ is considered [14].

Within the orthogonal dimer model the lowest-lying magnetically excited state is a single triplet excitation present on one of the dimers with the spin gap significantly suppressed, which is due to the presence of the geometrical frustration of the next-nearest neighbor exchange [5]. Experimentally, the first direct observation of the spin gap $\Delta = k_B \cdot 35\,\mathrm{K}$ was provided by high-field ESR experiments [15] and latter confirmed by various experimental techniques including inelastic neutron scattering experiments [16], far-infrared spectroscopy [17] and Raman light scattering [18]. An interesting feature of the single triplet excitation is its localized nature, which is reflected in almost flat dispersion of the lowest-lying excitation [16]. The single triplet

can hop to another dimer only from the sixth order of perturbation in J/J' [19] while correlated hopping or two-particle coherent motion is much more effective [20]. The direct consequence of the localized character of triplet excitations is also the presence of magnetization plateaus observed in $SrCu_2(BO_3)_2$ for the first time in two dimensions [2]. The gaped phases occur at 1/8, 1/4 and 1/3 of the saturated magnetization [21] and the lowest one exhibits magnetic superstructure [22].

Although the isotropic Shastry-Sutherland Hamiltonian can explain many of the magnetic features of the $SrCu_2(BO_3)_2$ system showing its quasi-two-dimensionality, it fails to account for some fine details. For instance, the single triple excitation exhibits a fine structure [15, 16], which calls for magnetic anisotropy to be included in the model Hamiltonian. In fact, in was shown by Cépas *et al*. that the observed splitting of the lowest-lying excitation can be explained by including Dzyaloshinsky-Moriya (DM) interaction between next-nearest neighbors [23],

$$H = \sum_{\{l,m\}} \pm D'_{\parallel} \mathbf{e}_c \cdot \mathbf{S}_l \times \mathbf{S}_m \,, \tag{4.2}$$

with the corresponding Dzyaloshinsky-Moriya vector $D'_{\parallel} = k_B \cdot 2.1\,\mathrm{K}$ pointing parallel to the crystal *c* axis. Such a form of the DM interaction was obtained by symmetry arguments with the small buckling of the $CuBO_3$ planes (see Fig. 4.1a) neglected. In fact, if these planes are treated as being completely flat there will be no DM coupling within nearest Cu^{2+} pairs due to the center of inversion positioned in the middle of each dimer.

However, there are numerous recent experimental findings suggesting also sizable intradimer DM interaction. Namely, the unusual ^{11}B NMR shifts at low temperatures and the observed enhanced staggered magnetization [24, 25], the relative intensities of singlet-triplet transitions observed in recent high-field ESR measurements [26], as well as the temperature dependence of the specific heat at low temperatures and in high magnetic fields, i.e., above 27 T [27], can all be explained by inclusion of the nearest-neighbor DM coupling. Second, though the interdimer DM interaction $D'_{\parallel}$ reproduces the observed fine splitting of the single triplet excitation and is of the expected amplitude, $D'_{\parallel} \approx \Delta g/g \cdot J' \approx k_B \cdot 6\,\mathrm{K}$, it cannot explain the observation of the otherwise forbidden singlet-triplet transition in ESR [15] and far-infrared absorption measurements [17] in the first place. In the first approximation of the isotropic Hamiltonian (Eq. (4.1)) any spin operator applied to the singlet ground state vanishes. As the direct consequence magnetic transitions from this state to any excited state are not possible. Since the interdimer DM interaction mixes a finite amount of the excited states into the ground state, these transitions are in principal allowed in $SrCu_2(BO_3)_2$ system. However, due to the symmetry of the system dictating the DM vector pattern, the above-mentioned DM terms still yield zero intensity of the magnetic dipole transitions between the ground state and the lowest-lying excited states of the system for $\mathbf{B} \parallel \mathbf{c}$ [23, 28]. The explanation of the observed ESR transition for this reason still stimulates theoretical work. Quite recently the exact

diagonalization approach of the model Hamiltonian on relatively small spin system of 6 sites [29] and the application of the standard Lanczos method on somewhat larger spin clusters of 20 sites [30] have been reported. The latter study provides a satisfactory explanation of many details of the observed single triplet splitting by inclusion of the intradimer DM anisotropy. Moreover, it shows that also a finite component of the symmetry-forbidden intradimer DM vectors $D_{\parallel}$ is required to account for the experimental findings, implying that the system should undergo a structural phase transition at very low temperatures.

Alternatively, Cépas *et al*. have proposed that electric dipole transitions between the ground state and the excited states is responsible for the observation of these "forbidden" transitions [28, 31]. The authors successfully explained the occurrence of the infrared-active modes as well as the dependence of their relative intensities on the external magnetic field [17] by introducing a novel concept of dynamical DM interaction. In this picture phonons induce instantaneous DM terms, which are otherwise forbidden by the crystal symmetry.

Nevertheless, a strong experimental evidence for the dynamic DM coupling is still lacking, which is why we employed a comprehensive X-band ESR study on a single crystal of the $SrCu_2(BO_3)_2$ system [32]. The temperature dependence and the angular dependence of the observed linewidth helped us to give the first quantitative estimation of the intradimer Dzyaloshinsky-Moriya coupling corresponding to high temperatures. The second aim of our ESR investigation was to try to determine the major anisotropy contributions in the case of the two-dimensional $SrCu_2(BO_3)_2$ system. Although the anisotropic spin interactions are expected to be weak, they can have a strong impact on spin dynamics due to the highly frustrated nature of the system. We conducted ESR experiments on powder samples [33] as well as on a single crystal [32, 34] in order to be able to clarify this issue. The experimental results from the single crystal enabled us to determine the direction of the intradimer DM vectors in addition to the interdimer ones. The results of the two above-mentioned topics are presented in the section that follows.

Another issue concerning the $SrCu_2(BO_3)_2$ system is the doping of this compound by whether electrons or holes. Due to its structural similarity with the high-T_c cuprates, already in the first report by Kageyama *et al*. [2] a possibility of superconductivity was suggested in the case of doped $SrCu_2(BO_3)_2$. This idea was then theoretically explored within the repulsive Hubbard model [35, 36]. However, no experimental evidence of the superconductivity of the doped $SrCu_2(BO_3)_2$ system has been reported up to date. On the other hand, the introduction of electrons or holes or the application of the chemical pressure on the system can have a pronounced effect also on the spin correlations developing in the system. Such disturbances can affect the spin gap and the overall low-lying magnetic excitations and possibly lead to novel magnetic phenomena. Our attempts of doping the powder $SrCu_2(BO_3)_2$ samples [37] will be presented in section 4.3, followed by a section of concluding remarks.

4.2 Determination of Magnetic Anisotropy by ESR

Electron spin resonance has been employed to determine the magnetic anisotropy contributions and the orientation of their principal axes since this technique probes the magnetic anisotropy on a local level and can thus serve as an additional source of information to those obtained from ^{11}B and ^{63}Cu NMR study on a single crystal [11]. For instance, the ^{11}B NMR lineshift with the boron ions acting as weakly interacting agents coupled to the electronic system implied on sizable anisotropy of the transferred hyperfine interaction just like our observation in the $PbNi_2V_2O_8$ system.

The X-band spectra corresponding to a high-purity powder sample recorded in the temperature range between room temperature and 5 K are presented in Fig. 4.2a. As evident the recorded derivative ESR signals are again rather broad indicating that the magnetic anisotropy is significant. In several samples also a narrower component corresponding to the *g*-factor around the free electron value has been observed at higher temperatures [33]. Its intensity varied from sample to sample, which is why we can now attribute it to paramagnetic impurities or a small amount of a different phase. The intensity of this additional narrow component is, however, insignificant with respect to the broad signal since it does not exceed few percents in any of the samples making the x-ray observation of this impurity "phase" nondetectable.

The ESR intensity at room temperature is around $0.8 \cdot 10^{-3}$ emu/Cu mol as determined from a comparison with a standard reference [33], which is very close to the value of the static susceptibility $1.0 \cdot 10^{-3}$ emu/Cu mol [2]. Moreover, the ESR signal follows the behavior of the latter parameter (see Fig. 4.2b), which implies that the measured ESR signal originates form the system of Cu^{2+} dimers. The small discrepancies between the temperature behavior of the ESR intensity and the susceptibility can be as in the previous chapter assigned to the broadness of the ESR spectra. However, contrary to the $PbNi_2V_2O_8$ compound the maxima of the two parameters in comparison are in clear accordance in the $SrCu_2(BO_3)_2$ system.

4.2.1 ESR Absorption Lineshape

The agreement of the ESR absorption spectra with the "broad"-Lorentzian lineshape (see Eq. (3.1)) in powder sample is satisfactory for the whole temperature range between room temperature and 5 K as shown in Fig. 4.2a. There are some minor discrepancies, which can however be attributed to the powder nature of the sample and the presence of a small amount of impurities. Namely, in powders there is a distribution of the linewidths and *g*-factors corresponding to a certain orientation of the magnetic field within the crystal frame, both of

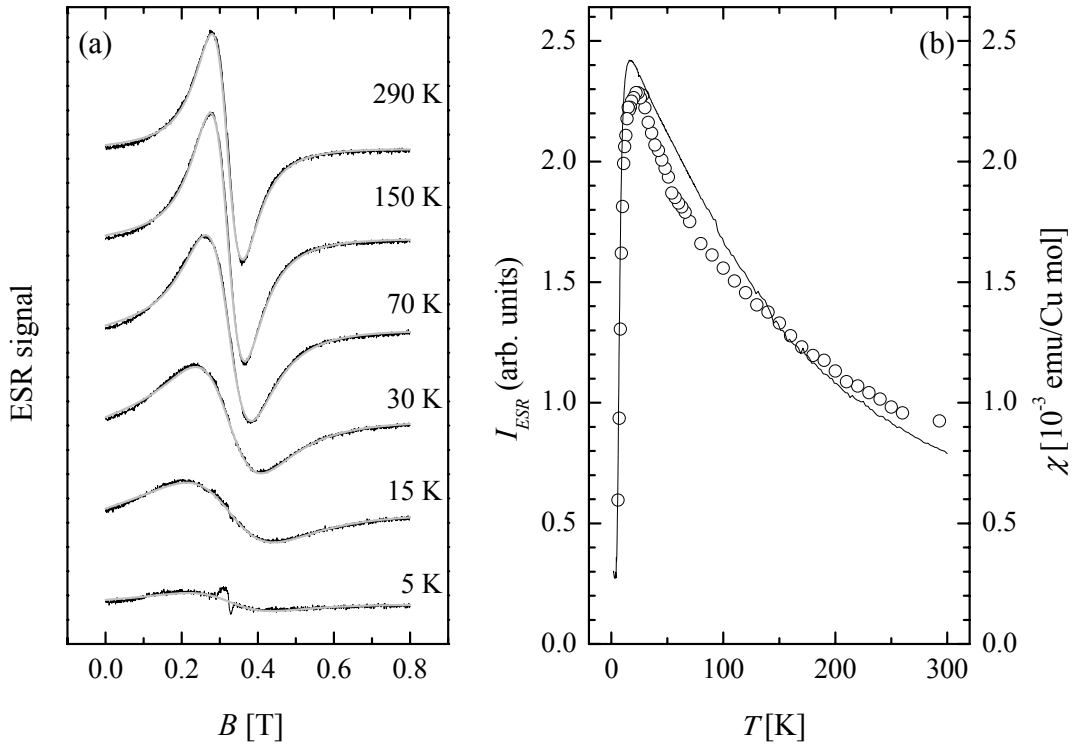

Fig. 4.2: (a) X-band ESR spectra of the $SrCu_2(BO_3)_2$ powder sample at selected temperatures with the gray lines corresponding to fits to the "broad"-Lorentzian model given by Eq. (3.1). (b) A comparison of the ESR intensity (○) and the static magnetic susceptibility (—).

which will be presented in what follows. The total ESR signal thus naturally deviates from the Lorentzian profile even though the individual components might be Lorentzian themselves.

For this reason the lineshape analysis is much more informative in case when single crystals are available. For the $SrCu_2(BO_3)_2$ system the accordance of the single-crystal spectra with the "broad"-Lorentzian distribution is excellent as illustrated in Fig. 4.3. The (a) part shows the experimental spectrum recorded at 525 K with the magnetic field oriented parallel to the *c* crystal axis. Although the recorded and the predicted lineshapes are practically identical, a more precise examination is possible by the standard test of the ESR lineshape [38]. In the plot $Y=\left(-2\left(B-B_0\right)I_{max}/\delta B_{pp}I(B)\right)^{1/2}$ versus $X=\left(2\left(B-B_0\right)/\delta B_{pp}\right)^2$, where I_{max} represents the maximum of the ESR derivative specter, the Lorentzian profile yields a linear dependence of the form $Y_L=X/4+3/4$ while the dependence for the Gaussian line is exponential $Y_G=\exp(X/2)/\sqrt{2e}$. Clearly, the character of the ESR line of the $SrCu_2(BO_3)_2$ compound is purely Lorentzian for both the external magnetic field parallel ($\theta=0°$) and perpendicular ($\theta=90°$) to crystal *c* direction defining the anisotropy direction. The plotted experimental data correspond to a rather high temperature of 525 K, which allows us to disprove the importance of the long-time diffusional decay of the spin correlation functions on the spin dynamics in the

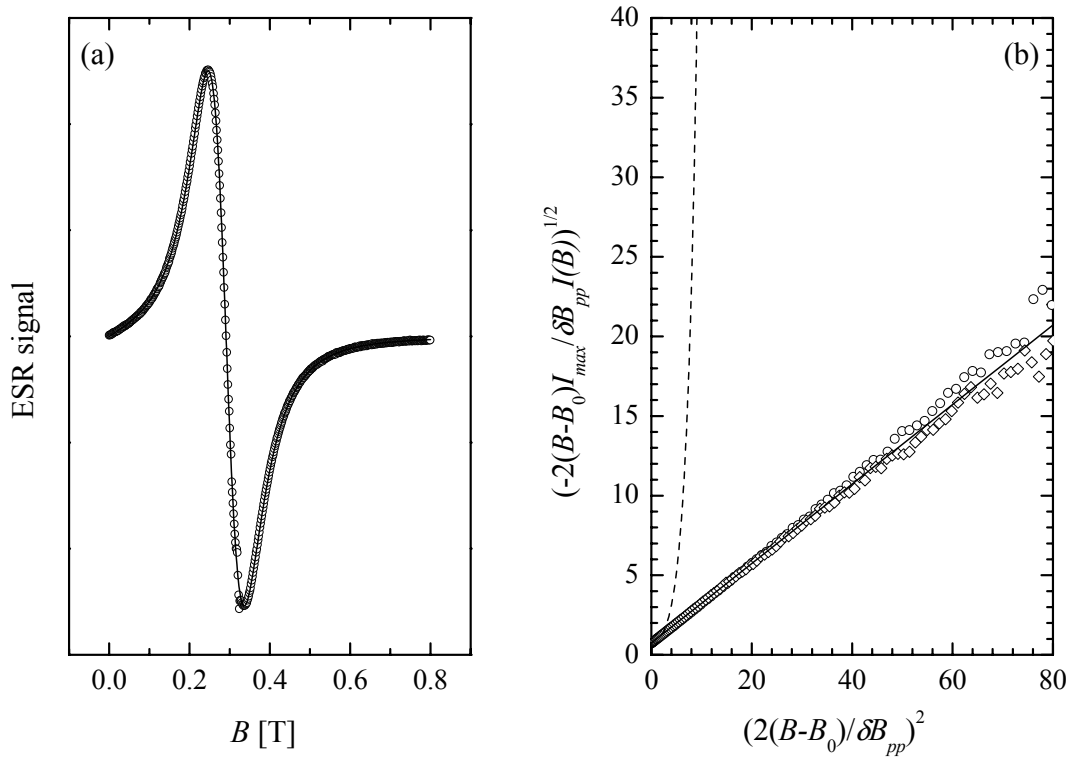

Fig. 4.3: A comparison of the experimentally detected X-band ESR spectrum of the $SrCu_2(BO_3)_2$ single crystal at 525 K with the Lorentzian (**—**) and the Gaussian (**--**) dependence for the external magnetic field parallel (○) and perpendicular (◇) to the crystal *c* axis. Part (a) shows the recorded spectrum as it appears, while part (b) illustrates the standard lineshape analysis.

time window of X-Band ESR for all temperatures below this value [34]. As in the $PbNi_2V_2O_8$ system the spin diffusion (see subsection 2.1.4) is also not important in $SrCu_2(BO_3)_2$ since the diffusional decay is basically thee-dimensional as $J_{\parallel} \gg g\mu_B B_0$. Second, the Lorentzian lineshape indicates that exchange narrowing is active allowing us to take advantage of the theory presented in subsection 2.1.3. Such a character is understandable since the ratio $J/g\mu_B\delta B_{pp}$ does not drop below 200 in the temperature interval of investigation indicating that the typical decay of the spin correlation function $\psi(\tau)$, regulated by the exchange interaction, is much faster than the decay of the ESR relaxation function $\varphi(t)$ determined by the magnetic anisotropy.

4.2.2 *g*-Factor Anisotropy

The *g*-factor anisotropy is a signature of the anisotropy of the local crystal structure around a certain localized magnetic moment defining the symmetry of the crystal field interaction as explained in chapter 2. In the case of the tetragonal local arrangement of the ligands (see Fig.

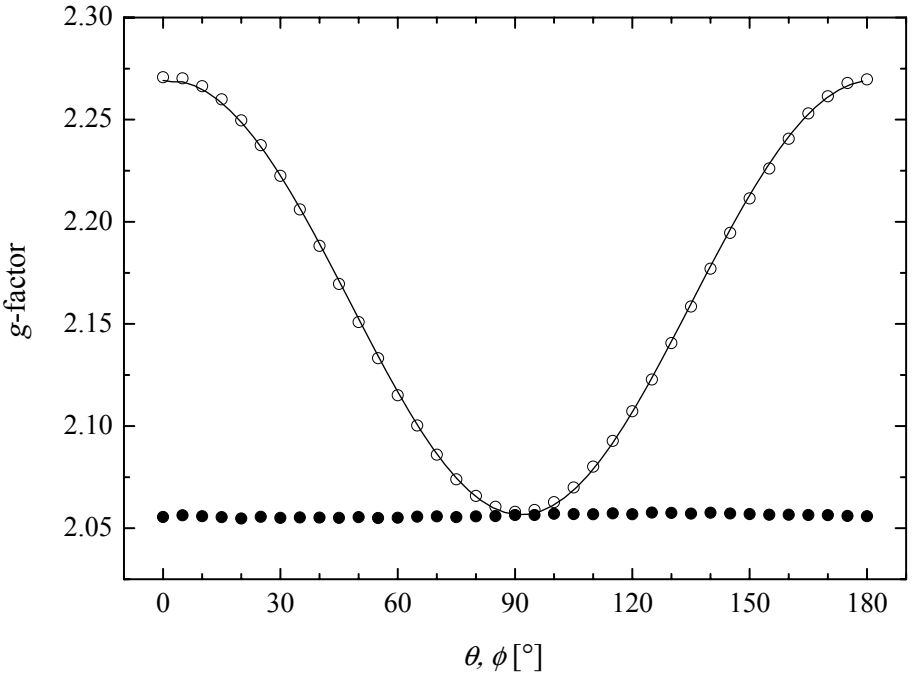

Fig. 4.4: The line-position anisotropy of the X-band ESR spectra recorded in the $SrCu_2(BO_3)_2$ single crystal at room temperature with the dependence on the polar angle θ between the direction of the external magnetic field and the crystal *c* direction (○) and the dependence with respect to the azimuthal angle ϕ (●). The solid line corresponds to the fit with the uniaxial-symmetry model given by Eq. (4.3).

4.1b) the *g*-factor is expected to depend on the polar angle θ between the direction of the external magnetic field and the anisotropy direction (*c* axis) while it should not show any dependence with respect to the azimuthal angle ϕ within the *ab* plane. This assumption is well justified in the case of the two-dimensional $SrCu_2(BO_3)_2$ system as presented in Fig. 4.4 corresponding to the angular dependence of the line position recorded at room temperature.

The dependence of the *g*-factor upon the polar angle can be described by the following equation

$$g = \sqrt{g_{\parallel}^2 \cos^2\theta + g_{\perp}^2 \sin^2\theta}\,, \tag{4.3}$$

where the parameter $g_{\parallel} = 2.269(2)$ represents the *g*-value along the *c* direction and $g_{\perp} = 2.057(2)$ the principal value for the perpendicular directions. The above expression can be derived in the same manner as presented below. The fairly small deviations of the *g*-factor from the free-electron value are a consequence of the relatively strong crystal field with respect to the spin-orbit coupling which then, in effect, partially restores the "quenched" orbital momentum as is characteristic for the iron-group ion Cu^{2+} ($3d^9$). The ratio $g_{\parallel} - g_0 / g_{\perp} - g_0 \approx 4$ is typical for the tetragonal symmetry in the case of the orbital part of the ground-state wave function being

of the form $\left|x^2-y^2\right\rangle=\left(x^2-y^2\right)f(r)$ with $f(r)$ being the isotropic electron-nucleus-distance dependent function [39]. In the other case of $\left|3z^2-r^2\right\rangle=\left(3z^2-r^2\right)f(r)$ function representing the ground state, which is also possible, a small and negative *g*-shift for the parallel direction should be observed [39]. Thus we can conclude that the orbital wave function of the ground state in $SrCu_2(BO_3)_2$ compound is the $\left|x^2-y^2\right\rangle$ function.

A more detailed look at the crystal structure shows that the local symmetry at Cu^{2+} sites is not perfectly tetragonal [4]. The arrangements of the oxygen ligands around the copper dimer and the corresponding angles at 100 K are shown in Fig. 4.5a. It should be emphasized that the angles do not change appreciably with the temperature. On the other hand, the buckling of the $CuBO_3$ planes (see Fig. 4.1a) characterized by the angle α between the normal of the plane containing the four oxygen ions corresponding to a certain CuO_4 plaquette, and the *c* crystal direction (see Fig. 4.5b) is a function of the temperature. The buckling angle at 100 K amounts to approximately 5.5° and decreases to 4° at room temperature. Moreover, it further decreases above this temperature and completely disappears at temperatures grater than $T_s=395\,\mathrm{K}$, which corresponds to the structural phase transition from the low-temperature $I\bar{4}2m$ crystal-symmetry phase to the high-temperature $I4/mcm$ one [4].

In what follows in this subsection, the effect of the buckling of the CuO_4 planes on the *g*-factor anisotropy is considered. Due to the crystal symmetry (a mirror plane perpendicular to the dimer direction positioned in the middle of it) one of the principal values of the *g*-factor is oriented along the η direction defined in Fig. 4.5. The other two principal directions are, however, shifted from the ξ and *c* crystal directions by the buckling angle α due to the finite corrugation of $CuBO_3$ planes. Let us assume that the principal values of the *g*-factor corresponding to the two principal directions within the plane of the plaquette have the same value. Then the transformation of the *g*-tensor written in the principal frame as

$$\underline{\mathbf{g}}'=\begin{bmatrix} g'_{\perp} & 0 & 0 \\ 0 & g'_{\perp} & 0 \\ 0 & 0 & g'_{\parallel} \end{bmatrix} \tag{4.4}$$

to the form in the modified crystal frame, where both *a* and *b* crystal axes are replaced by ξ and η axes, is obtained by the uniform rotation by $\pm\alpha$ around the η axis for the copper sites 1 and 2. The corresponding *g*-factor tensors have the following form

$$\begin{aligned} \underline{\mathbf{g}}_1 &= \mathrm{R}_{\eta}^{-\alpha}\,\underline{\mathbf{g}}'\,\mathrm{R}_{\eta}^{\alpha}=\begin{pmatrix} g'_{\perp}\cos^2\alpha+g'_{\parallel}\sin^2\alpha & 0 & -\left(g'_{\parallel}-g'_{\perp}\right)\sin\alpha\cos\alpha \\ 0 & g'_{\perp} & 0 \\ -\left(g'_{\parallel}-g'_{\perp}\right)\sin\alpha\cos\alpha & 0 & g'_{\parallel}\cos^2\alpha+g'_{\perp}\sin^2\alpha \end{pmatrix}, \\ \underline{\mathbf{g}}_2 &= \mathrm{R}_{\eta}^{\alpha}\,\underline{\mathbf{g}}'\,\mathrm{R}_{\eta}^{-\alpha}=\begin{pmatrix} g'_{\perp}\cos^2\alpha+g'_{\parallel}\sin^2\alpha & 0 & \left(g'_{\parallel}-g'_{\perp}\right)\sin\alpha\cos\alpha \\ 0 & g'_{\perp} & 0 \\ \left(g'_{\parallel}-g'_{\perp}\right)\sin\alpha\cos\alpha & 0 & g'_{\parallel}\cos^2\alpha+g'_{\perp}\sin^2\alpha \end{pmatrix}. \end{aligned} \tag{4.5}$$

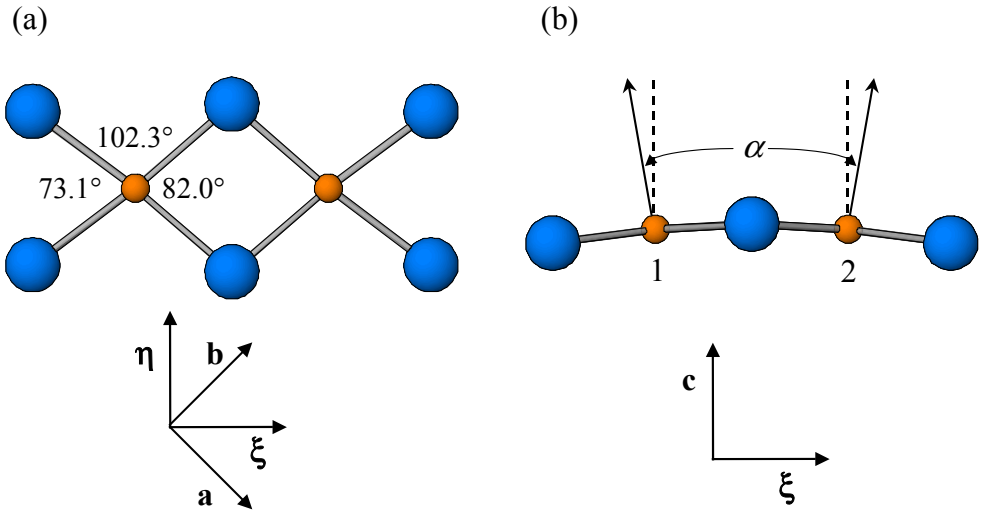

Fig. 4.5: The appearance of the two neighboring CuO_4 plaquettes in the (a) *ab* and (b) $c\xi$ crystal plane. The latter figure shows the buckling of these plaquettes with respect to the *c* crystal axis.

As the neighboring dimers are arranged perpendicular to each other, there are two more nonequivalent copper sites with the *g*-tensors

$$\begin{aligned}\underline{\mathbf{g}}_3 &= \mathrm{R}_\xi^{-\alpha}\,\underline{\mathbf{g}}\,\mathrm{R}_\xi^{\alpha} = \begin{pmatrix} g'_\perp & 0 & 0 \\ 0 & g'_\perp\cos^2\alpha + g'_\parallel\sin^2\alpha & \left(g'_\parallel - g'_\perp\right)\sin\alpha\cos\alpha \\ 0 & \left(g'_\parallel - g'_\perp\right)\sin\alpha\cos\alpha & g'_\parallel\cos^2\alpha + g'_\perp\sin^2\alpha \end{pmatrix}, \\ \underline{\mathbf{g}}_4 &= \mathrm{R}_\xi^{\alpha}\,\underline{\mathbf{g}}\,\mathrm{R}_\xi^{-\alpha} = \begin{pmatrix} g'_\perp & 0 & 0 \\ 0 & g'_\perp\cos^2\alpha + g'_\parallel\sin^2\alpha & -\left(g'_\parallel - g'_\perp\right)\sin\alpha\cos\alpha \\ 0 & -\left(g'_\parallel - g'_\perp\right)\sin\alpha\cos\alpha & g'_\parallel\cos^2\alpha + g'_\perp\sin^2\alpha \end{pmatrix}.\end{aligned} \tag{4.6}$$

Let us focus on the determination of the values of the *g*-factor corresponding to the crystal directions for the Cu^{2+} ion at site 1. The first one being $g_1^\eta = g'_\perp$ is trivial, however, for the case of the external magnetic field applied parallel to the ξ direction the following reasoning is in place. The Zeeman Hamiltonian of the form

$$H_Z = \mu_B \mathbf{S}\cdot\mathbf{g}\cdot\mathbf{B}_0 = \mu_B B_0\left(S^\xi g_1^{\xi\xi} + S^c g_1^{c\xi}\right), \tag{4.7}$$

with the corresponding *g*-factors written in the first column of the first tensor in Eq. (4.5), can be written in the basis of the two eigenstates $\left\langle S^\xi \right\rangle = \pm 1/2$, where ξ is taken as the quantization axis. In such a case the spin operator $S^c = \left(S^+ - S^-\right)/2i$ is a linear combination of the raising S^+ and the lowering operator S^-. In the introduced basis the Zeeman Hamiltonian reads

$$H_Z = \frac{\mu_B B_0}{2}\begin{pmatrix} g_1^{\xi\xi} & -ig_1^{c\xi} \\ ig_1^{c\xi} & -g_1^{\xi\xi} \end{pmatrix}, \tag{4.8}$$

which sets the corresponding eigenvalues

$$E = \pm\frac{\mu_B B_0}{2}\sqrt{\left(g_1^{\xi\xi}\right)^2 + \left(g_1^{c\xi}\right)^2} = \pm\frac{\mu_B B_0}{2}\sqrt{g_\perp'^{\,2}\cos^2\alpha + g_\parallel'^{\,2}\sin^2\alpha}\,. \tag{4.9}$$

The effective *g*-factor is thus $g_1^{\xi} = \sqrt{g_\perp'^{\,2}\cos^2\alpha + g_\parallel'^{\,2}\sin^2\alpha}$. Similar expressions can be obtained also for the other three nonequivalent sites. If the principal *g*-values are estimated in the first approximation as the parameters obtained from the fit of the experimental data presented above, i.e., $g_\parallel' = 2.269$ and $g_\perp' = g_1^{\eta} = 2.057$, and we take into account room temperature value of the buckling angle, the difference of the two extreme values of the *g*-factor within the *ab* crystal plane is evaluated to be of the size $g_1^{\xi} - g_1^{\eta} = 0.001$. In a similar manner the expression $g_1^{c} \approx g_\parallel'$ is realized.

As the corrections are rather small, the above approximation of the principal *g*-values with the experimental values is well justified. Furthermore, the buckling of the CuO_4 plaquettes away from the *c* direction does not induce an appreciable azimuthal-angle dependence of the position of the center of the ESR absorption line, which is in accordance with the experimental observations presented in Fig. 4.4. The assumption of the tetragonal local symmetry thus also seems to be reasonable, although, it has to be emphasized that the measured ESR signal reflects the average contribution of all the four nonequivalent Cu^{2+} sites.

4.2.3 ESR Linewidth

The X-band ESR spectra have been recorded in a broad temperature interval between 575 K and 5 K. However, the single crystal sample was found to contain some paramagnetic impurities unlike the powder sample. This fact disables a reliable determination of the linewidth below approximately 10 K due to the fact that narrow features positioned at the free-electron *g*-value with the Curie-like character of the ESR intensity dominate the low-temperature ESR spectra in the single crystal. The rather large linewidth of the powder sample at room temperature, which accounts to $\delta B_{pp}^{p} = 78(1)\,\mathrm{mT}$, can be attributed to considerable magnetic anisotropy present in the system. Moreover, also the linewidth anisotropy is substantial. The width corresponding to the magnetic field parallel to the crystal anisotropy direction is $\delta B_{pp}^{\parallel} = 91(1)\,\mathrm{mT}$ while it is $\delta B_{pp}^{\perp} = 69(1)\,\mathrm{mT}$ for the magnetic filed within the *ab* crystal plane. As with the *g*-factor also the linewidth exhibits no dependence on the azimuthal angle.

The temperature dependence of the linewidth of the powder sample as well as the single crystal is shown in Fig. 4.6. This ESR parameter shows a moderate linear decrease with decreasing temperature in the high-temperature regime, exhibits a minimum around room temperature and a strong broadening below room temperature. A maximum is observed around 10 K in the powder sample, while a reliable analysis is not possible in the single crystal below

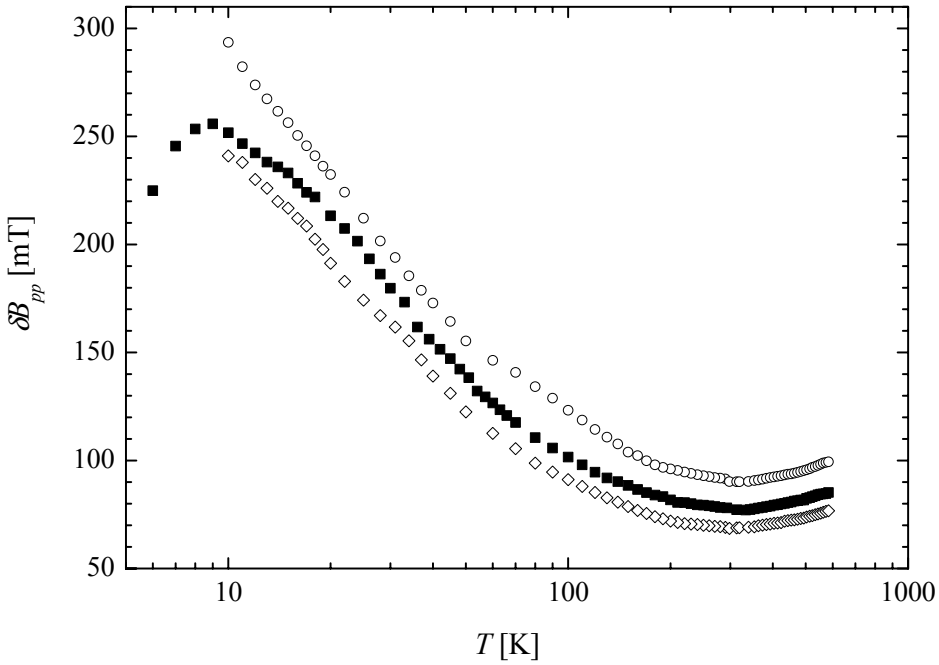

Fig 4.6: The temperature behavior of the X-band ESR linewidth in the $SrCu_2(BO_3)_2$ powder sample (■) and single crystal with magnetic field parallel (○) and perpendicular (◇) to the crystal *c* axis.

this temperature to confirm and evaluate the position of the maxima. The high-temperature increase of the linewidth with rising temperature does not depend on the orientation of the external magnetic field. Thus the slopes for the parallel direction $k_{\parallel} = 0.035(1)\,\mathrm{mT/K}$ and the perpendicular direction $k_{\perp} = 0.033(1)\,\mathrm{mT/K}$ with respect to the crystal *c* axis have the same value within the experimental error. Such a behavior will be shown to be extrinsic to the pure spin system, i.e., it is due to the coupling of the spin system with lattice vibrations. A further analysis of the temperature dependence in different regimes will be presented latter on in this subsection but first let us focus on the observed angular dependence of the linewidth and evaluate the effect of the possible line-broadening mechanisms.

Dzyaloshinsky-Moriya Interaction and Other Sources of Spin Anisotropy in $SrCu_2(BO_3)_2$

Before going to a detailed analysis of the linewidth anisotropy an estimation of the strength of all possible line-broadening mechanisms is in place [34]. As explained in chapter 2 the dominant anisotropy contributions to the spin Hamiltonian for a system of spins $S = 1/2$ are the magnetic dipolar interaction between the localized magnetic moments (H_{dd}), the hyperfine interaction of electronic and nuclear spins, the symmetric anisotropic exchange (H_{ae}), and the antisymmetric Dzyaloshinsky-Moriya interaction (H_{DM}). A superficial evaluation of the

importance of each of the mentioned spin anisotropies can be made by the approximate expression of the linewidth of the exchange-narrowed ESR absorption line corresponding to infinite temperatures given by Eq. (2.17). The approximation of the spin correlation time by $\tau_c = \hbar/J$ in the system with complicated exchange pattern seems rather careless, however, it proves to be sufficient for a mere order-of-magnitude prediction.

Knowing the crystal structure of the $SrCu_2(BO_3)_2$ the evaluation of the local dipolar fields is straightforward. The contribution of the nearest neighbor, which is at distance $r = 2.91\,\text{Å}$, is of the order of $\mu_0 g\mu_B/4\pi r^3 = 83\,\text{mT}$. The calculated second moment is similarly of the size $M_2^{dd} = (g\mu_B \cdot 100\,\text{mT})^2$, which yields according to Eq. (2.17) the linewidth of $\delta B_{pp}^{dd} \approx 0.2\,\text{mT}$. Second, the hyperfine coupling constants for the $|x^2 - y^2\rangle$ ground state of the Cu^{2+} ions in the tetragonal crystal field are given as [39]

$$\begin{aligned} A_\parallel &= 2\mathscr{P}\left(-\mathscr{K} - \frac{4}{7} + \frac{3}{7}\Delta g_\perp + \Delta g_\parallel\right), \\ A_\perp &= 2\mathscr{P}\left(-\mathscr{K} - \frac{2}{7} + \frac{11}{14}\Delta g_\perp\right), \end{aligned} \tag{4.10}$$

where the parameter $\mathscr{P}$ for free copper ions has the value $\mathscr{P} = \mu_0 \gamma_e \hbar g\mu_B/4\pi\langle r^3\rangle \approx g\mu_B \cdot 380\,\text{G}$. In crystals this parameter is typically lowered by 15-20% due to the covalency effect. The second parameter $\mathscr{K} \approx 0.3$ originates from the polarization of *s* electrons, which also induces the electron-nucleus magnetic coupling. From the experimentally determined *g*-shifts the principal values of the copper hyperfine coupling in $SrCu_2(BO_3)_2$ can be evaluated to be of the size $|A_\parallel| \approx g\mu_B \cdot 350\,\text{G}$ and $|A_\perp| \approx g\mu_B \cdot 20\,\text{G}$. The contribution of this anisotropic interaction to the ESR linewidth $\delta B_{pp}^{hf} \approx 0.03\,\text{mT}$ is thus even smaller than the dipolar contribution.

The two anisotropic parts of the spin Hamiltonian already considered in the previous paragraph evidently cannot account for the experimentally observed linewidths, which is why anisotropic exchange coupling has to be employed. The symmetric part of this interaction originates from the second order perturbation in the spin-orbit coupling and is thus of the order $d + e \sim (\Delta g/g)^2 \cdot J \approx k_B \cdot 1\,\text{K}$. According to Eq. (2.17) and Eq. (2.22) this pseudo-dipolar interaction then dictates ESR linewidths of $\delta B_{pp}^{ae} \approx 3\,\text{mT}$ again more than an order of magnitude narrower than the observed spectra. The last candidate is the antisymmetric part of the anisotropic exchange. As the Dzyaloshinsky-Moriya interaction is the result of the first order perturbation calculation its size can be as large as $D \sim \Delta g/g \cdot J$. In fact, as already explained the value of the interdimer DM coupling estimated from the fine splitting of the lowest-lying magnetic excitation is $D'_\parallel = k_B \cdot 2.1\,\text{K}$ [23], which is of the same order as the predicted value $D \sim \Delta g/g \cdot J' = k_B \cdot 6\,\text{K}$. The contribution of this interaction is then $\delta B_{pp}^{ae} \approx 46\,\text{mT}$.

The above analysis clearly shows that DM interaction is the only one giving linewidths of the correct order of magnitude. All the other contributions are at least an order of magnitude

smaller. It should be emphasized, though, that the presented estimations are strictly valid in the infinite-temperature regime where the static spin correlations effects are negligible. Second, the spin correlation time was evaluated from only the nearest-neighbor exchange, which is why the sole disagreement of the DM dictated linewidth and the experimental values by approximately the factor of 2 should not be treated as a failure. As it will be shown, a more accurate determination of the second and the fourth moment of the ESR absorption lines will help us to critically evaluate the current picture of only the next-nearest DM coupling with vectors pointing along the anisotropy axis, designated to be the dominant anisotropic interaction.

ESR Linewidth Anisotropy Determined by Dzyaloshinsky-Moriya Interaction

The angular dependence of the ESR linewidth resembles the behavior of the *g*-factor, as there is no anisotropy within the experimental error of $\pm 1\,\mathrm{mT}$ for external magnetic field within the *ab* crystal plane and a significant dependence on the polar angle. The anisotropies recorded at room temperature and at the temperature of 525 K are shown in Fig. 4.7. The dependence can be described by the equation of the form

$$\delta B_{pp} = A + B\left(1 + \cos^2\theta\right), \tag{4.11}$$

with parameters $A = 47.8(5)\,\mathrm{mT}$, $B = 21.8(5)\,\mathrm{mT}$ corresponding to 295 K and $A = 54.1(5)\,\mathrm{mT}$, $B = 22.0(5)\,\mathrm{mT}$ at 525 K. The parameter B is virtually unchanged as a consequence of the already mentioned fact that the high-temperature linear increase is not angular dependent. The form of the linewidth anisotropy given by Eq. (4.11) is preferred over the self-offering expression $\Delta B_{pp} = A' + B'\cos^2\theta$ for the reasons becoming unveiled shortly.

Let us first explore the originally proposed picture of only out-of-plane interdimer Dzyaloshinsky-Moriya interaction as the only one surviving the approximation of the planar $CuBO_3$ planes [23]. The way to the pattern of the DM vectors shown in Fig. 4.8 is paved with few fundamental symmetry arguments. A detailed analysis will be presented latter on in connection with a more general case of corrugated $CuBO_3$ planes. For the moment let us make only a single comment on the absence of the nearest-neighbor DM coupling. The crucial feature is the presence of the center of inversion in the middle of each dimer bond. Since this is a symmetry operation of the crystal space group, the Hamiltonian is invariant to its application. On the other hand, the DM interaction has odd parity with respect to the inversion due to its antisymmetric nature. Consequently, the intradimer DM coupling is identically equal to zero.

In the case of the Dzyaloshinsky-Moriya interaction as the dominant spin anisotropy contribution the ESR linewidth (see Eq. (2.19)) is determined by the second moment, given by Eq. (2.22), and the fourth moment [40]

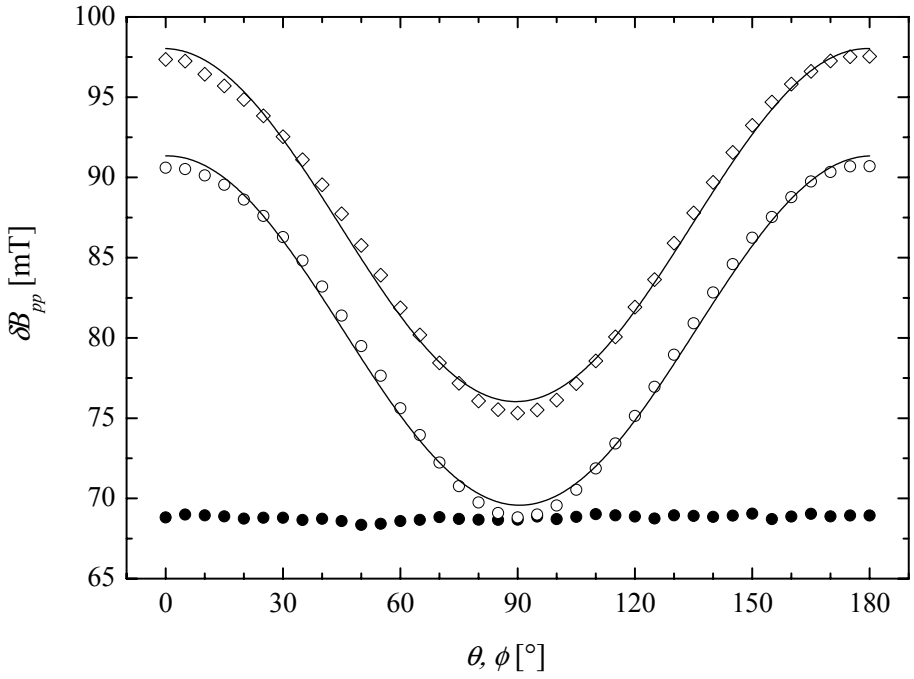

Fig. 4.7: X-band ESR linewidth anisotropy of the $SrCu_2(BO_3)_2$ single crystal at 525 K (◇) and at 295 K with respect to the polar angle θ (○) and the azimuthal angle ϕ (●). The solid lines correspond to the fit to the phenomenological model given by Eq. (4.11).

$$
\begin{aligned}
M_2^{DM} &= \frac{S(S+1)}{N}\frac{1}{3}\sum_{(i,j)}\left(D_{ij}^x\right)^2+\left(D_{ij}^y\right)^2+2\left(D_{ij}^z\right)^2, \\
M_4^{DM} &= \frac{S^2(S+1)^2}{N}\left[\frac{2}{3}\sum_{(ij)}J_{ij}^2\left(\left(D_{ij}^x\right)^2+\left(D_{ij}^y\right)^2+2\left(D_{ij}^z\right)^2\right)\right. \\
&\quad \left.+\frac{1}{18}\sum_{(ijk)}\sum_{\alpha=x,y,z}\left(\left(F_{ijk}^\alpha\right)^2+\left(F_{ijk}^z\right)^2+\left(F_{jki}^\alpha\right)^2+\left(F_{jki}^z\right)^2+\left(F_{kij}^\alpha\right)^2+\left(F_{kij}^z\right)^2\right)\right].
\end{aligned}
\tag{4.12}
$$

The three-site terms sum over functions $F_{ijk}^\alpha = J_{ij}\left(D_{ik}^\alpha - D_{jk}^\alpha\right)+J_{ik}\left(D_{ij}^\alpha + D_{jk}^\alpha\right)$. The above expressions correspond to the DM vectors written in the laboratory frame with z as the direction of the external magnetic field. The expected ESR linewidth anisotropy is then obtained by the transformation of the DM vector from the laboratory to the crystal frame

$$
\begin{aligned}
D_{ij}^x &= D_{ij}^a\cos\theta\cos\varphi + D_{ij}^b\cos\theta\sin\varphi - D_{ij}^c\sin\theta, \\
D_{ij}^y &= -D_{ij}^a\sin\varphi + D_{ij}^b\cos\varphi, \\
D_{ij}^x &= D_{ij}^a\sin\theta\cos\varphi + D_{ij}^b\sin\theta\sin\varphi + D_{ij}^c\cos\theta.
\end{aligned}
\tag{4.13}
$$

The orientation of the external magnetic field with respect to the crystal frame is here denoted as usually by the polar angle θ and the azimuthal angle ϕ. Plugging the Eq. (4.13) into Eqs. (4.11) and (4.12) and taking into account the pattern of the DM vectors as presented in Fig. 4.8a yields the expressions for the second and the fourth moment in the $SrCu_2(BO_3)_2$ compound,

$$M_2^{DM} = \frac{D_{\parallel}'^2}{2}\left(1+\cos^2\theta\right),$$
$$M_4^{DM} = \frac{3}{4}D_{\parallel}'^2\left(3J^2+3J'^2-2JJ'\right)\left(1+\cos^2\theta\right). \tag{4.14}$$

This according to Eq. (2.19) dictates the infinite-temperature linewidth angular dependence of the following appearance

$$\delta B_{pp}^{DM} = \frac{C}{g\mu_B}\frac{D_{\parallel}'^2}{\sqrt{6\left(3J^2+3J'^2-2JJ'\right)}}\left(1+\cos^2\theta\right). \tag{4.15}$$

The above-derived equation exhibits no ϕ-dependence, which is in excellent agreement with the experimental findings presented in Fig. 4.7. On the other hand, the predicted dependence on the polar angle is of the form $\left(1+\cos^2\theta\right)$. This defers from the observed behavior in one important detail. Namely, there is an additional constant parameter *A*, which has to be included to account for the experimental data. A satisfactory fit is obtained only when this supplementary parameter is of the same order as the parameter *B* giving the angular dependence. Therefore, the magnetic anisotropy responsible for the deviation of the theoretical prediction from the experiment must be significant and cannot be simply ignored. In this sense the picture of only out-of-plane interdimer DM coupling is insufficient.

Symmetric anisotropic exchange, which should provide the second larger contribution to the anisotropy in the $SrCu_2(BO_3)_2$ system as shown above, can be safely dismissed from the possible causes of the observed discrepancy for at least two reasons. First, it is more that an order of magnitude below the DM contribution and second, also the angular dependence dictated by the symmetric part of the anisotropic exchange does not improve the agreement between the theory and the experiment. Namely, the symmetric anisotropy can be presented by a symmetric traceless tensor with principal axes lying parallel to the principal axes of the *g*-tensor [41]. As the corresponding anisotropy tensor is thus axially symmetric, the linewidth anisotropy is again of the form $\left(1+\cos^2\theta\right)$ hence again failing to give an explanation of the extra parameter *A*. Here it should be emphasized that *A* and *B* remain of the same size even when the high-temperature line-broadening contribution is subtracted. The latter accounts to approximately 10 mT at room temperature.

Clearly, the key to resolving the above-presented inconsistency between the observed ESR linewidth and the theoretical prediction lies in improving the magnetic anisotropy Hamiltonian. It seems that the approximation of the $CuBO_3$ planes as being planar causes the observed discrepancy. In reality the $CuBO_3$ planes are buckled below the structural phase transition occurring at $T_s = 395\,\mathrm{K}$ [4], so there is no *ab* mirror plane containing the dimers. As a direct consequence the center of inversion present in the middle of each dimer is removed. This allows also for finite intradimer DM coupling. The bending of the neighboring CuO_4 plaquettes

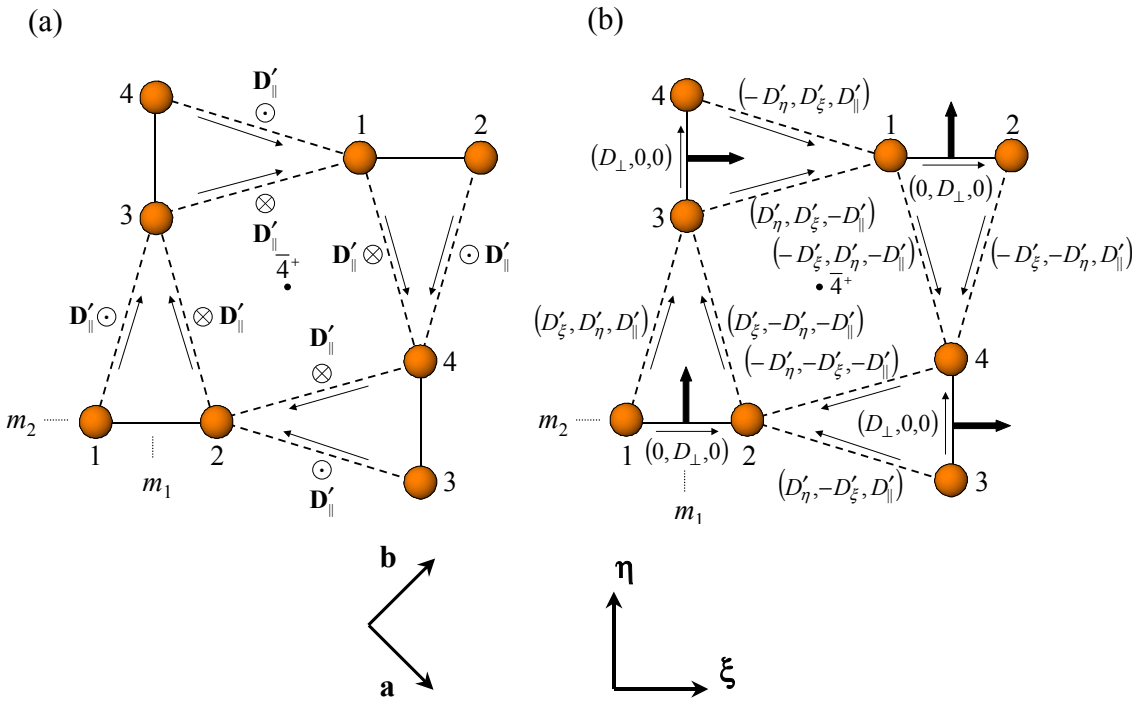

Fig. 4.8: The two-dimensional network of Cu^{2+} ions with the corresponding pattern of the Dzyaloshinsky-Moriya interaction for (a) only out-of-plane interdimer vectors and (b) also in-plane interdimer as well as intradimer DM vectors allowed by buckling of the $CuBO_3$ planes. The thin arrows represent the chosen direction of the DM bonds while the thick ones stand for the intradimer DM vectors.

can be the origin of nonzero in-plane components of the interdimer as well as the intradimer DM vectors. Moreover, the pattern of these vectors is well defined by the symmetry of the crystal as shown in Fig. 4.8b. Since the DM interaction is antisymmetric in its nature, the order of the spin operators is important. The orientation of the DM bonds is presented in Fig. 4.8 by thin arrows.

Let us first explore the possible pattern of the nearest-neighbor DM coupling vectors. The coupling between spin sites 1 and 2 is determined by the mirror plane m_2 corresponding to the ξc plane, which includes the dimer. When performing symmetry operations one has to take special care of transforming the spins as a vector field. A symmetry operation O changes the orientation of the spin vector and its coordinate according to $\mathbf{S}(\mathbf{r}) \to O[\mathbf{S}(\mathbf{r})] = O\mathbf{S}(O^{-1}\mathbf{r})$. As spins are axial vectors, the effect of the mirror plane m_2 is the following

$$\begin{bmatrix} S^{\xi}_{1,2} \\ S^{\eta}_{1,2} \\ S^{c}_{1,2} \end{bmatrix} \to \begin{bmatrix} -S^{\xi}_{1,2} \\ S^{\eta}_{1,2} \\ -S^{c}_{1,2} \end{bmatrix}. \tag{4.16}$$

The DM term connecting the spin sites 1 and 2

$$H_{12}^{DM} = D_{12}^{\xi}\left(S_1^{\eta}S_2^{c} - S_1^{c}S_2^{\eta}\right) + D_{12}^{\eta}\left(S_1^{c}S_2^{\xi} - S_1^{\xi}S_2^{c}\right) + D_{12}^{c}\left(S_1^{\xi}S_2^{\eta} - S_1^{\eta}S_2^{\xi}\right) \tag{4.17}$$

turns after the transformation to

$$H_{12}'^{DM} = D_{12}^{\xi}\left(-S_1^{\eta}S_2^{c} + S_1^{c}S_2^{\eta}\right) + D_{12}^{\eta}\left(S_1^{c}S_2^{\xi} - S_1^{\xi}S_2^{c}\right) + D_{12}^{c}\left(-S_1^{\xi}S_2^{\eta} + S_1^{\eta}S_2^{\xi}\right). \tag{4.18}$$

As m_2 is the symmetry operator of the space group, $H_{12}'^{DM} = H_{12}^{DM}$, which determines the DM vector $D_{1,2} = (0, D_{\perp}, 0)$. The relation of the remaining intradimer vectors with this one is determined by applying translations and rotoinversion operations. For instance, the orientation of the DM vector connecting sites 3 and 4 is obtained by the use of the rotoinversion axis $\bar{4}^{+}: 0,1/2,c; 0,1/2,1/4$ [42] combining the anticlockwise rotation around the axis $0,1/2,c$ and the inversion through the point $0,1/2,1/4$ with the coordinates given in the crystal frame. The position of the axis and the inversion point is presented in Fig. 4.8 by a dot. This symmetry operation causes the transformation of the spin operators

$$\begin{bmatrix} S_{1,2}^{\xi} \\ S_{1,2}^{\eta} \\ S_{1,2}^{c} \end{bmatrix} \rightarrow \begin{bmatrix} -S_{3,4}^{\eta} \\ S_{3,4}^{\xi} \\ S_{3,4}^{c} \end{bmatrix}. \tag{4.19}$$

By comparing the DM terms joining the spin sites 3 and 4 before and after the transformation

$$\begin{aligned} H_{34}^{DM} &= D_{34}^{\xi}\left(S_3^{\eta}S_4^{c} - S_3^{c}S_4^{\eta}\right) + D_{34}^{\eta}\left(S_3^{c}S_4^{\xi} - S_3^{\xi}S_4^{c}\right) + D_{34}^{c}\left(S_3^{\xi}S_4^{\eta} - S_3^{\eta}S_4^{\xi}\right), \\ H_{34}'^{DM} &= D_{12}^{\xi}\left(S_3^{\xi}S_4^{c} - S_3^{c}S_4^{\xi}\right) + D_{12}^{\eta}\left(-S_3^{c}S_4^{\eta} + S_3^{\eta}S_4^{c}\right) + D_{12}^{c}\left(-S_3^{\eta}S_4^{\xi} + S_3^{\xi}S_4^{\eta}\right), \end{aligned} \tag{4.20}$$

the following relations are obtained

$$D_{34}^{\xi} = D_{12}^{\eta} = D_{\perp}, \quad D_{34}^{\eta} = -D_{12}^{\xi} = 0, \quad D_{34}^{c} = D_{12}^{c} = 0. \tag{4.21}$$

Similarly, if the interdimer DM interaction connecting the sites 1 and 3 is chosen as $\mathbf{D}_{13}' = (D_{\xi}', D_{\eta}', D_{\parallel}')$ all the remaining interdimer vectors can be constructed. In general, if two oriented DM spin pairs are connected by a mirror plane (m_1 or m_2) as is the case of the bonds $(1,3)$ and $(2,3)$, the component of the DM vector perpendicular to the mirror plane will remain unchanged while the two components within the plane will change their sigh due to the fact that the same sigh transformation occurs for the spin operators. Second, the connection of the interdimer DM bonds originating from the dimers lying along ξ axis and those along η axis can be found by the use of the rotoinversion axes in the same manner as it was shown above for the intradimer DM coupling.

The symmetry arguments allow us to describe the DM vector pattern with only one intradimer DM coupling parameter $D_{\perp}$ and three interdimer parameters $D_{\xi}', D_{\eta}', D_{\parallel}'$ as shown in Fig. 4.8b. The buckling of the $CuBO_3$ planes thus induces additional in-plane DM vectors. Since it is expected that the size of the introduced in-plane intradimer DM interaction is greater than the size of the in-plane interdimer coupling, let us first neglect the latter interaction. The second

and the fourth moment of the expected ESR spectra in the limit of infinite temperature can be derived by the use of Eqs. (4.11) and (4.12) and the transformation given by (4.13),

$$\begin{aligned} M_2^{DM} &= \frac{1}{16}\left(8D_{\parallel}'^2 + 3D_{\perp}^2\right) + \frac{1}{16}\left(8D_{\parallel}'^2 - D_{\perp}^2\right)\cos^2\theta, \\ M_4^{DM} &= \frac{3}{128}\left(32D_{\parallel}'^2 J_1^2 + 3D_{\perp}^2 J_2^2\right) + \frac{3}{128}\left(32D_{\parallel}'^2 J_1^2 - D_{\perp}^2 J_2^2\right)\cos^2\theta, \end{aligned} \tag{4.22}$$

with the exchange coupling parameters $J_1^2 = 3J^2 + 3J'^2 - 2JJ'$ and $J_2^2 = 13J^2 + 6J'^2$. The anisotropy of the linewidth obtained by the use of Eq. (2.19),

$$\delta B_{pp}^{DM} = \frac{2\pi}{\sqrt{6}}\frac{1}{g\mu_B}\left(\frac{\left(8D_{\parallel}'^2 + 3D_{\perp}^2 + \left(8D_{\parallel}'^2 - D_{\perp}^2\right)\cos^2\theta\right)^3}{96\left(32D_{\parallel}'^2 J_1^2 + 3D_{\perp}^2 J_2^2 + \left(32D_{\parallel}'^2 J_1^2 - D_{\perp}^2 J_2^2\right)\cos^2\theta\right)}\right)^{1/2}, \tag{4.23}$$

again does not depend on the azimuthal angel as in the experiment, which is due to the orthogonal arrangement of spin dimers. In the above-derived expression the constant $C = 2\pi/\sqrt{6}$ corresponding to a product spectrum of a Lorentzian function and an exponentially decaying function $\exp\left(-|B - B_0|g\mu_B/J\right)$ was used as explained in chapter 2 below the Eq. (2.19). This approximation gives the highest value of the *C* constant and thus yields the best accordance of the experimentally deduced parameters with the known ones as shown in the following.

Although the above-obtained expression cannot be written in the form $A + B\left(1 + \cos^2\theta\right)$, there is not much difference between the two angular dependences. The fit of the experimental anisotropy at temperatures 295 K and 525 K with the model given by Eq. (4.23) is presented in Fig. 4.9a. The high-temperature linear broadening is subtracted as it will be latter shown that it is not intrinsic to the spin system alone, but is rather an effect of the coupling of this system with phonons. The derived model fits the experimental data rather well. The parameters of the DM interaction for the temperature of 525 K, where the effect of the static spin correlations is expected to be absent, have values $D_{\parallel}' = k_B \cdot 2.4(1)\,\mathrm{K}$ and $D_{\perp} = k_B \cdot 4.0(1)\,\mathrm{K}$. The parameters are only slightly larger at room temperature, i.e., by 0.1 K, which is due to the fact that the almost perfect linearly increasing broadening of the linewidth is seen above approximately 340 K. The estimated value of the interdimer exchange is in good agreement with the value evaluated from the fine splitting of the single triplet excitation $D_{\parallel}' = k_B \cdot 2.1\,\mathrm{K}$ [23]. When fitting the angular dependence of the linewidth the value of the isotropic exchange was taken as $J = k_B \cdot 85\,\mathrm{K}$ as evaluated from the temperature dependence of the static susceptibility [13]. However, recent analysis of the specific heat data in applied magnetic fields yields somewhat lower value of the nearest-neighbor exchange $J = k_B \cdot 74\,\mathrm{K}$ [27]. Such a value is also shown to be consistent with the magnetic susceptibility [27] as well as with the low-energy excitation spectrum determined from high-field ESR [30]. Smaller value of the isotropic exchange is also consistent with the

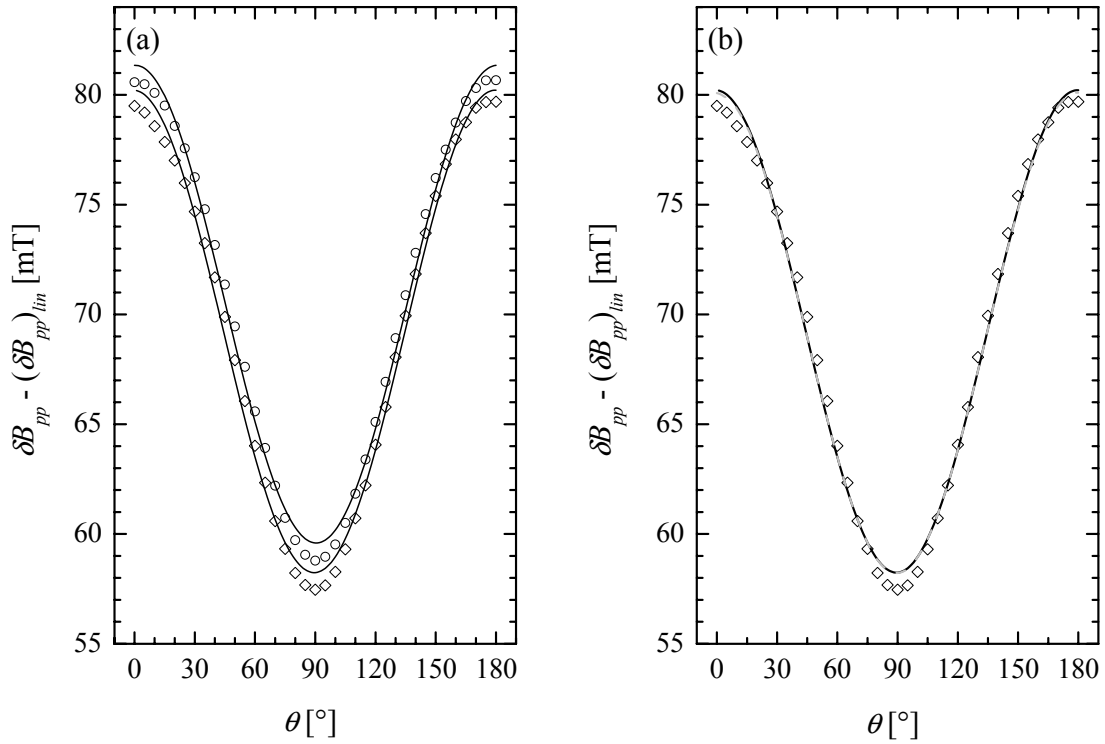

Fig 4.9: (a) The fit of the experimental X-band ESR linewidth anisotropy of the $SrCu_2(BO_3)_2$ single crystal measured at 525 K (◇) and 295 K (○), with the high-temperature linearly increasing contribution subtracted, with the model (—) including the intradimer DM coupling in addition to the interdimer out-of-plane components (Eq. (4.23)). (b) A comparison of the accuracy of the same model (—) and the model including also the in-plane interdimer DM vectors (--) on experimental data obtained at 525 K.

theoretical prediction of $J = k_B \cdot 72\,\mathrm{K}$ taking into account terms up to $(J'/J)^{14}$ [12]. As also the ratio J'/J is not changed in these reports, such lowered values of the exchange parameters would decrease the estimated DM parameters by approximately 7% thus making our evaluation of the interdimer exchange surprisingly accurate.

If also finite in-plane interdimer DM coupling is taken into account the expression of the linewidth anisotropy is considerably more complicated as different components of the DM vectors get coupled,

$$\delta B_{pp}^{DM} = \frac{\pi}{12 g \mu_B}\left(\frac{\left(8D_{\parallel}'^2 + 3D_{\perp}^2 + 12D_{\perp}'^2 + \left(8D_{\parallel}'^2 - D_{\perp}^2 - 4D_{\perp}'^2\right)\cos^2\theta\right)^3}{\left(32D_{\parallel}'^2 J_1^2 + 3D_{\perp}^2 J_2^2 + \psi_1 + \left(32D_{\parallel}'^2 J_1^2 - D_{\perp}^2 J_2^2 - \psi_2\right)\cos^2\theta\right)}\right)^{1/2}. \tag{4.24}$$

The two functions introduced in the denominator of the above expression,

$$\begin{aligned}\psi_1 &= 12D_{\perp}'^2\left(8J^2 + 13J'^2 - 4JJ'\right) + 4D_{\perp}D_{\perp}'\left(2JJ' - J'^2\right)\cos 2\phi,\\ \psi_2 &= 4D_{\perp}'^2\left(8J^2 + 13J'^2 - 4JJ'\right) + 4D_{\perp}D_{\perp}'\left(2JJ' - J'^2\right)\cos 2\phi,\end{aligned} \tag{4.25}$$

now introduce also the dependence on the azimuthal angle. The above expressions are strictly valid only when the values $D'_{\xi}=0$ and $D'_{\eta}=D'_{\perp}$ of the in-plane interdimer DM vectors are assumed [43]. Recent inelastic neutron scattering experiments have indicated finite values of these vectors. Namely, an anomalous fine structure at the "normalized" wave vector $q=(3\pi/2,0,0)$, where the out-of-plane component $D'_{\parallel}$ yields degenerated energy levels, was attributed to the in-plane component $D'_{\perp}$ [43]. The authors evaluated the latter component only in the limit $J'=0$ to be $D'_{\perp}\approx 0.4D'_{\parallel}$.

Taking into account this in-plane next-nearest neighbor DM component the quality of the fit is not essentially improved as shown in Fig. 4.9b. However, it leads to slightly lower intradimer interaction $D_{\perp}=k_B\cdot 3.6(1)\,\mathrm{K}$ while the inter-dimer one $D'_{\parallel}=k_B\cdot 2.4(1)\,\mathrm{K}$ is unchanged. This is due to the fact that the Eq. (4.24) couples only the in-plane components of the intradimer and the interdimer interaction. As the size of the latter interaction was evaluated in the limit of no next-nearest isotropic exchange and our experiment can not separate between the contributions of $D_{\perp}$ and $D'_{\perp}$ terms, we can only make an estimation of the intradimer DM interaction with slightly larger error, $D_{\perp}=k_B\cdot 3.6(5)\,\mathrm{K}$. It should also be emphasized, that the dependence on the azimuthal angle predicted by Eq. (4.24) is insignificant. Thus, for instance, the linewidth varies within 0.01 mT at the polar angle $\theta=0°$, in agreement with the experimental observation.

Nature of the in-Plane Dzyaloshinsky-Moriya Interaction

The evaluated value of the nearest-neighbor DM interaction seems to be surprisingly high, even more since it has been disregarded until very recently. This interaction should, however, be appreciable due to the static distortion of the $CuBO_3$ planes below the phase transition temperature [4]. As explained in subsection 4.2.2 considering the anisotropy of the *g*-factor in the $SrCu_2(BO_3)_2$ compound, the buckling angle of the CuO_4 plaquettes with respect to the crystal *c* axis amounts to $\alpha=4°$ at room temperature. The expected nearest-neighbor DM interaction is then of the order $D_{\perp}\approx 2\sin\alpha\,\Delta g/g\cdot J=k_B\cdot 1.8\,\mathrm{K}$, which is far from being insignificant with respect to the interdimer DM coupling.

As already mentioned in the first section of this chapter, recently, numerous experimental evidences of the presence of considerable intradimer DM anisotropic exchange have been reported, including unusual ^{11}B NMR lineshifts and the presence of the staggered magnetization [24, 25], the dependence of the relative intensities of the lowest-lying magnetically excited states observed by high-field ESR [26] and the magnetic field dependence of the specific heat measured at low temperatures [27]. The latter report also offers an estimation of the intradimer Dzyaloshinsky-Moriya interaction, $\mathbf{D}=k_B\cdot(2.2\,\mathrm{K},2.2\,\mathrm{K},5.2\,\mathrm{K})$. However, the authors

included also a sizable out-of-plane component not allowed by the crystal structure even when buckling is present, as described by the symmetry arguments above. Such symmetry-forbidden component could be due to a distortion on the crystal structure in high magnetic fields [27], as implicated by a drastic reduction of the sound velocity in the $SrCu_2(BO_3)_2$ system in magnetic field around 27 T [44]. The effect is believed to be due to a strong spin-phonon interaction coupling the lattice vibrations with the magnetic excitations. On the other hand, the evaluation of the in-plane component $D_\perp = 3.1\,\mathrm{K}$ is very close to our estimation. The splitting of the single triplet excitation has also been shown with the use of the Lanczos method on finite-size clusters of Shastry-Sutherland spin system, to be consistent with such a general form of the intradimer DM coupling [30]. Even more, the out-of-plane component is needed to explain the observed high-field ESR transitions for magnetic field applied along the anisotropy axis of the $SrCu_2(BO_3)_2$ system. Second, also the recent prediction of the in-plane intradimer DM coupling on the basis of the ^{11}B NMR lineshift, where the authors evaluated this interaction to be of the size $D_\perp = k_B \cdot 2.9(4)\,\mathrm{K}$ [45], is consistent with our prediction. However, it should be emphasized that contrary to ours all the estimations of the intradimer DM coupling were made for very low temperatures.

The intradimer Dzyaloshinsky-Moriya interaction should vanish above the phase-transition temperature of $T_s = k_B \cdot 395\,\mathrm{K}$, above which the $CuBO_3$ planes become flat in the static picture. Surprisingly, the observed ESR anisotropy is not affected by this structural phase transition at all. A credible explanation of this puzzle is provided if dynamical effects are taken into account [28, 31]. In this picture lattice vibrations instantaneously break local symmetry allowing for additional in-plane terms of the DM interaction. Due to the spin-orbit interaction the spin degrees of freedom cannot be decoupled from the space degrees of freedom. The Hamiltonian coupling the spin system with lattice vibrations is of the form [28]

$$H^{sl} = \sum_{i,j,d} \sum_{\alpha,\beta} g_d^\alpha u_{id}^\alpha \mathbf{S}_i \cdot \mathbf{S}_j + d_d^{\alpha\beta} u_{id}^\alpha \left(\mathbf{S}_i \times \mathbf{S}_j\right)^\beta . \tag{4.26}$$

The parameters α and β correspond to Cartesian coordinates while the variable u_{id}^α represents the displacement of the *d*-th ion in the vicinity of the spin site *i* from its equilibrium position. The first term is due to the isotropic spin-phonon coupling g_d^α while the second one represents the dynamical Dzyaloshinsky-Moriya effect.

There are, however, few general requirements to be fulfilled before including this mechanism into the interpretation of the X-band ESR results. First, dynamical effects can be observed when the characteristic phonon frequency is small compared to the characteristic exchange frequency $\omega_e \approx J/\hbar$ determining the spin correlation time τ_c. Since optical phonons are needed to produce required lattice distortions, significant softening of a particular normal mode should be present. Second, the mean square displacements of ions, participating in the

aforementioned lattice motion, from their equilibrium positions should be large enough to break the local symmetry significantly. It seems that both conditions are fulfilled in the $SrCu_2(BO_3)_2$ system.

Fortunately, the crystal structure and also the dynamical aspects of the $SrCu_2(BO_3)_2$ lattice have been thoroughly studied in the past [4]. Of our particular interest is the observation of a soft mode detected by Raman light scattering experiment. The analysis of the Raman shift of this mode based on the generally convincing symmetry argumentation was given quite recently [46]. The shift of the soft optical mode amounts to 62 cm^{-1} at T = 15 K. This value corresponds to a temperature of 89 K, which is thus very close to the isotropic exchange. It progressively softens, by 44 cm^{-1} just below T_s = 395 K, where the line disappears in a quasi-elastic tail as presented in Fig. 4.10a. Apart from the drastic softening also a broadening of the recorder Raman peak is present when raising the temperature. Both features suggest on the anharmonicity of the ionic potentials. This soft mode corresponds to in-phase motion of almost all ions within the primitive cell (with exception of Sr^{2+} ions) preferably along the crystal c direction thus being of the interlayer nature. The evidence of the vibrations along this axis is the intensity of the observed Raman mode, which is by two orders of magnitude larger in the case when the polarization of the initial and the detected scattered electric field is parallel to the c axis than in case of the polarization being within the ab plane. This vibrational mode corresponds to the center of the Brillouin zone and transforms to Raman-inactive buckling modes in the high-temperature structural phase. The normal coordinates for the case of Cu, B and O(1) ions are given by

$$Q_a = \frac{1}{2}\left(u_1^c - u_2^c + u_3^c - u_4^c\right), \tag{4.27}$$

and for the case of the O(2) ions by

$$Q_b = \frac{1}{2\sqrt{2}}\left(u_1^c + u_2^c - u_3^c - u_4^c + u_5^c + u_6^c - u_7^c - u_8^c\right). \tag{4.28}$$

The corresponding indexing of the displacements can be seen in Fig. 4.10b. A linear combination of the normal modes represents the observed soft mode. As already stressed, all the ions with exception of the Sr^{2+} ions vibrate preferably along the crystal anisotropy c axis, where also the movement of different ions is in phase. The latter feature is the origin of the large effective mass, i.e., low vibrational frequency [46].

The softening and the broadening of this soft mode as well as its symmetry are also consistent with the observed anomalous anharmonicity of lattice properties. Namely, a flattening of the local potentials of ions and a significant enhancement of their mean square dynamic displacements in the crystal c direction have been observed, both phenomena progressively getting larger when approaching the transition to the high-T phase [4]. The x-ray

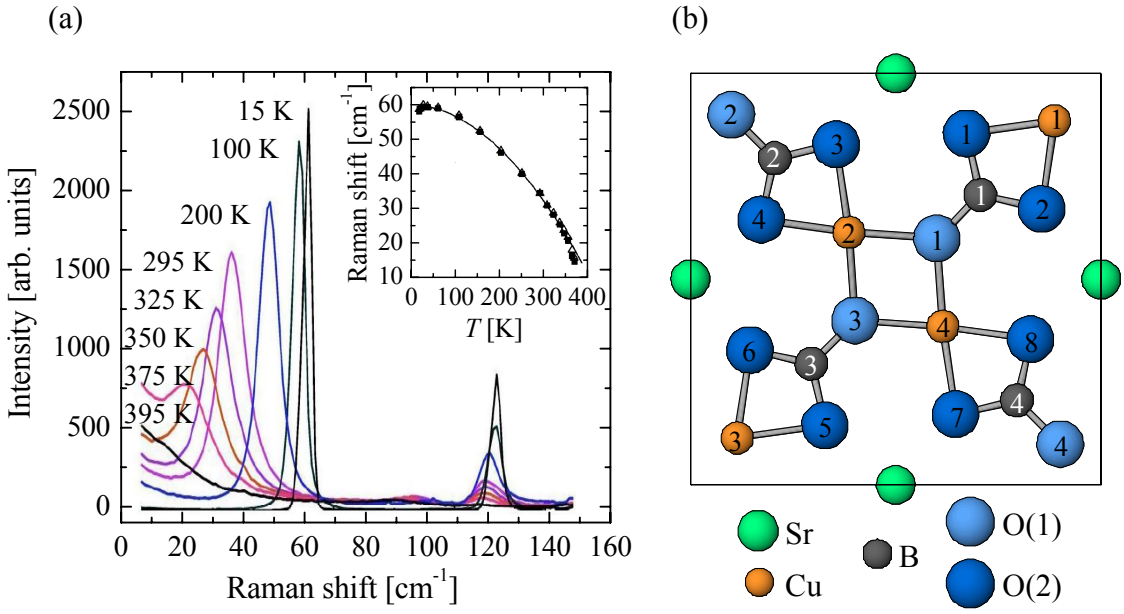

Fig. 4.10: (Ref. 46) (a) Softening of a phonon mode with temperature as observed by Raman light scattering experiments in $SrCu_2(BO_3)_2$ system and (b) site symmetry of the ionic vibrations within the prime cell corresponding to this lattice vibration as given by Eqs. (4.27) and (4.28).

diffraction experiments revealed that in the high-temperature phase the average squares of the displacements for all ions (with the exception of Sr^{2+}) are fairly large along the c axis and considerably smaller for the other directions. For instance, the U_{33} principal components of the displacement tensor of Cu and O(1) ions connecting them yield enhanced vibration amplitudes, which are virtually the same as static displacements (0.25 Å for Cu ions and 0.33 Å for O1 ions) of these ions at 100 K [4]. It is also interesting that the average displacements alongside two neighboring CuO_4 plaquettes increase from O(2) across Cu to O(1) ions. When lowering the temperature and crossing to the low temperature phase the amplitudes get progressively smaller, however, their decrease is unexpectedly slow. The phase transition can be thus characterized as displacive transition, where the local minima of the ionic potentials progressively move along c direction and become steeper when lowering the temperature in the low-temperature phase.

From the X-band ESR point of view, such lattice vibrations break the local symmetry in a very similar way as it is broken in the low-T phase by finite static buckling of $CuBO_3$ planes, since the distortions are quasi-static on the time-scale of the spin correlation time τ_c. Additionally, also the symmetry of the dynamic distortions is similar to the symmetry of the static one, as the in-phase movement of the ions corresponds to wave vector $q = 0$. Therefore, it is not surprising that the ESR linewidth anisotropy does not change qualitatively above room temperature despite crossing the structural phase transition. It is also worth mentioning that the isotropic exchange coupling constants are believed not to change significantly with temperature

[4]. For all the given reasons it seems most likely that the in-plane components of the DM interaction present in the high-temperature phase are due to the presence of the buckling soft modes, which instantaneously break the local symmetry. When crossing to the low-temperature structural phase the static displacements progressively take over the initiative. However, the origin of the nearest-neighbor DM interaction $D_{\perp} = 3.6\,\mathrm{K}$ can also be a combined effect of the static, i.e. buckling of $CuBO_3$ planes, and the dynamical mechanism and evolves progressively into a dynamical source with increasing temperature. The obtained DM parameter is thus an "averaged" value since the displacements are time dependent. Our experimental findings strongly support the recently proposed picture of the dynamical DM interaction [28, 31].

Lattice Vibrations as Line-Broadening Mechanism in High-Temperature Regime

The high-temperature increase of the X-band ESR linewidth in the $SrCu_2(BO_3)_2$ compound is essentially linear above approximately 340 K up to 590 K, which is the highest temperature that could be reached with our experimental set-up. Moreover, the slope is within the experimental error independent on the direction of the external magnetic field as shown in Fig. 4.11a for the case of the single crystal. Its value is estimated by $k_{\parallel} = 0.035(1)\,\mathrm{mT/K}$ and $k_{\perp} = 0.033(1)\,\mathrm{mT/K}$ for the magnetic field parallel and perpendicular to the anisotropy axis, respectively.

The increase of the linewidth between room temperature and 590 K amounts to approximately 10%. As already argued above, for a pure spin Hamiltonian, ESR linewidths are normally expected to approach a constant value for temperatures far above the characteristic exchange temperature J/k_B. Nevertheless, several mechanisms can lead to a temperature-dependent ESR linewidth at high temperatures, including spin diffusion, static spin correlations and spin-phonon coupling. Although the spin diffusion mechanism may become significant at higher temperatures, the measured Lorentzian ESR lineshape at 525 K speaks strongly against it. Second, the effect of static spin correlations on the linewidth can be observed in low-dimensional magnetic systems even up to temperatures of the order of $T \sim 10J$, as shown by Soos *et al*. [47]. Following this original paper, the temperature-dependent second moment due to the Dzyaloshinsky-Moriya interaction can be calculated to have the form

$$M_2^{DM}(T) = \frac{S(S+1)}{3N}\frac{\chi_C}{\chi(T)}\left[\sum_{(ij)}\left(\left(D_{ij}^x\right)^2 + \left(D_{ij}^y\right)^2 + 2\left(D_{ij}^z\right)^2\right)\left(1 - C_{ij}\right)\right.$$
$$+ \sum_{\substack{(ij)\\ m\neq i,j}}\left(D_{ij}^x D_{im}^x + D_{ij}^y D_{im}^y + 2D_{ij}^z D_{im}^z\right)C_{jm} + \qquad (4.29)$$
$$\left. + \sum_{(ij)}\sum_{\substack{(mn)\\ m,n\neq i,j}}\left(D_{ij}^x D_{mn}^x + D_{ij}^y D_{mn}^y + 2D_{ij}^z D_{mn}^z\right)\left(C_{im}C_{jn} - C_{in}C_{jm}\right)\right].$$

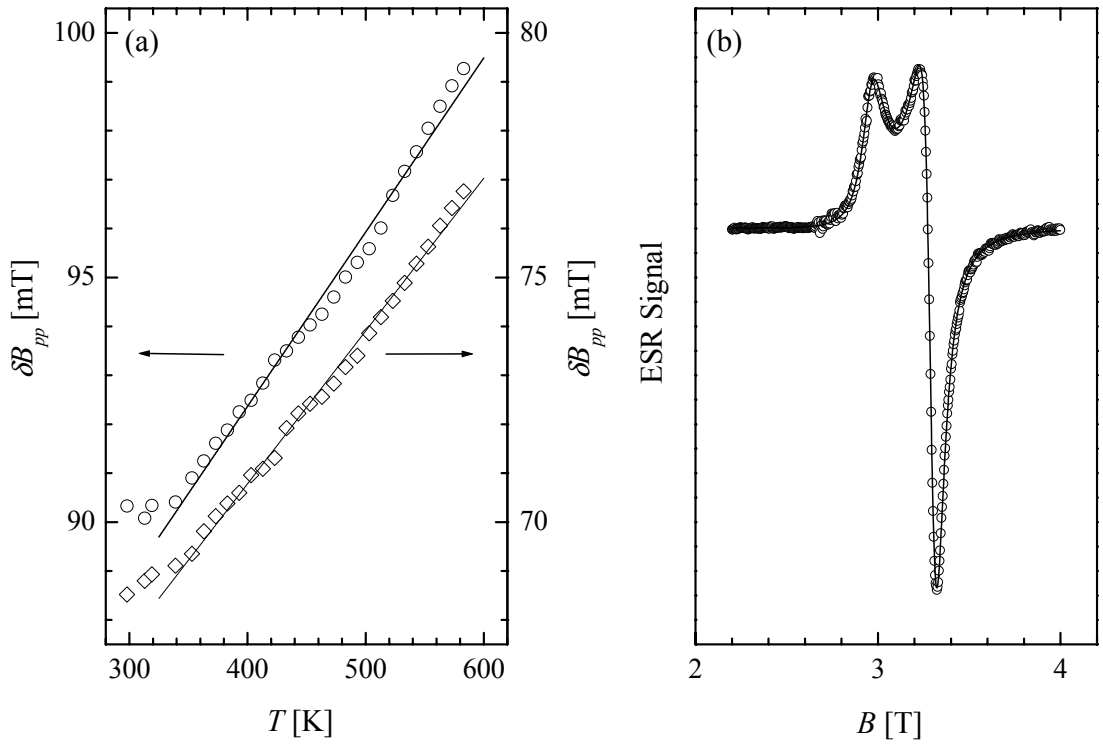

Fig 4.11: (a) The high-temperature linear increase of the X-band ESR linewidth of the $SrCu_2(BO_3)_2$ single crystal for the external magnetic field parallel (○) and perpendicular (◇) to the *c* crystal axis. Note that the two vertical scales have the same range. (b) The high-field ($\nu_L = 93.2\,\mathrm{GHz}$) ESR spectrum of the $SrCu_2(BO_3)_2$ powdered sample (○) with the corresponding theoretical Lorentzian curve for powder samples (**—**).

The temperature dependence due to static spin correlations is hidden in the ratio between the Curie susceptibility χ_C and the measured susceptibility $\chi(T)$ as well as in functions C_{ij} reflecting two-site static spin correlation between spins at sites *i* and *j* as described in Chapter 2.

Each of the three sums in Eq. (5) yields its own characteristic temperature behavior, with the first one approaching the infinite-temperature second moment and the last two going to zero when increasing the temperature. The first of the sums can clearly be factorized into an angular-dependent and a temperature-dependent part. The slope of the line broadening for this reason changes when changing the direction of the external magnetic field in the same manner as the magnetic anisotropy dictates the linewidth anisotropy. The influence of the other two sums on the angular dependence of the slope is not as easy to predict. However, it is highly unlikely that the two-site correlation functions C_{ij} would evolve with temperature in such a way to produce angular-independent line broadening as observed in current investigation. Another reason allowing us to dismiss static spin correlations as the possible origin of the observed broadening, is almost ideal linear dependence in a rather broad temperature range, i.e. between 3.5*J* and 7*J*.

In such a broad region one would expect significant bending of the linewidth curves towards the infinite temperature value if the broadening was due to short-range order effects.

Clearly, the spin Hamiltonian alone cannot provide an adequate explanation for the high-temperature linear increase of the linewidth. Additional degrees of freedom causing lifetime broadening effects must be important. As already mentioned, the spin-phonon interaction is considerable in the $SrCu_2(BO_3)_2$ system. Namely, the drastic decrease of the elastic constants, reflected in the reduction of the sound velocity as a function of temperature and even more in strong magnetic fields, speaks in favor of a strong coupling between the spin system and the lattice [44, 48]. Therefore, the spin-phonon coupling should be taken into account as a broadening mechanism at high temperatures.

As the increase of the linewidth is linear, normal direct phonon processes should be involved. Generally the line-broadening effects can be a consequence of different mechanisms. In particular, the observed line broadening can be due to the usual spin-lattice relaxation between Zeeman split excited states caused by the modulation of the dipolar coupling [49]. For this mechanism a strong dependence on the external magnetic field is typical as the spin-lattice relaxation rate increases proportionally to B_0^2. On the other hand, a modulation of the general anisotropic exchange can also lead to line broadening. The coupling of this kind is given in the Eq. (4.26). In connection with this expression, it is worth noting that the first term commutes with the Zeeman Hamiltonian due to its isotropic nature. Consequently, it does not induce line broadening. However, in some cases also the isotropic exchange coupling can induce a temperature dependence of the linewidth. Namely, when the ESR line is exchange narrowed the temperature variation of the isotropic exchange causes the linewidth to change with the temperature [50]. The temperature dependence of the exchange interaction follows from the thermal average of this parameter over the vibrational states in the case of an anharmonic potential. Second, the crystal lattice expands with increasing temperature, which causes a decrease of the isotropic exchange constant. It is expected that such changes of the isotropic exchange can noticeably affect the ESR linewidth only in systems with large thermal expansion constants [51]. To be precise, the mere modulation of the exchange constant due to the fluctuations of the interspin distances is only a secondary effect.

The effect of the time modulation of the Dzyaloshinsky-Moriya interaction on the lifetime of the magnetically excited states was studied by Seehra *et al*. [52]. The DM interaction in general causes mixing between the ground state and the excited states. The transitions between these states are then induced by a phonon modulation of the antisymmetric exchange interaction. Contrary to the case of the dipolar broadening, no magnetic field dependence is expected in the latter case. To test which of the two possible phonon-based broadening mechanisms is active in the $SrCu_2(BO_3)_2$ compound, we recorded also a high-field ($\nu_L = 93.2\,\mathrm{GHz}$) room-temperature ESR spectrum on a powder sample, which is shown in Fig.

4.11b. Contrary to the X-band case, the absorption profile in high magnetic field shows characteristic *g*-factor anisotropy. This is not surprising as the interval of the resonant field spans $\left(g_{\parallel}-g_{\perp}\right)/\overline{g}\approx 10\%$ of the average resonance field value, which is around 35 mT in the X-band and 350 mT in high magnetic field. The high-field ESR spectrum is nicely fitted by the Lorentzian function for powder spectra (see Fig. 4.11b), which yields anisotropic linewidths of $\delta B_{pp}^{a}=\delta B_{pp}^{b}=70(1)\,\mathrm{mT}$ and $\delta B_{pp}^{c}=89(1)\,\mathrm{mT}$. These parameters are virtually the same as the single-crystal X-band values $\delta B_{pp}^{\perp}=69(1)\,\mathrm{mT}$ and $\delta B_{pp}^{\parallel}=91(1)\,\mathrm{mT}$. Since the linear contribution to the linewidth at room temperature is of the order of 10 mT and is the same at the two resonance fields differing by approximately a factor of 10, we can deduce that the spin-lattice contribution to the linewidth is due to the fluctuating Dzyaloshinsky-Moriya interaction.

Making a rather crude approximation with neglecting correlation effects between a pair of interacting spins and their neighbors, the linewidth is determined by phonon-induced transitions between a singlet state and triplet states of a two spin system. Since *J* is two orders of magnitude larger than characteristic Zeeman energy and the phonon density scales with ω^2 in the Debye approximation, it is not surprising for the modulated-DM-interaction effect to dominate over the phonon-induced Zeeman transition between the excited states. In the simple picture of uncorrelated dimers the finite-lifetime contribution to the linewidth is given by [52]

$$\delta B_{pp}^{lin}\approx\frac{8Z}{9\sqrt{3}}\frac{1}{g\mu_B}\frac{(\lambda R)^2D^2J^2}{\rho\hbar^3}\left\langle\frac{1}{c_t^5}+\frac{2}{3}\frac{1}{c_l^5}\right\rangle_{\Omega}k_BT\,. \tag{4.30}$$

Taking the number of independent pairs as $Z=1$, the parameter $\lambda R=10$ where *R* represents the nearest-neighbor distance and $\mathrm{d}J/\mathrm{d}r=-\lambda r$ [53], the density $\rho=4.1\,\mathrm{kg/dm^3}$ [44], an approximate average velocity *c* = 4600 m/s [54] in place of the complicated angular average, and the above estimated intradimer DM interaction $D=D_{\perp}=k_B\cdot 3.6\,\mathrm{K}$, the slope of the linearly increasing part can be evaluated to be of the order of 0.014 mT/K. This result is in a reasonable agreement with the experimentally observed slope 0.034 mT/K bearing in mind that the mean velocity, which is burdened with the biggest uncertainty, is taken to the power of 5. Moreover, Eq. (4.30) is strictly valid only in the crude approximation of independent dimers. Since interactions with other neighbors in general shorten the lifetime of a spin in a certain energy level, the slope is expected to be larger in the real system. The fair agreement of this line-broadening mechanism with the experiment once again justifies the introduction of the intradimer DM interaction.

Spin dynamics in Low-Temperature Regime

Contrary to the high-temperature increase of the ESR linewidth, the low-temperature raise is much more enhanced as this parameter grows by approximately a factor of 3 between room

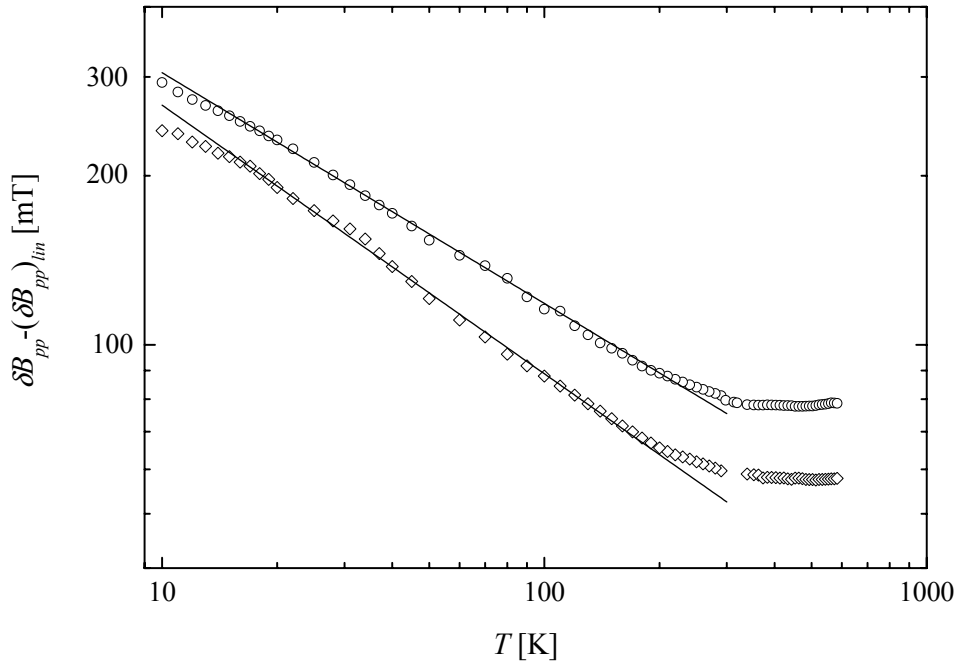

Fig. 4.12: The log-to-log plot of the linewidth of the $SrCu_2(BO_3)_2$ single crystal without the high-temperature linear contribution for the magnetic field at zero angle (○) and at right angle (◇) respectively to the crystal *c* axis showing the critical-type of the line broadening (—) as given by Eq. (4.31).

temperature and 10 K. Fig. 4.12 shows a log-to-log plot of the linewidth with the high-temperature linearly increasing part subtracted. It should be noted that the decrease of the number of phonons becomes a slower decreasing function than the linear function at temperatures around and below the spin-gap temperature. However, the phonon contribution to the linewidth at these temperatures is not appreciable.

The double logarithmic scale in Fig. 4.12 is appropriate for testing the potential dependence of the form

$$\delta B_{pp} = \frac{A}{\left(T - T^*\right)^p} . \tag{4.31}$$

The slope of the curve then simply corresponds to the exponent *p*, which is in our case given as $p_{\parallel} = 0.41(1)$ and $p_{\perp} = 0.47(1)$ for the external magnetic field applied parallel and perpendicular to the *c* axis of the crystal, respectively. The critical temperature T^* is equal to zero within the fitting error. Similar observation with the slope $p = 0.50(1)$ is made for the powder sample. The dependence of the linewidth given by the above expression is characteristic for critical slowing down of the spin fluctuations as observed when approaching a magnetic phase transition. However, the interval between 150 K and 15 K where the experimental broadening is well described by this equation is surprisingly broad. This can be a signature of the $SrCu_2(BO_3)_2$

system lying in the close vicinity of the quantum boarder-line between the spin-liquid and the magnetically ordered ground state, which could in principle lead to strong enhancement of antiferromagnetic spin correlations.

For temperatures below 15 K the increase of the linewidth is not so intense as predicted by Eq. (4.31). In powder samples, which are purer than the only single crystals we have, even a decrease of the linewidth behavior is found below 10 K (see Fig. 4.6). This could be attributed to a reduced number of the triplet excitations making the interactions between them smaller. In may also signal on some structural changes in this temperature range. In should be noted that in contrast to the $PbNi_2V_2O_8$ case the position of the line does not shift much with temperature even far below the spin-gap temperature. This can be seen by comparing the temperature evolution of the ESR spectra shown in Fig. 4.2. The origin of the ESR spectra must for this reason be hidden in the transitions within the energy continuum above the lowest-lying states [30]. In fact, employing the finite-temperature Lanczos method on finite-size spin clusters of Shastry-Sutherland lattice with the Dzyaloshinsky-Moriya interaction shows some preliminary indications of this sort. Namely, the predicted X-band signals corresponding to the *g*-factor around the free-electron value have very similar linewidth values as the observed signals. The linewidth seems to increase with temperature at very low temperatures similar to our experimental observations on powder samples below 10 K. However, the reverse of the behavior above this temperature is still not understood within the present spin model. Further analysis, currently in progress, is needed to resolve these issues.

4.3 Doping of $SrCu_2(BO_3)_2$

On the basis of the similarities of the $SrCu_2(BO_3)_2$ crystal and spin structure with high-T_c cuprates this material was suggested to possibly lead to superconductivity at low temperatures when properly doped with electrons or holes [2, 35, 36]. If this was indeed the case $SrCu_2(BO_3)_2$ could help to a better understanding of the superconductivity phenomena due to its relatively simple spin Hamiltonian. On the other hand, the investigated system is located close to the quantum boarder and features strongly frustrated exchange pathways. As in the case of the one-dimensional $PbNi_2V_2O_8$ spin-gap system presented in the previous chapter, small inhomogeneities introduced to $SrCu2(BO_3)_2$ could have a drastic impact on the magnetism of this material. In this sense doped $SrCu_2(BO_3)_2$ system could provide some novel physical phenomena, which was our initial motive for performing a number of different experimental doping approaches [37].

Before going into details, it should be mentioned that not many experimental reports on the doped $SrCu_2(BO_3)_2$ compounds have been given. Kageyama *et al*. [55] first reported their

successes of substitution doping. They managed to prepare phase-pure polycrystalline samples of $Sr_{1-x}A_xCu_2(BO_3)_2$ (A = Ba, Ca) at least up to $x = 0.3$. The effect of the substitution is an expansion/contraction of the cell constants for the Ba^{2+}/Ca^{2+} replacement, which can be attributed to a difference in ionic radii. On the other hand, the magnetic properties including susceptibility and the field dependence of the magnetization were not reported to change drastically, indicating that the spin-gap nature of the ground state was not altered. Besides the substitution-doped compounds at Sr site, only $SrCu_{1.98}Zn_{0.02}(BO_3)_2$ material has been reported in the literature [56]. The authors grew a single crystal of this compound and verified the successful Zn-substitution as well as phase-purity of the crystal. However, they failed to grow crystals with higher concentration of the Zn dopant. The Zn^{2+} impurities should naively brake copper singlet pairs thus creating localized S = 1/2 spins due to their spinless nature. Nevertheless, the magnetization curves once again showed no doping effect.

4.3.1 Solid-State Chemical Reactions and Electrochemical Doping

The most straightforward approach of doping is the conventional high-temperature solid-state reaction, where the choice of the starting materials is slightly altered with respect to the synthesis of the pure compound [1] in order to introduce the dopant into the crystal structure. High purity powders are weighted according to the purpose composition, pressed into pallets and then treated in the ordinary fashion.

Our initial attempt was to try to influence the magnetism of the copper planes by substituting the Sr^{2+}-ionic $CuBO_3$-plane spacers by ions with different valence states. The substitution of Sr^{2+} for La^{3+} was proved to be successful many times in different systems due to the similarity of the two corresponding ionic radii [57]. We tried to prepare different compositions of the $Sr_{1-x}La_xCu_2(BO_3)_2$ compounds with the substitution level ranging from $x = 0.02$ to $x = 0.5$. However, the common feature of all the resulting materials obtained after several heating/grinding cycles was their phase inhomogeneity. In Fig. 4.13 transmission-electron-microscopy image recorded in the back-scattered electrons mode on the sample with the stochiometry $Sr_{0.95}La_{0.05}Cu_2(BO_3)_2$ is compared with the image corresponding to the pure system. In the picture of the latter compound (Fig. 4.13a) the gray lamellas covering the majority of the observation window correspond to the $SrCu_2(BO_3)_2$, black holes are due to pores and the light-gray particles are the remains of the non-reacted CuO. Evidently, the size of the lamellas representing single-crystal grains is of the order of several tens of micrometers. On the other hand, in the case of the doped sample the dimension of the majority gray particles is much smaller and the material seems to be much more porous. The analysis of the ionic composition of the gray phase revealed that the percentage of the La content in it is significantly below the nominal concentration of 5%, which was verified by measuring the average composition in an

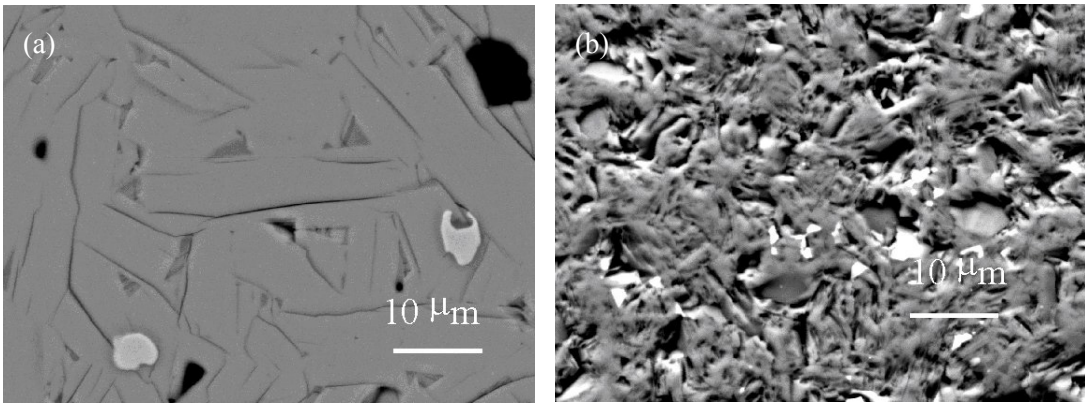

Fig. 4.13: Transmission-electron-microscopy image recorded in the back-scattered electrons mode for (a) the $SrCu_2(BO_3)_2$ powder sample and (b) a representative $Sr_{0.95}La_{0.05}Cu_2(BO_3)_2$ powder sample synthesized by the conventional solid-state chemical reaction. The major gray phase corresponds to the $SrCu_2(BO_3)_2$ phase, the lighter gray spots to a non-reacted CuO and black spots to pores. Additionally, the white parts in the (b) image represent La-reach phase as explained in the text.

observation window of $1\times1\,mm^2$. In addition, it varied from particle to particle and was usually even not seen. On the contrary, the bright (white) particles proved to contain an excess of lanthanum with its relative portion typically larger than that of the strontium. Unambiguously, the implementation of the lanthanum into the compound thus resulted in phase separation. Similar behavior was observed when the La^{2+} dopant was replaced with Pb^{2+}, which seems to work well in the lead-nickel vanadates presented in the preceding chapter. Moreover, also the solid-state chemistry substitutions of Sr^{2+} for various alkali-metal and earth-metal ions failed.

The second approach we took was again a solid-state reaction but this time between already synthesized $SrCu_2(BO_3)_2$ compound and a strong reducing agent. We measured stochiometric amounts of the strontium-copper borate and $LiBH_4$, which is known for its strong reducing capabilities [58]. The mixture was annealed and the resulting powder changed its color from the initial blue, characteristic for the $SrCu_2(BO_3)_2$ material, to brown, which could be an indication of a modified copper valence state. However, x-ray diffraction revealed that the crystal structure of the resulting material is not even similar to the starting one. Obviously some new material unrelated to the structure of the $SrCu_2(BO_3)_2$ was synthesized.

Another way to affect the magnetism of the copper layers in the $SrCu_2(BO_3)_2$ compound could be an intercalation of lithium ions into the crystal structure, since Li^+ ions are fairly small. The electrochemical approach of lithium intercalation can be performed by galvanostatic discharge using an electrochemical interface. The electrochemical lithium insertion was carried out in a laboratory-made three-electrode cell [59]. The $SrCu_2(BO_3)_2$ powder compound mixed with polyaniline, which improves electrical contact between grains, was used as the working

electrode. A lithium reference electrode and a lithium counter-electrode were used as the other two electrodes. The level of lithium insertion into the $SrCu_2(BO_3)_2$ material was monitored by measuring the electric charge transfer between the two electrodes. After the electrochemical treatment the color of the starting material was again changed. However, also the crystal structure was significantly altered, much similar to the case of the solid-state reduction product.

4.3.2 Liquid-Ammonia Method for n-Type Doping

As the crystal structure of the $SrCu_2(BO_3)_2$ compound seems to easily decompose if lithium is intercalated into the material by strong electrochemical potential, also a chemically soft method for n-type doping was used, previously proved to be successful in the case of fullerides [60]. In this case liquid ammonia was used as a solvent for the lithium metal and the alkali-metal liquid-ammonia solution was applied to the strontium-copper borate. In dilute solutions a metal is typically dissociated into solvated metal ions and electrons [61]. In very pure ammonia the solvated electrons lifetime is measured in days. They are trapped into a polarization field of the electrons of the solvent giving rise to a typical blue color of the solution. Indeed, our metal-ammonia solution turned blue from the initial colorless ammonia liquid. This solution was applied to the $SrCu_2(BO_3)_2$ powder and after several hours the solution above the powder turned transparent again while the color of the powder changed from initial blue to dark gray. The colorless nature of the solution indicated that the lithium ions and the electrons had left the ammonia solution while the change of the color of the powder $SrCu_2(BO_3)_2$ sample could be an indication of the modified valence state of copper ions. In this ideal scenario the Li^+ ions would intercalate into the strontium-copper borate and the accompanying electrons would change the characteristics of the copper spin system.

Structural Modifications due to Lithium Intercalation

The experimental data presented below corresponds to the sample, where the nominal stochiometric ratio of the lithium ions with respect to the parent compound before the lithium intercalation procedure was set at 1:1. Due to losses it is expected that the amount of lithium in the $Li_xSrCu_2(BO_3)_2$ intercalated compound is below this value. The modifications of the initial compound made by the lithium intercalation were first tested from the structural point of view. The x-ray diffraction pattern virtually matches the profile of the parent compound as indicated in Fig. 4.14a. This indicates that the static crystal structure of the resulting material is not significantly modified. Since lithium ionic ratio is fairly small, i.e. between 0.6 Å and 0.9 Å depending on the coordination [57], this could be an indication of Li^+ ions intercalating

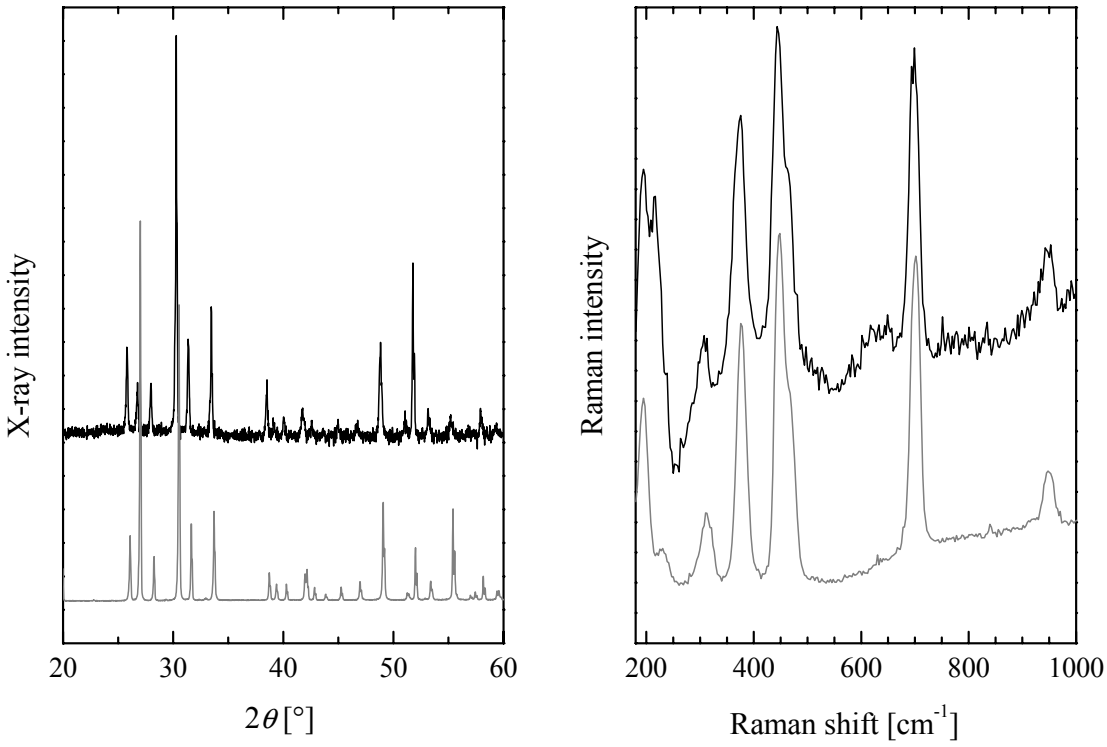

Fig 4.14: (a) X-ray diffraction pattern and (b) Raman light scattering absorption peaks of the parent $SrCu_2(BO_3)_2$ material (—) and the Li-intercalated $Li_xSrCu_2(BO_3)_2$ sample obtained by the liquid-ammonia method (**—**).

somewhere in the "free" space between the $CuBO_3$ planes, which are roughly displaced by $c/2 = 3.3$ Å . On the contrary of course, lithium ions might not have entered the crystal structure of the parent compound at all.

Second, also the dynamical aspect of the lattice modification was tested by Raman light scattering. The Raman spectra corresponding to the parent and the "doped" material are presented in Fig. 4.14b. Superficially speaking there is again no difference between the two materials. However, a closer look reveals that there are some minor dissimilarities as revealed in Table 4.1.

Table 4.1: The position of Raman peaks in $SrCu_2(BO_3)_2$ and $Li_xSrCu_2(BO_3)_2$ samples and the observed shift of the latter with respect to the former sample.

	Raman peak [cm^{-1}]								
$SrCu_2(BO_3)_2$	194.2	/	229.0	/	312.5	375.7	447.6	701.3	949.5
$Li_xSrCu_2(BO_3)_2$	194.1	215.5	~228	238.8	307	375.0	444.8	698	948.5
Shift	-0.1	/	~1	/	-5.5	-0.7	-2.8	-3.3	-1.0

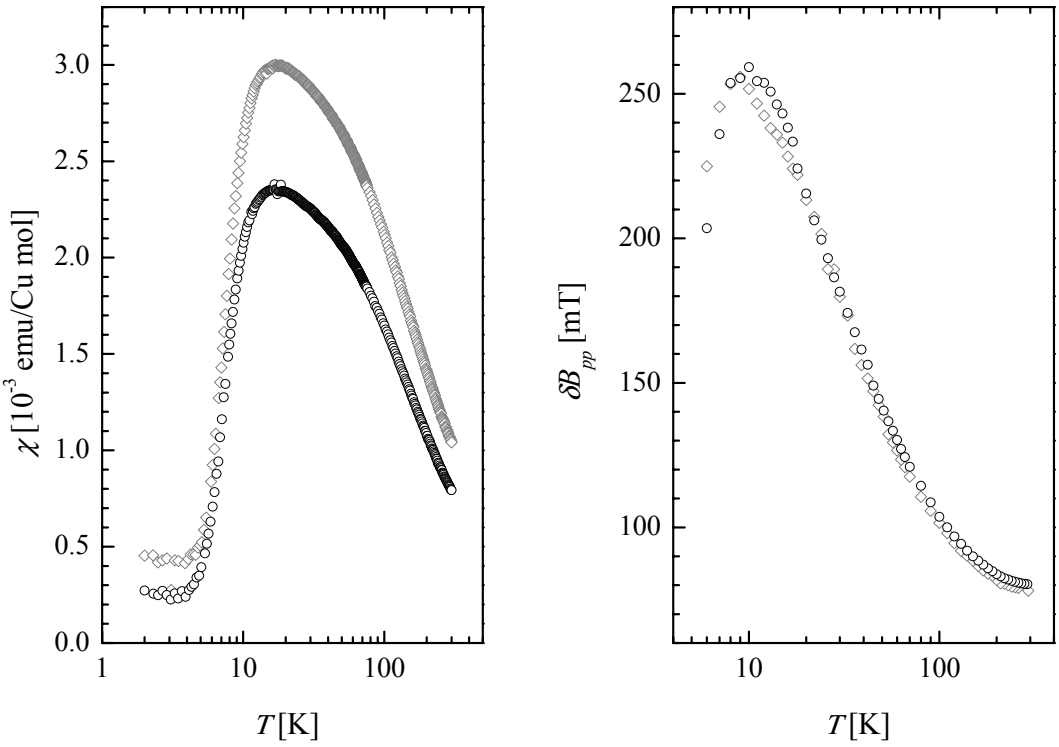

Fig. 4.15: A comparison of the temperature dependence of (a) the magnetic susceptibility and (b) the X-band ESR linewidth in the parent (◇) and the Li-intercalated (○) $SrCu_2(BO_3)_2$ samples.

The position of the observed Raman peaks agrees with previously published values [4, 46]. The relative Raman shifts vary between 0 and -5.5 cm^{-1}. In addition, there is an indication of a new resonant peak occurring at 215.5 cm^{-1}, which could also be the splitting of the peak positioned at 194 cm^{-1}. The intrinsic nature of the tiny hump at 238.8 cm^{-1} in the doped sample, on the other hand, is less certain. Moreover, the majority of the peaks corresponding to the doped sample are observably broader with respect to the peaks in the pristine compound, which indicates on a broader distribution of the vibrational frequencies.

Changes in Magnetic Character

As mentioned above, the color change of the $SrCu_2(BO_3)_2$ sample could be a signature of the charge transfer. One would then expect the magnetic properties of the compound to change after the intercalation of the lithium. The comparison of the magnetic susceptibilities measured in the field-cooled regime in external field of 50 mT and the ESR linewidth behavior of the two samples are shown in Fig. 4.15. The susceptibility of the doped sample is reduced with respect to the one corresponding to the parent material by approximately 25%. However, the overall

character of its temperature dependence is not altered, which would indicate that the spin gap is not affected. This behavior is similar to the one reported for the substitutional doping, where Sr^{2+} ions were partially replaced by Ba^{2+} or Ca^{2+} ions [55]. The susceptibility reportedly decreased after the substitution for both types of dopants regardless of the fact that Ca^{2+} is lighter and Ba^{2+} heavier ion than the Sr^{2+} ion.

Second, the ESR measurements show virtually no changes between the absorption spectra in both samples. As indicated in Fig. 4.15b the linewidth behavior is unaltered, which would imply that the magnetic anisotropy as well as the temperature development of the spin correlations is not affected by the Li intercalation procedure. We have previously reported some minor changes to occur at low temperatures [37]. A different behavior of the linewidth below the linewidth-maximum temperature around 12 K was accompanied by the presence of a small amount of nonresonant absorption emerging in zero field. Also the magnetic susceptibility of that particular sample exhibited a peculiar kink in that temperature region. However, further analysis on different Li-intercalated samples prepared according to the same experimental route showed that all these effects were not reproducible.

To verify if the lithium is present in our sample at all, we performed ^{7}Li NMR measurements in external magnetic field of 8.93 T. A relatively strong signal was observed close to the ^{7}Li Larmor frequency. The temperature dependence of the NMR spectra between room temperature and 5 K is presented in Fig. 4.16. Before trying to account for the relatively broad experimental spectra a comment of the absolute intensity of the observed signal is in place. The measured intensity of the absorption was compared with two reference samples of diluted Li_2CO_3 solutions with different molarities (54 mM and 273 mM). Knowing the quantity of the ^{7}Li I = 3/2 nuclei in all the samples allowed us to determine the stochiometry of the Li-intercalated sample $Li_xSrCu_2(BO_3)_2$, i.e., $x = 0.4(1)$. The ^{7}Li NMR signals were obtained with the solid-echo pulse sequence and since the resonance lines of the doped borate are fairly broad, also the decay of the echo intensity due to the spin-spin relaxation was taken into account by varying the duration τ between the two sequence pulses. The amount of the lithium within the doped sample is rather large, which seems to justify the exclusion of the possibility of the lithium intercalation resulting only in a “surface effect”.

Next, let us take a closer look at the observed spectra, which are plotted in Fig. 4.16 against the frequency shift with respect to the Li_2CO_3 solution. As evident there is virtually no frequency shift of the center of the resonance, which is further confirmed by the temperature independent first moment of the resonance of around $M_1 = 1.0(5)$ kHz corresponding to a chemical shift of ~7 ppm. This experimental finding suggests that the oxidation state of lithium in the sample is Li^+. If there were localized electrons at Li sites or itinerant electrons interacting with the Li nucleus significantly larger shifts would be expected. For instance the frequency

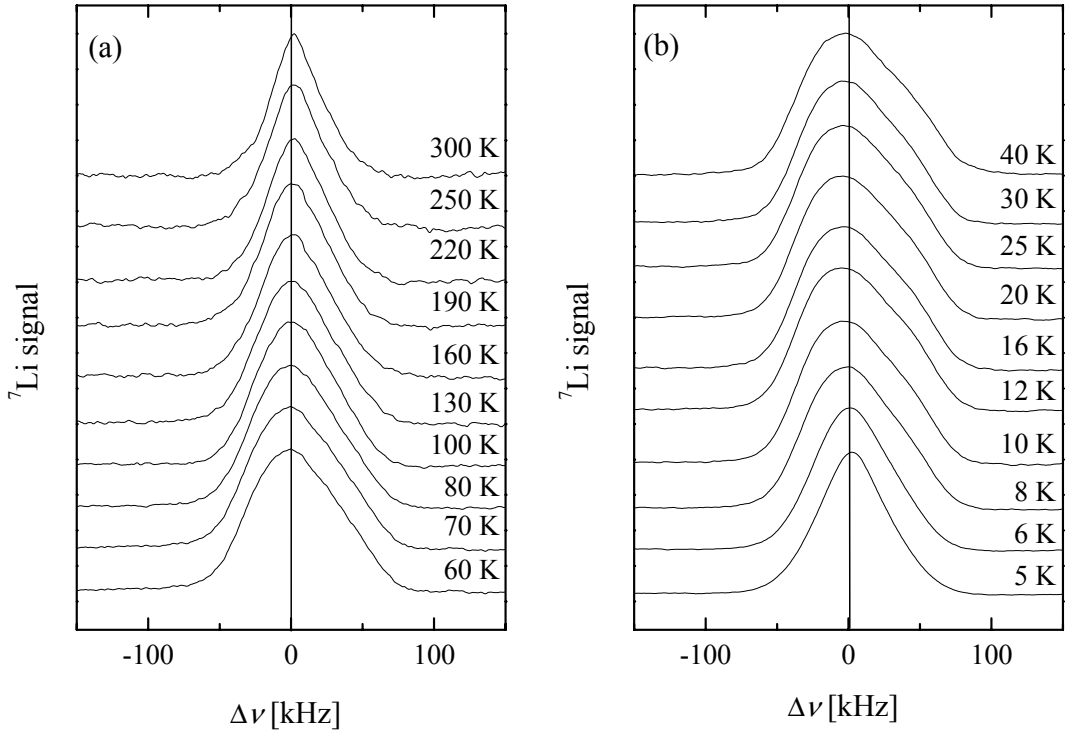

Fig. 4.16: A collection of ^{7}Li NMR spectra recorded in the Li-intercalated $Li_xSrCu_2(BO_3)_2$ compound in the magnetic field of 8.93 T.

shift typical for the Li metal is 240 ppm [62]. On the other hand considerably smaller chemical shifts up to ±10 ppm are typically observed for Li^+ ions [63].

Although ^{7}Li nuclei with spin $I = 3/2$ are "quadrupole" nuclei, the quadrupole splitting is not resolved in our case, which might be due to a distribution of the EFG components by magnitude and orientation. Second, the quadrupole structure of NMR spectra is not observed also when diffusion is present when the correlation time for the nuclear motion is short compared to the inverse of the quadrupole frequency. In this case, the quadrupole satellites collapse to a single line [64].

As the temperature is lowered from room temperature the spectra first exhibit broadening, reach a maximum around 15 K and then narrow observably as the temperature further decreases towards 5 K. In addition, the broader the resonance profile the more asymmetric it becomes. The appearance of the broad spectra is typical for the uniaxial-type of anisotropy, while the narrower ones at room temperature and 5 K appear symmetric. The temperature dependence of the second moment of the NMR lines shown in Fig. 4.17a mimics the dependence of the magnetic susceptibility and indicates that the observed broadening might be due to the interactions of Li nuclei with the paramagnetic spins within the parent $SrCu_2(BO_3)_2$ compound. Furthermore, Fig. 4.17b shows the resonant field dependence of the linewidth. When lowering

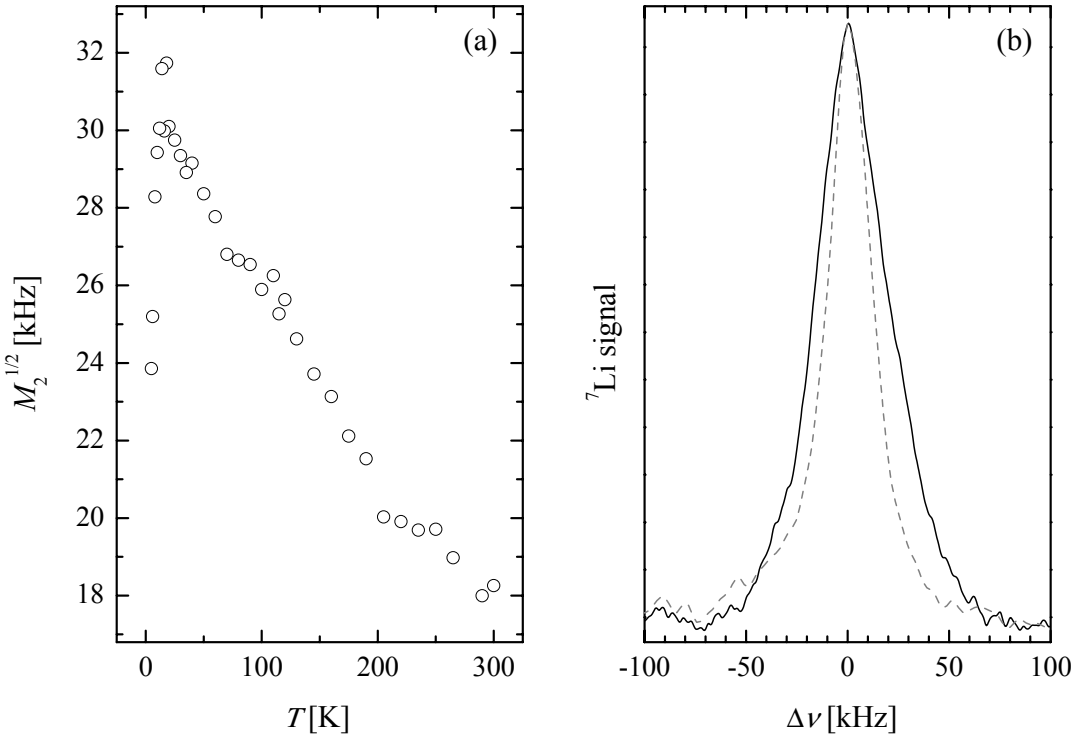

Fig. 4.17: (a) The variation of the square root of the second moment of the ^{7}Li NMR absorption line in the Li-intercalated $Li_xSrCu_2(BO_3)_2$ compound. (b) A comparison of the room-temperature NMR spectra recorded in the external magnetic field of 6.34 T (--) and 8.93 T (—).

the magnetic field from 8.93 T to 6.34 T the full width at half height of the ^{7}Li absorption spectrum at room temperature decreases from $39.5(2)$ kHz to $25.4(2)$ kHz. The linewidth thus nicely scales with the magnitude of the external magnetic field, indicating that the linewidth broadening is of magnetic origin. The coupling of the ^{7}Li nuclei with the copper spins strongly suggests that the intercalated lithium ions lay within the $SrCu_2(BO_3)_2$ crystal structure.

A similar conclusion can be drawn from the spin-lattice relaxation, which was measured by the saturation method. The evolution of the relaxation rate divided by temperature with respect to temperature is shown in Fig. 4.18. Again a gap-like behavior can be recognized from the direct comparison of the relaxation rate with the static magnetic susceptibility. In the case of the isotropic electron-nucleus magnetic coupling being the dominant magnetic interaction sensed by nuclei, the general expression for the spin-lattice relaxation rate obtained from Eq. (2.42) reads [65]

$$\frac{1}{T_1} = \frac{2k_B T}{(\hbar g \mu_B)^2} \sum_{\mathbf{q}} A_{\mathbf{q}} A_{-\mathbf{q}} \frac{\chi''_{\perp}(\mathbf{q}, \omega_0)}{\omega_0} \quad , \tag{4.32}$$

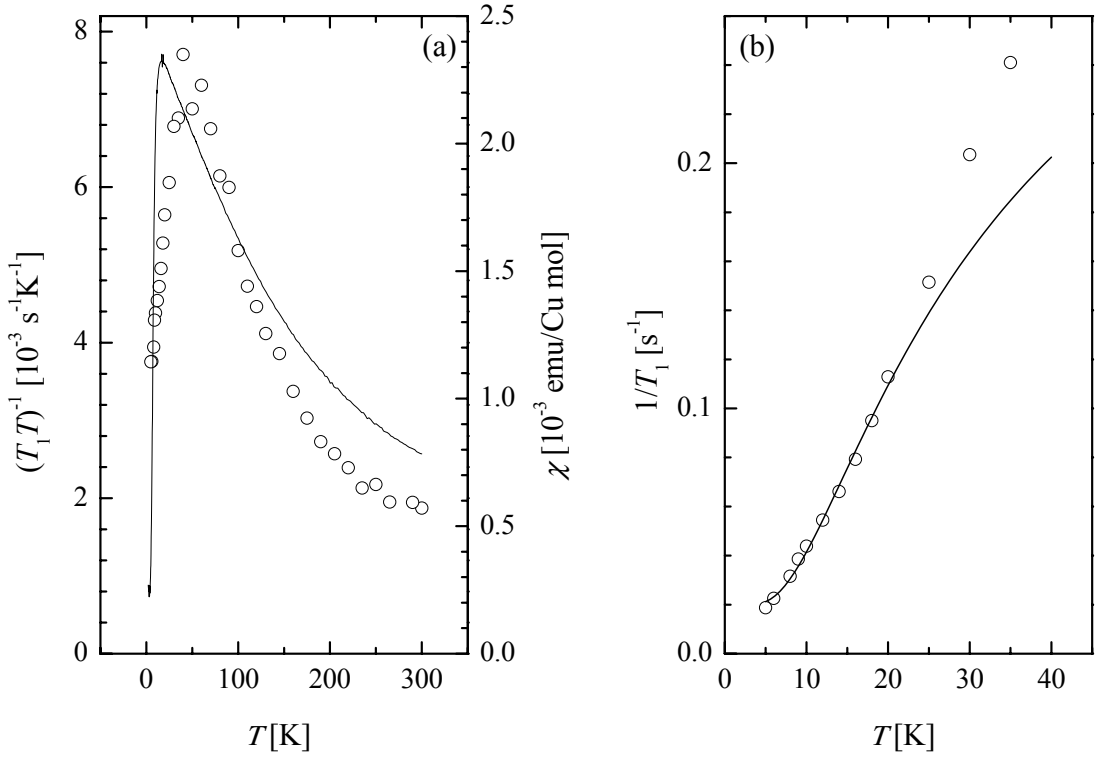

Fig. 4.18: (a) A comparison of the temperature evolution of the ^{7}Li NMR spin-lattice relaxation rate divided by temperature (○) with the dependence of the static susceptibility (—) in the Li-intercalated sample. (b) The activated behavior of the spin-lattice relaxation rate at low temperatures with the solid line given by Eq. (3.30).

where the sum runs over the wave vectors in the first Brillouin zone. The parameter $\chi''_{\perp}(\mathbf{q},\omega_0)$ represents the wave-vector-dependent dissipative part of the dynamic susceptibility for the directions perpendicular to the external magnetic field, evaluated at the Larmor frequency ω_0. In the case of anisotropic electron-nucleus interaction the expression is rather more involved. However, the general observation of the relaxation rate, being proportional to the product of the temperature and the imaginary portion of the dynamic susceptibility, still holds. This part of the susceptibility is expected to follow similar activated temperature dependence as the static uniform susceptibility as they are connected through the Kramers-Kronig relations.

Similar temperature dependence of the two quantities presented in Fig. 4.18a thus unambiguously points at the interaction between the lithium nuclei and the paramagnetic electrons. Moreover, the low-temperature spin-lattice relaxation rate exhibits the gap-like behavior (see Eq. (3.30)) as shown in Fig. 4.18b. The obtained dynamical gap $\Delta = k_B \cdot 29(2)\,\mathrm{K}$ is remarkably close to the spin gap value and the value of 30 K obtained from the copper spin-lattice relaxation at low temperatures, when fitted by the same model [2].

Since there is virtually no shift of the ^{7}Li resonance from the value characteristic for the nonmagnetic lithium, the *s* contribution of the electron-nucleus coupling must be insignificant.

The dominant interaction would then originate from the dipolar coupling of the lithium nuclei with the nearby copper magnetic moments. The estimation of the distance *r* between a particular lithium nucleus to the nearest copper spin can then be made in the following fashion. According to Eq. (3.29) the expected spin-lattice relaxation rate is

$$\frac{1}{T_1} = \sqrt{\frac{\pi}{2}} \frac{1}{h} \frac{S(S+1)}{3\hbar\omega_e} \overline{A}_d^2 , \tag{4.33}$$

where $\overline{A}_d$ is an average dipolar coupling of the order

$$\overline{A}_d = \frac{\mu_0}{4\pi} \frac{\gamma\hbar g\mu_B}{\langle r \rangle^3} . \tag{4.34}$$

If the latter expression is plugged into Eq. (4.33) and the exchange frequency of $\omega_e = \sqrt{M_4/\hbar^2 M_2} = 1.8J/\hbar$ [66] is calculated from the angle-averaged Eqs. (4.22) or equivalently (4.24), the evaluated lithium-nucleus–copper-spin distance of $r = 2.7\text{Å}$ is obtained. Such a distance corresponds to the intercalated lithium ions being between the $CuBO_3$ planes. The ^{7}Li spin-lattice relaxation thus, similarly to the temperature behavior of the linewidth, suggests on the lithium being within the crystal structure of the $SrCu_2(BO_3)_2$.

Moreover, the dipolar coupling as the dominant electron-nucleus interaction can also explain the shape of the NMR absorption spectra. Namely, the anisotropy of the dipolar interaction is again of the order $\overline{A}_d$. Now, due to the powder nature of the sample and the electrons being partially polarized in the external magnetic field, i.e., $\langle S \rangle = \chi_{mol(Cu)} B_0 / N_A g\mu_B$, the expected linewidth as a consequence of the dipolar broadening is

$$\delta\nu \approx \frac{\overline{A}_d \langle S \rangle}{h} = 13\,\text{kHz} . \tag{4.35}$$

This value is remarkably close to the magnitude of the observed linewidths. At high and low temperatures with respect to the spin gap the anisotropic character of the lineshape seems to be masked by an isotropic T_2 relaxation of perhaps by diffusional motion of the spins. However, at mid temperatures, corresponding also to the maximum of the spin susceptibility, the anisotropy of the lineshape clearly pops up.

4.4 Discussion on Magnetic Anisotropy and Doping Effects in $SrCu_2(BO_3)_2$

In summary, a comprehensive study of the magnetic properties of the two-dimensional spin-gap system $SrCu_2(BO_3)_2$ has been presented in this chapter together with the attempts of doping this material through several different experimental routes. The anisotropy of the crystal structure is

reflected also in the anisotropic magnetic properties. The angular dependence of the position of the ESR line indicates that it is justified to treat the individual Cu^{2+} localized magnetic moment as being in a uniaxial-type of crystal environment. The small corrugation of the $CuBO_3$ planes does not affect much the *g*-factor anisotropy.

On the other hand, this buckling of the crystal planes has a pronounce effect on the appearance of the magnetic anisotropy Hamiltonian in the $SrCu_2(BO_3)_2$ compound, reflected through the angular and the temperature dependence of the ESR linewidth. The anisotropy of the rather broad linewidth thus sheds some important additional light on the spin anisotropy of the investigated systems. Namely, the previously proposed picture of the out-of-plane interdimer DM interaction as being the dominant anisotropic contribution, cannot adequately account for the experimental findings. In addition to such anisotropy terms, which were evaluated to be of the size $D'_{\|} = 2.4(1)\,\mathrm{K}$ from our high-temperature ESR linewidth anisotropy, employing the concept of exchange narrowing due to strong isotropic exchange, also sizable in-plane component of the interdimer as well as the intradimer Dzyaloshinsky-Moriya coupling have to be included. The latter terms are not to be neglected as shown by various recent experiments including inelastic neutron scattering, high-field electron spin resonance, ^{11}B NMR and specific heat measurements in high magnetic fields.

A complete pattern of the allowed Dzyaloshinsky-Moriya vectors has been constructed on the basis of the symmetry operations of the space group $I\bar{4}2m$ as shown in Fig. 4.8b, corresponding to the low-temperature phase of the $SrCu_2(BO_3)_2$ system. The permitted intradimer DM vectors thus lie in the *ab* crystal plane perpendicular to the direction of the dimers. This model satisfactory explains the observed ESR linewidth anisotropy and yields the intradimer DM interaction of the order of $D'_{\|} = k_B \cdot 3.6(5)\,\mathrm{K}$. The relatively high degree of uncertainty of this parameter originates from the fact that the in-plane components of the nearest-neighbor and the next-nearest-neighbor Dzyaloshinsky-Moriya interaction are coupled in the expression of the ESR linewidth.

However, when crossing the boundary of the low-temperature structural phase and the high-temperature one at $T_s = 395\,\mathrm{K}$, the static buckling of the $CuBO_3$ planes disappears, which dictates the in-plane components of the Dzyaloshinsky-Moriya interaction to vanish due to the presence of the *ab* mirror plane containing the dimmers above the phase-transition temperature. On the contrary, our ESR linewidth anisotropy is not affected by this phase transition at all, which indicates that some additional mechanism to the static buckling has to be involved in creation of the finite intradimer DM coupling. In fact, the presence of soft-mode lattice vibrations with a particular symmetry in the low-temperature phase, as observed from the Raman scattering experiments, can be successfully associated with the dynamical braking of the local symmetry allowing for instantaneous antisymmetric interaction terms, otherwise forbidden by the crystal symmetry. These vibrational modes evolve into the high-temperature soft

buckling modes with large vibrational amplitudes along the crystal *c* axis thus making the phase transition masked on the time scale short with respect to the time scale of the lattice vibrations. Indeed, is has been argued above that the symmetry of the dynamical lattice distortion is very similar to the static distortion in the low-temperature phase. Additionally, also the amplitude of both types of deformation is comparable and the frequency of these optical soft-modes is far below the characteristic frequency of the ESR, which is determined by the isotropic exchange regulating the decay of the spin correlation functions. For all these reasons, it seems safe to propose that the origin of the intradimer Dzyaloshinsky-Moriya interaction in the high-temperature structural phase is hidden in the dynamical soft-mode distortions. When crossing to the low-temperature phase this source most probably progressively evolves from the dynamical into the static origin. However, it should be emphasized that the amplitudes of the lattice vibrations stay sizable, i.e., comparable to the static displacements even down to 100 K, which represents the lowest temperature at which the crystal structure has been thoroughly studied.

The temperature dependence of the linewidth in the high-temperature regime above room temperature supports the picture of the sizable intradimer Dzyaloshinsky-Moriya interaction. It reflects the interplay between the spin and the lattice degrees of freedom. Namely, the linear increase can be attributed to the phonon modulation of the antisymmetric anisotropic exchange inducing lifetime-broadening effects. A rather crude model, taking the spin dynamics of the neighboring dimers as uncorrelated, provides a surprisingly good prediction of the slope of the high-temperature ESR linewidth increase, which is only roughly by the factor of two below the observed one.

On the other hand, the low-temperature increase of the linewidth is probably a consequence of the evolving static spin correlations. It shows critical-like temperature dependence between approximately 150 K and 15 K. Below 10 K the linewidth behavior changes its character, as a maximum of this parameter is observed. Due to the fact that the position of the line does not shift much with the temperature, we can seek the origin of the observed X-band ESR signal in transitions within the higher-lying energy continuum.

Doping the $SrCu_2(BO_3)_2$ system proved to be a rather tedious job. It seems that unlike in the $PbNi_2V_2O_8$ compound, the spin gap in the borate is much more robust. Also the chemical system itself acts more hostilely to any outside disturbance in a form of an impurity. Among many different approaches used when trying to dope the system with either electrons or holes only the liquid-ammonia-metal-solution method resulted in some concrete results. Though the color of the sample changed, which is usually a characteristic of the charge transfer, the combined picture of the structural and the magnetic measurements performed on the intercalated system is rather perplexing. Namely, from the structural point of view, no serious changes of the crystal structure parameters can be observed. Additionally, also the bulk magnetization measurements show that the magnetic nature of the ground state and the lowest-

lying magnetically excited states is virtually unchanged, as only a reduction of the spin susceptibility can be observed while the activation behavior itself remains unaltered. Furthermore, also the spin dynamics reflected in the ESR linewidths is unaffected by the introduction of lithium.

On the other hand, ^{7}Li NMR measurement serve with some rather convincing proofs that the lithium from the ammonia solution has entered the $SrCu_2(BO_3)_2$ sample. However, it is well known that the intercalation mechanism involves the injection of both ions and electrons into the host matrix to balance the charge. One could then suppose that Li-clusters are formed inside or on the surface of the $SrCu_2(BO_3)_2$ grains. However, such clusters would be seen by ESR in a form of narrower absorption lines as well as the NMR line position would shift significantly from the Larmor frequency of nonmagnetic Li^+ ions. For these reasons, the possibility of the formation of the spin clusters can be ruled out. In fact, NMR linewidths, linear line-broadening with respect to the value of the external magnetic field, anisotropic lineshapes as well as the spin-lattice relaxation times speak in favor of lithium nuclei being dominantly coupled to the spin system of the host material by the magnetic dipole interaction. Even more, the value of the spin-lattice relaxation rate corresponds to Li nuclei being located at a distance of only few angstroms from the spin sites, thus probably lying between the $CuBO_3$ planes. Such an arrangement of the intercalated ions could also account for the small but observable shifts of the vibration frequencies of the eigenmodes of the $SrCu_2(BO_3)_2$ lattice observed by Raman light scattering.

The electrons introduced into the system should, though, in a naive picture, affect also the magnetism of the host system if we assume that the copper ions, which are the most serious candidates to except electrons, change their valence state from Cu^{2+} to Cu^{+}. As the latter ions are nonmagnetic, this would explain the reduction of the magnetic susceptibility of the intercalated sample. However, the injected electrons break the dimer singlets and should thus impinge on the value of the spin gap, which is determined also by the frustrated next-nearest neighbor exchange coupling. As the spin gap as well as the spin dynamics seem not to be influenced much by the lithium intercalation, a more reasonable would appear the assumption that the lithium has reacted with something else due to the leakage in the experimental setup. But then again, such molecules would hardly be able to enter into the crystal structure of the host material.

The position of the lithium ions as well as the form they take insight the $SrCu_2(BO_3)_2$ structure is, unfortunately, still vague despite the considerable experimental effort that was undertaken. Further experimental investigation like neutron powder diffraction is, therefore, needed to clarify this issue. For the moment, it is thus the wisest idea to leave the question about the true position of the Li ions and the nature of their bonding with the host material in suspense.

Bibliography

[1] R. W. Smith, D. A. Keszler. Synthesis, structure, and properties of the orthoborate $SrCu_2(BO_3)_2$, *J. Solid State Chem*. **93**, 430 (1991).

[2] H. Kageyama, K. Yoshimura, R. Stern, N. V. Mushnikov, K. Onizuka, M. Kato, K. Kosuge, C. P. Slichter, T. Goto, Y. Ueda. Exact dimer ground state and quantized magnetization plateaus in the two-dimensional spin system $SrCu_2(BO_3)_2$, *Phys. Rev. Lett*. **82**, 3168 (1999).

[3] H. Kageyama, K. Onizuka, T. Yamauchi, Y. Ueda. Crystal growth of the two-dimensional spin gap system $SrCu_2(BO_3)_2$, *J. Cryst. Growth* **206**, 65 (1999).

[4] K. Sparta, G. J. Redhammer, P. Roussel, G. Heger, G. Roth, P. Lemmens, A. Ionescu. M. Grove, G. Güntherodt, F. Hüning, H. Lueken, H. Kageyama, K. Onizuka, Y. Ueda. Structural phase transition in the 2D spin dimer compound $SrCu_2(BO_3)_2$, *Eur. Phys. J. B* **19**, 507 (2001).

[5] S. Miyahara, K. Ueda. Exact dimer ground state of the two dimensional Heisenberg spin system $SrCu_2(BO_3)_2$, *Phys. Rev. Lett.* **82**, 3701 (1999).

[6] B. S. Shastry, B. Sutherland. Exact ground state of a quantum mechanical antiferromagnet, *Physica* **108B**, 1069 (1981).

[7] A. Koga, N. Kawakami. Quantum phase transition in the Shastry-Sutherland model for $SrCu_2(BO_3)_2$, *Phys. Rev. Lett.* **84**, 4461 (2000).

[8] C. H. Chung, J. B. Marston, S. Sachdev. Quantum phases of the Shastry-Sutherland antiferromagnets: Application to $SrSu_2(BO_3)_2$, *Phys. Rev. B* **64**, 134407 (2001).

[9] A. Läuchli, S. Wessel, M. Sigrist. Phase diagram of the quadrumerized Shastry-Sutherland model, *Phys. Rev. B* **66**, 014401 (2002).

[10] S. Miyahara, K. Ueda. Theory of the orthogonal dimer Heisenberg spin model for $SrCu_2(BO_3)_2$, *J. Phys.: Condens. Matter* **15**, R327 (2003); and references therein.

[11] K. Kodama, J. Yamazaki, M. Takigawa, H. Kageyama, K. Onizuka, Y. Ueda. Cu nuclear spin-spin coupling in the dimer singlet state in $SrCu_2(BO_3)_2$, *J. Phys.: Condens. Matter* **14**, L319 (2002).

[12] C. Knetter, A. Bühler, E. Müller-Hartmann, G. S. Uhrig. Dispersion and symmetry of bound states in the Shastry-Sutherland model, *Phys. Rev. Lett.* **85**, 3958 (2000).

[13] S. Miyahara, K. Ueda. Thermodynamic properties of three-dimensional orthogonal dimer model for $SrCu_2(BO_3)_2$, *J. Phys. Soc. Jpn. Suppl. B* **69**, 72 (2000).

[14] A. Koga. Ground-state phase diagram for the three-dimensional orthogonal-dimer system, *J. Phys. Soc. Jpn.* **69**, 3509 (2000).

[15] H. Nojiri, H. Kageyama, K. Onizuka, Y. Ueda, M. Motokawa. Direct observation of multiple spin gap excitations in two-dimensional dimer system $SrCu_2(BO_3)_2$, *J. Phys. Soc. Jpn.* **68**, 2906 (1999).

[16] H. Kageyama, M. Nishi, N. Aso, K. Onizuka, T. Yosihama, K. Nukui, K. Kodama, K. Kakurai, Y. Ueda. Direct evidence for the localized single-triplet excitation and the dispersive multiplet excitations in $SrCu_2(BO_3)_2$, *Phys. Rev. Lett.* **84**, 5876 (2000).

[17] T. Rõõm, U. Nagel, E. Lippmaa, H. Kageyama, K. Onizuka, Y. Ueda. Far-infrared study of the two-dimensional dimer spin system $SrCu_2(BO_3)_2$, *Phys. Rev. B.* **61**, 14342 (2000).

[18] P. Lemmens, M. Grove, M. Fisher, G. Günteroth, V. N. Kotov, H. Kageyama, K. Onizuka, Y. Ueda. Collective singlet excitations and evolution of Raman spectral weights in the 2D spin dimer compound $SrCu_2(BO_3)_2$, *Phys. Rev. Lett.* **85**, 2605 (2000).

[19] S. Miyahara, K. Ueda. Superstructures at magnetization plateaus in $SrCu_2(BO_3)_2$, *Phys. Rev. B.* **61**, 3417 (2000).

[20] K. Totsuka, S. Miyahara, K. Ueda. Low-lying excitations of the Shastry-Sutherland model, *Phys. Rev. Lett.* **86**, 520 (2001).

[21] K. Onizuka, H. Kageyama, Y. Narumi, K. Kindom, Y. Ueda, T. Goto. 1/3 magnetization plateau in $SrCu_2(BO_3)_2$ – Stripe order of excited triplets, *J. Phys. Soc. Jpn*. **69**, 1016 (1999).

[22] K. Kodama, M. Takigawa, M. Horvatić, C. Bertier, H. Kageyama, Y. Ueda, S. Miyahara, F. Becca, F. Mila. Magnetic superstructure in the two-dimensional quantum antiferromagnet $SrCu_2(BO3)_2$, *Science* **298**, 395 (2002).

[23] O. Cépas, K. Kakurai, L. P. Regnault, T. Ziman, J. P. Boucher, N. Aso, M. Nishi, H. Kageyama, Y. Ueda. Dzyaloshinsky-Moriya interaction in the 2D spin gap system $SrCu_2(BO_3)_2$, *Phys. Rev. Lett.* **87**, 167205 (2001).

[24] K. Kodama, K. Arai, M. Takigawa, H. Kageyama, Y. Ueda. Spin Correlation and field induced staggered magnetization in the 2D orthogonal dimer spin system $SrCu_2(BO_3)_2$, *J. Magn. Magn. Mater.* **272-276**, 491 (2004).

[25] S. Miyahara, F. Mila, K. Kodama, M. Takigawa, M. Horvatić, C. Bertier, H. Kageyama, Y. Ueda. The effects of the intra-dimer Dzyaloshinsky-Moriya interaction on the properties of $SrCu_2(BO_3)_2$ in an external magnetic field, *J. Phys.: Condens. Matter* **16**, S911 (2004).

[26] H. Nojiri, H. Kageyama, Y. Ueda, M. Motokawa. ESR study on the excited state energy spectrum of $SrCu_2(BO_3)_2$ – A central role of multiple-triplet bound states, *J. Phys. Soc. Jpn.* **72**, 3243 (2003).

[27] G. A. Jorge, R. Stern, M. Jaime, N. Harrison, J. Bonča, S. El Shawish, C. D. Batista, H. A. Dubrowska, B. D. Gaulin. High field specific heat of 2D quantum spin system $SrCu_2(BO_3)_2$, *cond-mat/0309534v1* (2003, unpublished).

[28] O. Cépas, T. Sakai, T. Ziman. Dynamics, selection rules and Dzyaloshinsky-Moriya interactions in strongly frustrated magnets, *Prog. Theor. Phys. Suppl*. **145**, 43 (2002).

[29] S. Miyashita, A. Ogasahara. Effect of Dzyaloshinsky-Moriya interaction on the ESR of Shastry-Sutherland model, *J. Phys. Soc. Jpn.* **72**, 2350 (2003).

[30] S. El Shawish, J. Bonča, C. D. Batista, I. Sega. Electron spin resonance of $SrCu_2(BO_3)_2$ at high magnetic field, *cond-mat/0407632v1* (2004, unpublished).

[31] O. Cépas, T. Ziman. Theory of phonon-assisted "forbidden" optical transitions in spin-gap systems, *cond-mat/0401240v1* (2004, unpublished).

[32] A. Zorko, D. Arčon, H. van Tol, L. C. Brunel, H. Kageyama. X-band ESR determination of the Dzyaloshinsky-Moriya interaction in the two-dimensional $SrCu_2(BO_3)_2$ system. *Phys. Rev. B* **69**, 174420 (2004).

[33] A. Zorko, D. Arčon, A. Lappas, J. Giapintzakis. Near critical behavior in the two-dimensional spin-gap system $SrCu_2(BO_3)_2$, *Phys. Rev. B* **65**, 024417 (2001).

[34] A. Zorko, D. Arčon, H. Kageyama, A. Lappas. Magnetic anisotropy of $SrCu_2(BO_3)_2$ system as revealed by X-band ESR, to be published in *Appl. Magn. Reson.* **27**.

[35] B. S. Shastry, B. Kumar. $SrCu_2(BO_3)_2$: A unique Mott Hubbard insulator, *Prog. Theor. Phys. Suppl.* **145**, 1 (2002).

[36] T. Kimura, K. Kuroki, Y. Arita, H. Aoki. Possibility of superconductivity in the repulsive Hubbard model on the Shastry-Sutherland lattice, *Phys. Rev. B* **69**, 054501 (2004).

[37] A. Zorko, D. Arčon, C. J. Nuttall, A. Lappas. X-band ESR study of the two-dimensional spin-gap system $SrCu_2(BO_3)_2$, *J. Magn. Magn. Mater.* **272**, e699 (2004).

[38] J.-C. Bissey, R. Berger, Y. Servant. Differentiated *g*-values and exchange interaction between dissimilar copper ions as studied by EPR in the linear chain system $CuSO_4.5H_2O$, *Solid. State. Commun*. **93**, 243 (1995).

[39] J. R. Pilbrow. *Transition Ion Electron Paramagnetic Resonance* (Oxford University Press, Oxford, 1990).

[40] T. G. Castner, M. S. Seehra. Antisymmetric exchange and exchange-narrowed electron-paramagnetic-resonance linewidths, *Phys. Rev. B* **4**, 38 (1971).

[41] T. M. McGregor, Z. G. Soos. Anisotropic exchange in linear chain complexes of copper (II), *J. Chem. Phys.* **64**, 2506 (1976).

[42] T. Hahn (ed.). In *International Tables for Crystallography, Volume A: Space-group symmetry* (Kluwer Academic Publisher, Dordrecht, 1989), p. 416 .

[43] K. Kakurai, N. Aso, K. Nukui, M. Nishi, H. Kageyama, Y. Ueda, H. Kodowaki, O. Cépas. Inelastic neutron scattering experiments on Dzyaloshinsky-Moriya interaction in $SrCu_2(BO_3)_2$, in *Quantum Properties of Low-Dimensional Antiferromagnets*, edited by Y. Ajiro and J.-P. Boucher (Kyushu University Press, Fukuoka, 2002), p. 102.

[44] S. Zherlitsyn, S. Schmidt, B. Wolf, H. Schwerk, B. Lüthi, K. Kageyama, K. Onizuka, Y. Ueda, K. Ueda. Sound-wave anomalies in $SrCu_2(BO_3)_2$, *Phys. Rev. B* **62**, R6097 (2000).

[45] K. Kodama, S. Miyahara, M. Takigawa, M. Horvatić, C. Bertier, F. Mila, H. Kageyama, Y. Ueda. Field induced effects of anisotropic magnetic interactions in $SrCu_2(BO_3)_2$, *cond-mat/0404482v1* (2004, unpublished).

[46] K.-Y. Choi, G. Pashkevich, K. V. Lamonova, H. Kageyama, Y. Ueda, P. Lemmens. Strong anharmonicity and spin-phonon coupling in the quasi-two-dimensional quantum spin system $Sr_{1-x}Ba_xCu_2(BO_3)_2$, *Phys Rev. B* **68**, 104418 (2003).

[47] Z. G. Soos, T. T. P. Cheung, K. T. McGregor. Exchange narrowing in correlated spin systems: local field contributions, *Chem. Phys. Lett*. **46**, 600 (1977).

[48] B. Wolf, S. Zherlitsyn, S. Schmidt, B. Lüthi. Low-dimensional quantum spin systems in pulsed magnetic fields up to 50 T, *Phys. Stat. Sol. (a)* **189**, 389 (2002).

[49] A. Abragam. *Principles of Nuclear Magnetism* (Oxford University Press, Oxford, 1961), p 404.

[50] C. E. Zaspel, J. E. Drumheller. Temperature dependence of the exchange interaction and applications to electron paramagnetic resonance, *Phys. Rev. B* **16**, 1771 (1977).

[51] S. T. Bramwell. Temperature dependence of the isotropic exchange constant, *J. Phys.: Condens. Matter* **2**, 7527 (1990).

[52] M. S. Seehra and T. C. Castner. The paramagnetic line width in $Cu(HCOO)_2 \cdot 4H_2O$, *Phys. Kondens. Materie* **7**, 185 (1968).

[53] D. Bloch. The 10/3 law for the volume dependence of superexchange, *J. Phys. Chem. Solids* **27**, 881 (1966).

[54] B. Wolf, S. Zherlitsyn, S. Schimd, B. Lüthi, H. Kageyama, Y. Ueda. Soft acoustic modes in the two-dimensional spin system $SrCu_2(BO_3)_2$, *Phys. Rev. Lett.* **86**, 4847 (2001).

[55] H. Kageyama, K. Onizuka, Y. Ueda, S. Hane, H. Mitamura, T. Goto, K. Yoshimura, K. Kosuge. Ba- and Ca-substitution effect on the spin gap in $SrCu_2(BO_3)_2$ with the exact dimer ground state, in *Proceedings of the 4th international symposium on advanced physical fields*, edited by G. Kido (National Research Institute for Metals, Tsukuba, 1999), p. 235.

[56] H. Kageyama, Y. Narumi, K. Kindo, K. Onizuka, Y, Ueda, T. Goto. Quantized magnetization plateaus in the orthogonal dimer system $SrCu_2(BO_3)_2$, *J. Alloy. Compd*. **317-318**, 177 (2001).

[57] R. D. Shannon. Revised effective ionic radii and systematic studies of interatomic distances in halides and chalcogenides, *Acta Cryst. A* **32**, 751 (1976).

[58] H. I. Tsai, J. L. Schindler, C. R. Kannewurf, M. G. Kanatzidis. Plastic superconducting polymer-NbSe2 nanocomposites, *Chem. Mater.* **9**, 875 (1997).

[59] M. Gaberšček, M. Bele, J. Drofenik, R. Dominko, S. Pejovnik. Improved carbon anode for lithium batteries - Pretreatment of carbon particles in a polyelectrolyte solution, *Electrochem. Solid State Lett.* **3**, 171 (2000).

[60] W. K. Fullagar, P. A. Reynolds, J. W. White. Lithium and sodium fullerides prepared in liquid ammonia, *Solid State Commun.* **104**, 23 (1997).

[61] F. A. Cotton, G. Wilkinson, *Advanced Inorganic Chemistry* , *5th Edition* (John Wiley & Sons, New York,1988), p.127.

[62] W. R. McKinnon. *Chemical Physics of Intercalation (NATO ASI B), vol. B172*, edited by A. P. Legrand and S. Flanfrois (Plenum, New York, 1987), p. 181.

[63] J. Emery, O. Bohnke, J. F. Fourquet, J. Y. Buzare, P. Florian, D. Massiot. Polaronic effect on lithium motion in intercalated perovskite lithium lanthanum titanate observed by ^{7}Li NMR and impedence spectroscopy, *J. Phys.: Condens. Matter* **11**, 10401 (1999).

[64] I. S. Pronin, A. A. Vashman, S. E. Sygaryov. ^{7}Li and ^{31}P NMR studies of monoclinic $Li_3In_2(PO_4)_3$, *Phys. Rev. B* **48**, 16463 (1993).

[65] T. Moriya. The effect of the electron-electron interaction on the nuclear spin relaxation in metals, *J. Phys. Soc. Jpn.* **18**, 516 (1963).

[66] P. W. Anderson. Exchange narrowing in paramagnetic resonance, *Rev. Mod. Phys*. **25**, 269 (1953).

5 CONCLUDING REMARKS

The subject of this Thesis is a study of the role of magnetic anisotropy and doping on the magnetic properties of one- and two-dimensional antiferromagnets exhibiting a spin gap. We have chosen two recently discovered representatives, namely the one-dimensional Haldane system $PbNi_2V_2O_8$ and the two-dimensional orthogonal dimer system $SrCu_2(BO_3)_2$. As the extensive conclusions about the magnetic anisotropy, spin correlations and the effects of the impurities in these systems have already been given at the end of chapters 3 and 4, respectively, only short comments summarizing the general results in the light of the two topics presented in the introductive chapter are offered below. The experimental methods that were used in this work, namely the electron spin resonance and the nuclear magnetic resonance, were once again proven to be irreplaceable for extending the horizons about the magnetism in low-dimensional magnetic materials. Both experimental techniques yielded useful information on the nature of the low-energy excitations, the spin gap and the dominant magnetic anisotropy terms in the investigated compounds.

In both investigated parent materials, that is the $PbNi_2V_2O_8$ as well as the $SrCu_2(BO_3)_2$ compounds, the signature of the quantum mechanics in macroscopic spin systems is clearly expressed. Namely, the ground states of these systems have the "singlet" nature. Our experimental findings suggest a similar situation also in the $SrNi_2V_2O_8$ compound, which is isomorphous to the lead-nickel vanadate and was previously believed to exhibit magnetic order at low temperatures.

Second, there are many unsolved mysteries regarding the magnetism of these systems, which are a consequence of the presence of small but by no means negligible spin anisotropy. In this respect, the magnetic resonance experiments provided useful insight into this field. For both of the investigated materials the previously established picture of the dominant magnetic anisotropy terms was found to be inconsistent with our experimental results. For instance, in the case of the Haldane material $PbNi_2V_2O_8$ a simple uniaxial-type of the single-ion anisotropy was suggested as the leading contribution in the literature. However, our arguments presented in chapter 3 speak in favor of a more complicated picture due to significantly distorted local environment. Additionally, also sizable Dzyaloshinsky-Moriya interaction between the nearest-neighbor Ni^{2+} magnetic moments was evaluated. However, at present it seems rather unfeasible to check the validity of all our predictions since single crystals of this one-dimensional material do not yet exist.

On the contrary, the situation with the two-dimensional $SrCu_2(BO_3)_2$ system is quite opposite. Performing X-band ESR measurements on a single crystal sample enabled us to improve the picture of the magnetic anisotropy in this material in a quite precise manner.

Namely, in addition to the out-of-plane interdimer Dzyaloshinsky-Moriya interaction previously suggested to be the dominant anisotropic contributions, we were able to identify also sizable in-plane components of both the interdimer as well as the intradimer DM interaction. Using the symmetry arguments the pattern of DM vectors was constructed, which turned out to be in a good agreement with the experimental findings. Moreover, our experimental results highlighted also the importance of the spin-phonon coupling in the $SrCu_2(BO_3)_2$ compound. In this respect a novel mechanism of dynamically broken local symmetry inducing spontaneous Dzyaloshinsky-Moriya interaction was successfully implemented into the explanation of the experimental data.

The next open question presented in the introduction of this Thesis was the one regarding the impurity-doping effects. In this respect the two investigated spin systems turn out to be intrinsically different. In the case of substitutional doping the Haldane system $PbNi_2V_2O_8$ the spin singlet ground state is broken in favor of the magnetically ordered ground state at low temperature at very small doping concentrations irrespective of the spin or spinless nature of the dopants and. This situation resembles the one encountered in spin-Peierls systems and in spin ladders, where the origin of the singlet ground state of the parent material is explained within the framework of the valence-bond model. There is, however, a pronounced difference in the temperature evolution of the spin correlations in the doped $PbNi_2V_2O_8$ materials between the vacancy-doped (Mg^{2+}) and "spin"-doped (Co^{2+}) compounds. It was shown by our NMR measurement that magnetic fields of several tesla significantly suppress the antiferromagnetic correlations in the case of Mg-doping while these correlations are much more resistant in Co-doped samples.

On the other hand, doping the two-dimensional $SrCu_2(BO_3)_2$ compound is much more involved. Only intercalational doping with Li^+ ions seems to be producing some concrete results. Introducing lithium should result in electron doping of the copper planes. In contrast to the $PbNi_2V_2O_8$ compound the spin gap of the $SrCu_2(BO_3)_2$ system is much more robust. The ground state of the spin system thus remains the singlet state even though a sizable amount of lithium ions should be present in the Li-intercalated sample. In a way, our results thus resemble the case of hole-doped spin ladders. Since this two-dimensional spin-gap system could, according to theoretical predictions, lead to superconductivity, the future investigations should be oriented also towards the hole doping of this material. After all, if the superconductivity is observed in the $SrCu_2(BO_3)_2$ the accurate knowledge of the spin Hamiltonian of this system and its possible connection with the occurrence of the superconductivity could turn out to be a milestone in the understanding of this phenomenon.

EXTENDED ABSTRACT IN SLOVENE (RAZŠIRJEN POVZETEK V SLOVENŠČINI)

1 Uvod v sisteme s spinsko energijsko režo

Odkritje visokotemperaturnih superprevodnikov pred skoraj dvema desetletjema [1] je vzpodbudilo povečan interes tako po teoretičnih kot tudi po eksperimentalnih raziskavah nižjedimenzionalnih kvantnih magnetih sistemov. Vzrok temu gre iskati v dejstvu, da je spojine, ki pri ustreznem dopiranju postanejo superprevodne, moč obravnavati kot "idealne" planarne mreže lokaliziranih spinov $S = 1/2$, sklopljenih z izotropno antiferomagnetno izmenjalno interakcijo. Značilnosti visokotemperaturnih superprevodnikov so tako močne antiferomagnetne fluktuacije in pojav energijske reže v spektrih njihovih nizkoenergijskih ekscitacij ("pseudogap") v območju dopiranja pod optimalnim nivojem. Slednja se pojavi že nad temperaturo prehoda v superprevodno fazo in bi lahko bila povezana z mehanizmom tvorbe Cooperjevih parov pod temperaturo prehoda. Ker so v tvorbo energijske reže vpletene pretežno spinske prostostne stopnje [2, 3], so posebej zanimivi ostali nižjedimenzionalni spinski sistemi, ki kažejo spinsko energijsko režo ("spin gap") v spektrih nizkoenergijskih spinskih ekscitacij. Za razliko od dvodimenzionalnih so različni enodimenzionalni spinski sistemi podrobneje preučevani že vse od samih začetkov kvantne mehanike v prvi polovici prejšnjega stoletja. Spinske verige namreč v nasprotju z višjedimenzionalnimi spinskimi strukturami pogosto nudijo analitične rešitve [4] oziroma omogočajo natančnejše numerične približke. Nadaljnji vzrok razcveta področna nižjedimenzionalnih magnetnih sistemov je prav gotovo tudi znaten napredek na področju sinteze materialov, saj je kemija trdne snovi dandanes zmožna sinteze različnih "eksotičnih" in hkrati potencialno tehnološko uporabnih materialov.

Sama nižjedimenzionalna narava določenega spinskega sistema je povezana z izmenjalno interakcijo med spini, v pretežni meri omejeno bodisi na eno ali dve dimenziji. Vzrok takšne redukcije dimenzije spinskega prostora je sama kristalna struktura. Tako ta pogosto narekuje zmanjšano interakcijo v določeni smeri zaradi večjih razdalj med ioni ali pa zaradi manjkajočih nemagnetnih ionov, mediatorjev interakcije med posameznimi magnetnimi ioni. Sledni mehanizem izmenjalne interakcije imenujemo superizmenjalna interakcija ("superexchange"). Velikost magnetne sklopitve je v tem primeru kritično odvisna od same postavitve magnetnih ionov in nemagnetnih mediatorjev interakcije preko prekrivanja ustreznih ionskih orbital, kar popisujejo Kanamori-Goodenoughova pravila [5, 6]. Posledica zmanjšane dimenzionalnosti so močne kvantne fluktuacije, ki preprečujejo magnetno urejanje. Le-te so pogojene s samo topologijo izmenjalne interakcije, z medsebojno velikostjo različnih sklopitev in s prisotnostjo nečistoč, ki lahko bistveno vplivajo na osnovno stanje in nizkoenergijske ekscitacije [7, 8].

Čeprav je sama spinska konfiguracija posameznih osnovnih stanj, pripadajočih različnim magnetnim sistemom s spinsko energijsko režo, precej raznolika, pa je vsem skupen koncept tvorbe spinskih parov. Za sistem dveh spinov $S = 1/2$ je na primer osnovno stanje podano z antisimetrično kombinacijo Néelovih stanj, $\left(\left| \uparrow\downarrow \right\rangle - \left| \downarrow\uparrow \right\rangle \right) / \sqrt{2}$, in je kot tako klasično nepredstavljivo. V primeru večjega števila sklopljenih spinov je formacija takšnih singletnih parov otežena. Posledično je splošna tendenca makroskopskih spinskih sistemov tudi v primeru zmanjšane dimenzionalnosti orientirana proti magnetnemu urejanju in odpravljanju spinske energijske reže, kar je delno povezano tudi s prisotnostjo členov magnetne anizotropije, kot bo to predstavljeno v nadaljevanju. Sistemi z energijsko režo in singletnim osnovnim stanjem so zato v naravi relativno maloštevilni. Ker je za njihovo nemagnetno osnovno stanje značilno hitro (eksponentno) padanje spinskih korelacij z razdaljo, jih imenujemo tudi spinske tekočine. Do takšnega osnovnega stanja in pripadajoče spinske energijske reže vodi več mehanizmov. Lahko sta posledica posebne oblike izmenjalne topologije, tekmovanja nasprotujočih se izmenjalnih mehanizmov, ki vodi do frustracije v spinskem prostoru, celoštevilčne narave spinov v primeru spinskih verig, ali pa dimerizacije mreže, ki je posledica zlomljene translacijske simetrije.

Sistemi s spinsko energijsko režo so relativno številčni v eni dimenziji glede na dve dimenziji. Prvo družino takšnih sistemov predstavljajo spin-Peierlsove organske [9, 10] in anorganske spojine [11, 12], za katere je značilno, da pride pod temperaturo prehoda v spin-Peierlsovo stanje do dimerizacije kristalne mreže vzdolž verig, ki je posledica zamrznitve določenega mrežnega nihanja. Takšna deformacija kristalne strukture sicer povzroči povečanje elastične energije kristala, vendar pa je celokupna energija zmanjšana na račun urejanja spinov v singletne pare. Direktna posledica alternirajočih razdalj med sosednjimi spini vzdolž verige je namreč tudi alternirajoča izmenjalna interakcija, ki vodi do tvorbe spinskih singletov, kot to ponazarja slika 1.1. Podobna slika je realizirana tudi v primeru spojin $Cu(NO_3)_2 \cdot 2.5\ H_2O$ [13] in $(VO)_2P_2O_7$ [14], kjer je alternirajoča narava izmenjalne interakcije v osnovi zagotovljena že brez prisotnosti mrežnih nihanj. Do energijske reže lahko vodi tudi tekmovanje interakcij med najbližjimi in drugimi najbližjimi sosedi znotraj spinske verige [15], lahko pa njen izvor sploh nima geometrijskega ozadja, kot v primeru celoštevilskih spinskih verig.

Haldane je v začetku 80ih let prejšnjega stoletja predlagal, da je narava osnovnega stanja celoštevilčnih spinskih verig precej drugačna od polceloštevilčnih verig [16]. Tako so za primer prvih značilni spinsko singletno osnovno stanje, eksponentno padajoče spinske korelacije v tem stanju in energijska reža do najnižjega vzbujenega stanja, medtem ko so v primeru slednjih spinske korelacije počasneje (potenčno) padajoče, med osnovnim in najnižjim vzbujenim energijskim stanjem pa ni končne energijske reže. Nadalje je osnovno stanje z energijsko režo tudi precej obstojnejše na zunanje perturbacije kot so sklopitev med verigami ali magnetna anizotropija [17]. Po drugi strani nemagnetno osnovno stanje na račun magnetnega v primeru

polcelоštevilčnih spinov podre že vsaka najmanjša perturbacija [16]. Trenutno najboljši približek osnovnega stanja celoštevilčnih (Haldaneovih) spinskih verig predstavlja tako imenovano "valence-bond solid" (VBS) osnovno stanje [18]. Shematsko je vzpostavitev spinske konfiguracije v Haldaneovem osnovnem stanju za primer spinov $S = 1$ prikazana na sliki 1.2. V tem primeru iz vsakega mrežnega mesta izvirata dve valenčni vezi, ki sklapljata obe izmed prostostnih stopenj $S = 1/2$ na tem mestu s sosednjima mestoma v singletno stanje. Upravičenost predlagane slike je bila tudi eksperimentalno dokazana z detekcijo prostih spinov $S = 1/2$, induciranih v spinskih verigah $[Ni(C_2H_8N_2)_2(NO_2)]ClO_4$ (NENP) s spinom $S = 1$ poleg nemagnetnih nečistoč [19]. Danes obstaja že kar nekaj znanih Haldaneovih sistemov. Nekateri izmed njih so prikazani na faznem diagramu na sliki 1.4. Med njimi je tudi nedavno odkriti sistem $PbNi_2V_2O_8$ [20], ki je predmet raziskave te disertacije.

Sistemi, ki povezujejo eno dimenzijo z dvema, so tako imenovane spinske lestve ("spin ladders"), v katerih je z znatno izmenjalno interakcijo povezano končno število spinskih verig. V primeru parov sklopljenih verig, kot v spojine $SrCu_2O_3$, je osnovno stanje zopet singletno [21]. Zanimiva lastnost spinskih lestev je prisotnost energijske reže v primeru sodega števila sklopljenih verig in odsotnost le-te v primeru, ko je število sklopljenih verig liho [22], kar je kvantna manifestacija dejstva, da je le sodo število spinov moč sklopiti v singletno stanje. S povečevanjem števila sklopljenih verig v limiti pridemo do dvodimenzionalnega primera, vendar pa tudi sama velikost energijske reže konvergira proti ničelni vrednosti [22]. Zato ni presenetljivo, da je znanih le malo dvodimenzionalnih magnetnih sistemov z energijsko režo.

Prvi primer dvodimenzionalne spojine z energijsko režo je CaV_4O_9, kjer je takšna narava osnovnega stanja posledica posebne topologije kristalne mreže [23]. Drug možen mehanizem, ki vodi do spinske tekočine, pa je frustracija izmenjalne interakcije v primeru spojine $SrCu_2(BO_3)_2$ [24], kjer je pomen antiferomagnetne sklopitev med drugimi najbližjimi sosedi zadušen na račun antiferomagnetne sklopitve znotraj parov najbližjih spinov zaradi geometrijskih razlogov, kot to prikazuje slika 1.3. Hamiltonka, ki popisuje omenjen sistem ortogonalnih spinskih dimerov, je topološko ekvivalentna s Shastry-Sutherlandovim modelov (glej sliko 1.3), obravnavanim pred več kot dvema desetletjema [25]. Gre za prvo fizikalno realizacijo omenjenega modela, katerega posebnost je eksaktno izračunljivo osnovno stanje, ki je preprost produkt singletov na posameznih dimerih. Magnetna anizotropija in efekt dopiranja na omenjeno spojino predstavljata drugi predmet raziskave te disertacije.

Kot je bilo že povedano, lahko na osnovno stanje in nizkoležeče magnetne ekscitacije odločilno vplivajo magnetna anizotropija, tridimenzionalna topologija izmenjalne interakcije in prisotnost nečistoč, ki podrejo homogenost v spinskem sistemu. V primeru energijske reže so osnovna stanja ponavadi obstojna glede na naštete dejavnike do neke mejne vrednosti, ko je energija določene ekscitacije v recipročnem prostoru znižana do mere, da povzroči ta ekscitacija vzpostavitev reda dolgega dosega. Primer energijskega diagrama rahlo sklopljenih Haldaneovih

verig v prisotnosti magnetne anizotropije oblike $D_{cf}S_z^2$ na posameznem mestu ("single-ion") je prikazan na sliki 1.4. Kot je lepo razvidno, obe perturbaciji nasprotujeta tvorbi nemagnetnega Haldaneovega osnovnega stanja [26]. Podoben efekt na osnovno stanje Haldaneovih verig imajo tudi spinske nečistoče. Če koncentracija nečistoč brez spina na spinskih verigah preseže določeno mejno vrednost, se v snovi vzpostavi magnetni red dolgega dosega [17]. Ta efekt, ko nered v obliki nečistoč povzroči magnetno urejanje, je v literaturi znan pod imenom "order-by-disorder effect" [27]. Omenjen učinek za primere različnih dopiranj tako z magnetnimi kot z nemagnetnimi nečistočami je bil pogosto opažen v $S = 1/2$ spinskih sistemih, kot so spin-Peierlsov sistem $CuGeO_3$ [11, 28] ali spinska lestev z dvema sklopljenima verigama $SrCu_2O_3$ [29, 30]. Hiter razpad energijske reže in vzpostavitev antiferomagnetnega reda dolgega dosega v primeru nemagnetnih nečistoč je bila v primerih obeh spojin pripisana spinskim prostostnim stopnjam $S = 1/2$, induciranim v neposredni bližini nečistoč kot posledica razdrtja singletnih vezi [29, 31]. Problem dopiranja sistemov z energijsko režo z lokaliziranimi nečistočami in superprevodnost v visokotemperaturnih kupratih, kjer mobilni nosilci naboja podrejo antiferomagnetno ureditev, se na prvi pogled zdita dva povsem nekorelirana pojava. Po drugi strani pa bi moral biti vpliv mobilnih nosilcev na ekscitacije določene spinske tekočine v tesnejši povezavi z visokotemperaturno superprevodnostjo. V tej luči je zanimiva nedavno opažena superprevodnost v spinski verigi/lestvi $Sr_{0.4}Ca_{13.6}Cu_{24}O_{41.84}$, dopirani z vrzelmi [32].

Čeprav je v splošnem magnetno urejanje spinov kot posledica nečistoč precej raziskano področje, pa koherentne teorije še vedno ni. Ta disertacija zato ponuja nov eksperimentalni vpogled v to tematiko na primeru družine Mg- in Co-dopiranih spojin $PbNi_2V_2O_8$, ki so prva realizacija Haldaneovega sistema z izraženim "order-by-disorder" efektom [20]. Po drugi strani je potencialno zanimivo tudi dopiranje dvodimenzionalne spojine $SrCu_2(BO_3)_2$ [33, 34], zaradi formalne podobnosti njene strukture s strukturami visokotemperaturnih superprevodnikov [24].

Drugi cilj te disertacije je podrobneje raziskati magnetno anizotropijo v obeh sistemih. Kot je bilo omenjeno, lahko ta bistveno vpliva na osnovno stanje in nizkoležeče ekscitacije v spinskih sistemih. Pri tolmačenju različnih pojavov, povezanih s spinskimi prostostnimi stopnjami nekega sistema, je zato dobro imeti kar se da jasno sliko o dominantnih prispevkih k magnetni anizotropiji.

S stališča reševanja zastavljenih vprašanj se zdijo magnetno-resonančne spektroskopske metode idealne [35]. Elektronska spinska resonance (ESR) lahko namreč nudi direktno sliko o magnetni anizotropiji in spinskih korelacijah v določenem spinskem sistemu, saj so končni eksperimentalni spektri odraz končne anizotropije, njihovo temperaturno spreminjanje pa odraža razvoj spinskih korelacij. Po drugi strani lahko tudi meritve jedrske magnetne resonance (NMR) uporabimo kot vir dodatnih, komplementarnih informacij o sistemu elektronskih spinov. To je mogoče, ko je sistem preučevanih jeder le rahlo sklopljen s sistemom spinov, da lokalna magnetna polja, ki jih ustvarjajo paramagnetni centri na mestu jeder, niso prevelika [36].

2 Spinske korelacije in magnetna anizotropija v 1D Haldaneovem sistemu $PbNi_2V_2O_8$

O prvi sintezi enodimenzionalnega spinskega sistema $PbNi_2V_2O_8$ so Uchiyama *et al.* prvič poročali šele na prelomu prejšnjega stoletja [20]. Gre za spojino, ki je izomorfna že kar nekaj let poznani spojini $SrNi_2V_2O_8$ [37]. Kristalno strukturo obeh sistemov prikazuje slika 3.1a. V obeh primerih imajo le Ni^{2+} ioni magnetni moment. Kot je prikazano na sliki 3.1b, ti magnetni momenti z efektivnim spinom $S = 1$ tvorijo nenavadne spiralno oblikovane verige. Dominantna izmenjalna interakcija $J = k_B \cdot 95\,\mathrm{K}$ antiferomagnetnega značaja [20] med najbližjima sosedoma v verigi je posredovana preko dveh kisikovih ionov. Omenjena vrednost izmenjalne sklopitve je bila določena na podlagi visokotemperaturnih meritev magnetne susceptibilnosti in je nekaj pod napovedjo rezultatov neelastičnega nevtronskega sipanja [38, 39]. Slednje meritve so postregle tudi z oceno izmenjalne interakcije med drugimi najbližjimi sosedi v verigi $J' = k_B \cdot 5\,\mathrm{K}$ in med sosednjimi verigami $J_\perp = -k_B \cdot 2\,\mathrm{K}$. Enodimenzionalno naravo spinskega sistema so potrdile karakteristične magnetne ekscitacije z energijsko režo v primeru spojine $PbNi_2V_2O_8$. Ta reža v limiti neskloplјenih verig znaša $\Delta_\parallel = k_B \cdot 36\,\mathrm{K}$ za Haldaneove ekscitacije polarizirane vzdolž spinskih verig in $\Delta_\perp = k_B \cdot 46\,\mathrm{K}$ za pravokotno polarizirane ekscitacije.

Najpomembnejši vir magnetne anizotropije v sistemu $PbNi_2V_2O_8$ je distorzija NiO_6 oktaedrov. Avtorji prvega prispevka so predlagali dominanten člen magnetne anizotropije oblike $D_{cf} S_i^{z\,2}$, kjer *z* sovpada s smerjo kristalne osi *c*. Na podlagi tega modela, ki temelji na tetragonalni kristalni simetriji osnovne celice, je bila tudi ocenjena velikost magnetne anizotropije za posamezni ion, $D_{cf} = -k_B \cdot 5.2\,\mathrm{K}$ [38, 39].

Ustreznost te napovedi je moč oceniti z eksperimentom elektronske paramagnetne resonance [40, 41]. Spektri posneti v območju X ($\nu_0 = 9.3\,\mathrm{GHz}$) na praškastem vzorcu $PbNi_2V_2O_8$, prikazani na sliki 3.2, potrjujejo, da gre za sistem z energijsko režo, saj intenziteta signala kaže tipično aktivacijsko obnašanje pri nizkih temperaturah. Širine eksperimentalnih spektrov δB so relativno velike, saj so primerljive z vrednostjo resonančnega polja B_c. Zato je potrebno upoštevati tako absorpcijo pri pozitivnem kot tudi negativnem resonančnem polju, kar jemlje v obzir Lorentzova funkcija

$$I(B) = -\frac{16A}{\pi}\delta B\left(\frac{(B-B_c)}{\left(4(B-B_c)^2+\delta B^2\right)^2}+\frac{(B+B_c)}{\left(4(B+B_c)^2+\delta B^2\right)^2}\right), \qquad (1)$$

kjer A predstavlja intenziteto signala. Ujemanje te funkcije z eksperimentalnimi spektri je zadovoljivo, kot to prikazuje slika 3.2a. Pri temperaturah nad 150 K širina kot tudi vrednost resonančnega polja ne kažeta tako intenzivnega spreminjanja s temperaturo, kot pri nizkih temperaturah (glej sliko 3.3). Spreminjanje v tem območju lahko pripišemo temperaturnemu razvoju spinskih korelacij ali pa sklopitvi s fononskimi nihanji. Ker gre za manjše spremembe,

lahko širino spektra pri sobni temperaturi $\delta B_{pp} = 0.36(1)\,\mathrm{T}$ direktno primerjamo s teoretično napovedjo v limiti neskončne temperature. Širina resonančnega spektra med obema vrhovoma je podana z drugim in četrtim momentom tega spektra, ki sta v primeru dominance izotropne izmenjalne sklopitve oblike [42]

$$\begin{aligned} M_2 &= \left\langle \left[H', M^+\right]\left[M^-, H'\right]\right\rangle \Big/ \left\langle M^+ M^-\right\rangle = D_{cf}^2\left(1+\cos^2\theta\right)/2, \\ M_4 &= \left\langle \left[H - H_Z, \left[H', M^+\right]\right]\left[H - H_Z, \left[H', M^-\right]\right]\right\rangle \Big/ \left\langle M^+ M^-\right\rangle = 4J^2 D_{cf}^2\left(1+\cos^2\theta\right)/2. \end{aligned} \tag{2}$$

Pri tem je celotna hamiltonka razdeljena na del $H_0 = H_{ex} + H_Z$, ki vključuje le izmenjalno interakcijo in Zeemansko sklopitev, in del H', ki ponazarja magnetno anizotropijo v sistemu. Operator $M^{\pm}$ je operator celotne magnetizacije, oglati in trikotni oklepaji pa zapored določajo komutator in operacijo termičnega povprečenja. Parameter θ v gornjem izrazu označuje kot med smerjo vektorja anizotropije za posamezni ion $\mathbf{D}_{\mathrm{cf}}$ (kristalna os *c*) in smerjo zunanjega magnetnega polja $\mathbf{B}_0$. Širino spektra v limiti neskončne temperature podaja izraz [43, 44]

$$\delta B_{pp}^{L} = \frac{C}{g\mu_B}\left(\frac{M_2^3}{M_4}\right)^{1/2}, \tag{3}$$

kjer nedoločenost konstante *C* (reda velikosti 1) izvira iz divergence obeh momentov v primeru povsem Lorentzovih spektrov. Predlagana magnetna anizotropija oblike $D_{cf} S_i^{z\,2}$ tako v praškastem vzorcu narekuje širino velikosti

$$\delta B_{pp} = \frac{\pi}{3\sqrt{3}}\frac{1}{g\mu_B}\frac{D_{cf}^2}{J} = 0.12\ \mathrm{T}, \tag{4}$$

kar je približno za faktor tri pod eksperimentalno vrednostjo.

Zgoraj predstavljeni model magnetne anizotropije se torej izkaže za neprimernega v sistemu $PbNi_2V_2O_8$. To je moč pričakovati, saj temelji na simetriji osnovne celice in ne na dejanski lokalni simetriji kristalnega polja, ki ga čuti posamezni Ni^{2+} magnetni moment. Le-to je dominantno določeno s postavitvijo šestih najbližjih okoliških kisikovih ionov, kot to prikazuje slika 3.4 za primer spojine $PbNi_{1.88}Mg_{0.12}V_2O_8$, ki se po svoji kristalni strukturi naj ne bi bistveno razlikovala od starševske spojine [45]. Ker je distorzija lokalne postavitve kisikovih ionov od kubične postavitve daleč od tetragonalne simetrije, je pričakovati, da lasna os, pripadajoča dominantni lastni vrednosti tenzorja anizotropije na posameznem ionu, ne bo kazala v smeri kristalne osi *c* in da bodo vse tri lastne vrednosti bistveno različne.

V splošnem obstaja več pristopov, kako določiti tenzor anizotopije na posameznem ionu v primeru distorziranega polja ligandov [46]. Vendar pa je edina dostopna metoda kristalnega polja, ki obravnava interakcije med magnetnim ionov in njegovimi ligandi s stališča elektrostatskih interakcij v približku točkastih nabojev [47]. Kot taka, je direktno uporabna le v primeru redkih zemelj, za katere je značilno, da so njihove valenčne orbitale locirane bliže jedra

in se zato ponavadi znatno ne prekrivajo z orbitalami ligandov. V primeru Ni^{2+} ionov v spojini $PbNi_2V_2O_8$ je prekrivanje valenčnih *p* orbital z okoliškimi kisikovimi orbitalami znatno zaradi relativno majhnih razdalj, velikosti 2 Å. Ta kovalenčni efekt onemogoča uporabo metode kristalnega polja in s tem natančnejšo določitev parametrov hamiltonke anizotropije za posamezen ion

$$H_{cf} = D_{cf} S_z^2 + E_{cf}\left(S_x^2 - S_y^2\right). \tag{5}$$

Na podlagi ne(simetrije) NiO_6 oktaedrov je mogoče napovedati le, da sta parametra D_{cf} in E_{cf} istega reda velikosti.

Nadalje je distorzija NiO_6 oktaedrov lahko vzrok tudi antisimetrični anizotropni izmenjalni interakciji med dvema spinoma, imenovani interakcija Dzyaloshinsky-Moriya (DM) [48, 49], ki je oblike

$$\mathbf{D}_{ij} \cdot \mathbf{S}_i \times \mathbf{S}_j . \tag{6}$$

Gre za interakcijo, ki je posledica prvega reda perturbacije v spinsko-orbitalni sklopitvi, njena velikost pa je omejena tudi s simetrijskimi argumenti [49]. Za primer spojine $PbNi_2V_2O_8$ je te vrste anizotropna interakcija med najbližjimi sosedi oblike $\mathbf{D}_{ij} = D\left(\mathbf{n}^i_{O(2)} \times \mathbf{n}^j_{O(2)} + \mathbf{n}^i_{O(3)} \times \mathbf{n}^j_{O(3)}\right)$, kjer so ustrezni vektorji definirani na sliki 3.4 in je parameter $D \approx \Delta g / g \cdot J$. Velikost interakcije je tako reda $D_{ij} \approx 0.15 \Delta g / g \cdot J \approx k_B \cdot 1.5\,\mathrm{K}$, kar je primerljivo z oceno anizotropije za posamezni ion D_{cf}. Tako sta verjetno obe interakciji odgovorni za eksperimentalno širino resonančnih spektrov ESR. Natančnejša analiza pa bo mogoča šele, ko bo moč izvajati eksperimente tudi na kristalnih vzorcih.

Nadaljnji vpogled v sistem elektronskih spinov omogočajo meritve jedrske magnetne resonance na jedrih, ki so le rahlo sklopljeni s paramagnetnimi Ni^{2+} momenti. V ta namen smo si izbrali jedra ^{51}V s spinom $I = 7/2$ [50], ki se v kristalni strukturi nahajajo med nikljevimi verigami in v obliki VO_4 tetraedrov le-te povezujejo, kot kaže slika 3.1a. Spektri posneti v resonančnem polju $B_0 = 6.34\,\mathrm{T}$ in temperaturno spreminjanje položaja njihovega centra so prikazani na sliki 3.6. Slednji parameter nedvoumno priča, da sta sistema nikljevih paramagnetnih spinov in vanadijevih jedrskih spinov sklopljena. Temperaturna odvisnost premika resonančne črte, ki izvira iz statične komponente lokalnega magnetnega polja na mestu določenega jedra, od vrednosti $\nu_L^{dia} = 70.974\,\mathrm{MHz}$, pričakovane za povsem diamagnetne V^{5+} ione, namreč zadovoljivo sledi magnetni susceptibilnosti tega vzorca. Ker gre za meritev na praškastem vzorcu, neničelne premike povzroča le del efektivne prenesene hiperfine interakcije

$$\widetilde{H}_i^{hf} = \mathbf{I}_i \cdot \sum_j \underline{\widetilde{\mathbf{A}}}_{i,j} \cdot \mathbf{S}_j , \tag{7}$$

ki je povezan z redistribucijo elektronske gostote v vanadijevim orbitalah *s*, kot posledica delne kovalence, to je prekrivanja nikljevih valenčnih orbital s kisikovimi in nadaljnjega prekrivanja

le-teh z vanadijevimi. Iz premika ^{51}V resonančne črte $\Delta\nu = 300\,\mathrm{kHz}$ in vrednosti molarne susceptibilnosti $\chi_{mol} = 2N_A g\mu_B \langle S_j \rangle / B_0 = 5.6\cdot 10^{-3}$ emu/mol pri sobni temperaturi, je potem moč oceniti velikost tega izotropnega prispevka k hiperfini interakciji na mestu vanadija

$$\tilde{A}_{i,j}^{iso} = \frac{h\Delta\nu 2N_A g\mu_B}{6\chi_{mol} B_0} \approx k_B \cdot 0.17\,\mathrm{mK}\,. \tag{8}$$

Kot rečeno, ta prispevek izvira iz redistribucije elektronske gostote v sicer zapolnjeni vanadijevi lupini 3*s*, ki je posledica interakcije s povprečnimi nikljevimi magnetnimi momenti, zato jo velja primerjati z velikostjo interakcije v primeru, ko je elektron v tej orbitali nesparjen [51],

$$A_{3s}^{iso} = \frac{\mu_0}{4\pi} g\mu_B \gamma\hbar \frac{8\pi}{3} |\psi(0)|_{3s}^2 = k_b \cdot 0.4\,\mathrm{K}\,, \tag{9}$$

kjer $|\psi(0)|_{3s}^2 = 601\,\text{Å}^{-3}$ ponazarja gostoto tega elektrona na mestu jedra za primer V^{5+} ionov [52]. Preprosta primerjava izrazov (8) in (9) govori o tem, da je delež nesparjenosti elektrona na mestu vanadija, ki je posledica interakcije z nikljevimi valenčnimi elektroni preko kovalenčnega efekta, enak $w \approx 2.5\cdot 10^{-3}$. Ta delež je znaten in upravičuje relativno veliko izmenjalno interakcijo med nikljevimi spini na sosednjih verigah, pri čemer pot izmenjalne interakcije poteka preko vanadijevih ionov. Podobnega efekta nikljevih elektronov na redistribucijo vanadijevih elektronov v orbitalah tipa *p* s stališča premika resonančne črte v praškastih vzorcih ni moč opaziti, saj se ta premik v povprečju izniči [53]. Lahko pa se anizotropni del hiperfine interakcije (7) odraža v obliki in širini absorpcijskih spektrov NMR.

Spektri NMR, posneti v celotnem temperaturnem območju med 300 K in 4.2 K, imajo karakteristično obliko kvadrupolnega spektra (glej sliko 3.7a), kjer so poleg centralnega prehoda $-1/2 \leftrightarrow 1/2$ prisotni še satelitski prehodi, simetrično premaknjeni od centralne črte za [54]

$$\nu_m^{(1)} = \frac{E_{m-1} - E_m}{h} = -\nu_Q \left(m - \frac{1}{2} \right) \left(3\cos^2\theta - 1 + \eta\left(1 - \cos^2\theta\right)\cos 2\phi \right). \tag{10}$$

Parameter $\nu_Q = 3e^2 qQ / 4I(2I-1)h$ ponazarja kvadrupolno frekvenco, kota θ in ϕ pa zapored polarni in azimutni kot smeri zunanjega magnetnega polja v lastnem sistemu tenzorja gradienta električnega polja. Zaradi praškaste narave vzorca je položaj satelitskih prehodov izpovprečen glede na ta dva kota, iz položajev vrhov pa je moč oceniti velikost kvadrupolne frekvence na $\nu_Q \approx 85\,\mathrm{kHz}$. Same razširitve centralne črte ($-1/2 \leftrightarrow 1/2$) na polovični višini $\delta\nu_0 = 60\,\mathrm{kHz}$ ni moč pripisati kvadrupolni interakciji, ki ta prehod razširi šele v drugem redu perturbacije [55] in povzroča širine reda velikosti $5\nu_Q^2/\nu_L \approx 1\,\mathrm{kHz}$. Nasprotno, naraščanje širine črte z naraščajočim resonančnim poljem (glej sliko 3.7b) priča o magnetnem izvoru te razširitve. Le-ta je lahko posledica že zgoraj omenjenega anizotropnega dela efektivne hiperfine interakcije, ali pa anizotropije kemijskega premika lokalnega polja $\mathbf{B}_i = \mathbf{B}_0(1 - \underline{\boldsymbol{\sigma}}_i)$. Slednji je namreč v primeru ionov V^{5+} tipično velikosti nekaj sto ppm in je negativen [56, 57], kar ustreza eksperimentu.

Nadaljnji problem, povezan z enodimenzionalnim Haldaneovim sistemom $PbNi_2V_2O_8$, predstavlja razumevanje vzpostavitve reda dolgega dosega pri nizkih temperaturah v primeru, ko nikljeve ione delno zamenjamo z nečistočami. Že Uchiyama *et al*. so s pomočjo meritev magnetne susceptibilnosti pokazali, da delna zamenjava magnetnih ionov Ni^{2+} z nemagnetnimi ioni Mg^{2+} vodi do magnetnega urejanja pod ~3.5 K [20]. To so naknadno potrdile še termodinamske meritve specifične toplote, s pomočjo katerih so natančno določili potek temperature prehoda v urejeno fazo v odvisnosti od koncentracije dopiranja [58]. Kritična koncentracija za vzpostavitev reda dolgega dosega naj bi bila enaka nič oziroma zelo blizu tej vrednosti. Zamenjava Mg^{2+} ionov za prav tako nemagnetne ione Zn^{2+} bistveno ne vpliva na magnetno urejanje [59], kar priča o tem, da same nečistoče niso direktno vključene v formiranje magnetnega reda. Nasprotno pa nečistoče s spinov znatno spremenijo temperaturo prehoda v urejeno fazo. Tako recimo dopiranje z ioni Cu^{2+} ($S = 1/2$) naj ne bi vodilo do urejanja nad 2 K pri majhnih koncentracijah [59], medtem ko kobaltovi ioni Co^{2+} ($S = 3/2$) zvišajo temperaturo faznega prehoda, ki v primeru spojine $PbNi_{1.92}Co_{0.08}V_2O_8$ znaša 7.2 K [60].

Razvoj tridimenzionalnih spinskih korelacij v okolici prehoda v magnetno urejeno fazo v primeru družine z magnezijem dopiranih spojin smo preučevali z elektronsko spinsko resonanco [40]. Preučevane materiale lahko okarakteriziramo kot zamrznjene raztopine ("solid solutions"), saj je položaj zamenjave nikljevih ionov z nečistočami povsem naključen [45, 61]. Primerjava parametrov ESR na slikah 3.8 in 3.9 nazorno kaže, da je obnašanje signala v dopiranih vzorcih precej drugačno od starševskega vzorca. Spektri pri sobni temperaturi so si dokaj podobni z izjemo rahlega širjenja resonančnih spektrov v odvisnosti od koncentracije dopiranja (glej sliko 3.12), pri nizkih temperaturah, to je pod karakteristično temperaturo spinske energijske reže, pa so razlike veliko bolj izrazite. Nizkotemperaturno komponento spektrov lahko pripišemo spinskim prostostnim stopnjam $S = 1/2$, induciranim kot posledica pretrganih Haldaneovih vezi poleg nečistoč [19], saj tako širina resonančnih spektrov pri najnižjih temperaturah, premik *g*-faktorja, kot tudi intenziteta nizkotemperaturnega signala sledijo stopnji dopiranja. Temperaturno odvisnost zadnjega izmed parametrov je na primer moč opisati v luči kooperativnega tridimenzionalnega urejanja spinov, ki ga popisuje Curie-Weissov zakon $I_{ESR} = C/(T - T_N)$ (slika 3.9b in tabela 1).

Tabela 1: Parametri prilagajanja modela $I_{ESR} = C/(T - T_N)$ z nizkotemperaturnimi meritvami ESR na spojinah $PbNi_{2-x}Mg_xV_2O_8$. Konstanti *C* in *C*/*x* imata poljubni enoti.

x	0.04	0.08	0.10	0.12	0.15	0.24
T_N	2.5 K	3.0 K	3.3 K	3.4 K	3.5 K	3.4 K
C	4.7	9.0	13.5	15.2	18.9	27.4
C/x	118	113	135	127	126	114

Širine nizkotemperaturnih signalov ESR v dopiranih spojinah $PbNi_2V_2O_8$ so precej večje kot v primeru Haldaneovega sistema NENP, dopiranega z nemagnetnimi nečistočami [62, 63], in primerljive s širinami v magnetno dopiranih vzorcih NENP [19]. Ker sta širini signalov, posnetih pri sobni temperaturi v območju X $\delta B_{pp}^{X} = 0.429(5)\,\mathrm{T}$ in v visokem polju pri 10-krat višji frekvenci $\delta B_{pp}^{HF} = 0.445(5)\,\mathrm{T}$, praktično enaki (slika 3.10), lahko anizotropijo *g*-faktorja [62] izločimo kot možnega kandidata za razlago nepričakovano širokih spektrov v sistemu $PbNi_2V_2O_8$. Inducirani spini $S = 1/2$ poleg nečistoč morajo biti zato med seboj sklopljeni. Magnetna anizotropija je v primeru feromagnetno sklopljenega para spinov oblike [64]

$$D^{*} = -3\frac{\mu_0}{4\pi}\frac{(g\mu_B)^2}{r^3} - \frac{3d}{2}, \tag{11}$$

kjer je prvi člen posledica dipolarne interakcije med spinoma, drugi pa simetrične anizotropne izmenjalne interakcije, ki je reda velikosti $d = (\Delta g/g)^2 \tilde{J}'$. Iz znane kristalne strukture je moč oceniti velikost dipolarnega polja $B^d = 45\,\mathrm{mT}$ in velikost prispevka simetrične anizotropne izmenjalne interakcije $3d/2g\mu_B \approx 90\,\mathrm{mT}$, ki pa oba skupaj še zdaleč ne dosegata eksperimentalne širine. Le-ta v primeru največje stopnje dopiranja doseže pri temperaturi 5 K vrednost 515 mT. Pri oceni zadnjega prispevka je bila uporabljena velikost sklopitve med drugimi najbližjimi sosedi v čisti verigi *J'*, ki pa v primeru pretrganih verig ob nečistočah verjetno ne daje prave slike. Inducirana spina $S = 1/2$ ob določeni nečistoči namreč povezuje drug vezni mehanizem, ki ne izvira iz prekrivanja nikljevih in kisikovih orbital med sosedi v verigi [17, 39]. Vsak "osvobojen" spin namreč na sosednji verigi inducira otoček alternirajoče urejenih spinov ("staggered magnetization"), ki efektivno sklaplja oba izmed spinov od neki nečistoči, kot to prikazuje slika 3.11.

Feromagnetna sklopitev med induciranimi spini $S = 1/2$ je sicer v nasprotju z napovedjo, ki so jo na podlagi paramagnetne in antiferomagnetne resonance naredili Smirnov *et al*. [65], vendar pa so nedvoumno potrditev naše hipoteze [40] dale nedavne meritve specifične toplote. Le-te so pokazale, da nečistoče Mg^{2+} efektivno inducirajo prostostne stopnje $S = 1$, torej feromagnetno sklopljene pare spinov $S = 1/2$ [66]. Takšna sklopitev pa sama po sebi še ne pojasnjuje linearne odvisnosti širine spektrov ESR od stopnje dopiranja pri temperaturi 5 K, kot to prikazuje insert v sliki 3.8a, saj sama temperatura urejanja kot parameter velikosti sklopitve med spini ne kaže podobnega monotonega obnašanja. Linearno širjenje kot posledica nečistoč je bilo v literaturi že obravnavano [67]. Pripišemo ga lahko delokalizirani naravi spinov, induciranih ob nečistočah, zaradi česar posamezni spini interagirajo med sabo. Poleg feromagnetne interakcije znotraj posameznega para spinov $S = 1/2$, sklopljenega v spin $S = 1$, je tako pomembna tudi interakcija med temi efektivnimi spini.

Za razliko od dopiranja z nemagnetnimi ioni magnezija pa dopiranje z magnetnim kobaltom bistveno vpliva na absorpcijske spektre ESR že pri sobni temperaturi, kot to prikazuje

slika 3.12. Vzrok temu lahko iščemo v dejstvu, da so ioni Co^{2+} znani po svoji hitri spinsko-mrežni relaksaciji zaradi močne spinsko-mrežne sklopitve [68, 69]. Mehanizem spinske relaksacije na Ni^{2+} mestih poteka preko izmenjalne sklopitve J^* z ioni Co^{2+} in sklopitve le-teh z mrežo ter povzroča razširitev resonančnih črt ESR oblike [68]

$$\delta B = \delta B_0 + \frac{\eta}{1-\eta}\delta B_{imp}\,, \tag{12}$$

kjer δB_0 in δB_{imp} zapored označujeta širino v čistem sistemu in inducirano razširitev kot posledico nečistoč. Parameter η predstavlja razmerje med stopnjo relaksacije ionov nečistoč in stopnjo prenosa magnetne energije iz sistema nikljenih na sistem kabaltovih ionov. Ker je spinsko-mrežna relaksacija močno temperaturno odvisna [70],

$$\frac{1}{T_1} = a\left(\frac{T}{\theta_D}\right)^7 \int_0^{\theta_D/T} \frac{x^6\, \mathrm{e}^x \mathrm{d}x}{\left(e^x-1\right)^2}\,, \tag{13}$$

je pričakovati tako imenovano "bottleneck" obnašanje spreminjanja odstopanja širine črt ESR v dopiranih vzorcih od nedopiranjega vzorca, kot to nazorno kaže slika 3.13 za primer spojine $PbNi_{1.98}Co_{0.02}V_2O_8$. V izrazu (13) θ_D predstavlja Debyejevo temperaturo, neznani parameter a pa lahko na podlagi eksperimenta fiksiramo z relacijo $\eta(T) = T_1(55\,\mathrm{K})/T_1(T)$. Prilagajanje tega modela meritvam (glej insert k sliki 3.13) narekuje Debyejevo temperaturo $\theta_D = 500(50)\,\mathrm{K}$ in velikost razširitve črt ESR zaradi nečistoč $\delta B_{imp} = 120\,\mathrm{mT}$. Zadnji parameter določa velikost izmenjalne sklopitve med nikljevimi in kobaltovimi ioni $J^* = k_B \cdot 11\,\mathrm{K}$ preko relacije [69]

$$\delta B_{imp} \approx \frac{1}{\sqrt{3}}\frac{32}{g\mu_B}\frac{\left(J^*\right)^2 S^*\left(S^*+1\right)}{3\hbar\omega_e}\frac{x}{2}\,, \tag{14}$$

kjer S^* predstavlja velikost kobaltovih spinov in $\omega_e = \sqrt{2J^2 Z' S(S+1)/3\hbar^2}$ izmenjalno frekvenco znotraj sistema nikljevih spinov. Ta enačba napoveduje linearno odvisnost razširitve spektrov ESR od stopnje dopiranja z ioni Co^{2+}, kar je evidentno izraženo na sliki 3.12. Vnos nečistoč Co^{2+} v spinski sistem $PbNi_2V_2O_8$ tako nudi informacijo o fononskih nihanjih tega sistema preko parametra Debyejeve temperature. Žal pa trenutno še ni objavljena nobena druga eksperimentalna meritev, ki bi lahko služila kot referenca oceni tega parametra.

Direktna primerjava razvoja spinskih korelacij pri temperaturah reda velikosti energijske reže in obnašanje le-teh v okolici temperature magnetnega urejanja za obe vrsti dopiranj ni mogoča na podlagi meritev ESR, saj so v primeru dopantov s spinov eksperimentalni spektri preširoki. Po drugi strani pa nam to primerjavo nudijo meritve NMR na jedrih ^{51}V, kjer vanadijeva jedra služijo kot sonde, šibko sklopljene s sistemom nikljevih paramagnetnih momentov. Primerjava spektrov NMR v dopiranih vzorcih s starševsko spojino (glej sliki 3.6a in 3.14) pričakovano pokaže znatne razlike pri nižjih temperaturah, presenetljivo pa razkrije tudi odvisnost spektrov od narave dopanta. Tako je nizkotemperaturna razširitev spektrov v

dopiranih vzorcih precej bolj izrazita pri dopiranju z ioni Mg^{2+}, različna pa je tudi sama oblika resonančnih črt. Le-te so v primeru magnezija asimetrične, v primeru kobalta pa simetrične. Primerjava temperaturne odvisnosti prvega in drugega momenta resonančnih spektrov, to je njihovega položaja in širine, je za obe vrsti dopiranja prikazana na sliki 3.15. Očitna je razlika tako prvega momenta, ki je odraz statične komponente lokalnih magnetnih polj, kot tudi drugega momenta, ki predstavlja fluktuacije teh polj pri Larmorjevi frekvenci. Kljub temu da v primeru obeh vrst dopiranja spojine kažejo antiferomagnetno urejanje pri nizkih temperaturah, pa je razvoj spinskih korelacij v bližini magnetnega prehoda povsem drugačen, vsaj kar se tiče eksperimentalnega magnetnega polja 6.34 T. To opažanje je v skladu z nedavno ugotovitvijo, da vzorci dopirani z magnezijem kažejo metamagnetizem [61, 66]. V relativno majhnih magnetnih poljih se namreč antiferomagnetno urejeno osnovno stanje podre na račun feromagnetnega urejanja spinov [71]. Eksperimentalni spektri tako implicirajo, da pri nizkih temperaturah v vzorcih z nečistočami Mg^{2+} prevladujejo feromagnetne spinske korelacije, samo asimetrično obliko pa lahko pripišemo efektivni hiperfini interakciji tipa *p*. Po drugi strani v primeru kobalta kot dopanta dominanco ohranijo antiferomagnetne fluktuacije, v kar nas dodatno prepričajo meritve spinsko-mrežnega relaksacijskega časa, ki pri temperaturi 7 K v primeru spojine $PbNi_{1.92}Co_{0.08}V_2O_8$ kaže očitne indikacije magnetnega prehoda (glej sliko 3.17). Iz simetrične oblike spektrov lahko sklepamo, da pri takšni antiferomagnetni konfiguraciji spinov postane dominantna izotropna efektivna hiperfina interakcija tipa *s*, dvogrbo strukturo v urejeni fazi pa lahko pripišemo efektu statičnih dipolarnih polj urejenih spinov.

Spojina $SrNi_2V_2O_8$ naj bi za razliko od njej izomorfne spojine $PbNi_2V_2O_8$ na Sakai-Takahashijevem faznem diagramu ležala v področju z magnetno urejenim osnovnim stanjem (glej sliko 1.4). Ta ugotovitev je plod neelastičnega nevtronskega sipanja [38], vendar pa je nekoliko kontradiktorna. Že njeni avtorji so priznali, da pod temperaturo 7 K, kjer naj bi prišlo do magnetnega urejanja, niso v eksperimentih rentgenskega sipanja opazili nobenih dodatnih Braggovih vrhov, kar so upravičili s predpostavko, da so velikosti urejenih magnetnih momentov zelo majhne. Po drugi strani pa zaradi same eksperimentalne nenatančnosti v primeru nevtronskega sipanja niso izključili možnosti prisotnosti manjše, a končne energijske reže. Da bi razjasnili ta nesoglasja smo sami opravili eksperimente ESR in NMR na jedrih ^{51}V v tej spojini, katerih rezultati so prikazani na sliki 3.18. Primerjala spektrov ESR kaže, da med obema izomorfnima sistemoma ni bistvenih razlik. Sicer opazna razlika v širini spektrov se s temperaturo zmanjšuje, v okolici temperature domnevnega magnetnega prehoda pa ni zaznati nobenih sprememb. Nedvoumno podobnost med sistemoma, to je obstoj energijske reže tudi v spojini $SrNi_2V_2O_8$ pa da primerjava parametrov NMR. Tako prvi moment resonančne črte kot spinsko-mrežna relaksacija namreč kažeta na aktivacijsko obnašanje pri nizkih temperaturah. Odsotnost kakršnihkoli anomalij pri temperaturi 7 K tako implicira, da vsaj v primeru resonančnega polja 6.34 T v sistemu $SrNi_2V_2O_8$ ne prihaja do magnetnega urejanja.

3 Magnetizem v 2D sistemu ortogonalnih dimerov $SrCu_2(BO_3)_2$

Spojina $SrCu_2(BO_3)_2$ je bila prvič sintetizirana že v začetku 90ih let prejšnjega stoletja [72], vendar pa je pravo revolucijo v smislu njene prepoznavnosti povzročil šele članek Kageyame *et al*. [24]. Spojina je požela veliko zanimanje tako eksperimentalne kot tudi teoretične raziskovalne sfere, kar gre v pretežni meri pripisati relativno enostavni osnovni hamiltonki sistema in uspešni sintezi precej velikih kristalnih vzorcev zadovoljive kvalitete [73]. Osnovna celica te spojine je prikazana na sliki 4.1 in kaže tipično planarno strukturo, kjer si ravnine $CuBO_3$, razmaknjene z Sr^{2+} ioni, sledijo vzdolž kristalne osi *c*. Bakrovi ioni Cu^{2+}, ki imajo edini v strukturi magnetni moment ($S = 1/2$), tvorijo dvodimenzionalno mrežo ortogonalnih dimerov, prikazano na sliki 1.3. Izmenjalna sklopitev znotraj dimerov je antiferomagnetna $J = k_B \cdot 85\,\mathrm{K}$. Sklopitev s štirimi drugimi najbližjimi sosedi $J' = 0.63J$ je tudi znatna, medtem ko je sklopitev med ravninami $J_{\|} = 0.09J$ precej manjša, kar upravičuje dvodimenzionalno naravo tega spinskega sistema. Ta nabor konstant izmenjalne interakcije najbolje popiše temperaturni potek magnetne susceptibilnosti vzorca [74], predlaganih pa je bilo tudi nekaj nekoliko, a ne bistveno različnih naborov [75, 76]. Spinski sistem $SrCu_2(BO_3)_2$ je bil kmalu prepoznan kot prva realizacija teoretičnega modela Shastry-Sutherlanda [24]. Topološka ekvivalentnost omenjenih kristalnih mrež je prikazana na sliki 1.3. Posebnost modelske hamiltonke

$$H = J\sum_{(i,j)} \mathbf{S}_i \cdot \mathbf{S}_j + J'\sum_{\{l,m\}} \mathbf{S}_l \cdot \mathbf{S}_m \tag{15}$$

je eksaktno rešljivo osnovno stanje do kritičnega razmerja izmenjalnih konstant $\left(J'/J\right)_c = 0.68$ [77]. To je preprost produkt singletnih spinskih funkcij na posameznih dimerih, ki ostane osnovno stanje tudi v primeru končne sklopitve med ravninami [78].

Znotraj modela ortogonalnih dimerov ("orthogonal dimer model") je najnižje vzbujeno stanje preprosta tripletna ekscitacija na enem od dimerov, ki je bila prvič eksperimentalno opažena z meritvami ESR v visokih poljih [79] in nato potrjena z različnimi eksperimentalnimi tehnikami [80, 81, 82]. Čeprav je model ortogonalnih dimerov ustrezen za marsikatero magnetno lastnost sistema $SrCu_2(BO_3)_2$, med drugim upraviči tudi prisotnost platojev v magnetizacijski krivulji [24, 83, 84], pa ne pojasni nekaterih manjših detajlov, kot je recimo fina struktura najnižje tripletne ekscitacije [79, 80]. Kot rešitev te uganke so Cépas *et al.* predlagali magnetno anizotropijo tipa Dzyaloshinsky-Moriya [85]

$$H = \sum_{\{l,m\}} \pm D'_{\|}\mathbf{e}_c \cdot \mathbf{S}_l \times \mathbf{S}_m \,. \tag{16}$$

Takšna oblika antisimetrične spinske interakcije le med drugimi najbližjimi sosedi sledi ob aproksimaciji $CuBO_3$ struktur s planarnimi ravninami, ko center inverzije na sredini vsakega dimera prepoveduje intradimerno interakcijo DM, interdimerni vektorji $D'_{\|} = k_B \cdot 2.1\,\mathrm{K}$ pa so

tudi zaradi simetrijskih razlogov usmerjeni pravokotno na te ravnine. Vendar pa množica nedavnih eksperimentov priča, da takšna aproksimacija ni upravičena. Tako na primer nenavadni premiki črt NMR na jedrih ^{11}B pri nizkih temperaturah in znatna alternirajoča magnetizacija ("staggered magnetization") [86, 87], relativne intenzitete prehodov med osnovnim in najnižjimi vzbujenimi stanji [88], kot tudi temperaturna odvisnost specifične toplote pri nizkih temperaturah v visokih magnetnih poljih [89] vsi implicirajo na znatno intradimerno interakcijo Dzyaloshinsky-Moriya. Le-ta je ob upoštevanju gubanja ("buckling") $CuBO_3$ ravnin [90] simetrijsko dovoljena v primeru, da vektorji DM ležijo v kristalni ravnini *ab*. Kljub temu da takšna interakcija meša tripletna stanja k singletnemu v osnovnem stanju sistema in s tem v osnovi omogoča magnetne dipolne prehode med osnovnim in vzbujenimi stanji, pa povsem ne pojasni eksperimentalno detektiranih spektrov ESR v visokih magnetnih poljih [85, 91]. Zato je bila pri nizkih temperaturah upoštevana tudi prisotnost simetrijsko prepovedane intradimerne komponente, vzporedne s kristalno osjo *c* [89, 91], ki pa bi zahtevala strukturni fazni prehod. Alternativno so Cépas *et al*. predlagali, da bi v sistemu $SrCu_2(BO_3)_2$ lahko bil pomemben dinamični mehanizem zloma lokalne simetrije [92, 93]. V dinamični sliki fononi zlomijo lokalno simetrijo in tako omogočijo dinamične komponente interakcije Dzyaloshinsky-Moriya, ki so v statičnem modelu zaradi simetrijskih razlogov lahko prepovedane.

Vendar pa trdnega dokaza o pomembnosti dinamičnih komponent interakcije DM v sistemu $SrCu_2(BO_3)_2$ še vedno ni. Ker je elektronska spinska resonanca občutljiva na magnetno anizotropijo te vrste smo izvedli serijo meritev v področju X tako na praškastih vzorcih [94], kot tudi na kristalnem vzorcu [95, 96]. Slednji eksperimenti zaradi možnosti opazovanja kotne odvisnosti magnetne anizotropije preko razvoja širine resonančnih spektrov pri različnih orientacijam zunanjega magnetnega polja glede na kristalne osi ponujajo tudi možnost razlikovanja in ovrednotenja posameznih prispevkov k magnetni anizotropiji sistema.

Intenziteta spektrov ESR, posnetih na praškastem vzorcu med sobno temperaturo in 5 K, kaže aktivacijsko obnašanje (glej sliko 4.2), kar je v skladu z energijsko režo. Spektri so Lorentzove oblike (enačba (1)) tako na praškastih kot tudi na kristalnem vzorcu, kot to nazorno prikazujeta sliki 4.2a in 4.3a. Natančnejšo določitev odstopanja eksperimentalnih spektrov od te oblike omogoča standardna primerjava spremenljivke $Y = \left(-2\left(B - B_0\right)I_{max}/\delta B_{pp} I\left(B\right)\right)^{1/2}$ v odvisnosti od $X = \left(2\left(B - B_0\right)/\delta B_{pp}\right)^2$, prikazana na sliki 4.3b, kjer $I(B)$ označuje intenziteto signala in I_{max} njen maksimum. Opažena linearna odvisnost potrdi domnevo o Lorentzovi obliki spektrov in izloči možnost večjega vpliva spinske difuzije na absorpcijske spektre ESR [97].

Širine eksperimentalnih spektrov so podobno kot v primeru enodimenzionalne spojine $PbNi_2V_2O_8$ precejšnje, kar priča o znatni magnetni anizotropiji v sistemu. Temperaturni potek tega parametra, prikazan na sliki 4.6, govori o dveh različnih območjih obnašanja med 5 K in 600 K, saj kaže širina minimum okoli sobne temperature tako v praškastih vzorcih kot tudi pri različnih orientacijah zunanjega magnetnega polja v kristalnem vzorcu. Visokotemperaturni

linearni porast širine z naraščajočo temperaturo je posledica sklopitve spinskega sistema z mrežnimi nihanji, kot bo pokazano v nadaljevanju. Ker torej ne gre za intrinzično širino, ki bi sledila iz samega spinskega sistema, bomo ta prispevek v nadaljevanju pri interpretaciji eksperimentalnih rezultatov s spinsko hamiltonko preprosto odšteli. Izmerjena širina spektrov med obema vrhovoma, ki v minimumu za praškaste vzorce znaša $\delta B_{pp}^{p} = 78(1)\,\mathrm{mT}$, za kristalni pa $\delta B_{pp}^{\parallel} = 91(1)\,\mathrm{mT}$ in $\delta B_{pp}^{\perp} = 69(1)\,\mathrm{mT}$ v primeru magnetnega polja vzdolž in pravokotno na kristalno os *c*, ni mogoče pojasniti ne z magnetno dipolarno interakcijo med spini niti z hiperfino interakcijo na mestih Cu^{2+}, ampak je zanjo odgovorna anizotropija izmenjalne interakcije [94, 96]. Simetrični del te interakcije, ki je velikosti $d + e \sim (\Delta g/g)^2 \cdot J \approx k_B \cdot 1\,\mathrm{K}$, v skladu z enačbama (2) in (3) napoveduje širine reda velikosti $\delta B_{pp}^{ae} \approx 3\,\mathrm{mT}$, antisimetrični del $D'_{\parallel} = k_B \cdot 2.1\,\mathrm{K}$ pa velikosti $\delta B_{pp}^{ae} \approx 46\,\mathrm{mT}$. Tako je le antisimentrična interakcija Dzyaloshinsky-Moriya zmožna upravičiti eksperimentalne širine absorpcijskih spektrov ESR.

V limiti neskončne temperature ta interakcija vodi do anizotropije širine spektrov, ki jo določata drugi in četrti moment. V laboratorijskem sistemu z osjo *z* vzdolž zunanjega magnetnega polja imata momenta obliko [44]

$$\begin{aligned} M_2^{DM} &= \frac{S(S+1)}{N}\frac{1}{3}\sum_{(i,j)}\left(D_{ij}^{x}\right)^2 + \left(D_{ij}^{y}\right)^2 + 2\left(D_{ij}^{z}\right)^2, \\ M_4^{DM} &= \frac{S^2(S+1)^2}{N}\left[\frac{2}{3}\sum_{(ij)} J_{ij}^2\left(\left(D_{ij}^{x}\right)^2 + \left(D_{ij}^{y}\right)^2 + 2\left(D_{ij}^{z}\right)^2\right)\right. \\ &\qquad \left. + \frac{1}{18}\sum_{(ijk)}\sum_{\alpha=x,y,z}\left(\left(F_{ijk}^{\alpha}\right)^2 + \left(F_{ijk}^{z}\right)^2 + \left(F_{jki}^{\alpha}\right)^2 + \left(F_{jki}^{z}\right)^2 + \left(F_{kij}^{\alpha}\right)^2 + \left(F_{kij}^{z}\right)^2\right)\right], \end{aligned} \tag{17}$$

kjer so funkcije $F_{ijk}^{\alpha} = J_{ij}\left(D_{ik}^{\alpha} - D_{jk}^{\alpha}\right) + J_{ik}\left(D_{ij}^{\alpha} + D_{jk}^{\alpha}\right)$. Izračun momentov s komponentami vektorjev DM v kristalnem sistemu je mogoč s transformacijo

$$\begin{aligned} D_{ij}^{x} &= D_{ij}^{a}\cos\theta\cos\varphi + D_{ij}^{b}\cos\theta\sin\varphi - D_{ij}^{c}\sin\theta, \\ D_{ij}^{y} &= -D_{ij}^{a}\sin\varphi + D_{ij}^{b}\cos\varphi, \\ D_{ij}^{x} &= D_{ij}^{a}\sin\theta\cos\varphi + D_{ij}^{b}\sin\theta\sin\varphi + D_{ij}^{c}\cos\theta. \end{aligned} \tag{18}$$

Ob upoštevanju Cépasovega predloga o obliki vzorca vektorjev interakcije DM (enačba (16)), ki ga povzema slika 4.8a, sta oba momenta resonančne črte oblike

$$\begin{aligned} M_2^{DM} &= \frac{D_{\parallel}'^2}{2}\left(1+\cos^2\theta\right), \\ M_4^{DM} &= \frac{3}{4}D_{\parallel}'^2\left(3J^2 + 3J'^2 - 2JJ'\right)\left(1+\cos^2\theta\right), \end{aligned} \tag{19}$$

kar določa kotno odvisnost širine spektrov ESR

$$\delta B_{pp}^{DM} = \frac{C}{g\mu_B}\frac{D_{\parallel}'^2}{\sqrt{6\left(3J^2 + 3J'^2 - 2JJ'\right)}}\left(1+\cos^2\theta\right). \tag{20}$$

Primerjava te napovedi z eksperimentalno anizotropijo širine pri 295 K in 525 K (glej sliko 4.7) nazorno pokaže na neustreznost modela, saj izmerjeno odvisnost od polarnega kota θ zadovoljivo popiše šele odvisnost oblike $\delta B_{pp} = A + B\left(1+\cos^2\theta\right)$ s parametri $A = 47.8(5)\,\mathrm{mT}$, $B = 21.8(5)\,\mathrm{mT}$ pri 295 K in $A = 54.1(5)\,\mathrm{mT}$, $B = 22.0(5)\,\mathrm{mT}$ pri 525 K. Parameter *A*, ki ostane tudi v primeru, ko odštejemo visokotemperaturni linearni prispevek širini, reda velikosti parametra *B*, pričakovanega po napovedi (20), priča o znatni dodatni anizotropiji v sistemu $SrCu_2(BO_3)_2$ poleg predlagane sklopitve DM med drugimi najbližjimi sosedi z vektorji vzporednimi s kristalno osjo *c*, kot to povzema enačba (16). Simetrični del anizotropne izmenjalne interakcije kot drugi največji prispevek k magnetni anizotropiji ne more upravičiti tega odstopanja, saj je za več kot red velikosti premajhen in povzroča kotno odvisnost širine, ki je "napačne" oblike. Lastne smeri tenzorja te interakcije namreč sovpadajo z lastnimi smermi *g*-tenzorja, ki ima tetragonalno simetrijo z osjo anizotropije usmerjeno vzdolž kristalne osi *c*, kot to prikazuje slika 4.4. Posledično je anizotropija širine črte ESR spet oblike $\left(1+\cos^2\theta\right)$ [98], torej ni v skladu z dodatnim konstantnim prispevkom *A*.

Rešitev te dileme ponuja natančnejša obravnava kristalne strukture. Ravnine $CuBO_3$ pod temperaturo strukturnega faznega prehoda $T_s = 395\,\mathrm{K}$ namreč niso planarne, ampak so nagubane, kot to prikazuje slika 4.1a [90]. Posledično je na primer odpravljen center inverzije na sredini vsakega dimera in so neničelne intradimerne komponente vektorjev DM dovoljene. Do natančnega vzorca vektorjev interakcije DM, prikazanega na sliki 4.8b, je moč priti z upoštevanjem simetrijskih operacij prostorske grupe kristala in ustreznimi transformacijami vektorskega polja spinov $\mathbf{S}(\mathbf{r}) \to O[\mathbf{S}(\mathbf{r})] = O\mathbf{S}\left(O^{-1}\mathbf{r}\right)$. Le-te razkrijejo, da so vsi vektorji DM določeni le s štirimi različnimi parametri. Intradimerna komponenta $D_\perp$ leži v kristalni ravnini *ab* in je vedno orientirana pravokotno na smer dimera spinov, ki ga povezuje, interdimerne komponente pa so v splošnem tri, torej poleg tiste vzporedne s smerjo kristalne anizotropije $D'_\parallel$ še komponenti D'_ξ, D'_η znotraj kristalne ravnine *ab*. Ker je moč pričakovati, da je velikost intradimerne komponente večja od velikosti interdimernih D'_ξ, D'_η v ravnini *ab*, slednji najprej zanemarimo. Izračun drugega in četrtega momenta črte ESR določa kotno odvisnost širine

$$\delta B_{pp}^{DM} = \frac{2\pi}{\sqrt{6}}\frac{1}{g\mu_B}\left(\frac{\left(8D_\parallel'^2 + 3D_\perp^2 + \left(8D_\parallel'^2 - D_\perp^2\right)\cos^2\theta\right)^3}{96\left(32D_\parallel'^2 J_1^2 + 3D_\perp^2 J_2^2 + \left(32D_\parallel'^2 J_1^2 - D_\perp^2 J_2^2\right)\cos^2\theta\right)}\right)^{1/2}, \qquad (21)$$

pri čemer sta konstanti $J_1^2 = 3J^2 + 3J'^2 - 2JJ'$ in $J_2^2 = 13J^2 + 6J'^2$. Ujemanje modela in meritev je v tem primeru zadovoljivo, kot je to prikazano na sliki 4.9a, ocenjena parametra interakcije DM pa znašata $D'_\parallel = k_B \cdot 2.4(1)\,\mathrm{K}$ in $D_\perp = k_B \cdot 4.0(1)\,\mathrm{K}$. Interdimerna sklopitev je tako zelo blizu oceni, dobljeni iz razcepa najnižje tripletne ekscitacije v visokih magnetnih poljih $D'_\parallel = k_B \cdot 2.1\,\mathrm{K}$. Pri tem je bila za izotropno izmenjalno interakcijo uporabljena uveljavljena vrednost $J = k_B \cdot 85\,\mathrm{K}$ [74], nedavne eksperimentalne [89, 91] in teoretične ocene

[76] pa napovedujejo tudi do 15% nižje vrednosti, kar bi še dodatno izboljšalo ujemanje našega eksperimenta z znanimi podatki. Nadaljnje upoštevanje komponent interdimerne interakcije v ravnini *ab* bistveno ne spremeni kakovosti ujemanja eksperimenta in teorije (glej sliko 4.9b), uvede pa negotovost v oceni parametra intradimerne sklopitve, saj je le-ta v končnem izrazu za širino sklopljen z na novo vpeljanima komponentama. Če za interdimerno komponento vektorja DM v ravnini *ab* upoštevamo oceno $D'_{\perp} \approx 0.4 D'_{\parallel}$, narejeno v limiti $J' = 0$ [99], je velikost sklopitve DM znotraj vsakega dimera podana z $D_{\perp} = k_B \cdot 3.6(5)\,\mathrm{K}$, kar predstavlja prvo kvantitativno oceno te interakcije pri visokih temperaturah. Naša ocena je primerljiva z nedavnima napovedma velikosti te interakcije pri nizkih temperaturah. Na osnovi meritev specifične toplote v magnetnem polju je bila komponenta v ravnini *ab* intradimerne interakcije DM ocenjena na $D_{\perp} = 3.1\,\mathrm{K}$ [89], meritve NMR na jedrih $^{11}\mathrm{B}$ pa so dale napoved $D_{\perp} = k_B \cdot 2.9(4)\,\mathrm{K}$ [100].

Primerjava izmerjene anizotropije širine spektrov ESR pri 295 K in 525 K vodi do ključnega vprašanja o izvoru detektirane interakcije DM. Sama oblika kotne odvisnosti je namreč nespremenjena pri obeh temperaturah, ki sta zaporedoma daleč pod in daleč nad temperaturo strukturnega faznega prehoda $T_s = 395\,\mathrm{K}$ v tej spojini. V statični sliki bi bilo moč pričakovati bistvene spremembe, saj je v visokotemperaturni fazi dovoljena samo komponenta $D'_{\parallel}$ interakcije DM. Verjetno razlago tega nesoglasja nam ponuja dinamična slika, kjer nihanja kristalne mreže začasno podrejo lokalno simetrijo in omogočajo končne prej simetrijsko prepovedane komponente interakcije DM [92, 93]. Takšen mehanizem vpliva na spektre ESR v primeru, če so v to vpletena mehka optična fononska nihanja ("soft optical modes") s karakterističnimi fononskimi frekvencami pod tipično izmenjalno frekvenco razpada spinskih korelacij v sistemu $\omega_e \approx J/\hbar$. Nadalje morajo biti povprečni kvadrati odmikov ionov od ravnovesnih leg znatni, to je primerljivi s statičnimi odmiki v nizkotemperaturni fazi.

Prisotnost ustreznega optičnega nihajnega načina je bila ugotovljena z eksperimenti ramanskega sipanja [90, 101]. Frekvenca nihanja usteza velikosti izmenjalne frekvence pri 15 K, kar se da razbrati iz energije ramanskega premika 62 cm^{-1} pri tej temperaturi. Z višanjem temperature pa se ta premik znatno zniža in doseže vrednost 18 cm^{-1} nekaj pod temperaturo strukturnega prehoda, ko črta izgine v signalu ozadja (glej sliko 4.10). Omenjeno nihanje ustreza nihanju v fazi skoraj vseh ionov znotraj osnovne celice (razen Sr^{2+}), preferenčno vzdolž kristalne osi *c* in kot tako spominja na statično deformacijo ravnin v nizkotemperaturni fazi. Nadalje so tudi sami odmiki precejšnji, saj znašajo na primer za bakrove ione 0.25Å in 0.33Å za kisikove ione O(1), ki bakrove ione povezujejo, kar je primerljivo s statičnimi odmiki pri temperaturi 100 K. Ker gre dodatno še za nihanje v centru Brillouinove cone, se s stališča meritev ESR povzročene dinamične distorzije bistveno ne razlikujejo od statičnih v nizkotemperaturni fazi. Izvor intradimerne interakcije DM gre tako iskati v kombiniranem efektu obeh mehanizmov, ocenjen parameter pa predstavlja časovno povprečeno vrednost.

Temperaturno odvisnost širine spektrov ESR nad sobno temperaturo lahko, kot je že bilo omenjeno, pripišemo sklopitvi spinskega sistema s fononi. Preostali dve možnosti razlage opaženega linearnega spreminjanja širine črte s temperaturo, to je spinsko difuzijo [97] in vpliv statičnih spinskih korelacij [102], lahko namreč zanemarimo. O nepomembnosti prvega mehanizma govori Lorentzova oblika absorpcijskih spektrov, drugega pa ovrže regularen linearen porast v zelo širokem temperaturnem območju med 3.5*J* in 7*J* (glej sliko 4.11a) in kotno neodvisen naklon tega porasta ($k_{\parallel} = 0.035(1)\,\mathrm{mT/K}$, $k_{\perp} = 0.033(1)\,\mathrm{mT/K}$). Omenjeno razširitev lahko pripišemo efektu končnega življenjskega časa vzbujenih nivojev, ki je posledica modulacije parametrov spinske hamiltonke zaradi mrežnih nihanj. Po mehanizmu predlaganem s strani Seehre *et al*. mrežna nihanja povzročijo fluktuacije interakcije Dzyaloshinsky-Moriya, ki nato inducira prehode med osnovnim in vzbujenimi stanji spinskega sistema [103]. V limiti nesklopljenih dimerov je ta dodatna razširitev črte podana z izrazom

$$\delta B_{pp}^{lin} \approx \frac{8Z}{9\sqrt{3}} \frac{1}{g\mu_B} \frac{(\lambda R)^2 D^2 J^2}{\rho \hbar^3} \left\langle \frac{1}{c_t^5} + \frac{2}{3} \frac{1}{c_l^5} \right\rangle_{\Omega} k_B T \,, \tag{22}$$

kjer $Z = 1$ predstavlja število neodvisnih parov, $\lambda R = 10$, pri čemer je *R* razdalja med spinoma znotraj dimera in $\mathrm{d}J/\mathrm{d}r = -\lambda r$ [104], gostota znaša $\rho = 4.1\,\mathrm{kg/dm^3}$ [105], kompliciran kotno povprečje zvočnih hitrosti pa lahko ocenimo s pomočjo povprečne hitrosti *c* = 4600 m/s [106]. V primeru zgoraj ocenjene intradimerne interakcije DM $D = D_{\perp} = k_B \cdot 3.6\,\mathrm{K}$ enačba (22) napove vrednost naklona grafa širine črte ESR v odvisnosti od temperature, 0.014 mT/K, kar je istega reda velikosti kot povprečen izmerjen naklon 0.034 mT/K. Teoretični in eksperimentalni rezultat se zadovoljivo ujemata, saj sta zgornja aproksimacija s povprečno hitrostjo in neupoštevanje spinskih korelacij med dimeri precej površni oceni.

Kot je bilo že omenjeno v uvodu v to poglavje, drug potencialno zanimiv problem predstavlja dopiranje $SrCu_2(BO_3)_2$ sistema z elektroni oziroma vrzelmi [33, 34] zaradi formalne podobnosti kristalne strukture tega sistema s strukturami visokotemperaturnih superprevodnikov [24]. Po drugi strani lahko vnos nečistoč v sistem tudi bistveno vpliva na spinsko energijsko režo in v splošnem na energije nizkoležečih magnetnih ekscitacij, še posebej ker sistem leži blizu kvantne meje med različnimi osnovnimi stanji [107]. Zaradi teh razlogov smo se sami lotili različnih pristopov dopiranja [108], ki pa so se v pretežni meri končali kot neuspešni. V splošnem so namreč botrovali fazni nehomogenosti vzorcev (glej sliko 4.13).

Potencialno pomembni se zdijo le rezultati dopiranja z metodo raztapljanja alkalnih kovin v tekočem amoniaku [109]. Le te disociirajo na ione kovin in proste elektrone [110], zato lažje prodirajo v določeno kristalno strukturo. Sami smo poizkusili z interkalacijo litijevih ionov v strukturo $SrCu_2(BO_3)_2$, vzporeden vnos elektronov pa naj bi služil za kompenzacijo električnega naboja. Elektroni naj bi po predvidevanjih vplivali predvsem na valenco bakrovih ionov v spojini, na kar je implicirala tudi sprememba barve vzorcev iz začetne modre v temno sivo.

Natančne strukturne analize s pomočjo rentgenskega sipanja (glej sliko 4.14) so pokazale, da sam vnos litijevih ionov, če je do njega sploh prišlo, zaznavno ne spremeni kristalne strukture spojine, manjši premiki ramanskih absorpcijskih črt, pa implicirano na možne rahle spremembe v normalnih nihanjih kristalne mreže. Tudi sam magnetni karakter spojine z interkaliranim litijem ni bistveno spremenjen od starševske spojine. Tako na primer magnetna susceptibilnost še vedno kaže na aktivacijsko obnašanje in nespremenjeno vrednost spinske energijske reže, sama velikost izmerjene susceptibilnosti pa je v dopiranih vzorcih nekoliko manjša (glej sliko 4.15a). Podobno obnašanje je bilo opaženo v primeru dopiranja spojine $SrCu_2(BO_3)_2$ na mestu stroncija z barijem in kalcijev, ki sta oba vodila do zmanjšane vrednosti susceptibilnosti, čeprav je Ca^{2+} lažji in Ba^{2+} težji ion od iona Sr^{2+} [111].

Vendar pa so prisotnost litija v vzorcu nedvomno potrdile meritve NMR. Primerjava intenzitete signala NMR na jedrih ^{7}Li v polju 8.93 T v interkaliranem vzorcu $Li_xSrCu_2(BO_3)_2$ in referenčni raztopini Li_2CO_3 so namreč pokazale, da je molarni delež litija $x = 0.4(1)$, kar je približno za faktor dva pod nominalno določenim stohiometrijskim razmerjem mola litija na mol starševske spojine. Širine izmerjenih spektrov so relativno velike, kot to prikazuje slika 4.16. Še več, tudi temperaturni potek tega parametra in njegova linearna odvisnost od amplitude zunanjega statičnega polja (slika 4.17) implicirata, da je dominantna magnetna anizotropija na mestu ^{7}Li jeder elektronskega izvora. O sklopitvi sistema litijevih jeder s sistemom paramagnetnih elektronov na ionih Cu^{2+} dodatno priča aktivacijsko obnašanje spinsko-mrežne relaksacije, prikazano na sliki 4.18. Sama velikost spinsko-mrežnega relaksacijskega časa in širine resonančnih spektrov služi tudi za oceno povprečne razdalje med litijevimi jedri in bakrovimi ioni $r = 2.7\text{Å}$, torej bi se morala litijeva jedra nahajati znotraj kristalne strukture. Majhni premiki resonančne črte od Larmorjeve frekvence reda velikosti nekaj ppm pričajo, da je litij v spojini v obliki ionov Li^+, saj bi litijevi skupki povzročili znatno večje premike, ki v primeru litijeve kovine znašajo 240 ppm [112]. Po preprostem pričakovanju naj bi elektroni, intenkalirani v starševsko spojino poleg ionov Li^+, vplivali na spremembo valence bakrovih ionov iz Cu^{2+} v Cu^+, ki so nemagnetni. Vendar pa bi uničenje singletnih parov v osnovnem stanju moralo vplivati tudi na velikost spinske energijske reže. Zato ni izključena možnost, da je med reakcijo interkalacije litij reagiral z neznano snovjo iz okolice zaradi nepopolnega tesnjenja eksperimentalne aparature, čeprav bi potem takšne strukture še bistveno težje "neopazno" prodirale v kristalno strukturo spojine $SrCu_2(BO_3)_2$.

4 Zaključne opombe

Predmet raziskave te disertacije je vpliv magnetne anizotropije in dopiranja na magnetizem dveh nedavno sintetiziranih sistemov s spinsko energijsko režo, to je enodimenzionalnega

Haldaneovega sistema $PbNi_2V_2O_8$ in dvodimenzionalnega sistema ortogonalnih dimerov $SrCu_2(BO_3)_2$. V obeh spojinah se očitno izraža kvantna mehanika na makroskopskem nivoju, saj sta pripadajoči osnovni stanji obeh spinskih sistemov singletne narave. Rezultati naših magnetno-resonančnih meritev na sistemu $SrNi_2V_2O_8$, ki je spojini $PbNi_2V_2O_8$ izomorfen, so pokazali podobno sliko o prisotnosti spinske energijske reže, čeprav je prej prevladovalo mnenje, da v tem sistemu prihaja do magnetnega urejanja pri nizkih temperaturah.

Magnetna anizotropija je v sistemih $PbNi_2V_2O_8$ in $SrCu_2(BO_3)_2$ znatna in bistveno vpliva na njune magnetne lastnosti, zato je njeno podrobno poznavanje ključno za razumevanje magnetizma v teh sistemih. S pomočjo magnetno-resonančnih meritev smo uspeli nadgraditi uveljavljeni sliki o dominantnih prispevkih magnetne anizotropije v obeh spojinah. V primeru Haldaneovega sistema $PbNi_2V_2O_8$ je tako prevladovalo prepričanje o anizotropiji na posameznem mestu uniaksialne oblike kot vodilnem členu magnetne anizotropije. Tako naše meritve ESR kot tudi simetrijski argumenti na podlagi natančnejšega poznavanja kristalne strukture pa so pokazali na precej bolj zapleteno strukturo te interakcije in na dodatno nezanemarljivo interakcijo Dzyaloshinsky-Moriya. Slednji prispevek je bil tudi kvantitativno ovrednoten, vendar pa kritičen test predlaganega modela zaenkrat onemogoča praškasta narava razpoložljivih vzorcev.

Po drugi strani pa je ravno kristalna narava vzorcev spojine $SrCu_2(BO_3)_2$ omogočila natančno določitev oblike magnetne anizotropije v tem sistemu. Analiza meritev elektronske spinske resonance je tako pokazala, da so poleg prej predlaganih interdimernih komponent interakcija Dzyaloshinsky-Moriya pomembne tudi intradimerne interakcije, saj je njihova velikost istega reda velikosti. Vzorec vektorjev Dzyaloshinsky-Moriya, ki je bil narejen na podlagi simetrijskih operacij prostorske grupe pripadajoče kristalne strukture, je tako v skladu z meritvami. Nadalje je eksperiment razkril tudi pomen spinsko-mrežne sklopitve na spinsko dinamiko v tem sistemu. Interakcija Dzyaloshinsky-Moriya je namreč tudi dinamičnega izvora, saj sledi iz podrtja lokalne simetrije kot posledica fononskih nihanj.

S stališča drugega izmed zastavljenih vprašanj v tej disertaciji, to je vprašanja vpliva dopiranja z nečistočami na magnetizem obeh spinskih sistemov, sta se preučevana sistema izkazala kot popolni nasprotji. V primeru spojine $PbNi_2V_2O_8$ že zelo majhna koncentracija nečistoč podre spinsko singletno osnovno stanje in povzroči magnetno urejanje pri nizkih temperaturah neglede na spinsko naravo dopantov, kar je v skladu s sliko valenčnih vezi. Sama spinska narava pa bistveno vpliva na razvoj spinskih korelacij v večjih magnetnih poljih velikosti nekaj tesla. Kot kaže namreč ta zadušijo razvoj antiferomagnetnih korelacij v primeru dopiranja z nemagnetnimi ioni Mg^{2+}, ne pa tudi v primeru magnetnih ionov Co^{2+}.

Po drugi strani je dopiranje sistema $SrCu_2(BO_3)_2$ precej težavnejša naloga, saj se zdi, da samo metoda interkalacije ionov alkalijske kovine v kristalno strukturo starševske spojine kaže konkretnejše rezultate. Interkalacija litija bi tako morala povzročiti vnos elektronov v bakrove

ravnine, vendar pa je ta rezultat vprašljiv. Spinska energijska reža se namreč izkaže za zelo odporno proti takšni perturbaciji, kar priča o singletni naravi osnovnega stanja kljub znatni količini interkaliranega litija. Na nek način ta rezultat spominja na primer spinskih lestev, dopiranih z vrzelmi v manjših koncentracijah, kjer se izkažejo podobne tendence o ohranitvi spinske energijske reže. Dopiranje z vrzelmi pa bi moral biti tudi eden izmed najpomembnejših ciljev v nadaljnjem raziskovanju dvodimenzionalnega spinskega sistema $SrCu_2(BO_3)_2$, saj bi lahko vodilo do superprevodnosti. V tem primeru bi se natančno poznavanje spinske hamiltonke tega sistema in njena možna povezanost s superprevodnostjo lahko izkazala kot mejnik v razumevanju tega pojava.

Bibliografija

[1] J. G. Bednorz, K. A. Müller. Possible high-Tc superconductivity in the Ba-La-Cu-O system, *Z. Phys. B* **64**, 189 (1986).

[2] B. Batlogg, V. J. Emery. Crossovers in cuprates, *Nature* **382**, 20 (1996).

[3] T. Shibauchi, L. Krusin-Elbaum, M. Li, M. P. Maley, P. H. Kes. Closing the pseudogap by Zeeman splitting in $Bi_2Sr_2CaCu_2O_{8+y}$ at high magnetic fields, *Phys. Rev. Lett.* **86**, 5763 (2001).

[4] H. A. Bethe. Zur Theorie der Metalle. I. Eigenwerte und Eigenfunktionen der linearen Atomkette, *Z. Phys*. **71**, 205 (1931).

[5] J. Kanamori. Superexchange interaction and symmetry properties of electron orbitals, *J. Phys. Chem. Solids* **10**, 87 (1959).

[6] J. B. Goodenough. Theory of the role of covalence in the perovskite-type manganites [La, *M*(II)]MnO_3, *Phys. Rev*. **100**, 564 (1955).

[7] P. Lemmens, G. Güntherodt, C. Gros. Magnetic light scattering in low-dimensional quantum spin systems, *Phys. Rep*. **375**, 1 (2003).

[8] K. Katsumata. High-frequency electron spin resonance in magnetic systems, *J. Phys.: Condens. Matter* **12**, R589 (2000).

[9] J. W. Bray, H. R. Hart, L. V. Interrante, I. S. Jocobs, J. S. Kasper, G. D. Watkins, S. H. Wee, J. C. Bonner. Observation of a spin-Peierls transition in a Heisenberg antiferromagnetic linear-chain system, *Phys Rev. Lett*. **35**, 744 (1975).

[10] S. Huizinga, J. Kommendour, G. A. Sawatzky, B. T. Thole, K. Kopinga, W. J. M. de Jong, J. Roos. Spin-Peierls transition in N-methyl-N-ethyl-morpholinium-ditetracyanoquinodimethanide [MEM-$(TCNQ)_2$], *Phys. Rev. B* **19**, 4723 (1979).

[11] M. Hase, I. Terasaki, K. Uchinokura. Observation of the spin-Peierls transition in linear Cu^{2+} (spin-1/2) chains in an inorganic compound $CuGeO_3$, *Phys. Rev. Lett.* **70**, 3651 (1993).

[12] M. Isobe, Y. Ueda. Magnetic susceptibility of quasi-one-dimensional compound α'-NaV_2O_5 - possible spin-Peierls compound with high critical temperature of 34 K, *J. Phys. Soc. Jpn.* **65**, 1178 (1996).

[13] J. C. Bonner, S. A. Fridberg, H. Kobayashi, D. L. Meier, H. W. J. Blöte. Alternating linear-chain antiferromagnetism in copper nitrate $Cu(NO_3)_2 \cdot 2.5\ H_2O$, *Phys. Rev. B* **27**, 248 (1983).

[14] A. W. Garrett, S. E. Nagler, D. A. Tennant, B. C. Sales, T. Barnes. Magnetic excitations in the S = 1/2 alternating chain compound $(VO)_2P_2O_7$, *Phys. Rev. Lett.* **79**, 745 (1997).

[15] C. K. Majumdar, D. P. Ghosh. On next-nearest neighbor interaction in linear chains. I, *J. Math. Phys.* **10**,1388 (1969).

[16] F. D. M. Haldane. Nonlinear field theory of large spin Heisenberg antiferromagnets: semiclassically quantized solitons of the one-dimensional easy-axis Néel state, *Phys. Rev. Lett*. **50**, 1153 (1983).

[17] E. F. Shender, S. A. Kivelson. Dilution-induced order in quasi-one-dimensional quantum antiferromagnets, *Phys. Rev. Lett*. **66,** 2384 (1991).

[18] I. Affleck, T. Kennedy, E. H. Lieb, H. Tasaki. Rigorous results of valence-bond ground states in antiferromagnets, *Phys. Rev. Lett*. **59**, 799 (1987).

[19] M. Hagiwara, K. Katsumata, I. Affleck, B. I. Harpelin, J. P. Renard. Observation of S = 1/2 degrees of freedom in an S = 1 linear-chain Heisenberg antiferromagnet, *Phys. Rev. Lett.* **65**, 3181 (1990).

[20] Y. Uchiyama, Y. Sasago, I. Tsukada, K. Uchinokura, A. Zheludov, T. Hayashi, N. Miura, P. Böni. Spin-vacancy-induced long-range order in a new Haldane-gap antiferromagnet, *Phys. Rev. Lett*. **83**, 632 (1999).

[21] E. Dagotto, J. Riera, D. J. Scalapino. Superconductivity in ladders and coupled planes, *Phys. Rev. B* **45**, 5744 (1992).

[22] E. Dagotto, T. M. Rice. Surprises on the way from one- to two-dimensional quantum magnets: The ladder materials, *Science* **271**, 618 (1996).

[23] S. Taniguchi, T. Nishikawa, Y. Yasui, Y. Kobayashi, M. Sato, T. Nishioka, M. Kotani, K. Sano. Spin gap behavior of S = 1/2 quasi-two-dimensional system CaV_4O_9, *J. Phys. Soc. Jpn.* **64**, 2758 (1995).

[24] H. Kageyama, K. Yoshimura, R. Stern, N. V. Mushnikov, K. Onizuka, M. Kato, K. Kosuge, C. P. Slichter, T. Goto, Y. Ueda. Exact dimer ground state and quantized magnetization plateaus in the two-dimensional spin system $SrCu_2(BO_3)_2$, *Phys. Rev. Lett*. **82**, 3168 (1999).

[25] B. S. Shastry, B. Sutherland. Exact ground state of a quantum mechanical antiferromagnet, *Physica* **108B**, 1069 (1981).

[26] T. Sakai, M. Takahashi. Effect of the Haldane gap on quasi-one-dimensional systems, *Phys. Rev. B* **42**, 4537 (1990).

[27] J. Villain, R. Bidaux, J. P. Carton, R. Conte. Order as an effect of disorder, *J. Phys. - Paris* **41**, 1263 (1980).

[28] G. B. Martins, E. Dagotto, J. A. Riera. Rapid suppression of the spin gap in Zn-doped $CuGeO_3$ and $SrCu_2O_3$, *Phys. Rev. B* **54**, 16032 (1996).

[29] Y. Motome, N. Katoh, N. Fukuwara, M. Imada. Impurity effect on spin ladder systems, *J. Phys. Soc. Jpn.* **65**, 1949 (1996).

[30] M. Azuma, Y. Fujishiro, M. Takano. Switching of the gapped singlet spin-liquid state to an antiferromagnetically ordered state in $Sr(Cu_{1-x}Zn_x)_2O_3$, *Phys. Rev. B* **55**, R8658 (1997).

[31] M. Laukamp, G. B. Martins, C. Gazza, A. L. Malvezzi, E. Dagotto. Enhancement of antiferromagnetic fluctuations induced by nonmagnetic impurities: Origin and predictions for NMR experiments, *Phys. Rev. B* **57**, 10755 (1998).

[32] M. Uehara, T. Nagata, J. Akimitsu, H. Tkahashi, N. Mori, K. Kinoshita. Superconductivity in the ladder material $Sr_{0.4}Ca_{13.6}Cu_{24}O_{41.84}$, *J. Phys. Soc. Jpn.* **65**, 2764 (1996).

[33] B. S. Shastry, B. Kumar. $SrCu_2(BO_3)_2$: A unique Mott Hubbard insulator, *Prog. Theor. Phys. Suppl.* **145**, 1 (2002).

[34] T. Kimura, K. Kuroki, Y. Arita, H. Aoki. Possibility of superconductivity in the repulsive Hubbard model on the Shastry-Sutherland lattice, *Phys. Rev. B* **69**, 054501 (2004).

[35] R. Kubo, K. Tomita. A general theory of magnetic resonance absorption, *J. Phys. Soc. Jpn*. **9**, 888 (1954).

[36] V. Jaccarino. Nuclear Resonance in Atiferromagnets, v *Magnetism, Vol. II, Part A*, ur. G. T. Rado in H. Suhl (Academic Press, New York, 1965), str. 307.

[37] R. Wichman, H. Müller-Buschbaum. SrNi2V2O8: ein nuer Strukturtyp der Erdalkali-Oxometallate, *Rev. Chim. Miner*. **23**, 1 (1986).

[38] A. Zheludov, T. Masuda, I. Tsukada, Y. Uchiyama, K. Uchinokura, P. Böni. Magnetic excitations in coupled Haldane spin chains near the quantum critical point, *Phys. Rev. B* **62**, 8921 (2000).

[39] A. Zheludov, T. Masuda, K. Uchinokura, S. E. Nagler. Zone-boundary excitations in coupled Haldane spin chain systems $PbNi_2V_2O_8$ and $SrNi_2V_2O_8$, *Phys. Rev. B* **64**, 134415 (2001).

[40] A. Zorko, D. Arčon, A. Lappas, J, Giapintzakis, C. Saylor, L. C. Brunel. Effect of vacancy doping on the Haldane spin-liquid state in $PbNi_{2-x}Mg_xV_2O_8$, *Phys. Rev. B* **65**, 144449 (2002).

[41] D. Arčon, A. Zorko, A. Lappas. X-band ESR and ^{51}V NMR study of the Haldane system $PbNi_{2-x}Mg_xV_2O_8$, to be published in *Appl. Magn. Reson*. **27**.

[42] J. H. Van Vleck. The dipolar broadening of magnetic resonance lines in crystals, *Phys. Rev*. **74**, 1168 (1948).

[43] J. E. Gulley, D. Hone, D. J. Scalapino, B. G. Silbernagel. Exchange narrowing: Magnetic resonance lineshapes and spin correlations in paramagnetic $KMnF_3$, $RbMnF_3$, and MnF_2, *Phys. Rev. B* **1**, 1020 (1970).

[44] T. G. Castner, M. S. Seehra. Antisymmetric exchange and exchange-narrowed electron-paramagnetic-resonance linewidths, *Phys. Rev. B* **4**, 38 (1971).

[45] I. Mastoraki, A. Lappas, J. Giapintzakis, D. Többens, J. Hernández-Velasco. Relation of crystal structure to magnetic properties in the quasi-one-dimensional compound $PbNi_{1.88}Mg_{0.12}V_2O_8$, *J. Solid State Chem.* **177**, 2404 (2004).

[46] K. Yosida, *Theory of Magnetism* (Springer-Verlag, Berlin, 1996), str. 25.

[47] W. Low. Paramagnetic resonance in solids, v *Solid State Physics, supplementary Vol. 2*, ur. F. Seitz in D. Turnbull (Academic Press, New York, 1960), str. 8.

[48] I. Dzyaloshinky. A thermodynamic theory of "weak" ferromagnetism of antiferromagnetisc, *J. Phys. Chem. Solids* **4**, 241 (1958).

[49] T. Moriya. Anisotropic superexchange interaction and weak ferromagnetism, *Phys. Rev.* **120**, 91 (1960).

[50] D. Arčon, A. Zorko, A. Lappas. ^{51}V NMR study of the doped chain compounds $PbNi_{2-x}Mg_xV_2O_8$, *Europhys. Lett.* **65**, 109 (2004).

[51] A. J. Freeman, R. E. Watson. Hyperfine Interaction in Magnetic Materials, v *Magnetism, Vol. II, Part A*, ur. G. T. Rado in H. Suhl (Academic Press, New York, 1965), str. 167.

[52] E. Clementi, C. Roetti. Roothaan-Hartree-Fock atomic wavefunctions: Basis functions and their coefficients for ground and certain excited states of neutral and ionized atoms, $Z \leq 54$, *At. Data Nucl. Data Tables* **14**, 177 (1974).

[53] R. G. Shulman, V. Jaccarino. Nuclear magnetic resonance in paramagnetic MnF_2, *Phys. Rev.* **108**, 1219 (1957).

[54] C. P. Slichter, *Principles of Magnetic Resonance, 3rd Enlarged and Updated Edition* (Springer-Verlag, Berlin, 1990), str 485.

[55] P. P. Man. Quadrupole coupling in nuclear magnetic resonance, general, v *Encyclopedia of Analytical Chemistry*, ur. R. A. Meyers (John Wiley & Sons Ltd, Chichester, 2000), str. 12224.

[56] S. Hayashi, K. Hayamizu. ^{51}V NMR chemical shift and anisotropy in solid metavanadates, *Bull. Chem. Soc. Jpn.* **63**, 961 (1990).

[57] B. A. Gee, A. Wong. Vanadium-51 MAS and static NMR studies of the binary V_2O_5-WO_3 system, *J. Phys. Chem. B* **107**, 8382 (2003).

[58] K. Uchinokura, Y. Uchiyama, T. Masuda, Y. Sasago, I. Tsukada, A. Zheludov, T. Hayashi, N. Miura, P. Böni. Phase diagram of spin-vacancy-induced antiferromagnetism in a new Haldane compound $PbNi_2V_3O_8$, *Physica B* **284-288**, 1641 (2000).

[59] K. Uchinokura, T. Masuda, Y. Uchiyama, R. Kuroda. Impurity-induced antiferromagnetic phase in a new Haldane-gap compound $PbNi_2V_2O_8$, *J. Magn. Magn. Mater.* **226-230**, 431 (2001).

[60] I. Mastoraki, A. Lappas, R. Schneider, J. Giapintzakis. Spin-gap and antiferromagnetic correlations in low-dimensional $PbNi_{2-x}A_xV_2O_8$ (A = Mg, Co), *Appl. Phys. A* **74** (Suppl.), S640 (2002).

[61] A. Lappas, V. Alexandrakis, J. Giapintzakis, V. Pomjakushin, K. Pressides, A. Shenck. Impurity-induced ordering in the Haldane-gap compound $PbNi_{2-x}Mg_xV_2O_8$ (x = 0.24), *Phys. Rev. B* **66**, 014428 (2002).

[62] S. H. Glarum, S. Geschwind, K. M. Lee, M. L. Kaplan, J. Michel. Observation of fractional Spin S = 1/2 on open ends of S = 1 linear antiferromagnetic chains: nonmagnetic doping, *Phys. Rev. Lett.* **67**, 1614 (1991).

[63] Y. Ajiro, T. Uchikawa, T. Asano, M. Mekata, N. Mori. ESR of "the magnetic dangling bond" in the Haldane state, *J. Phys. Soc. Jpn*. **66**, 971 (1997).

[64] H. Manaka, I. Yamada. Crossover from S = 1/2 to S = 1 Haldane state in the ferromagnetic and antiferromagnetic alternating Heisenberg chain system $(CH_3)_2CHNH_3CuCl_3$ observed with EPR at 24 GHz, *Phys. Rev. B* **62**, 14279 (2000).

[65] A. I. Smirnov, V. N. Glazkov, H.-A. Krug van Nidda, A. Loidl, L. N. Demianets, A. Ya. Shapiro. Paramagnetic and antiferromagnetic resonance in the diamagnetically diluted Haldane magnet $PbNi_2V_2O_8$, *Phys. Rev. B* **65**, 174422 (2002).

[66] T. Masuda, K. Uchinokura, T. Hayashi, N. Miura. Impurity-induced antiferromagnetic phase in a doped Haldane system $Pb(Ni_{1-x}Mg_x)_2V_2O_8$, *Phys. Rev. B* **66**, 174416 (2002).

[67] V. N. Glazkov, A. I. Smirnov, R. M. Eremina, G. Dhalenne, A. Revcolevschi. Magnetic resonance of spin clusters and triplet excitations an a spin-Peierls magnet with impurities, *JETP* **93**, 143 (2001).

[68] J. E. Gulley, V. Jaccarino. Impure exchange-coupled paramagnets: Electron paramagnetic-resonance studies, *Phys. Rev. B* **6**, 58 (1972).

[69] K. Nagata, T. Nishino, T. Hirosawa, T. Komatsubara. EPR in the impure Heisenberg linear chain $CsMn_{1-x}Co_xCl_3 \cdot 2H_2O$, *J. Phys. Soc. Jpn*. **44**, 813 (1978).

[70] A. Zorko, D. Arčon, K. Biljaković, C. Carcel, J. M. Fabre, J. Dolinšek. Spin-Peierls fluctuations in $(TMTTF)_2Br$ studied by pulsed electron spin resonance spin-lattice relaxation, *Phys. Rev. B* **64**, 172404 (2001).

[71] E. Stryjewski, N. Giordano. Metamagnetism, *Adv. Phys*. **26**, 487 (1977).

[72] R. W. Smith, D. A. Keszler. Synthesis, structure, and properties of the orthoborate $SrCu_2(BO_3)_2$, *J. Solid State Chem*. **93**, 430 (1991).

[73] H. Kageyama, K. Onizuka, T. Yamauchi, Y. Ueda. Crystal growth of the two-dimensional spin gap system $SrCu_2(BO_3)_2$, *J. Cryst. Growth* **206**, 65 (1999).

[74] S. Miyahara, K. Ueda. Thermodynamic properties of three-dimensional orthogonal dimer model for $SrCu_2(BO_3)_2$, *J. Phys. Soc. Jpn. Suppl. B* **69**, 72 (2000).

[75] S. Miyahara, K. Ueda. Exact dimer ground state of the two dimensional Heisenberg spin system $SrCu_2(BO_3)_2$, *Phys. Rev. Lett.* **82**, 3701 (1999).

[76] C. Knetter, A. Bühler, E. Müller-Hartmann, G. S. Uhrig. Dispersion and symmetry of bound states in the Shastry-Sutherland model, *Phys. Rev. Lett.* **85**, 3958 (2000).

[77] A. Koga, N. Kawakami. Quantum phase transition in the Shastry-Sutherland model for $SrCu_2(BO_3)_2$, *Phys. Rev. Lett.* **84**, 4461 (2000).

[78] A. Koga. Ground-state phase diagram for the three-dimensional orthogonal-dimer system, *J. Phys. Soc. Jpn.* **69**, 3509 (2000).

[79] H. Nojiri, H. Kageyama, K. Onizuka, Y. Ueda, M. Motokawa. Direct observation of multiple spin gap excitations in two-dimensional dimer system $SrCu_2(BO_3)_2$, *J. Phys. Soc. Jpn.* **68**, 2906 (1999).

[80] H. Kageyama, M. Nishi, N. Aso, K. Onizuka, T. Yosihama, K. Nukui, K. Kodama, K. Kakurai, Y. Ueda. Direct evidence for the localized single-triplet excitation and the dispersive multiplet excitations in $SrCu_2(BO_3)_2$, *Phys. Rev. Lett.* **84**, 5876 (2000).

[81] T. Rõõm, U. Nagel, E. Lippmaa, H. Kageyama, K. Onizuka, Y. Ueda. Far-infrared study of the two-dimensional dimer spin system $SrCu_2(BO_3)_2$, *Phys. Rev. B.* **61**, 14342 (2000).

[82] P. Lemmens, M. Grove, M. Fisher, G. Günteroth, V. N. Kotov, H. Kageyama, K. Onizuka, Y. Ueda. Collective singlet excitations and evolution of Raman spectral weights in the 2D spin dimer compound $SrCu_2(BO_3)_2$, *Phys. Rev. Lett.* **85**, 2605 (2000).

[83] K. Onizuka, H. Kageyama, Y. Narumi, K. Kindom, Y. Ueda, T. Goto. 1/3 magnetization plateau in $SrCu_2(BO_3)_2$ – Stripe order of excited triplets, *J. Phys. Soc. Jpn*. **69**, 1016 (1999).

[84] K. Kodama, M. Takigawa, M. Horvatić, C. Bertier, H. Kageyama, Y. Ueda, S. Miyahara, F. Becca, F. Mila. Magnetic superstructure in the two-dimensional quantum antiferromagnet $SrCu_2(BO3)_2$, *Science* **298**, 395 (2002).

[85] O. Cépas, K. Kakurai, L. P. Regnault, T. Ziman, J. P. Boucher, N. Aso, M. Nishi, H. Kageyama, Y. Ueda. Dzyaloshinsky-Moriya interaction in the 2D spin gap system $SrCu_2(BO_3)_2$, *Phys. Rev. Lett.* **87**, 167205 (2001).

[86] K. Kodama, K. Arai, M. Takigawa, H. Kageyama, Y. Ueda. Spin Correlation and field induced staggered magnetization in the 2D orthogonal dimer spin system $SrCu_2(BO_3)_2$, *J. Magn. Magn. Mater.* **272-276**, 491 (2004).

[87] S. Miyahara, F. Mila, K. Kodama, M. Takigawa, M. Horvatić, C. Bertier, H. Kageyama, Y. Ueda. The effects of the intra-dimer Dzyaloshinsky-Moriya interaction on the properties of $SrCu_2(BO_3)_2$ in an external magnetic field, *J. Phys.: Condens. Matter* **16**, S911 (2004).

[88] H. Nojiri, H. Kageyama, Y. Ueda, M. Motokawa. ESR study on the excited state energy spectrum of $SrCu_2(BO_3)_2$ – A central role of multiple-triplet bound states, *J. Phys. Soc. Jpn.* **72**, 3243 (2003).

[89] G. A. Jorge, R. Stern, M. Jaime, N. Harrison, J. Bonča, S. El Shawish, C. D. Batista, H. A. Dubrowska, B. D. Gaulin. High field specific heat of 2D quantum spin system $SrCu_2(BO_3)_2$, *cond-mat/0309534v1* (2003, unpublished).

[90] K. Sparta, G. J. Redhammer, P. Roussel, G. Heger, G. Roth, P. Lemmens, A. Ionescu. M. Grove, G. Güntherodt, F. Hüning, H. Lueken, H. Kageyama, K. Onizuka, Y. Ueda. Structural phase transition in the 2D spin dimer compound $SrCu_2(BO_3)_2$, *Eur. Phys. J. B* **19**, 507 (2001).

[91] S. El Shawish, J. Bonča, C. D. Batista, I. Sega. Electron spin resonance of $SrCu_2(BO_3)_2$ at high magnetic field, *cond-mat/0407632v1* (2004, unpublished).

[92] O. Cépas, T. Sakai, T. Ziman. Dynamics, selection rules and Dzyaloshinsky-Moriya interactions in strongly frustrated magnets, *Prog. Theor. Phys. Suppl*. **145**, 43 (2002).

[93] O. Cépas, T. Ziman. Theory of phonon-assisted "forbidden" optical transitions in spin-gap systems, *cond-mat/0401240v1* (2004, unpublished).

[94] A. Zorko, D. Arčon, A. Lappas, J. Giapintzakis. Near critical behavior in the two-dimensional spin-gap system $SrCu_2(BO_3)_2$, *Phys. Rev. B* **65**, 024417 (2001).

[95] A. Zorko, D. Arčon, H. van Tol, L. C. Brunel, H. Kageyama. X-band ESR determination of the Dzyaloshinsky-Moriya interaction in the two-dimensional $SrCu_2(BO_3)_2$ system. *Phys. Rev. B* **69**, 174420 (2004).

[96] A. Zorko, D. Arčon, H. Kageyama, A. Lappas. Magnetic anisotropy of $SrCu_2(BO_3)_2$ system as revealed by X-band ESR, to be published in *Appl. Magn. Reson.* **27**.

[97] P. M. Richard. Magnetic resonance in one- and two-dimensional systems, v *Local Properties of Low-Dimensional Antiferromagnets*, ur. K. A. Müller (Nord Holland Publishing Company, Amsterdam, 1976), str. 539.

[98] T. M. McGregor, Z. G. Soos. Anisotropic exchange in linear chain complexes of copper (II), *J. Chem. Phys.* **64**, 2506 (1976).

[99] K. Kakurai, N. Aso, K. Nukui, M. Nishi, H. Kageyama, Y. Ueda, H. Kodowaki, O. Cépas. Inelastic neutron scattering experiments on Dzyaloshinsky-Moriya interaction in $SrCu_2(BO_3)_2$, v *Quantum Properties of Low-Dimensional Antiferromagnets*, ur. Y. Ajiro in J.-P. Boucher (Kyushu University Press, Fukuoka, 2002), str. 102.

[100] K. Kodama, S. Miyahara, M. Takigawa, M. Horvatić, C. Bertier, F. Mila, H. Kageyama, Y. Ueda. Field induced effects of anisotropic magnetic interactions in $SrCu_2(BO_3)_2$, *cond-mat/0404482v1* (2004, unpublished).

[101] K.-Y. Choi, G. Pashkevich, K. V. Lamonova, H. Kageyama, Y. Ueda, P. Lemmens. Strong anharmonicity and spin-phonon coupling in the quasi-two-dimensional quantum spin system $Sr_{1-x}Ba_xCu_2(BO_3)_2$, *Phys Rev. B* **68**, 104418 (2003).

[102] Z. G. Soos, T. T. P. Cheung, K. T. McGregor. Exchange narrowing in correlated spin systems: local field contributions, *Chem. Phys. Lett*. **46**, 600 (1977).

[103] M. S. Seehra and T. C. Castner. The paramagnetic line width in $Cu(HCOO)_2 \cdot 4H_2O$, *Phys. Kondens. Materie* **7**, 185 (1968).

[104] D. Bloch. The 10/3 law for the volume dependence of superexchange, *J. Phys. Chem. Solids* **27**, 881 (1966).

[105] S. Zherlitsyn, S. Schmidt, B. Wolf, H. Schwerk, B. Lüthi, K. Kageyama, K. Onizuka, Y. Ueda, K. Ueda. Sound-wave anomalies in $SrCu_2(BO_3)_2$, *Phys. Rev. B* **62**, R6097 (2000).

[106] B. Wolf, S. Zherlitsyn, S. Schimd, B. Lüthi, H. Kageyama, Y. Ueda. Soft acoustic modes in the two-dimensional spin system $SrCu_2(BO_3)_2$, *Phys. Rev. Lett.* **86**, 4847 (2001).

[107] S. Miyahara, K. Ueda. Theory of the orthogonal dimer Heisenberg spin model for $SrCu_2(BO_3)_2$, *J. Phys.: Condens. Matter* **15**, R327 (2003); in vsebovane reference.

[108] A. Zorko, D. Arčon, C. J. Nuttall, A. Lappas. X-band ESR study of the two-dimensional spin-gap system $SrCu_2(BO_3)_2$, *J. Magn. Magn. Mater.* **272**, e699 (2004).

[109] W. K. Fullagar, P. A. Reynolds, J. W. White. Lithium and sodium fullerides prepared in liquid ammonia, *Solid State Commun.* **104**, 23 (1997).

[110] F. A. Cotton, G. Wilkinson, *Advanced Inorganic Chemistry* , *5^{th} Edition* (John Wiley & Sons, New York,1988), str.127.

[111] H. Kageyama, K. Onizuka, Y. Ueda, S. Hane, H. Mitamura, T. Goto, K. Yoshimura, K. Kosuge. Ba- and Ca-substitution effect on the spin gap in $SrCu_2(BO_3)_2$ with the exact dimer ground state, v *Proceedings of the 4^{th} international symposium on advanced physical fields*, ur. G. Kido (National Research Institute for Metals, Tsukuba, 1999), str. 235.

[112] W. R. McKinnon. *Chemical Physics of Intercalation (NATO ASI B), vol. B172*, ur. A. P. Legrand in S. Flanfrois (Plenum, New York, 1987), str. 181.

IZJAVA

Izjavljam, da je ta disertacija plod lastnega znanstveno-raziskovalnega dela.

Ljubljana, 5. 10. 2004

Andrej Zorko